A sensor system and related models to determine irregular shaped 3-D objects

Hartmut Gall

A thesis submitted for the degree of Doctor of Philosophy

A collaboration between
Agronomy Department, SAC and
Department of Physics, University of Edinburgh

March, 2000

Abstract

This work comprises several parts, the initial part of which is a review of the techniques in use at present for measuring shape and characterising products. The major work details a ring sensor system, which consists of a large number of transmitters and receivers alternately arranged on the circumference of a metal annulus. Using a modified polar co-ordinate system and trigonometric functions, two enveloping spirals of an object can be determined. One or both spirals can then be used for further data analysis. Each spiral consists of intersections between enveloping chords and parts of the chords. The area surrounding the object is segmented and properties such as volume and axis measurements can be determined. A model was developed to simulate artificial objects of various shapes. Simulation tests were carried out to determine the limits of the system concerning position within the ring, shape and speed of the object and resolution of the ring. A ring was manufactured for actual tests, which were carried out mainly on potatoes to confirm the possible use in practice and to show the relative merits compared with existing systems. Interesting side issues are introduced, such as the low number of primary data, possibilities of further reduction using differential coding, and the consumption time of the algorithms. Finally, a model for the simulation of more than one object in the ring at the same time is introduced and a possible way of separation is investigated.

I hereby declare that all work presented in this thesis
is original and has been carried out by the author
unless otherwise stated.

Hartmut Gall

Table of Contents

List of Symbols

2_13	code for object situation, e.g. here object 2 is separated from object 1 and 3, which shadow each other
a	side of a rectangle
A1-3	actual chords
A_C	area of a segment of the ring (circle)
A_O	cross-sectional area of an object
A_R	area of the ring
A_S	segment in the ring consisting of one triangle and a segment of the ring (circle)
A_S*	A_S in a circle with radius 1
A_T	area of the triangle
b	side of a rectangle
case 9	situation where chords can not be assigned during process of separation
C_A	intersect on the actual chord with the perpendicular from the intersection opposite
C_P, C_S	intersection of the actual chord with the predecessor or successor
C_P[n]	intersection of the actual chord with the predecessor
C_P'[n]	temporary position of the intersection C_P[n]
C_S[n]	intersection of the actual chord with the successor $k_{Tx,TRy}$ numbers of receivers between different transmitters or receivers determined using the variables n for the marked transmitter or m_B1[n] for the marked receivers. Multiplied by angle β, angles $\varphi_{M,Tx,TRy}$ will be determined.
C_X, C_X*	intersection between the perpendicular of the actual chord and the apparent parallel chord or the opposite intersection
C_Z	intersection of the perpendicular from the actual receiver R_A[n] to the apparent chord
d, d1, d2	distances
d_O	distance between the midpoint of the object and each vertex.
d_R	difference between two neighbouring radii
d_{REL}	relative distance of the 'front' spiral to the 'back' spiral
d_S	distance which the object moves during one scanning revolution
D_A	length of an axis
D_{ED}	distance from the outside of the ring
D_I	midpoint of the object
e_A, e_B	half of the major axis and minor axis of an ellipse

e_X	eccentricity of the ellipse
FCHM	array of $m_B1[n[i]]$ of used snapshots
FCHN	array of n[i] of used snapshots
FCHR	array of distances |TA:CP[n[i]]| of used snapshots
GC	generalised cylinder
i	actual number of an investigation
i_{N_POS}, i_{N_NEG}	maximum and minimum factor for finding the maximum expansion of an ellipse
i_{OBJ}	total number of determined remaining area segments A_S or volume segments
i_V	vertex
i_{VN}	total number of vertices of a polygon
IIC	image improvement code
IN_2, IN_{3A}, IN_{3B}	intersections
k1 - k5	factors for regression
k_R	constant determining the slope of a spiral
$k_{TA.TP}$, $k_{TX,RX*}$, $k_{TX,RX}$	numbers of receivers between different transmitters and/or receivers
k_Z	constant
log	logarithm
L	length
LSL	largest slice major axis
LSS	largest slice minor axis
m_B,m_{B1}, m_{B2}, m_{B3}	number of receivers from the actual activated transmitter n anti-clockwise to the receiver of the 'back' chord of an object for a snapshot
m_F,m_{F1}, m_{F2}, m_{F3}	number of receivers from the actual activated transmitter n anti-clockwise to the receiver of the 'front' chord of an object for a snapshot
$m_{TR0}[n]$ - $m_{TR5}[n]$	number of receivers from the actual activated transmitter n anti-clockwise to the receiver of the 'front' or 'back' chord of object 1-3
M	midpoint
MAX	maximum
MIN	minimum
M_O	midpoint of the object
MSL	middle slice major axis
MSS	middle slice minor axis
n	number of the actual activated transmitter
N_{CH}	maximum possible number of chords
N_I	number of intersections
N_{OBJ}	total number of snapshot of one object
NPO	number of order of objects in the scene
N_P	number of possible positions of parts of objects

N_{RAN}	rational random number between 0..1
N_R	number of installed receivers
N_{REV}	number of revolutions
N_T	number of installed transmitters
OBJ0 - OBJ5	multiple primary data sorted by objects, 'back' and 'front' chord
OOC	object order code
p_3	polygon with 3 corners
P	parallels
P1-3	predecessor chords
P_C	point of intersection
P_H	position in horizontal direction
POT	primary object transformation code
r	radius
r_A, r_S	radii of neighbouring circles
r_{CIR}	radius of cross section of sphere and cylinder
rev	revolution
r_O	maximum expansion of the object in central position
r_{O3D}	distance of surface point of an 3D object from the rotationary axis (midpoint) of a symmetrical object
r_{OD}	actual distance from the midpoint of the ring to the surface of the displaced object
R	receiver
R_A, R_S, R_P	actual receiver, successor and predecessor
R_X, R_Y, R_X*	receiver on the opposite side
s	displacement of the object between each snapshot
stdev	standard deviation
S2, S3	successor chords
SOC[n]	Snapshots of changes regarding the order of chords to the objects
SPO	position of the largest slice
t	time
t[case1]	time needed to process case1
t[case2]	time needed to process case 2
t[case3]	time needed to process case 3
t_{CMIN}	minimal time required for processing
t_{TOD2D}	time required to process cross-sections (2-D case)
t_{TOD3D}	time required to process whole objects (3-D case)
T	transmitter
TE	number of transmitter and receiver with TE = N_T =N_R
T_A, T_S, T_P	actual transmitter, successor and predecessor
T_X[n], T_Y[n]	transmitter on the opposite side
TR0 - 5	chord between transmitter and receiver
TRC	transfer code

u	number of receivers from the actual transmitter anti-clockwise to the actual investigated receiver during the process of simulation
V_C	volume of cylinder
V_{MEAS}	measured volume
V_{C_MEAS}	corrected volume using regression
V_O	volume of the object
V_R	volume of spline
V_S	volume of segment
w_{BIT}	necessary width in bits for coding distance between transmitter and receiver
x,y	label for actual chord A, the predecessor P or the successor S
x_{MO}, y_{MO}	co-ordinates of the midpoint of a cross-section
$x[i]$, $y[i]$	Cartesian co-ordinates of intersections of the major and minor axes
X, Y, Z	axes of the Cartesian co-ordinate system
Z0, Z1, Z2, Z3	arrays with coded primary data of snapshots
α	angle between adjacent transmitters
β	angle (displacement) between transmitter and receiver = $\frac{1}{2}\alpha$
χ_D	direction of expansion of object
χ_P	pivot point of the object related to the co-ordinate system of the ring
μ	angle between transmitter and receiver beams
γ, γ_M, ε, ε_M, φ, δ, ψ, η	angles
π	PI
$\sigma 1$, $\sigma 2$	accuracy
σ_M	middle error
$\tau 1$-3	angle in the triangles
$\omega_{M,Tx.TRy}$	angle at the circumference centred on a transmitter created with the radius of the ring (with the midpoint M) and a further transmitter or receiver
ϑ	fixed minimum angle of 0.5° for simulation of ellipse

List of Figures

List of Tables

Acknowledgements

In 1995 I arrived in Scotland to work on the project 'ring sensor system' and lived in Edinburgh for 2½ years. This was possible, because the project was planned and set up by D. C. McRae and myself and supported by a grant from the European Union. I want to thank Douglas for his initial work and support.

The start was a challenge for me, because my English was very poor at that time. Nevertheless, the project working on the ring sensor system made good progress and my supervisor for the project A.Y. Muir and I decided that I should become a PhD student. Because my grant was limited I changed my work place in 1998. Since then I have been working for the company R J Herbert Engineering Ltd in England. Outside my normal work I was able to continue the development of the system, hardware, software and writing the thesis.

Without support it would not have been possible to get the results described in this thesis. At first I want to give my special thanks to my two supervisors A.Y. Muir and W. Hossack for their critical views and helpful advice. Over the years I made progress in the English language. Nevertheless, I needed the help from a native English speaker to get my written proposals corrected; therefore I want to give my special thanks to J. Fleming. Also I want to thank my former colleagues at the SAC, C. Dewar, D. Kennedy, J. Kirkland, F. Milne, D. Ross for their support.

For many years I have had a good relationship with the company Argus Electronic GmbH in Rostock / Germany. We worked together setting up the hardware solution and the development of the surrounding software; thanks to R. Pohlmann and L. Göcke.

Further I want to thank R.J. Herbert and N. Herbert, who supported the project with technically and with a special work time arrangement within the company R J Herbert Engineering Ltd. since 1998. Special thanks to my colleague Dr. L. Defty, who always encouraged finishing the work and gave helpful advice.

Finally my thanks are going to P. Covell, who supported the set-up of the presentation system and A. Johnson and S. Levene, who helped by reading my proposals for the thesis.

I liked to work on this project from the point of technical and language challenge, but it also gave me the opportunity to improve my knowledge on many surrounding technical fields especially in the post-harvest handling of agricultural products. Last but not least I am grateful to have been given the opportunity to meet lots of people in many countries at conferences, discussions about projects and cultural events.

1. Introduction

1.1. Background

Vision is the most important recognition system of the higher developed species and is used for self location, controlled movement, object location and to select food in the three-dimensional world. The main factors are position, size and shape of objects. A grey level or shadow picture can give information about these factors in simple terms. The colour or spectral reflectance of objects gives additional information about the properties of the surface of objects.

In nature, many organisms vary greatly in their sensitivity to light. Simple and very complex sensor systems can in nature be found combined to give information about position, size and shape. For example, and in the simplest form the Euglena, a one cell creature, is only sensitive to the presence and direction of a light source, while the retina in the eyes of higher developed animals delivers a 2-D image, but by itself it only contains information about a scene from one viewpoint with no information about the third dimension. Two spatially separated 2-D sensors of this kind can be used to measure the difference between the relative positions of corresponding features from two viewpoints, the so-called binocular disparity, and information about the third dimension, the depth, then becomes available. Another possibility of obtaining 3-D information is through the use of motion around objects to get several viewpoints, for example as used by the common house fly (Times 1997).

General technical developments of the last four decades have led to the recognition of 3-D objects by automatic vision systems. The fascinating machine vision problem still remaining is parameter determination and the comprehensive description of objects in real time. Today for many processes the human can be replaced by visual systems coupled with automatic manipulated systems. New kinds of viewing with different kind of 'eyes' (vision sensors) have been developed which allow viewing from the micro (structure of molecules) to macro worlds (space). Image recognition systems may also use arrangements of lighting and detection, which are not possible in nature. These techniques allowed the development of new kinds of 'eyes', for example the laser scanner technique using triangulation, which can better cope with the needs of processes and technical surroundings. Another example are the use of the very simple cross-beam solution, which is based on locating where is light and shadow (Namco 1990). Using

such techniques a number of image analysis problems can be solved using less expenditure than other conventional video systems.

As opposed to image analysis, synthesis is for example used in CAD systems and for simulations. Theories and models can also be used to describe objects captured by image analysis systems (Foley 1997).

This work is about a comprehensive 3-D size, shape and position detection system and accompanying 3-D modelling for the description particularly of predominantly convex agricultural products with a large variability of shape (Brice 1996, Tillett 1991). Recovery of shape from contour remains one of the hardest problems in computer vision. For a one camera system this means that difficulty results from the loss of one dimension and the production of imperfect contours (Zerroug 1996). Obtaining 3-D properties from a 2-D image is the current common practise. This tends to be inaccurate, as the 2-D information only contains the contour and cross-sectional area of the object from one viewpoint. Generally three dimensional detection systems take a number of snapshots from different viewpoints to cover parts of, or as in this work, the whole object.

The position of an object in space can be defined using a point in the 3-D world and the orientation of its axes to the object. The size is then considered as volume and has a single physical value. Shape on the other hand is a complex matter depending on the structure variation of the object. There are different meanings of 'shape' which are not necessarily closely related (Koendrink 1990). In this work 'shape' is especially considered as the geometry of the hull of the outside surface of, in the first instance, single predominantly diffuse, reflecting closed convex opaque objects. Apples, potatoes and torsos of pigs, chickens, humans etc. conform to these requirements.

Overall shape detection requires 'wrapping' the surface of the whole object as closely as possible and creates a data set of co-ordinates. Shape can also be described by a number of shape factors such as axis measurements. In most industrial applications, objects do not vary much, but measurement accuracy might require to be in microns. In agriculture and the food industry, accuracy to this level is not necessary. However, speed, real-time use, reduced computer-power and last but not least the price of the system are more important. The accuracy compared with industrial applications is normally less important and is typically in the millimetre range. For products such as potatoes, onions, apples etc. the minimum limit of interest for size can be set at around 10mm and for axis

measurements about 1-2 mm. This latitude allows the use of different solutions and technologies for sensor systems as will be introduced in this work.

The choice of sensor is not the only deciding factor in the quality and performance of a system. The presentation of the object and the adaptation of the sensor system must match. In particular, correct presentation of objects to the sensor has as much influence on the efficiency of image assimilation as has the choice of sensor.

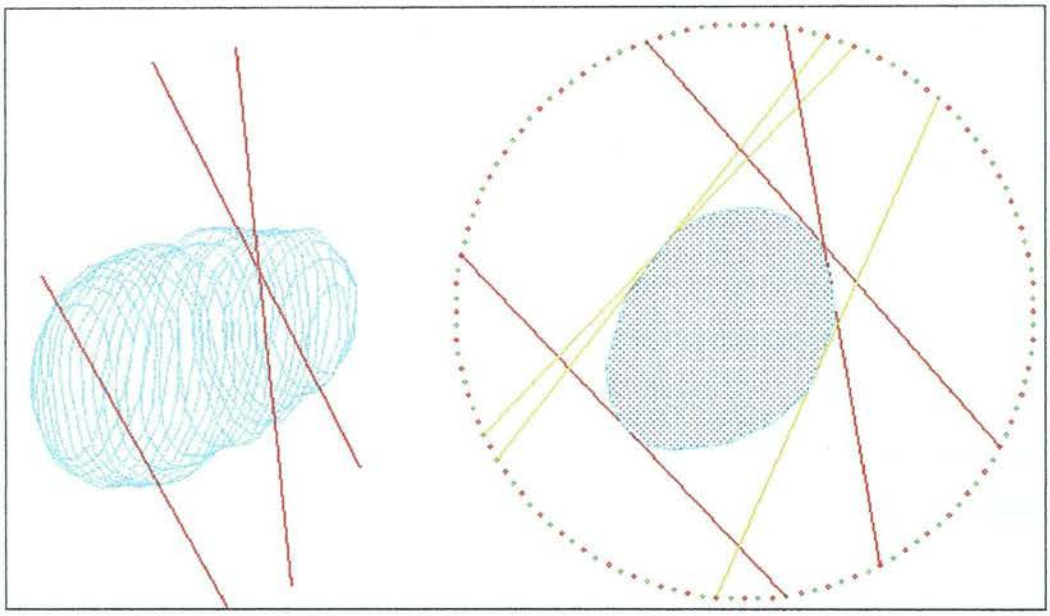

Figure 1.1. Image of the middle slice and the whole object scanned by the ring sensor system

The main goal of this work is the description of new developments of an optical ring sensor system with particular applications in agriculture. The arrangement was first described by Farchmin and Gall (1990) (see figure 1.1). This sensor system can be used for the determination of the size, shape and position of opaque convex 3-D objects in a defined space in real time.

1.2. Directly related works

Earlier work was done concerning a ring sensor system solution. An introduction was given by Gall (1990, 1992). More information can be found in Gall (1994, 1996a,

1996b). Partial results of this thesis have already been released by Gall *et al* (1997, 1998, 1999).

The basic work done by Gall (1992) shall be mentioned. It includes

- A short overview of some vision systems existing at that time as well as a general introduction into image analysis techniques
- Different ring sensor arrangements and the use of parallel light beams for data analysis
- Description of a co-ordinate system with the origin at the centre of the ring
- Description of basic algorithms for the determination of attaching chords with a proposed system scanning clockwise and viewing the scene clockwise.
- Only the first attached chord of each snapshot in the clockwise direction is used and only one object within the ring system is considered
- Basic algorithms for volume and axis measurements under the existing conditions
- Limited theoretical error investigations on worst case conditions of centrally positioned objects
- Theoretical investigation into the physics of light and optics in the ring sensor system
- Description of a first test solution and results of simple practical tests

1.3. Scope of the thesis

Because of the expanding complexity of analysing the developments in the technical world, describing a solution for a shape detection system and a model for shape description, this work will focus on the following points:

- A review of the principal construction of sensor systems for size and shape detection is given, but is limited to geometric optical systems. (Details of systems such as general tomography and laser scanner in detail will be out with the scope of the work)
- The importance of presentation systems will be discussed

- The basic properties of the ring sensor system, as the solution to be introduced in this work, will be compared with related solutions
- A new 3-D model will be developed using a new modified polar co-ordinate system to describe the shape of irregular objects (Gall 1997) for a system scanning clockwise and viewing the scene anti-clockwise
- The use of one or two polar helices enveloping an object will be investigated
- The mathematics for the determination of volume (size) and axis measurement (shape) and position will be introduced (Gall *et al* 1998) with a different perspective of enveloping as described in Gall (1992)
- A model for the simulation of objects in the ring, which can also be used for the general

  3-D world will be introduced
- A comprehensive error investigation on simulations as well as on real measurements will demonstrate the limits of the system
- The possibilities of data compression are investigated
- The computational cost of the main algorithms will be analysed
- Multiple objects will be simulated in the ring
- One proposal for a separation of multiple objects will be described

2. Optical sensor systems for size and shape detection

In this chapter, basic facts, definitions and an overview are given of possible optical sensor systems for size and shape detection within a size range of 10mm - 1m, including the crucial issue of the presentation of objects. It concentrates on optical systems using mainly light within the infra-red, visible and X-ray spectra. Methods such as holography, interferometry, spectroscopy and measurement based on speed of light are not investigated. Scanning size and shape with for example tactile, weighing, capacitive, inductive and ultrasonic sensors are also outside the scope of this work. A more general overview is given in Gall (1992).

2.1. General classification of systems

Optical vision systems for shape detection can be classified by their main features:

1. The lighting and detector beam angle characteristics of the sensor systems can be distinguished by the use of diffuse and/or directed light.

2. Light interaction with the object such as shadowed, reflected or transmitted light is used.

3. The objects have to be presented to the vision system, and must be spatially separated (singulated and oriented).

4. Getting the 3-D object 'boxed-in', the construction and the cost of the sensor system is linked to the consistency of the presentation of the object. In most practical cases this determines the need for either the movement of the object and/or the light sources and/or complexity of the sensor system. Movement also means that hardware can be saved, but it must be compensated for by more 'snapshots' to get the whole object enveloped step by step, often necessitating more complex algorithms and higher computer power.

5. To describe the 3-D shape of objects different models are necessary for different sensor systems. If an interesting parameter, for example axes, can not be measured it can only be estimated, knowledge of the population statistics relating these values is necessary.

The construction and resulting properties of the sensor systems for 3-D detection must always relate to a combination of these features.

2.2. Interaction with light and definitions

The light used is crucial for the illumination of the objects and interaction with the object. The light can interact with the object in different ways, which will generate the potential for different kinds of shape detection. These are now explained:

Shadowing: includes the edge detection where the object is turned away from the light source or another surface intercepts the light from the source, for example between sun and earth between night and day and eclipses. Shadow pictures taken around an object give silhouettes, which can be taken to reconstruct the object (Koendrink 1990). Shadow systems recognising the silhouette are often used for the determination of size and shape of objects.

Transmission: light from an external source which passes through the object is detected and analysed. It is used for computer tomography (Rosenfeld *et al* 1982, Herman 1980) and in principle is based on the same arrangements as shadow systems.

Emission: the transmitter is within the object itself. This is used in medical imaging where the object is injected with a radioactive isotope and the decay products of radiation detected (usually γ - rays), but because the lighting is not from the outside of the object this case will not be considered further.

Reflection: without analysis of brightness within the image of the object, only edge detection is possible. The result is the silhouette, the same as it would be by the use of a shadow system.

Shape from shading: is based on reflection, investigating the whole image for its pattern of brightness and is based on the assumption that image radiance is a function of purely local geometric property, the surface normal (Forsyth *et al* 1990). Shading depends on the variation of brightness in a region of an image of an object which is constantly illuminated and which has properties of reflection all over the object. With one sensor such as an eye or a CCD-camera it is possible to interpret the brightness pattern on the image as shading to the spatial fluctuation of surface orientation of constantly bright objects (Horn *et al* 1989). Limited information about the shape of the surface can be recognised, often counted as a 'half dimension'. The arrangements used are usually the same as for normal reflection systems.

Stereo vision: is a 3-D method for shape detection, based on reflection of the different brightness levels in the reflected light caused by the texture (structure) of objects or by the use of structured light (Davies 1990). A minimum of two images from two different known viewpoints to a point of same brightness on the object are used and the known geometrical relation of the two viewpoints allows the determination of 3-D shape parameters. It is a passive method, but structured lighting with not necessarily known direction and flexible pattern can support the method especially on plane objects. Stereo vision relies on being able to uniquely locate the same object point in two or more images. This is computationally difficult with enormous calculation required for smooth natural objects. Shape from shading cannot build up an accurate shape from degraded images (Noborio 1988). This problem can usually be solved by the use of structured light (Turing 1999) but still requires complex computer processing to locate points and build the 3-D model.

Triangulation: is close to stereo vision, the difference being that it is an active method, using structured light with a known pattern and direction (e.g. a line) to focus the system on the points of interest. Angles and distances between light source and receiver are known. The position of a known lighted spot on the surface of an object can be determined (Gronewäller *et al* 1990). In principle it is very accurate, but requires the object to have a non-blurring or scattering surface. It is also limited to a predetermined distance range.

2.3. Basic optical arrangements

The different possible methods of influenced light as described above require different arrangements of transmitters and receivers. In this chapter the fundamental three arrangements, which are the basis for all comprehensive systems, are described.

The illumination or lighting (in this work in the range between X-ray and near infra-red light) of the scene depends on the beam angle characteristic of the single elements of which the system is built, the kind of arrangement and their number (Siemens 1993, Texas 1975, Gall 1992). For different systems, different light beam angle characteristics of the transmitter and receiver are required. In principle, every complex lighting system with characteristics such as homogeneous (isotropic), structured and diffused light can be built up by a number of basic elements of a point source with a single point and/or wide beam lighting characteristic or anything between. The same characteristic can also be achieved using transmitters combined with optical units such as lenses, gratings and diffusers, which will have a geometrical extension in at least one dimension. More about lighting is addressed in Slusallek *et al* (1995), Kim *et al* (1995), Foley *et al* (1997), Shafer (1985), Belhumeur *et al* (1996). The same as for transmitters can be said about the beam angle characteristic of receivers with regard to the number of single elements it consists of, the characteristics of the whole receiving sensor unit and the use of optical units for a characteristic change.

Linked with the characteristic of lighting are the simplest arrangements of vision systems (see figure 2.1) using light beam detectors (light beam barrier) consisting of a single spot transmitter and a single spot receiver for the detection of the presence of objects on a line or a spot. Most of the more complex arrangements can be attributed to this simple arrangement, they are in principle a collection of a number of these basic presence detection systems.

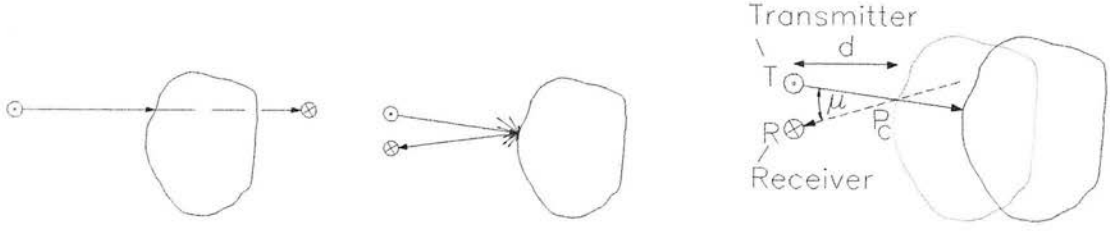

a) Shadowing transmission

b) Reflection diffuse lighted

c) Reflection structured lighted

Figure 2.1. Fundamental arrangements (light beam sensors)

The transmitted light interacts with the object and will have its properties changed. There are different possibilities for constructing a basic system (see figure 2.1) for detection of objects:

1. Transmitter and receiver are arranged on opposite sides of the object and can detect objects on the straight line between them (see figure 2.1.a).

- Shadowing, outline

  If the object breaks the light path, the line between transmitter and receiver, an object is present. The beam angle characteristic of the optical elements is not crucial.

- Transmission

  If an object is in the field of view the transmitted light can be detected and an internal property detection of the object can be carried out. This is the basic of tomography and relies on the object being semi-transparent to the imaging radiation.

2. The beam angle characteristics of transmitter and receiver (viewing angle) face into the same direction in the space. Without an object, the detector does not receive any signal (see figure 2.1.b).

- Reflection

  If an object is present on the line of view, light is reflected and detected by the sensor determining the presence of the object. To obtain the accurate location by this method the transmitter or receiver beam angle characteristic (viewing angle) must be a point (or spot).

- Shading

  The level of reflection can also be determined, which can give information about the distance of the viewed point of a homogeneous object from the transmitter, or the reflectance characteristics of the object.

3. The transmitter and receiver are arranged separately. Both have very narrow beam angle characteristics (points) and the beams cross at one point (see figure 2.1.c).

- Triangulation

  Based on the use of reflected light for the determination of the presence of an object on a defined point and including the knowledge of the position in space, only a reflection light beam sensor can be used. Only if an object with reflecting surface is at a defined single point is any signal received in the detector. The angle μ in the triangle transmitter, receiver and crossing point is known, as is the distance such as d between them. Only one known point P in space can be observed for presence at one time, so a more complex scanning system is required in practise to get one dimension or more. For machine vision in 3-D space, pictures including distances are more useful than intensity, because the segmentation is easier (Rosenfeld 1987).

Stereo vision in its simplest form is a multiple arrangement, which is based on a combination of two basic arrangements shown in figure 2.1.b or the use of movement (see also chapter 2.5.3).

2.4. Presentation of objects

In practice, presentation of the object is probably one of the most crucial points and is frequently under-estimated in setting up image analysis systems for shape detection. This task demands a great deal of engineering attention (Affeldt 1993). Presentation determines the number of dimensions of view in space, speed and accuracy, costs and success of a system on a large scale. The problem of presentation can be split into two tasks:

1. Movement or scanning of the object and/or the sensor system. Fixed sensor and object positions are predominantly used in medical and scientific applications while process maintaining applications always involve movement of objects or sensors. Each dimension of movement in space of a sensor system gives the opportunity for a dimension in shape detection.

2. Separation of the objects to a level where they can be isolated by the sensor system and/or software. If separation is not possible, more complex arrangements of sensors or algorithms using splitting techniques are necessary. This complicates the system and results in many practical difficulties.

Most 3-D recognition systems can in principle be reduced to the use of a 2-D or 1-D application or at least to presence detection (see chapter 2.3) using horizontal or vertical motion and/or rotation. As a result of motion and separation of objects and /or sensor systems, new dimensions of viewing for the vision system become possible.

The main known presentation systems particularly used in the food industry are shown in the tables 2.1-2.3.

Device for horizontal or vertical presentation of the object	**Notes**	**Important properties**	**Examples / literature**
Flat conveyor belt	Objects lying on the belt for presentation	Very high throughput possible, simple mechanical solution, normally only limited inspection from the top possible	Arnarson *et al* (1993), Marel (1999), Hirotoshi (1991), Samro (1994, 1995)
V-belts	Objects lined up and stabilised	Longitudinal orientation of objects possible, throughput high per line, top view and part side view are possible	Mörtl (1992), Select (1998) Tao *et al* (1995), Lefebre *et al* (1993)
Wire system (consists of 2-4 separate parallel running wires)	Often fed out of a shaker	Longitudinal orientation can be reached if correctly fed, very stable simple system, disadvantage objects partly hidden by wires	Exeter (1994)
Net or transparent hose	The object is guided through the sensor system	Net has to be added and partially hides object, stable presentation	Wartenberg (1989)
Finger system attached to a long chain	Fed by a shaker	Longitudinal orientation can be reached if correctly fed, complex system, disadvantage – objects hidden by fingers	Mafroda (1998)
Flight (drop) through the air	Presented from a flat or V-belt	High throughput, from a V-belt no hidden parts of objects	Mörtl (1992), Select (1998), Argus (1997)
Rotation	On a plate	No throughput, bottom partly hidden	Wright (1984)

Table 2.1. Horizontal and vertical movement of objects

Movement of the sensor system	Notes	Important properties	Examples / literature
Along a line	-	Slow, mechanical wear	-
Mechanical rotation around the object	-	Slow, mechanical wear, only cross-section	See figure 2.4.e, Klingenbeck *et al* (1990), Limbach (1997)
Pseudo movement (rotation)	Switching transmitter on a multiple arrangement on different times	Fast, no wear, especially used by light beam sensors, only cross-section	Ring sensor system as shown in this work

Table 2.2. Horizontal or vertical movement of the sensor system

Moving part	Description	Notes	Important properties	Examples / literature
Object	Rotational and vertical movement on a roller table in front of the system	Camera takes snapshots, the object will be wrapped	Very high throughput, neither end of the object can be seen, only for round and nearly round objects	Crezee (1996), McCrea (1981) , Marchant *et al* (1988), Herbert (1998), Loctronic (1989)
Object	Rolling down a ramp	For clod detection and separation	Only for nearly round objects, if not round, track of the object unknown, instabilities	Samro (1995)
Object	Shaker tray	-	No controlled speed, if object not round parts will be hidden	-
Object	Flight with rotation	-	The set-up is unstable unless object is round	-
System	Rotating around an object and movement	-	-	Satellites around the earth, Konecny *et al* (1996), Raggam *et al* (1994)
Both	Horizontal movement of the object and rotation of the sensor around	-	A stable arrangement can be built up	See figure 2.4.e, ring sensor system as below, Limbach (1997)

Table 2.3. Combination of linear movement with rotation of the object and/or sensor system

Some, but not all of these systems also include separation or singulation of the objects with varying degrees of success.

In practise a lot of attention is paid to good separation. Combinations consisting of separation and movement systems can often be found. The separation of objects is often carried out by increasing the speed of objects, for example

- combination of belts with increasing speed
- riddle channels
- circular vibratory feeder elevating single objects (pills and cereal grains)
- two contra-rotating drums with an increasing spiral on the surface for horizontal movement
- using gravity acceleration in free fall, on slanting planes or belt systems

or with

- an expanding roller singulator (McRae 1988)
- a roller table with self-controlled infeed by special roller size and angle of rise (Herbert 1998).

2.5. Practical arrangements

In this chapter, practical 1-D up to 3-D sensor-systems will be briefly introduced as used in practice and research applications, mainly focusing on the possible use for objects as defined in chapter 1 or similar to the ring sensor system described later. They can be fundamentally built up by different sensor systems consisting of simple basic presence detectors (see also chapter 2.3) up to a 3-D detection arrangement. They can carry out a multiple scan with one snapshot, or use multiple snapshots based on pseudo-movement of alternately arranged transmitters and receivers, or mechanical movement of the system itself (see also chapter 2.4). The lack of multiple arrangements can be compensated using mechanical motion, which can deliver a simple system and saving a lot of expense. The disadvantage is a need for more time than one snapshot of a multiple arrangement.

For a complex 3-D scan of one static object a complex 3-D arrangement of a sensor system is required. Because in most industrial processes movement is always present, 2-D arrangements are predominantly used, allowing the collection of a number of cross-sections. Possible arrangements (based on triangulation and stereo vision) directly giving

3-D information only from one side of the object have also to be moved or configured in multiple arrangements to cover whole objects.

2.5.1. Shadow and transmission sensors

On the basis of the shadow presence detector (see figure 2.1.a), a number of different arrangements of shape detectors can be built. Solutions for 1, 2 and 3-D detection will be introduced.

1-D detection

1. Movement

Moving detection system can be built up using

- movement of a shadow light beam sensor (see figure 2.1.a) along an object at a known speed. The beginning and end break of the light beam indicate the edges of the object and thus its position in space.
- one receiver or transmitter carrying out a movement around the object (see figure 2.2.a). Provided that the position and shape (e.g. circular) of the object is known, a 1-D measurement can be taken.

2. Arrangement

Stable arrangements can be built up using

- a large number of presence detectors (see figure 2.2.b). The receiver and/or the transmitter must have a narrow beam angle characteristic. If not, a pseudo-movement (switching the transmitters sequentially) is necessary.
- one transmitter, one receiver and two lenses to obtain parallel light in an inspection area (see figure 2.2.c). The disadvantage is that no information about the position of the object will be given (Molitor 1988).
- one transmitter and many receivers on a known curve (see figure 2.2.d).

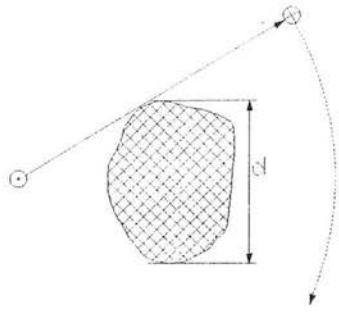

a) Fixed transmitter and moving receiver

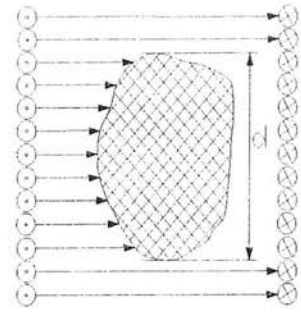

b) Rows of transmitters and receivers

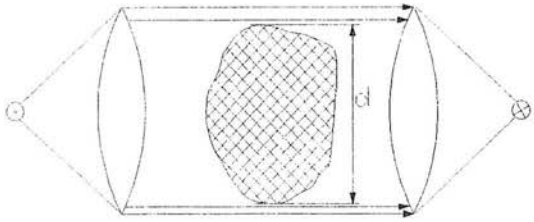

c) Transmitter, receiver and lenses

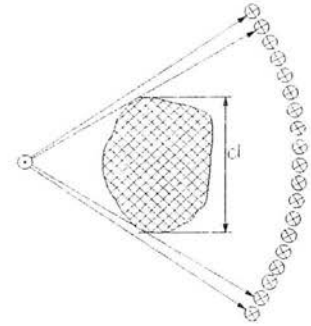

d) Fixed transmitter and a part circle of receivers

Figure 2.2. Different arrangements to gain 1-D information

2-D and 3-D detection

1. Movement

   A 2-D vision system can be built for convex objects using a 1-D shadow system and vertical motion of the object (see figure 2.3.a). Uses of single frame systems for agriculture have been described by Streenstrup *et al* (1993), Chen *et al* (1992), Fon *et al* (1990), Schulz (1986) and Wallack *et al* (1993, 1995). This system will only give information about the varying diameter of the cross-section of the object from one viewpoint.

2. Arrangement

   Two sets of crosswise arranged lines (see figure 2.3.b) build up into a rectangular frame which gives a rectangular picture of the cross-section of an object in the vertical direction. Such frames are used in agriculture (Aquametric 1995, Exeter 1994) and for sorting parcels (Pepperl 1995). Gall (1992) shows a hexagonal solution based on two line sets of transmitters and two line sets of sensors not crosswise arranged.

Further arrangements are described by Wallack *et al* (1997a, 1997b) (see figure 2.3.c) using vertical crossbeam sensors, which form a set of co-planar orientated binary light-beam sensors. A similar solution with many transmitters is described by Knight (1973).

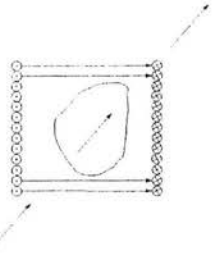

a) Line of transmitters and receivers

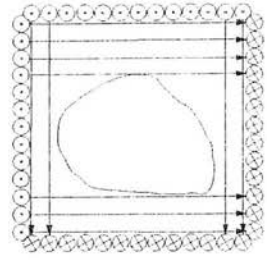

b) Rectangle built up of lines

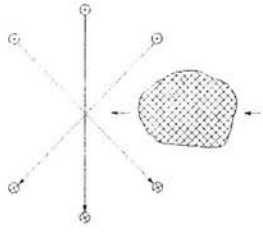

c) Vertical cross-beam sensors

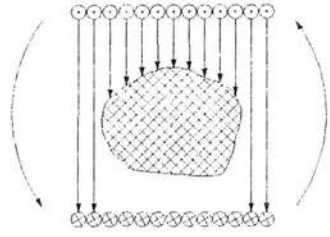

d) Rotating lines

Figure 2.3. 2-D and 3-D shadow (transmission) sensor principles (part 1)

3. Mechanical rotation

Rotation has the advantage that many viewpoints around the objects can be used and the whole object scanned comprehensively. A solution using the mechanical rotation of systems is shown in figure 2.3.d. A rotating cylinder using parallel lighting is described by Takada (1983). One other solution describes a rotating sensor in a mechanical ring scanning a helix around a human body (Limbach 1995). Many systems use transmission which results in tomographic reconstruction. A review is outside the scope of this thesis, however an overview of arrangements used in computer tomography is given by Herman (1980), Rosenfeld *et al* (1982), Tellkamp (1989), Klingenberg *et al* (1990) and illustrated in figure 2.4.a-e. It should be noted at the solution in figure 2.4.e, that it includes also pseudo rotation, because the transmitter can be switched.

4. Pseudo rotation

Another solution (see figure 2.4.f) is the ring sensor system (Farchmin 1990, Gall 1992, 1997, 1998) consisting of a number of single emitters and receivers arranged alternately and equispaced on the circumference of a circle (ring), which will be further investigated in this work. Pseudo movement is obtained by

switching the transmitters in sequence (comprehensive description in chapter 3). Similar solutions are used in computer tomography with a transmitting source (X-ray generator) in a moving ring consisting of 10 or more elements (Schaffrath 1989, Mullani 1986). A simple similar arrangement with a large number of transmitters and only two receivers is described by Wögenbauer (1991) for measuring trunks of wood.

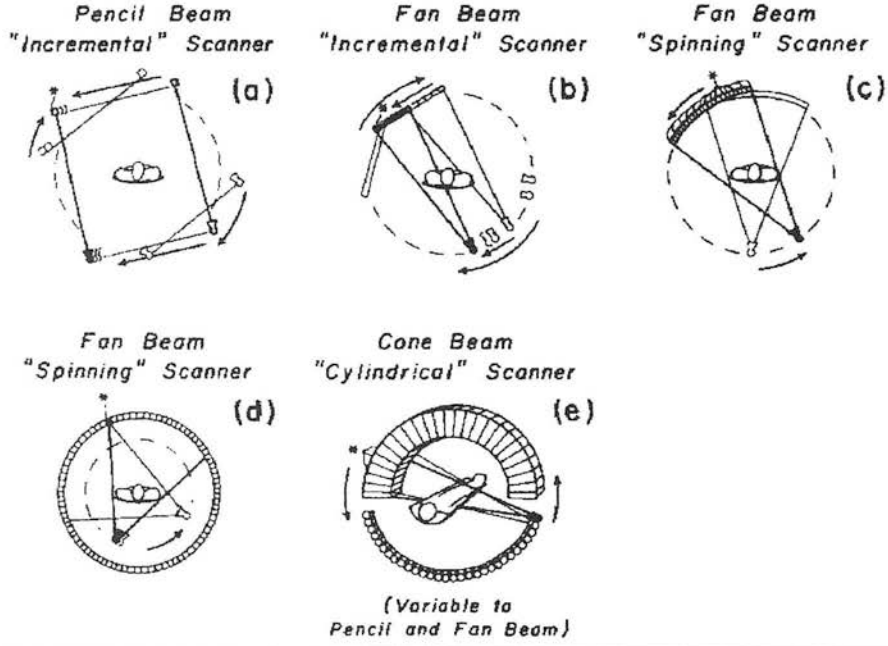

	a	b	c	d	e
Profile scan per angle of view, sec	1	1	~0.001	>0.25	<0.0004
Circumferential scan, sec	~200	18	5	≥ 1	0.01

Arrangements and timing for computer tomographs (Herman 1989)

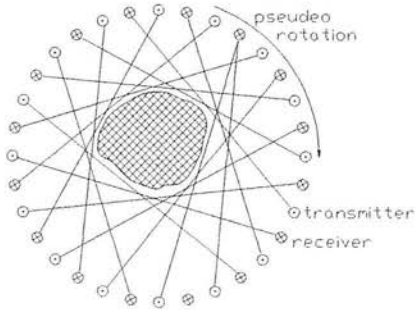

f) Full pseudo-rotation with a ring construction (Farchmin *et al* 1990)

Figure 2.4. 2-D and 3-D shadow (transmission) sensor principles (part 2)

The main properties of 2-D shadow systems are

- only the convex hull can be determined
- concavities in the cross-section can not be seen.
- simple construction of the system
- direct switching of light beams guarantees stability under difficult lighting and environmental conditions

The extension of all these systems for the 3-D world is realised by passing the object through the sensor system. An added advantage is that concave areas in the direction of movement can then be seen.

2.5.2. Reflection - light-beam sensor systems for edge detection and shading techniques

The use of light-beam sensors working on the basis of reflection for presence detection (see figure 2.1.b) is a common practice. The dimension of viewing can be expanded using this basic arrangement.

1-D detection

1. Horizontal mechanical movement

   Edge detection and therefore the 1-D measurement of an axis of an object can be carried out using a movement of a reflection beam or of the object as in figure 2.1.b. Beginning and end of reflection can be used for edge detection and the 1-D measurement. The object can be either brighter than the background or vice versa.

2. Arrangement

   The arrangement (see figure 2.5.a) consists of a number of receivers in a row and typically a line camera.

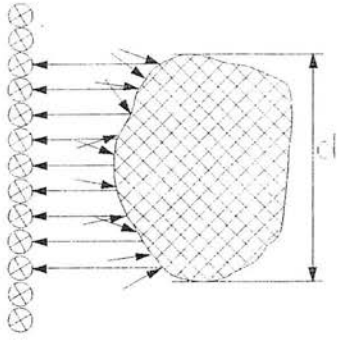

a) Row of receivers (line camera)

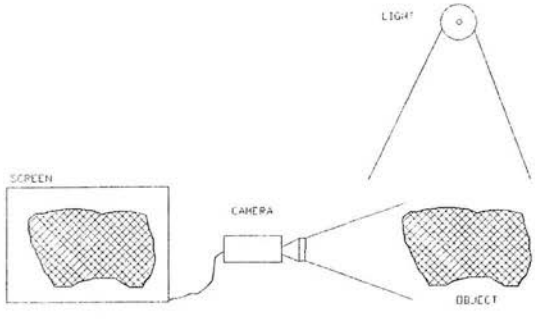

b) 2-D image with matrix camera and object

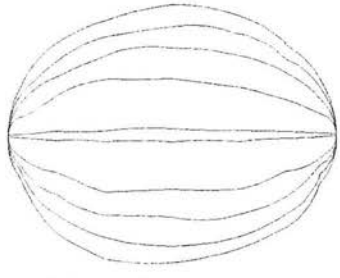

c) Multiple views taken around an object by a matrix camera system and put together again

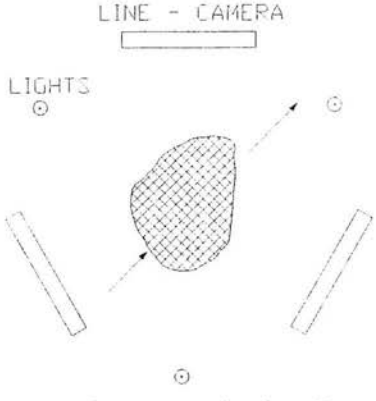

d) Object passing 3 enveloping line cameras

Figure 2.5. Detection systems for objects using reflection

2-D and 3-D detection

A 2-D reflection system can be built up using a line camera moving along an object. Each image recognised using this technique is basically monocular vision (Davies 1990).

1. Horizontal movement in front of a camera

The 2-D case employed in all commercial matrix or line cameras is the most commonly used scanning method for shape (see figure 2.5.b). It gives the image from one cross-section in the field of view of one object. The image is threshold around a brightness level to separate the object (for example fish or mushrooms on flat belts) from the black or white background (Strachan 1993, De Silva 1993, Schulz 1986, Heinemann *et al* 1994). From the pixel picture the envelope can be distinguished and this gives the silhouette.

An overview for agriculture especially for potatoes is given in Larsson (1994). Similar systems for sizing vegetables and fruits are described (Alt 1992, Herbert 1989, Greefa 1995, Resource 1995, OLE 1996).

2. Rotation

The objects are rotating in front of a matrix camera on a roller table. These systems are used to get 3-D information, for example in the potato industry (Marchant *et al* 1990, Herbert 1998). A collection of images from different angles (see figure 2.5.c) can 'box-in' the whole object and the shape can be determined.

3. Arrangements of line cameras

An arrangement of multiple line cameras combined with movement can be used to generate 3-D images. Systems with 3 or 4 cameras around passing objects are described by Mörtl (1992) and used in practise by Riese (1992) and Select (1998). The images received give the shape information (see figure 2.5.d) in the form of a polygon with twice as many vertices as viewpoints.

4. Arrangements of matrix cameras and mirrors

A mirror ring around the scene for optically scanning the surface of an object is described by Birkle (1993). Solutions with a number of mirrors surrounding an object reflecting the images to one or more cameras are described by Hirotoshi (1991), Hiroshi (1989) and Ross (1995).

The design of shading systems is as described above. More about shape from shading systems can be found in Davis (1990), Horn *et al* (1989), Forsyth *et al* (1990), Nayar (1989), Liu (1992) and Rashid *et al* (1992). An alternative solution involves the use of a large number of LEDs flashing around sequentially with the picture taken by a camera as described by Crezee (1996).

There is one solution for vision systems with a completely different basic principle, the artificial retina (Karnali 1997), only used for determination of size. Based on reflection, it is a dome over the object and includes a large number of receivers with a wide beam angle and a trained neural network to obtain information about the size but not the shape of the object.

2.5.3. Reflection - stereo vision

Stereo vision is a special case using reflection and is a very popular field of research. Different dimensions can be investigated using different arrangements and movement.

1-D detection

1. Horizontal movement and rotation of the receiver

   The combination of a translatory and turning movement of a receiver with a narrow beam characteristic (see figure 2.6.a) always follows the same point of brightness on the object and is called monocular stereo decoding. If the position of the detector is known during its movement, the distance to the spot on the object can be found by the triangle formed. The 1-D measurement does not give size or shape, but is a flexible measurement of position of a surface point on the object.

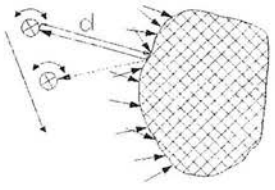

a) One moving and turning receiver

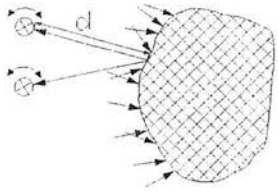

b) Two fixed but turning receivers

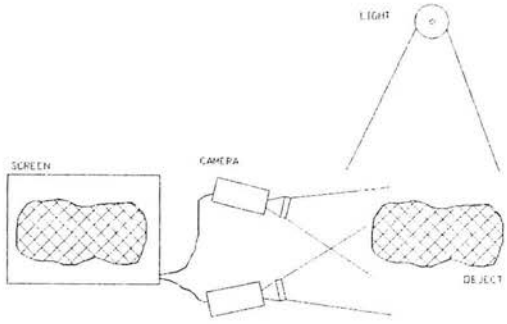

c) 3-D stereo-vision with 2 cameras

Figure 2.6. Stereo vision

2. Arrangement

To obtain a stable arrangement requires at least two single receivers (sensor cells) which can turn around their centre position and focus on the point of interest as shown in figure 2.6.b. In principle it works like the human eyes.

2-D and 3-D detection

Matrix cameras are mainly used in stereo systems, with a minimum of two images from different angles of the same part of the surface of an object. This can then be used to determine the 3-D structure of an object (see figure 2.6.c) by matching points in the two images. The structure of the object or the use of structured light gives spots of different brightness on the surface, aiding point location. Observed from different angles in space, the point distribution varies depending on the shape which can be determined by the geometry of the system.

1. Movement

If one camera moves from different known positions the co-ordinate of a fixed point on an object can be determined. Monocular stereo decoding is used for example in space experiments and from aircraft for map making (Lanzl 1985, Raggam 1994, Konecny *et al* 1996), to scan the shape of the surface of the earth and other objects. Multiocular images from a moving sensor of objects are analysed by Wu *et al* (1997). Techniques for moving objects are described in Shen *et al* (1994) and Kajiki (1997).

2. Arrangements

With two cameras it is called binocular or stereo vision. If the object does not move, part of a 3-D image can be determined (see figure 2.6.c) from stereo images which can cover up to 50% of an object (Antonsson 1989).

2.5.4. Reflection - triangulation (structured light)

Triangulation is based on reflection of scanned beams of objects and is typically used in high accuracy systems.

1-D detection

For the determination of a 1-D measurement, the monocular case only requires one moving receiver (see figure 2.7.a). The fixed arrangement can be built up with receivers in a line (line camera) (see figure 2.7.b). In both cases, with a constant angle μ for the parallel beams, the surface of the object is detected at the distance d2.

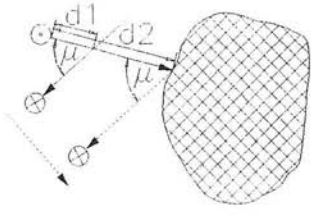

a) Fixed transmitter moving receiver

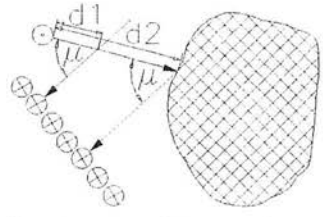

b) Fixed transmitter and receiver

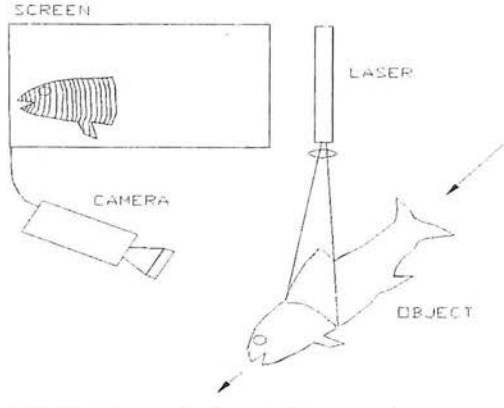

c) 3-D triangulation with matrix-camera

Figure 2.7. Triangulation

2-D and 3-D detection

This is a common method for determination of the shape of objects.

1. Movement

Movement is mostly used to get 3-D images out of 2-D systems, typically objects pass through vertical to the scanning line. Examples in practice for biological

objects are described in Elad (1990) and Minowa (1994). A different light strip pattern is utilised to determine the height of an object on a belt by Zwahlen (1992).

2. Arrangements

A matrix camera and a strip of light usually generated by a laser gives a 2-D profile of part of a cross-section (see figure 2.7.c) of an object (Molitor 1988, Leu *et al* 1992). By using structured light with more lines or grids, multiple parts of an object from one viewpoint can be investigated.

Further possible solutions for scientific, industrial and agricultural use are described by Vosseler (1997) with a flexible adjustable sensor unit, Biswas (1990) with two or more sensor units rotating around the object and Hata *et al* (1988) with two cross-wise installed sensor units and a rotating light line. Inoue *et al* (1995) introduces a solution with a wide angle between the lighting and receiver unit, Fatehi *et al* (1991) a solution especially for bulk material on conveyer belts, Thomson *et al* (1991) a solution with rotating light source to classify wheat kernels. Monnin (1994) is scanning crackers in a bakery, Bhatia *et al* (1994) surface changes on the human face with a multiple arrangement. Yang (1996) investigates the shape of apples with line structured light. A multi-triangulation system for use in a robot hand is described by Lee (1990) and similarly by Yamazaki (1995).

2.6. Modelling and reconstruction of objects

Depending on the sensor system used, computer vision requires different geometrical models for the reconstruction of an object. The image data description and the geometrical world model information must match. Computer vision has always attempted to understand biological vision systems from a computational point of view and to build useful automated visual perception systems consisting of computers, software and image sensors. Geometric modelling, however, has been primarily concerned with mechanical design, finite-element analysis, numerical control machining, and visualisation by computer graphics (Besl 1988).

There is a range of general theories regarding the shape and surface description of three-dimensional objects. One theory uses the idea of wrapping the object with a flexible elastic band with geodesics in many directions (Stewart, 1993). Closed geodesics will be

found, but on most surfaces, geodesics wander around forever without closing up. A mathematical method for the construction of piecewise surfaces parameterized as single-valued surfaces in spherical co-ordinates is described by Sánchez (1994).

There are many different methods and models which describe objects. In this work they will be ignored if they do not bear close relation to the ring sensor system. Information concerning 3-D surface reconstruction depending on the method of detecting or creating an object can be found for:

- tomography: Rosenfeld *et al* (1982), Herman (1980), Gardner (1995)
- reflection (silhouette): Mörtl (1992)
- shading: Boyer *et al* (1997), Cipolla *et al* (1997), Oren *et al* (1996), Weinshall (1994) and Brooks *et al* (1994)
- stereo vision: Robert *et al* (1995), Chung (*et al* 1996), Raggam (*et al* 1994)
- triangulation: Elad *et al* (1990), Crowe *et al* (1996), Eigler *et al* (1988) and Shen *et al* (1995)
- computer graphics and models: Foley (1997), Preparata (1985), Chiokura *et al* (1983), Faux *et al* (1985), Klein (1986), O'Rourke *et al* (1979).

2.7. The ring sensor system compared with three other systems

Because of the interest in using a sensor system especially for shape detection in agriculture and the food industry, the requirements for a system looked for in this work are:

- comprehensive 3-D scan of objects
- high throughput
- simple structure
- low costs
- low computer power
- limited accuracy of about 2.5% standard deviation
- resolution 1-2mm
- object size range between 20 - 140 mm diameter (length 250mm)
- simple presentation of objects
- reliability in a tough practical environment

The essential properties of the ring sensor system (see figure 2.4.f) are now compared with three other systems. The three other systems were chosen because with all of them, shape detection is possible and they are used in practice for biological objects:

1. computer tomograph: the arrangements are very similar, it uses transmitted light instead of shadowed and is used in medicine and agriculture
2. laser scanner: 3-D shape detection from one viewpoint (side), used in quality control in the food industry
3. camera system: 2-D (3-D) system used in agriculture for colour quality control and grading and sometimes for limited size grading

Every system has advantages and disadvantages. All of the points discussed are crucial for the design and operation of a system. All methods are only as good as their ability to 'box in' and 'wrap' the objects (Gall 1998). The number of viewpoints of a system around an object is often the limiting factor.

Methods based on reflection such as stereo vision, shape from shading or triangulation require in addition enormous calculation time for solving matching problems.

Under these circumstances, the ring sensor system as suggested by Gall (1992, 1997) is a solution for practical use (see figure 1.1, 2.4.f), provided that the objects are in a limited but reasonable size-range, are singulated and presented on a line.

Sensor system	Ring	Tomograph	Laser scanner	Camera system
Presentation of object	On a single line passing horizontally	On a single line passing horizontally	On a single line passing horizontally	Rows in vertical direction passing horizontally
Possible rotation of the system	Electronically	Mechanically, electronically	-	-
Number of viewpoints without rotation of objects	High 32 and more	High 16 and more	Low 1-3 (arrangement of 3 systems)	Low 1-6 (mirrors or cameras)
Speed of the system	High 200-800 rev/s	Slow 5 sec/rev (see figure 2.4.e)	High 10000 lines /s	Very high 3-10 images/s
Interaction of light with the object	Shadow	Transmission, emission	Triangulation	Shadowing, shading, triangulation
Limitations in the shape of objects for a correct detection	Vertical cross-section has to be always convex	No limitations in shape	Lightbeam has to touch surface from the viewpoint (not possible in holes)	1. each point of surface has to reflect 2. use of shadowing / shading methods are necessary on concave areas
Accuracy for 2-D detection	Low (1mm) for 64x64 transmitters and receivers	-	Very high (μm)	High (0.1mm depending on resolution)
Accuracy for global 3-D detection without rotation of objects	Relatively high (1mm)	Very high (0.1mm)	Low (only one viewpoint)	Low (only one viewpoint)
Complexity of hardware for global 3-D shape detection	Low	Very high	High	High
Complexity of algorithms for 3-D shape detection	Low	Very high	High	High
Estimated price per unit, inclusive of real-time software in 1998	$6000 (3-D)	$200000 (3-D)	$13000 (only 2-D)	$4000 (only 2-D)
Lighting / requirement for safety	LED infra-red / low	X-Ray / high	Laser infra-red / high	Infra-red - visible light / low
Influence of environment	Low	High	High	High

Table 2.4. Comparison of four different shape detector systems

2.8. Summary

This chapter gives an overview of the construction of sensor systems for shape recognition and analysis. Optical systems consist of presence detectors using reflection, shadowing or transmission. Dimensions of the view of the optical system can be compensated for by movement of the sensor or the object. Presentation and singulation of objects are crucial for a successful system and determine the dimension of the required sensor array. Special tasks require special solutions adapted to the process and these are determined by the needs of accuracy, size and shape of the object, dimension of view, speed, throughput, environmental factors and the aim. A short introduction into modelling and the reconstruction of objects by the computer is given. The requirements are defined for a system for agricultural use and compared with existing methods.

3. The ring sensor system and the 3-D reconstruction of one object

This chapter describes the construction of a ring sensor system, the basic algorithm and mathematics for contour detection and a modified co-ordinate system (Gall 1997) based on the fundamental development by Gall and Farchmin (1990) and Gall (1992).

3.1. Construction of the ring sensor system

The ring sensor system (see figure 3.1), consists of a number N_T of single emitters and receivers N_R arranged alternately and equispaced on the circumference of a circle (ring). Other arrangements are possible, for example, an unequal number of emitters and receivers could be used. The emitters and receivers have a Lambertian angular response. The emitters are switched on in sequence round the ring. From one activated transmitter, the signal at each optical receiver can be likened to a 'snapshot'. If no object is present within the ring, for each switched on transmitter, each detector will detect light. If an object is introduced, then one or more receivers will be obscured from the emitter. The two closest non-interrupted light paths (chords in the circle) can be used to describe the curvature of objects. They are referred to as the 'front' and 'back' chord of each 'snapshot' (viewpoint, transmitter).

For basic operation only the 'back' chord of each 'snapshot' is used (instead of the 'front' chord, described by Gall (1992)). It is permissible to make this simplification because the method and the result are similar to those obtained using only the 'front' chords. The decision for using the 'back' chord is that the use of different hardware from that of a test device gives the 'back' chord as the first extracted chord from each 'snapshot' (see figure 3.1.b). From the mathematical point of view the difference is that one co-ordinate in the 3-D world is inverted. Using both chords of many 'snapshots' would give two similar independent enveloping spirals of an object in the 3-D (see chapters 3.6 and 5.2.4).

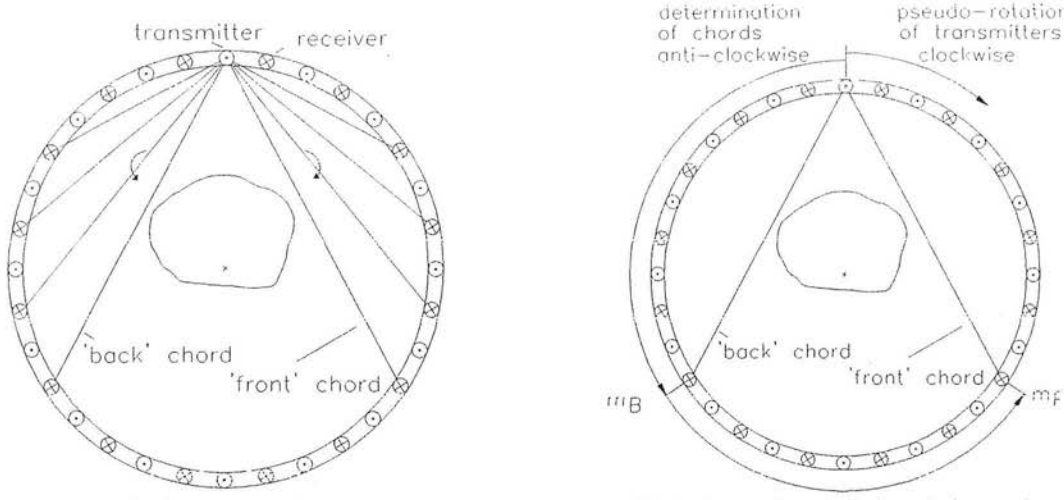

a) Light-beams try to cover b) Orientation of chord detection

Figure 3.1. 'Snapshot' from one viewpoint indicating tangential light paths at the 'front' and the 'back' of an object.

A scanning revolution means, that each transmitter in a clockwise direction is turned on one after the other. For each transmitter the last receiver in the anti-clockwise direction received light before shadowed by an object is recorded as a 'back' chord. If there are N_T transmitter, these 'back' chords can be written as $m_B[n]$ describing a vector, where m_B is the number of lighted receivers between transmitter and 'back' chord and n is the actual activated transmitter between 1 and N_T.

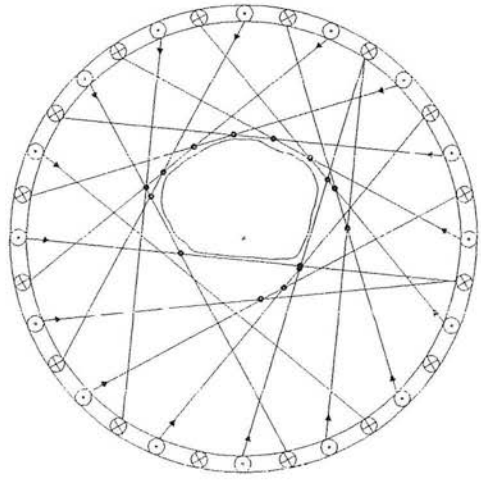

Figure 3.2. The 'back' chords of one revolution including the cross-section of an object (the intersections between adjacent chords are marked).

After a scanning revolution of the ring, when there is a static object within the scanned area a 'basic' picture showing all 'back' chords, including the cross-section of the object

(see figure 3.2), is obtained. There is no restriction on the position of the object in the ring.

For each transmitter n with $0 \leq n < N_T$ the relative position of the receiver to the actual transmitter ('snapshot') $m_B[n]$ is coded in one dimensional integer array Z0 (for more about data in memory management see chapter 6.2, 10.7), whose size, in the two-dimensional case, equals to the number of transmitters on a ring N_T. The addressing of the array is the same as the number of the related transmitter ('snapshot'). In a three-dimensional case the array will be extended but remains one-dimensional. It can be seen for example that a ring sensor solution with 64 transmitters and 64 receivers 64 x 6 bit ~ 64 Bytes are required to store a whole picture of a cross-section of an object of flexible shape and position. This compact primary data format is one of the major advantages of this system.

3.2. Contour-tracking

3.2.1. Conditions

Consider first the two-dimensional case. The following conditions are set:

1. Only one object is in the ring (multiple objects will be considered in chapter 8).
2. The same number of transmitters and receivers will be arranged alternately. Pairs of transmitters are diametrically opposite each other, as are pairs of receivers.
3. To simplify the following description, the ring shall scan clockwise and from each 'snapshot' (see figure 3.1) only the 'back' chords will be investigated.

As shown in figure 3.2 the description of the curvature of a section of the object is contained within this set of chords. Using any shadow method it is impossible to scan concave areas in the curvature in the two-dimensional case, so under these conditions, the result of determination will always be a convex hull.

Determination of a convex hull has often been discussed in mathematics and computer geometry literature. For a given set (cloud) of points (pixels) the task is to find the smallest polygon by excluding extraneous points (Jarvis 1973, AKL 1979, Petkov 1990, Preparata 1985, Robert 1995). Similarly a wider range of cases can be considered by the use of generalised cylinders (GC) (Shafer 1985, Zerroug 1996, Chung *et al* 1996). They

consist for example of surfaces generated with discs of varying radius as the envelope of a sphere is swept along a not necessarily straight cylinder (Pillow *et al* 1995). Because it is mainly based on pixel images, the use of GCs is often complex. Additionally it is combined with the loss of detailed shape information, because GCs impose symmetry constraints on objects they represent. A deformed model for 3-D shape, which has a preference for axial symmetry and is based on symmetry seeking models, is described by Terzopoulos *et al* (1987).

Considering the ring sensor system, starting with components of vectors instead of a pixel picture offers a different situation. The following points define the geometric conditions:

1. The chords and intersections (marked points in figure 3.2) of the adjacent chords are all on or outside the convex hull.
2. The number of intersections with adjacent chords is limited, is equal to the number of chords and also equal to the number of transmitters.
3. The chords are formed sequentially around the object.

This problem is similar to the intersections of half-planes (Preparata 1985, Teillaud 1993, Chen 1987). They describe the set-up of a polygon limited in size by a large number of half-planes and methods to exclude redundant constraints in the polygon description. In our case (see figure 3.2), if the chords were stretched to form segments of the circle, or into straight lines building up half-planes around the convex hull, the same conditions hold and this same method could be used. In practice the ring-sensor has limited numbers of transmitters and receivers and the object has to be in the area of the ring, which means that the conditions are much more controlled. A simplified algorithm can be used.

3.2.2. Method

The 'basic' picture is generated in one scan consisting of N_T sequential snapshots which gives a set of N_T 'back' chords. All chords are sequentially investigated as they are generated. All redundant chords have to be excluded from further consideration, since they are not part of the envelope of the contour of the object.

To do this, each chord (actual chord), its successfully tested predecessor and it's successor have to be investigated (see figure 3.3).

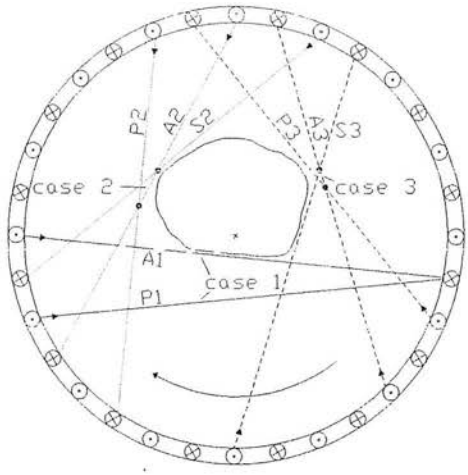

Figure 3.3. The three different cases of adjacent chords

The following cases are possible:

Case 1: The actual chord A1 reaches the same receiver as the predecessor P1, P1 is therefore redundant and is excluded from further investigations.

Case 2: The intersection of the actual investigated chord A2 with the predecessor P2 lies further from the transmitter than does the intersection with the successor S2. The actual chord A2 can therefore be part of the convex hull. It might be excluded by investigation on subsequent steps.

Case 3: The intersection of the actual investigated chord A3 with the predecessor P3 lies closer to the transmitter than does the intersection with the successor S3. The actual chord is redundant and has to be excluded from further investigations. At this point, the predecessor P3 will become the actual chord, and the chord tested before the predecessor is now the predecessor chord. The successor remains the same. The 'turning back' and excluding of previously successfully tested chords, but in this instance recognised as redundant, will continue until case 2 occurs.

The chords are then renumbered and rechecked sequentially using the above rules until no more chords can be excluded (see figure 3.4).

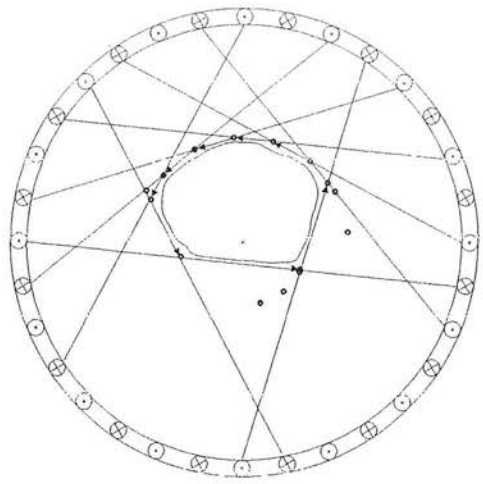

Figure 3.4. Remaining chords building up the convex hull (included and excluded intersections are marked).

The contour is described using the remaining chords and the distance to the intersections of the chords.

3.3. The modified polar co-ordinate system

Using the 'basic' picture and a modified polar co-ordinate system it can be shown how the positions of intersections $C_P[n]$ of the actual chord n and the predecessor n-1 of the convex hull can be described (see figures 3.3-3.5). From each transmitter with the position $T_A[n]$ we get one distance stored, being the 'back' chord, some of which will be excluded by the above procedure. These values will be components of the vectors and intersections, which will describe the convex hull of the object. The origin of the co-ordinate system is transmitter $T_A[0]$.

The parameters of the ring are: α, angle from the centre between adjacent transmitters (in this case also between the receivers); β, angle (displacement) between transmitter and receiver; N_T, number of installed transmitters; N_R number of installed receivers; r, radius. The variables are: n, number of the transmitter with $0 \leq n < N_T$; $m_B[n]$, number of receivers from the activated transmitter n anti-clockwise to the receiver of the 'back' chord with $0 \leq m < N_R$. The positions of transmitters and receivers are given for the actual investigated chord by $T_A[n]$ and $R_A[n]$ and for the predecessor by $T_P[n]$ and $R_P[n]$.

The maximum possible number of chords is N_{CH} which is set by the numbers of transmitters N_T and receivers N_R being:

$$N_{CH} = N_T N_R$$

It will first be shown that the position of the vector $T_A[0]:C_P[0]$ from the chord with the first transmitter in the origin with n=0 (position [0,0]) to the intersection with the predecessor starting in $T_P[0]$ can be described as follows. For equally spaced transmitters and receivers, we have:

$$\alpha = 2\pi / N_T \qquad \beta = \alpha / 2$$

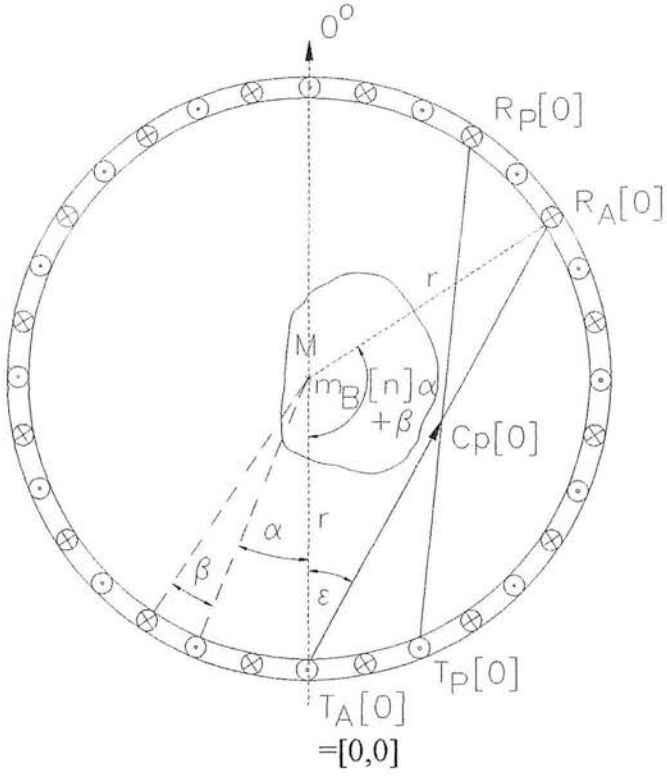

Figure 3.5. The vector $T_A[0]:C_P[0]$ in the co-ordinate system

The position of the actual receiver $R_A[0]$ from the 'back' chord depends on the shape of the object. With $R_A[0]$ related to $m_B[0]$ we get that

$$\varepsilon = \pi/2 - \tfrac{1}{2} (m_B[0]\, \alpha + \beta)$$

and $T_A[0]$ within the origin the chord $T_A[0]:R_A[0]$ can be described by the vector

$$T_A[0]:R_A[0] \quad = \quad [\,\varepsilon\,,\, 2\,r\cos\varepsilon\,]$$

where 2 r cos ε is the distance from $|T_A[0]:R_A[0]|$. The distance between the transmitter of the actual chord with n=0 and the interception with the predecessor in $C_P[0]$ (determination in chapter 3.4) can be used to determine the position of the intersection.

$$T_A[0]:C_P[0] \quad = \quad [\,\varepsilon,\, |T_A[0]:C_P[0]|\,]$$

The first step for the investigation of all chords is the use of $m_B[n]$ from the actual chord and starting with the temporary transmitter in position $T_A[0]$ as the origin for the determination of the temporary vector $T_A[0]:C_P'[n]$ (see figure 3.6.a). Because the ring is symmetrical the same algorithms can be used as for snapshot of transmitter n=0 as described above, which is an advantage.

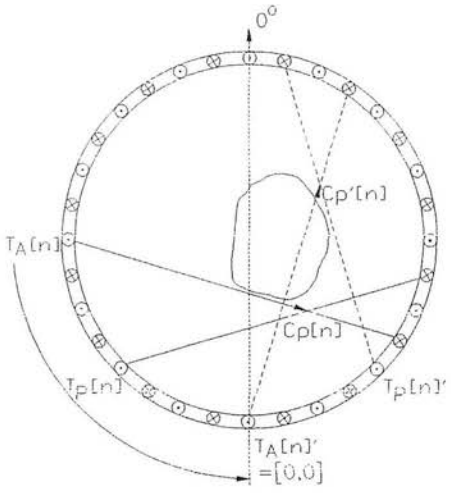

a) Temporary shift of chords into the [0,0]position

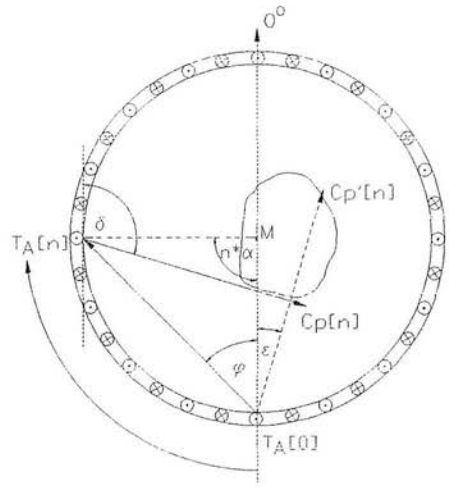

b) Turning the vector Cp'[n] into the correct position

Figure 3.6. Creation of the vector $T_A[n]:C_P[n]$ for every left transmitter

It is now necessary to 'move' the vector $T_A[0]:C_P'[n]$ into the correct position (see figure 3.6.b). The position of the starting point with the angle φ to the zero axis and the distance from $T_A[0]$ to $T_A[n]$ will be determined.

With

$$\varphi \quad = \quad \pi/2 \; - n\,\beta$$

and

$$|T_A[0]: T_A[n]| = 2\,r\cos\varphi$$

the vector

$$T_A[0]:T_A[n] = [\varphi\,,\,2\,r\cos\varphi\,]$$

can be determined.

The angle δ of the real vector $T_A[n]:C_P[n]$ will be determined by the angle $T_A[0]$, M, $T_A[n]$ and ε

$$\delta = n\alpha + \varepsilon\ .$$

The position of $C_P[n]$ can than be described by the vector

$$T_A[0]:C_P[n] = [\varphi\,,\,2\,r\cos\varphi] + [\delta\,,\,|T_A[0]:C_P'[n]|\,] \qquad (3.1.)$$

The use of this co-ordinate system results in simpler mathematical equations than does the use of the polar co-ordinate system with the origin at the midpoint. It should be noted that for this description only two variables are necessary, the number of the activated transmitter n and the distance from the transmitter to the receiver of the 'back' chord $m_B[n]$. The position of the intersections with the successor chords $C_S[n]$ (see chapter 3.2.2) can be described in the same way.

3.4. Intersections of chords

To find the redundant chords where the successor does not have an intersection as shown in case 1 (see figure 3.3), the data of the 'back' chords of the snapshots $m_B[n]$ and $m_B[n-1]$ have to be observed. If the distance between transmitter and receiver of the actual 'back' chord $m_B[n]$ and its predecessor $m_B[n-1]$ is $m_B[n] = m_B[n-1]-1$ then there will not be an intersection between the chords.

For intersecting chords the main task is the determination of the distances from the transmitter of the actual 'back' chord $T_A[n]:R_A[n]$ to the intersections with the adjacent chords. It would also be possible to use the distances of the intersections to the receiver of the actual chord. As previously stated the determination of the distance between the

actual transmitter n with the position $T_A[n]$ to the intersection $C_P[n]$ is independent of $T_A[n]$, because it is the same distance between $T_A[0]$ and Cp'[n] (see figure 3.6).

The distance between each position of the transmitter $T_A[n]$ and the intersection with predecessor $T_A[n]$:$C_P[n]$ will be determined (see figure 3.7).

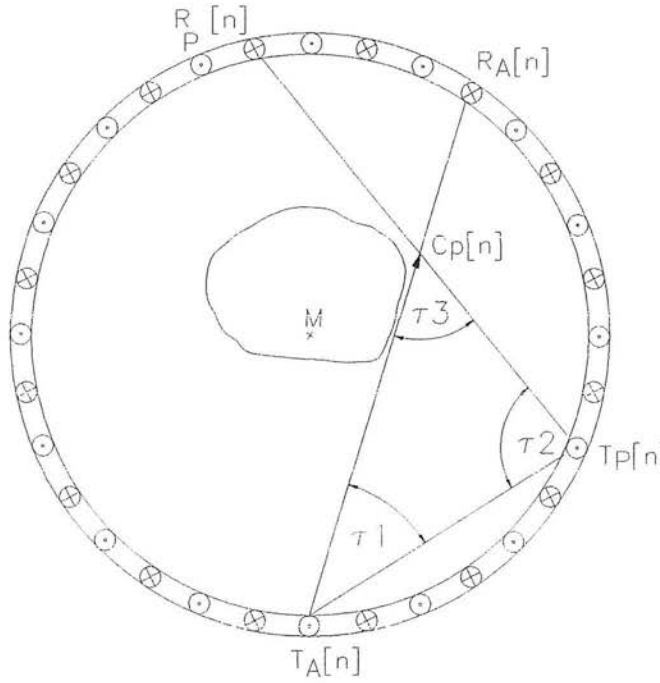

Figure 3.7. Intersection between actual chord and predecessor

Using trigonometry (sine rule)

$$|T_A[n]:C_P[n]| = |T_A[n]:T_P[n]| \sin \tau 2 / \sin \tau 3 \qquad \text{(see appendix 1)}$$

The distance between the transmitter and the intersection with the successor $|T_A[n]:C_S[n]|$ can be determined (see figure 3.8).

$$|T_A[n]:C_S[n]| = |T_A[n]:T_S[n]| \sin \tau 1 / \sin \tau 3 \qquad \text{(see appendix 2)}$$

If

$$|T_A[n]:C_P[n]| < |T_A[n]:C_S[n]|$$

then the actual investigated chord has to be eliminated (rule 3, chapter 3.2.2) otherwise the chord may be a tangential chord of the convex hull unless eliminated by further checking. Clockwise each chord has to be checked in this way. The equations are valid for all $T_A[n]$.

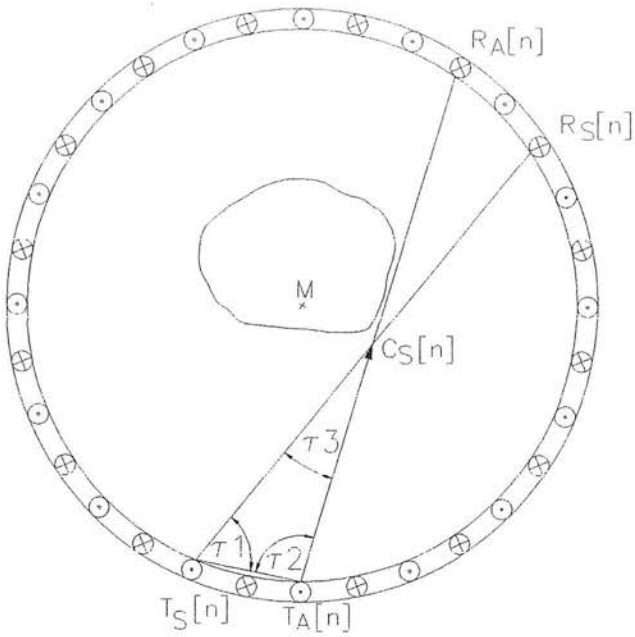

Figure 3.8. Intersection between actual chord and successor

3.5. The three-dimensional system

The extension of the co-ordinate system (see chapter 3.3) into three dimensional space can easily be done with the ring sensor determining the object section at intervals with the object moving through the sensor (see figure 3.9). If the movement is at a constant speed, this will guarantee a constant distance 's' between each snapshot. In relation to the object the ring is now an enveloping helix describing a cylinder of the sensor system (see figure 3.10). The helix will have a pitch of N_T s where s in the sampling distance in the third dimension determined by the speed of the object. The object has to pass through the ring and will be positioned in the cylinder.

The apparent number n of transmitters is now unlimited. N_T transmitters will be activated in one revolution. The distance $m_B[n]$ between each activated transmitter and the receiver building up the touching chords on the object is the same as in the two-dimensional case $0 \leq m_B[n] < N_R$. The algorithms used are the same as described in chapter 3.2.2. An object starts if $m = m_B[0] < N_R$. The end is reached when $m_B[n] = N_R$ again.

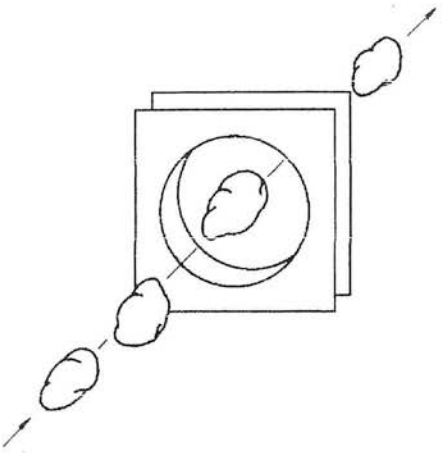

Figure 3.9. Potato on the way through the sensor system (Gall 1992)

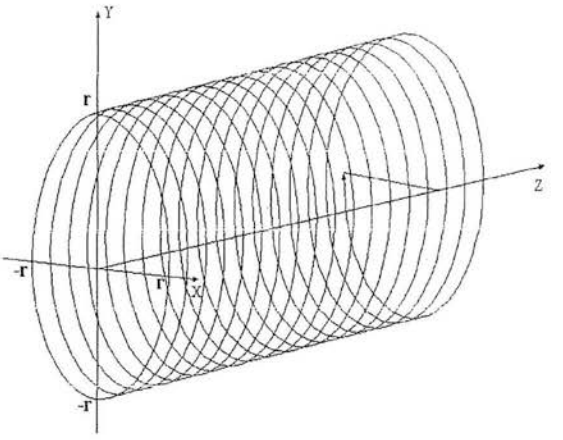

Figure 3.10. The sensor ring building up a 3-D cylinder space

Analogous to the 2-D case the intersection Cp can be determined by using equation 3.1. The picture of the object is composed of part of the chords between intersections including the determined intersections. The result is an enveloping spiral (see figures 3.11-3.13). These display pictures created by a ring with $N_T = 64$ and $N_R = 64$ using the 'back' spiral which consists of 'back' chords only.

It should be noted that one difference from the 2-D case is that concavities can be seen in the direction of movement of the system (see figure 3.13), however concave areas in the cross-section can not be seen. The probability of concave areas on the longest axis of an object (potato or other agricultural products) is higher than in other directions, and is the reason for a preferred direction of an object passing the sensor system. As an additional result of this condition the determination of the length L of the object is simply the total number of counted snapshots N_{OBJ} multiplied with the distance the object moved between each snapshot s, so that $L = N_{OBJ}\ s$.

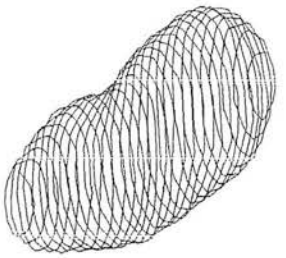

Figure 3.11. An enveloping spiral of a potato

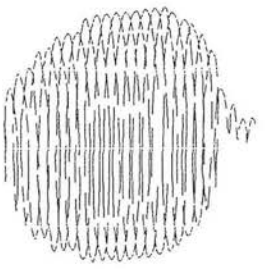

Figure 3.12. An enveloping spiral of an apple

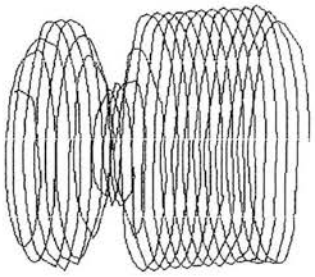

Figure 3.13. Example for object with concavity

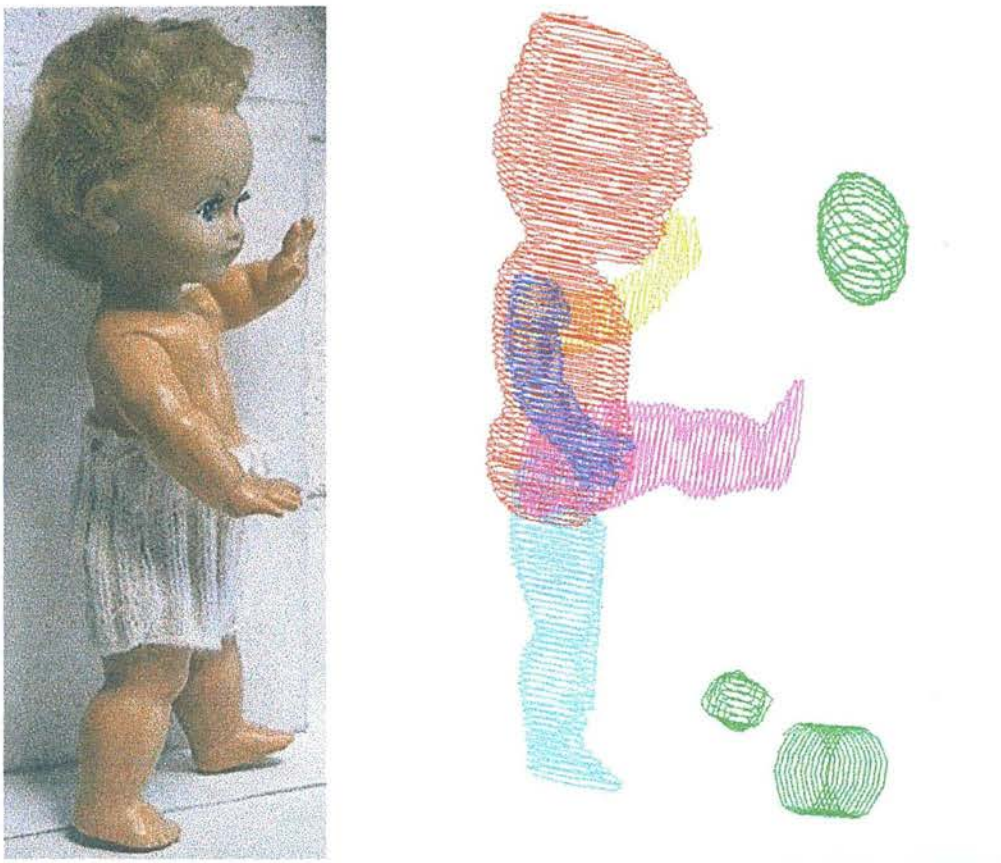

a) Original picture b) Multiple scan and simulation

Figure 3.14. A doll created from independent scans of the torso and limbs and simulated objects

A further example is an image containing the results of scans of different objects such as the torso and limbs of a doll, their combination in a scene and added to other objects (see figure 3.14) which are simulated (see chapter 5.1). A complete scene can be built up by using the data for different objects, positioning the start points of the cylinders (see figure 3.10) and the angle of expansion into space.

Compared with other models such as the wire frame model (Delibasis *et al* 1994, Mitchell 1995) to describe whole 3-D shaped objects this method is much simpler and results in more compact data (see chapters 6.2, 6.3). Slicing the object as described in a model by Takada (1983), Yang *et al* (1989) is not necessary, where the object moves and a helical scan is carried out by the ring sensor.

3.6. The use of two helices

A snapshot gives two touching chords for one object in the ring, the 'front' and the 'back' chords. So far only the 'back' chord has been used, but this means that for special sensor constructions with alternately arranged transmitters and receivers, and for all scans on moving objects, information is lost.

1. In the two-dimensional case there are two possibilities. In the first case, transmitters and receivers are alternately arranged. In this case (see figure 3.15.a) the 'front' chords never cover 'back' chords. In the second arrangement, the transmitters and receivers are at the same places (see figure 3.15.b). For each 'front' chord a 'back' chord exists, which covers the 'front' chord. Using a different number of transmitters from receivers a mixture of both cases is possible.

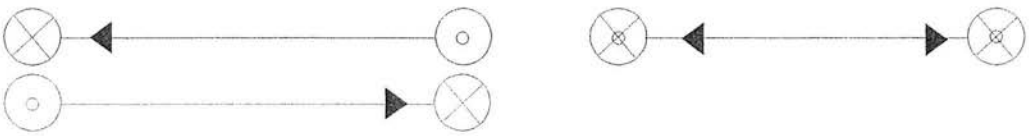

a) Alternately - different position b) Covering - same position

Figure 3.15. Possible arrangement of transmitter or receiver (cover)

2. In the 3-D case two independent spirals are always built up (see figure 3.16), which never touch each other. The distance between them varies if shape or position of the object in the ring changes. The distance also depends on the angle or phase between the 'back' chord described by the number of receivers between the transmitter and the actual receiver anti-clockwise $m_B[n]$ and the 'front' chord described by the number anti-clockwise $m_F[n]$ (see figure 3.1.b). For all cases it is

$$0 < m_B[n] < m_F[n] < N_R$$

For cylinders with different diameters centrally positioned, the function of the relative distance d_{REL} of the 'front' spiral from the 'back' spiral in one turn is with the $m_B[n]$ and $m_F[n]$ generated anti-clockwise (see figure 3.1.b).

$$\begin{aligned} 0 &<= m_B[n] < N_R / 2 \\ N_R/2 &<= m_F[n] < N_R \end{aligned}$$

$$m_B[n] = N_R - m_F[n]$$

then $$d_{REL} = (m_F[n] - m_B[n]) / N_R$$

For a cylinder with $m_B[n] = N_R/2-1$ and $m_F[n]=N_R/2$ the diameter of the spiral is small and the maximal distance 50% (see figure 3.16.a). Theoretically for a large (maximum) diameter with $m_B[n] =0$ and $m_F[n] = N_R$ the distance would be zero. This is not possible in practice. Typically there is a limit of about

$$m_B[n] >= 1/20\ N_R$$
$$m_F[n] <= 19/20\ N_R$$

which corresponds to a minimum distance of 5% of pitch (see figure 3.16.b).

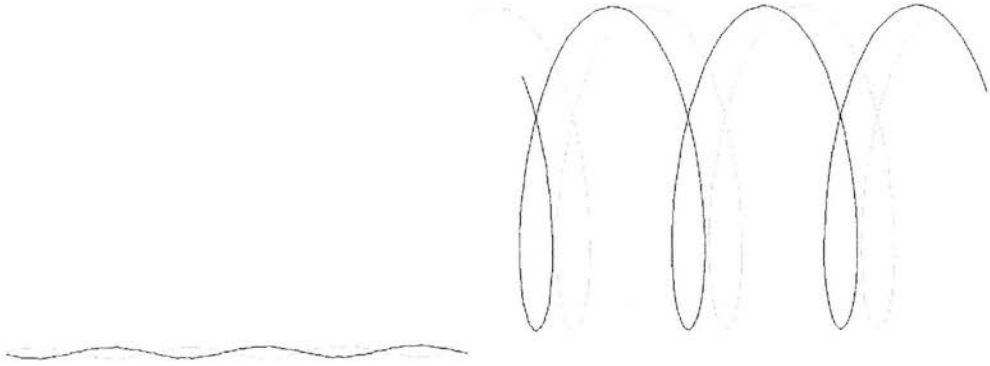

a) Small diameter (s_spiral)
$m_B[n] = N_R/2-1$,
$m_F[n] = N_R/2$

b) Large diameter (b_spiral)
$m_B[n]=1/20$ r, $m_F[n]=19/20$ r

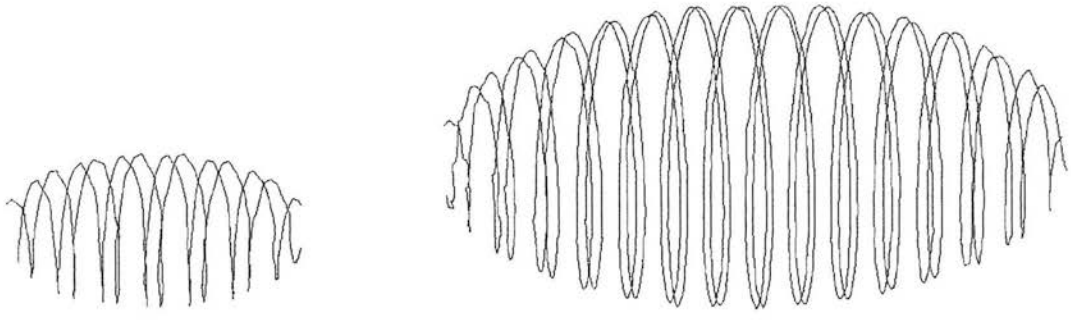

c) Thin small object

d) Thick object (maximal diameter on the limit of ring)

Figure 3.16. 'Back' and 'front' spiral enveloping a cylinder (a,b) and two ellipsoids (c,d)

Another investigation was made to connect both spirals into one. This is possible if the transmitters and receivers are arranged alternately and works in the 2-D case. This can be done by inverting the orientation (receiver become transmitter and transmitter becomes receiver) of the 'front' chords and including them in the array of the 'back' chords or vice versa. The advantage is that all chords can be investigated in one step, building up one envelope with double the number of chords and hence resolution. The disadvantage is that it can only be used with restrictions in the 3-D. The reason for this is, although the two displaced spirals become one, due to the movement of the object, they contain information about different points on the surface of the object. For example, if an object with an increasing diameter is entering the ring, the 'back' chord will touch the 'same' spot of the object later than the 'front' chord. During this time the object has moved and the diameter has increased. In each case the algorithm will take the 'front' chord because it was 'closer' to the object. Therefore this means information is lost and an error will result.

This basic necessary transformation of the 'front' chords includes also a shift of phase related to time of the real snapshot. The hardware of the ring has to fulfil the Nyquist criteria working with a higher sampling rate than a major change of the object geometry will happen to avoid this problem. If the transmitter and receiver are arranged alternately as in this case, their number will be 'doubled' virtually as the resolution.

The use of both chords, the 'back' chord stored in array Z0 and the 'front' chord stored in array Z1 (see chapter 6.2, 10.7), means the amount of primary data investigated doubles.

3.7. Summary

This chapter introduces the construction and operation of the ring sensor system. It explains how the contour-tracking is carried out on 'back' chords as a multiple adaptation process. The introduction of the modified co-ordinate system is an important aspect which has the advantage that immediately after the scan, a vector description of the scene is available. The extension from 2-D into the 3-D world is shown. The amount of primary data describing the enveloping spiral of a complex object is very low. Examples show agricultural products as well as an assembly of a scene created using compact data of multiple scans. The facility to use the 'back' and 'front' chord is discussed, which builds up two shifted independent enveloping spirals.

4. Geometrical measurements of one object

4.1. Area and volume

4.1.1. Segmentation of the picture

A main step in computer vision is the segmentation of a picture into known simple geometric units. Most of these systems try to segment the objects, and the origin of the co-ordinate system is placed within the object.

The ring sensor is built with the same number of transmitters N_T and receivers N_R, symmetrically arranged on the circumference of a circle (Gall 1997, 1992). The environment around the object is defined by the ring and the data obtained describes the outline curvature of the object. Since there is no information about the inside of the silhouette, it is more logical to segment the space between the ring and the object.

The surface of the object is described by vectors from each transmitter of the remaining chords to the intersection with its predecessor (Gall 1997). In figure 4.1 a cross-section built up by these vectors is shown. The segmentation of the picture becomes obvious.

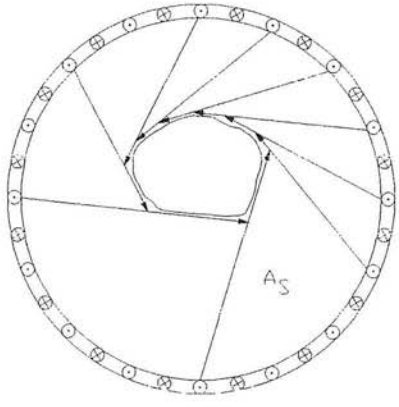

Figure 4.1. Segmentation anti-clockwise

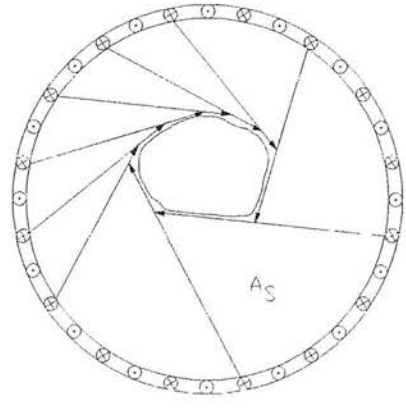

Figure 4.2. Segmentation clockwise

There are two possibilities for segmenting the picture, anti-clockwise (see figure 4.1) or clockwise (see figure 4.2). Both ways are feasible and will deliver the same results for the area and volume determination. Each element A_S is defined by part of one chord and part of its predecessor chord which intersect, and an arc of the ring.

In the following investigations, the anti-clockwise orientation was used. Each element A_S is made up of a triangle A_T and a segment of a circle A_C (see figure 4.3). These units are basic geometrical figures and can be calculated and used for area and volume determination.

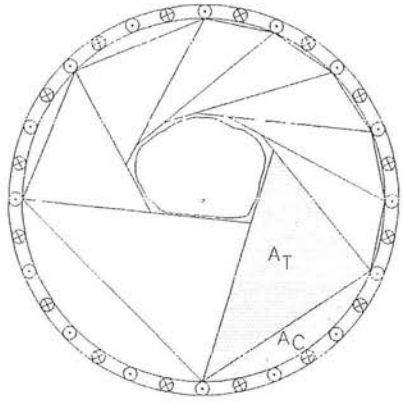

Figure 4.3. Segmentation into definite elements - triangle A_T and segment of circle A_C

4.1.2. Areas of segments

The segmentation of the picture offers a simple method of determination of cross-section areas and volumes of objects with the ring sensor system. The investigation uses results from the investigation in chapter 3. The solution of the geometrical shapes is shown in figure 4.4 where $T_A[n]$, $T_P[n]$ are the positions of transmitters and $R_P[n]$, $R_A[n]$ are the positions of receivers of two neighbouring touching chords of the object. n is the number of the actual activated transmitter which creates the specified chord in the image. α is the angle between two neighbouring transmitters or receivers and β the angle between neighbouring transmitter and receiver. All values are known, excepted the areas A_T and A_C .

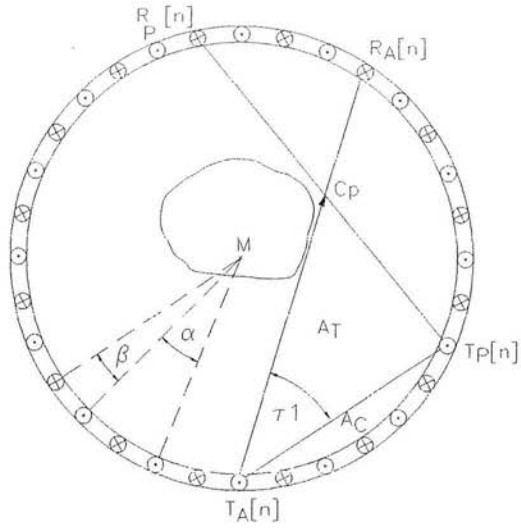

Figure 4.4. Intersection between actual chord and predecessor creating triangle A_T, segment A_C and vector $T_A{:}C_P$.

The area of the triangle A_T for all possible circles with radius r is

$$A_T = \tfrac{1}{2}\, r^2\, |T_A{:}C_P|\, |T_A{:}T_P| \sin \tau 1$$

The area for the segment of the circle using the number $k_{TA,TP}$ of receivers between the transmitters $T_A[n]$ and $T_P[n]$ and the angle α is

$$A_C = \tfrac{1}{2}\, r^2\, (k_{TA,TP}\, \alpha - \sin (k_{TA,TP}\, \alpha))$$

The sum of A_T and A_C gives the area for the element A_S

$$A_S = \tfrac{1}{2}\, r^2\, (|T_A{:}C_P|\, |T_A{:}T_P| \sin \tau 1 + k_{TA,TP}\, \alpha - \sin (k_{TA,TP}\, \alpha))$$

In the case of the unit circle ,

$$A_S{}^* = A_S / r^2 \qquad (4.1)$$

An advantage of this method is that main values such as the length of the vector $T_A{:}C_P[n]$ and angle $\tau 1$ can be taken from previous investigations and the determination of all the other values is not difficult. This allows real time use.

4.1.3. Area of a cross-section

The area for the whole circle (inside of the ring), A_R, is simply

$$A_R = \pi r^2$$

The sum of the determined remaining i_{OBJ} segments A_S gives the area surrounding the object. Subtracted from A_R this gives the resulting cross-sectional area A_O of the object

$$A_O = A_R - \sum_{i=1}^{i=i_{OBJ}} A_S(i) \quad .$$

Since the minimum set of 'back' chords have been found as described in chapter 3 the area determination of a cross-section of an object is a simple and rapid calculation.

4.1.4. Volume of an object

Using the ring sensor system, the extension of algorithms into 3-D space is simple as already described in chapter 3.5. First take the ring with no object and the maximal cylinder described by it (see figure 4.5.a). The ring describes a cylindrical spiral about the length L of the object. The volume of this cylinder V_C is the number of recognised snapshots N_{OBJ} times the volume of a spline V_R or the sum of all splines V_R (see figure 4.5.b). The volume of a spline is given by the area (circle sector) between the centre of the ring, the part of the circle between adjacent transmitters and distance d_S which the object moves during one scanning revolution.

$$d_S = N_T \, s$$

$$V_R = \pi r^2 \, d_S / N_T = \pi r^2 \, s$$

$$V_C = N_{OBJ} \, V_R$$

$$V_C = N_{OBJ} \, \pi r^2 \, s$$

The area elements A_S surrounding the object become volumes V_S when multiplied by the distance d_S.

$$V_S = A_S \; d_S = A_S \; s \; N_T$$

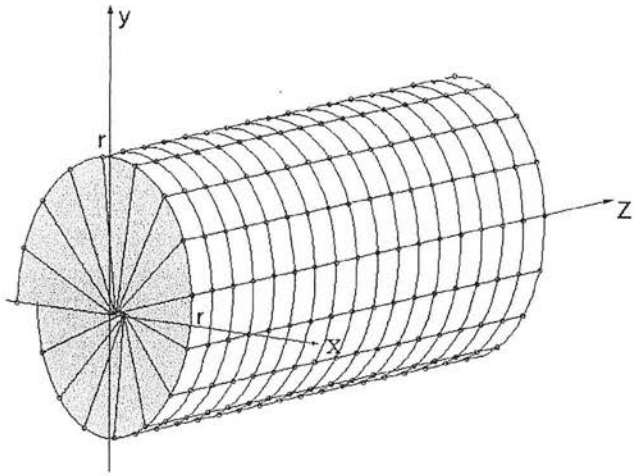

a) Basic volume cylinder for an object

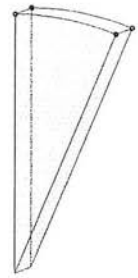

b) Basic spline

Figure 4.5. Volume of 3-D ring (cylinder)

The volumes V_S have to be subtracted from the cylinder volume V_C to get the object volume V_O.

$$V_O = V_C - \sum_{i=1}^{i=i_{OBJ}} V_S(i)$$

$$V_O = N_{OBJ} \; \pi r^2 \; s \; - \sum_{i=1}^{i=i_{OBJ}} A_S(i) \; s \; N_T$$

In the last formula the radius of the ring r is constant and the distance s between each snapshot is dependent on the speed of the object through the ring. They can be excluded during the data processing until the final calculation using A_S* (see equation 4.1).

$$V_O = r^2 \; s \; (\; N_{OBJ} \; \pi - \sum_{i=1}^{i=i_{OBJ}} A_S^*(i) \; N_T \;)$$

4.2. Axis measurements

4.2.1. Characteristic axes of an object

In this work a simple description of the determination of major axes with length D_A is made, which requires the largest axis of the object to be parallel to the axis of passage through the ring sensor. The advantages of this are that only a two dimensional investigation is necessary to determine the axis measurements, and the co-ordinate system (see chapter 3) need not be changed. If the presentation of objects were random, a different co-ordinate system would be necessary with subsequently more complex 3-D algorithms.

The determination of one of these axes, the length L of the object has been discussed previously. One revolution of the enveloping spiral of the object creates a cross-section vertical to the longitudinal direction. For an ellipsoid the other two axes are the minor and major axes of the middle slice cross-section (see figure 4.6.a).

In nature, many variable forms of fruit and vegetables can be found. If the object is not an ellipsoid, these three parameters will not be adequate to describe the shape.

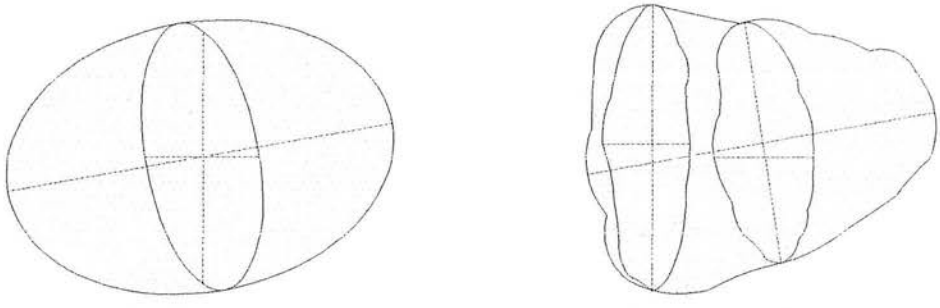

a) Ellipsoid b) Irregular object

Figure 4.6. Different shaped objects

One possible solution (see figure 4.6.b) is based on finding the position of the largest slice SPO based on finding the largest axis LSL of an object in a cross-section, which means that the data for the whole object has to be examined.

The relationship between the length, the axes of the largest slice and the middle slice, and the position of the largest slice can give a shape description of the object (see also chapter 4.3).

4.2.2. Positions of the chords for axes at a cross-section

Three different positions of axes are possible in an object. They can be defined as lying between:

1. two parallel chords P (see figure 4.7.a)
2. a chord and an intersection IN_2 (see figure 4.7.b)
3. two intersections IN_{3A} , IN_{3B} (see figure 4.7.a) .

For the minor axis, variants 1, 2 and 3 are possible, a major axis in each case requires variant 3.

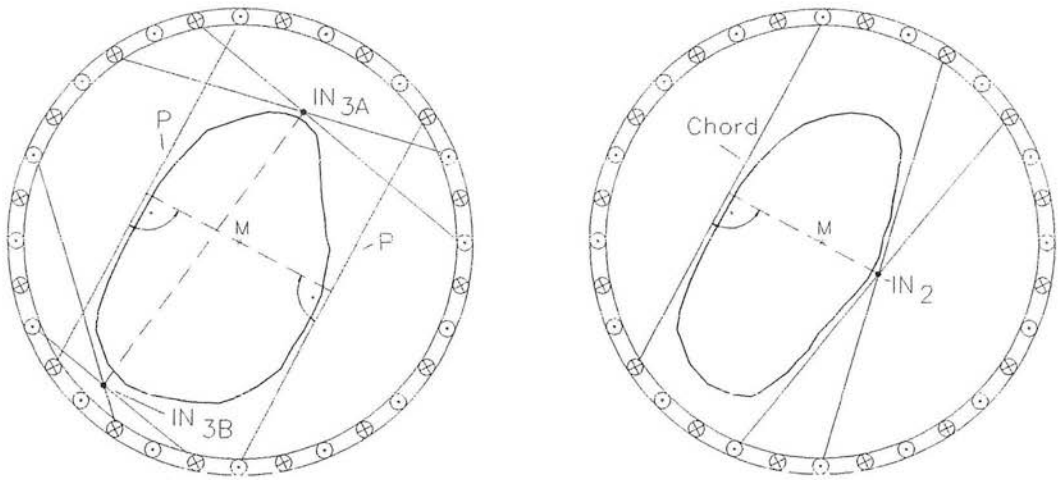

a) b)

Figure 4.7. Possible axes in an object with parallels and opposite intersections

The following chapters describe the mathematical background of the axis determination.

4.2.3. The distance between parallel chords (variant 1)

Looking for minor and major axes of cross-sections, each chord touching an object will be investigated for a parallel chord opposite (see figure 4.8). This case is valid when the distances $|T_A{:}R_X|$ and $|R_A{:}T_X|$ are the same. The distance $|C_A{:}C_X|$ which equals the length of the axis is:

$$D_A = |C_A{:}C_X| = r \,|\cos(k_{TA,RA} + 1)\,\beta + \cos(k_{TX,RX} + 1)\,\beta| \quad \text{(see appendix 3)}$$

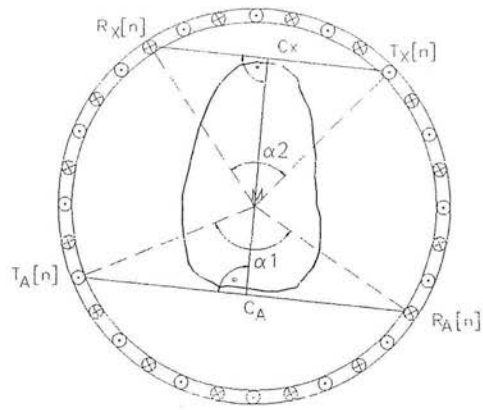

Figure 4.8. Distance between two parallel chords

If parallel chords are found, the investigation is finished. The distance $|C_A:C_X|$ includes no information about the position of the axis.

4.2.4. The distance between a chord and an intersection of chords (variant 2)

In most cases parallel chords will not be found (see figure 4.9). In this case, the most distant intersection C_X on the opposite side has to be found and the shortest distance $C_A:C_X$ to the actual chord $T_A:R_A$ has to be determined.

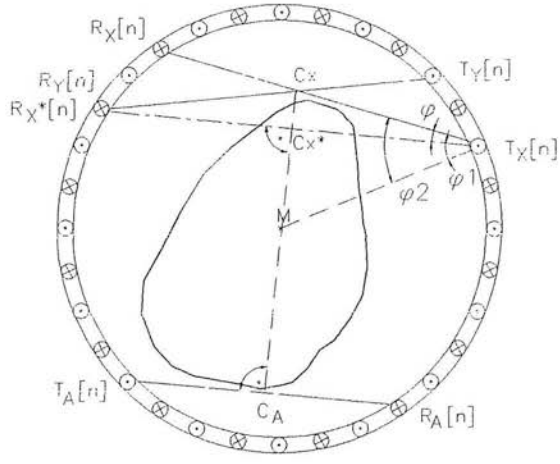

Figure 4.9. Distance between a chord and an intersection

The first step is to find the chord $T_X[n]$:$R_X[n]$ in the clockwise direction of rotation of the ring, which is 'one of' parallel to $T_A[n]$:$R_A[n]$.

Next an apparent parallel chord T_x:R_x* has to be fixed for the determination of the distance $|C_A:C_X^*|$ using the method from the previous chapter. The intersection C_X is always further from the chord T_A:R_A [n] than this parallel. Finally the distance $D_A = |C_A:C_X|$ can be determined.

$$|C_A:C_X| = |C_A:C_X^*| + |C_X:C_X^*|$$
$$|C_A:C_X| = |C_A:C_X^*| + |T_X:C_X| \sin ((k_{TX,RX^*} - k_{TX,RX})\,\beta) \qquad \text{(see appendix 4)}$$

The distance $|T_X:C_X|$ is known from the determination of intersections (see chapter 3.4). So in this case the location and length of C_A:C_X can be found.

4.2.5. The distance between two intersections (variant 3)

Because the major axis of a cross-section can only lie between two intersections, and the minor axis could also do this (see chapter 4.2.2), a second intersection has to be found by investigating the distance from the receiver of the actual chord to the intersection with the predecessor $|R_A:C_P|$, and also $|R_A:C_S|$, the distance to the intersection with the successor chord (see figure 4.10).

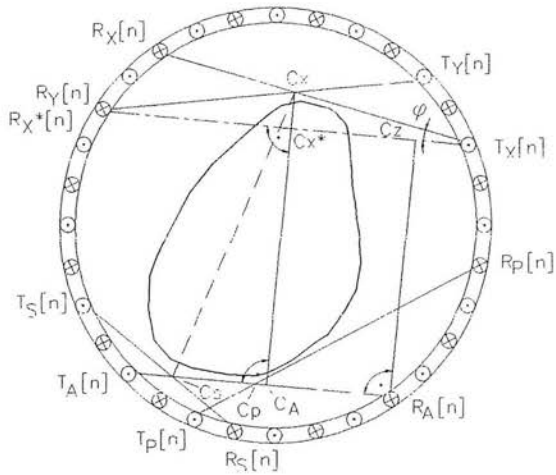

Figure 4.10. Distance between two opposite positioned intersections

Both can simply be produced as a 'by product' during the determination of the intersections (see chapter 3.4). The distance $|R_A:C_A|$ is also required.

$$|R_A:C_A| = \tfrac{1}{2} (|T_A:R_A| + |T_X:R_X^*|) - |T_X:C_X^*| \qquad \text{(see appendix 5)}$$

Investigating the distances $|C_A:C_P|$ and $|C_A:C_S|$, the larger has to be evaluated.

$$|C_A:C_P| = |R_A:C_P| - |R_A:C_A|$$
$$|C_A:C_S| = |R_A:C_S| - |R_A:C_A|$$

The larger distance $|C_A:C_P|$ or $|C_A:C_S|$ determines the required intersection (C_S in figure 4.10). Using Pythagoras' theorem the result is either

$$D_A = |C_X:C_S| = (|C_A:C_X|^2 + |C_A:C_S|^2)^{1/2} \qquad \text{or}$$
$$D_A = |C_X:C_P| = (|C_A:C_X|^2 + |C_A:C_P|^2)^{1/2} .$$

All requirements for the evaluation of the length of the axes are now known. The largest value found around the cross-section is the major axis. The position in longitudinal direction of the object is known. Information about the vertical positions of the axes in the cross-sections and in the ring are not considered, because they are not required for the shape classification.

4.3. Classification of shape

As a result of the determination of volumes, areas and axes an object can be classified for its shape by using these parameters. In this work, classification is only briefly discussed because the right choice of parameters should be decided by the requirements of practical use in further investigations. A Fourier based method is described by Tao *et al* (1995). Axis measurements and other geometrical properties have been used for potatoes and vegetables to estimate the shape and volume of objects (Sistler 1991, Mörtl 1992, McRae *et al* 1986, Miller (1992) (see figure 4.11.a).

One advantage of the ring-sensor system is that the 3-D shape description is based on the use of 2-D algorithms, in difference to other systems based on 3-D shape analysis techniques (Yang *et al* 1989).

Recognition of the species and position of fishes by shape is described in Strachan *et al* (1993), De Silva *et al* (1993) and Arnarson *et al* (1994). For an accurate, detailed shape description the surface curvature of fish areas or curvature lines could be partly classified as convex, straight and concave (see figure 4.11.b) (Cinque *et al* 1995).

Parameter	Definition
area ratio	Area (object) / area of rectangle (a b)
circularity	perimeter^2 / area (object)
diameter (D_A) range	MAX (D_A) - MIN (D_A)
diameter (D_A) ratio	D_A (b orientation) / D_A (a orientation)

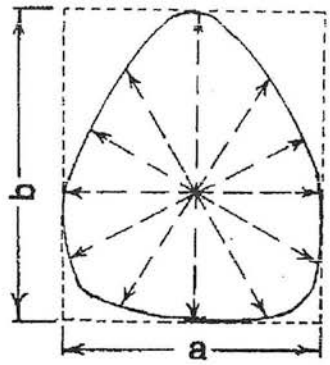

a) Classification of fruit (Miller 1992)

Segment classification	Labels
Very concave	W
Concave	C
Straight	S
Convex	X
Very convex	Y

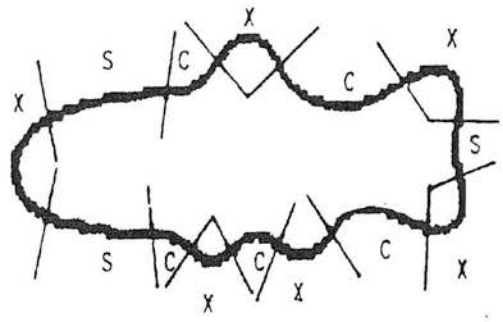

b) Classification of fish (Cinque 1995)

Figure 4.11. Classification of shape

Depending on the level of accuracy needed, simple or more complex descriptions can be taken.

4.4. Position (midpoint) of the object

For handling agricultural products information about the position of an object is very important. Only when the position is known, can directed mechanical handling of objects be possible. A 'position' in this case is defined as a single point in space for one object, which will change with movement of the object. Finding this single point, in this

case the midpoint of the object, will be described in this chapter. For the determination it is important that the objects are lined up in horizontal direction (see figures 3.9) and passing through the ring. The main axis in horizontal direction and the largest and smallest axes in vertical direction of one cross-section can then be used (see figure 4.6).

4.4.1. Position of the midpoint in horizontal direction

The position depends on the definition of the midpoint. The position of the object P_H in horizontal direction (horizontal axis of the object) can be found for example

1. in the middle of the object

$$P_H = s\ N_{OBJ} / 2$$

2. on the position of the largest cross-sectional slice (SPO) determined by the largest vertical major axis (LSL) of the object

$$P_H = s\ n\ [MAX\ [D_A[n]]]$$

3. the midpoint of volume (mass) distribution, which copes with the situation of separation in a grading unit using a central side impetus to avoid spinning of the object. The algorithm described in chapter 4.1.4 can be used.

$$P_H = s\ n\ [V_O\ [n] / 2]$$

4.4.2. Position of the midpoint in vertical direction

The determination of the object in the vertical direction is reduced to a 2-D problem within one cross-section, because of the directed passage of the object through the ring. The simplest possible solution is the use of the minor and the major axes of cross-section as determined in chapter 4.2. The beginnings and ends of the two axes are determined by four intersections from the enclosing chords which are given in modified polar co-ordinates (see chapter 3.3.-3.4). One possibility uses the intersection of the axes marking the midpoint M_O of the object (see figure 4.12.a).

For the determination of M_O it is much easier to use the Cartesian co-ordinate system (X, Y). The origin of the system shall be the midpoint M of the ring as in the polar-co-ordinate system. The transformed intersections with the number i will have the co-ordinates x[i], y[i].

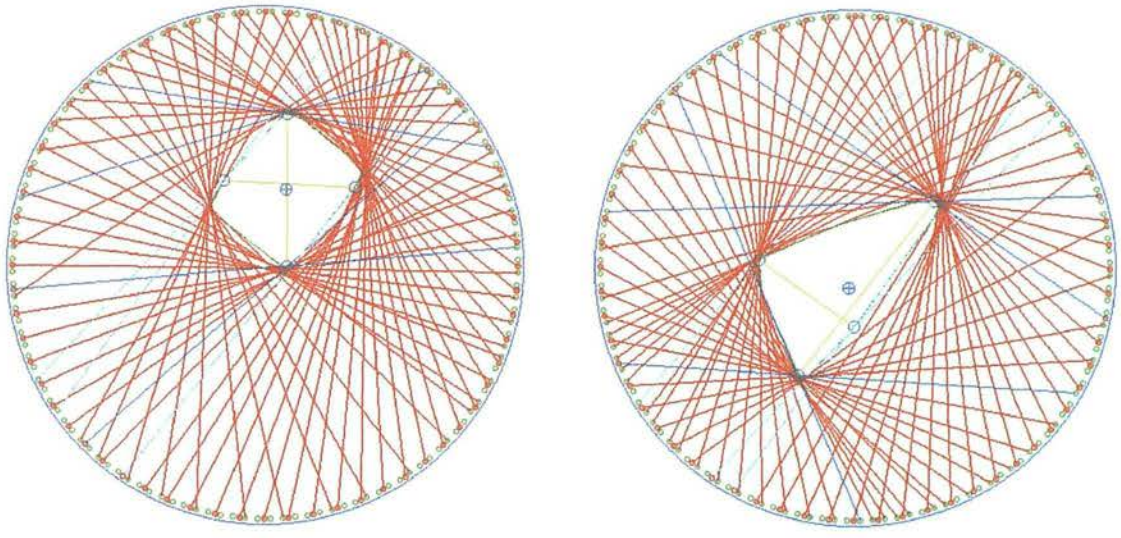

a) Rectangle b) Triangle

Figure 4.12. Cross-sections with marked positions (circles for intersections on surface and cross for the midpoint found)

The polar co-ordinates of each intersection of the envelope of the object have to be transferred into the midpoint of the ring (see figures 4.13 and 4.14, see also chapter 3.4)

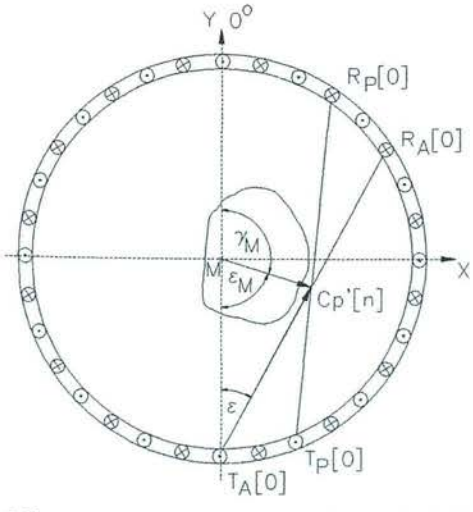

Figure 4.13. Determination of M:C_P'

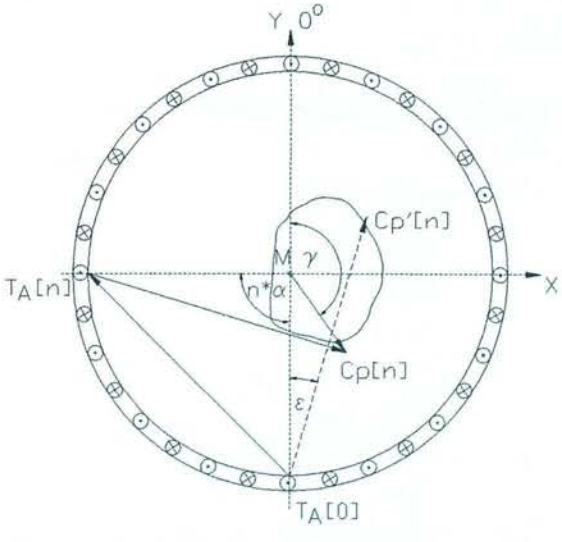

Figure 4.14. Determination of the angle γ in the Cartesian co-ordinate system

Using the cosine rule (see figures 4.13 and 3.5) in the zero position, the distance

$$|M{:}C_P'[n]| = (r^2 + |T_A[0]{:}C_P'[n]|^2 - 2\, r\, |T_A[0]{:}C_P'[n]| \cos \varepsilon)^{1/2}$$
$$|M{:}C_P'[n]| = |M{:}C_P[n]|$$

Using the sine rule the angle γ_M can be determined.

$$\gamma_M = \pi - (\arcsin |T_A[0]{:}C_P'[n]| \sin \varepsilon) / |M{:}C_P'[n]|$$

Using the clockwise turn in the scene (see figure 4.14) to finally get the angle γ simply means the addition of the angle $n\,\alpha$

$$\gamma = \gamma_M + n\,\alpha$$

with $\pi = N_T/2\,\alpha$

$$\gamma = (N_T/2 + n)\,\alpha - (\arcsin |T_A[0]{:}C_P'[n]| \sin \varepsilon) / |M{:}C_P'[n]|$$

The transformation into Cartesian co-ordinates for each intersection is

$$x[i] = |M{:}C_P[n]| \sin \gamma$$

$$y[i] = |M{:}C_P[n]| \cos \gamma$$

For the intersection of the major and minor axes the position of M_O with its co-ordinate $[x_{MO}, y_{MO}]$ of the largest slice in Cartesian co-ordinates is

$$x_{MO} = \sum_{i=1}^{i=4} x[i] / 4$$

$$y_{MO} = \sum_{i=1}^{i=4} y[i] / 4$$

As can be seen in figure 4.12.b however, the intersection of the two axes is well away from the middle, because the major axis and area is on one side of the triangle. A better way to obtain a more central position is to observe at the maximum and minimum in the x and y direction. Under this view M_O is given by

$$x_{MO} = (\text{MAX}_{i=1}^{i=4} [x[i]] - \text{MIN}_{i=1}^{i=4} [x[i]) / 2$$

$$y_{MO} = (\text{MAX}_{i=1}^{i=4} [y[i]] - \text{MIN}_{i=1}^{i=4} [y[i]) / 2$$

There are other ways to get a more precise midpoint, for example by taking into account more axes from different views around the cross-section of the object. The principal way of dealing with the data will be the same.

4.5. Summary

The segmentation of the environment of the object in the ring is described by creating a number of area segments. Based on this the cross-sectional area of the object is calculated. The extension into 3-D space produces surrounding volume segments and finally the volume of the object. It is shown how axis measurements which can also be used for shape classification can be determined. The methods for finding the position of midpoints of objects is described. The results contained in this chapter provide the basis for the carrying out investigations into the limitations of the ring sensor system.

5. Simulation of objects and tests of accuracy

Simulation can be used to find the accuracy limits of the system for determination of geometrical properties of objects. For this reason, models have to be developed to produce the data. In this chapter the imaging of cylinders, spheres, ellipsoids and symmetrical polyhedra with 2-5 vertices passing through the ring sensor will be simulated. The simplest cases use a cylinder and a sphere because of the overall symmetry of the 2-D cross-section. More complex analysis is required for ellipsoids and polygons because of there is limited symmetry. The 2-D case will be described first, followed by the 3-D case. Simulations carried out with different defined objects will confirm the principles.

5.1. Models for the creation of objects

5.1.1. Polar co-ordinate description of cross-sections of objects with their midpoints at the centre of the ring

The cross-sections of objects are first centred in the ring (see figure 5.1). The radius $r_O[\chi_D]$ is the distance from the midpoint M to the tangent of the object in each direction χ_D. The description in polar co-ordinates is for a sphere and cylinder with radius r_{CIR}

$$r_O[\chi_D] = r_{CIR} \tag{5.1}$$

For the ellipse and polygons (see figure 5.1, 5.2.a), information about the pivot point of the object relative to the co-ordinate system of the ring is needed, and can be described by the angle χ_P. The ellipse in a polar co-ordinate system is described by half of the major axis, e_A and by the minor axis, e_B. The numerical eccentricity e_X is given by (Gellert 1971)

$$e_X = ((e_A^2 - e_B^2)/e_A^2)^{1/2}$$

The formula for the ellipse for the tangential expansion on a line in a specific direction is then

$$r_O[\chi_D] = (e_B^2 / (1-e_X^2 \cos^2(\chi_D + \chi_P))^{1/2}$$

The maximum tangential expansion of an ellipse can be on a different surface point (see figure 5.1.b). Because of this, for the simulation the expansion of neighboured surface points has to be investigated. The maximum expansion of the ellipse has to be found into by an iterative search. To limit the number of investigations a step sin of $\vartheta = 0.5°$ and a varying factor $i_{N\_NEG} < i < i_{N\_POS}$ for the following investigations was used. Using this settings and the formula above the neighbourhood has to be investigated until a maximum is found.

$$r_O[\chi_D] = \underset{i=i_{N\_NEG}}{\overset{i=i_{N\_POS}}{MAX}} (\cos(i\vartheta)\,(e_B^2 / (1-e_X^2 \cos^2(i\vartheta + \chi_D + \chi_P))^{1/2} \qquad (5.2)$$

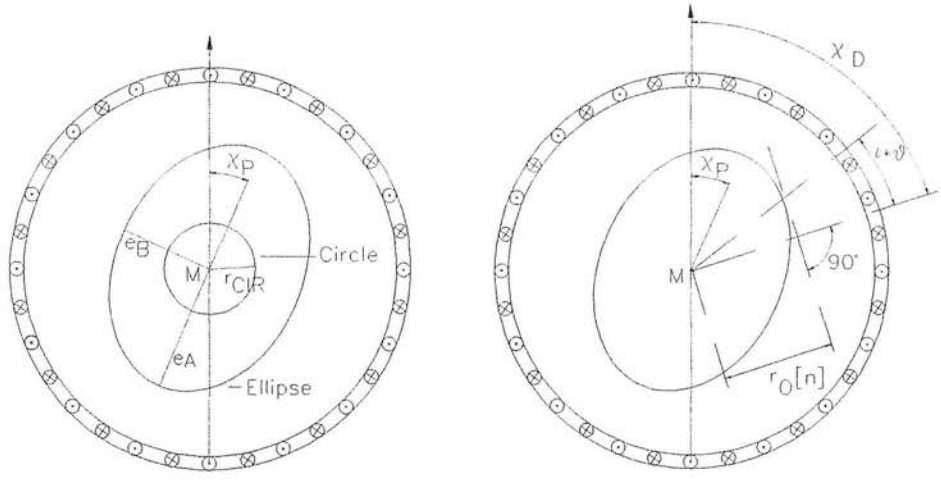

a) Circle and ellipse b) $r_O[n]$ on an ellipse

Figure 5.1. Cross-sections of centrally positioned circle and ellipse

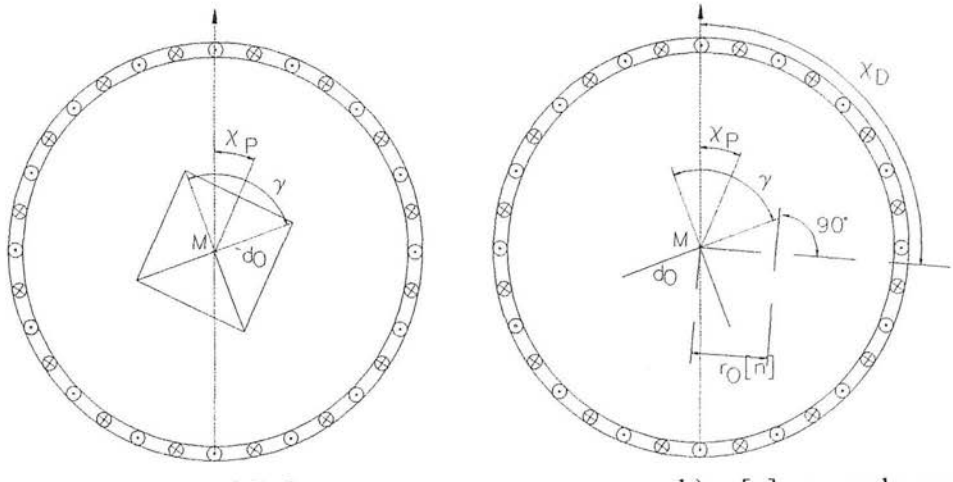

a) Polygon b) $r_O[n]$ on a polygon

Figure 5.2. Cross-section of a centrally positioned polygon

For a regular polygon (see figure 5.2.a) with the total number of vertices i_{VN} the partial angle between two neighboured vertices from its midpoint is γ. To find the maximum tangential expansion r_O of a polygon from its centre in each direction, all vertices have to be investigated using the distance d_O between the centre of the polygon and each vertex (see figure 5.2.b).

With $$\gamma = 2\,\pi / i_{VN}$$

$$r_O[\chi_D] = \max_{i=1}^{i=i_{VN}} (d_O \cos(i\,\gamma + \chi_D + \chi_P)) \qquad (5.3)$$

The only difference of irregular polygons is the variation of the angle γ and/or the distance d_O of the vertices.

$$r_O[\chi_D] = \max_{i=1}^{i=i_{VN}} (d_O[i] \cos(\gamma[i] + \chi_D + \chi_P))$$

5.1.2. Displacement of the cross-section and discovering enveloping chords

Displacing the midpoint of the object from the midpoint of the sensor ring (see figure 5.3), the displacement $M{:}D_I$ consists of the distance $|M{:}D_I|$ and the angle ψ (shown in figure 5.3.a).

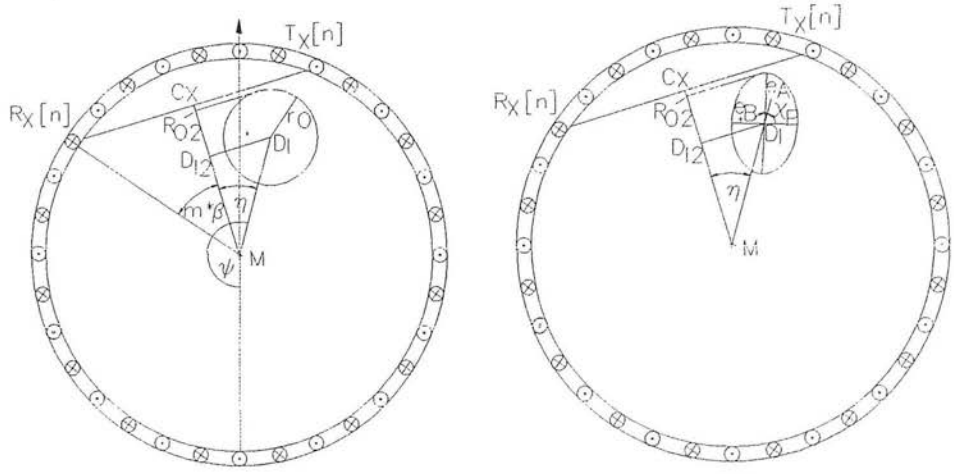

a) Circle b) Ellipse

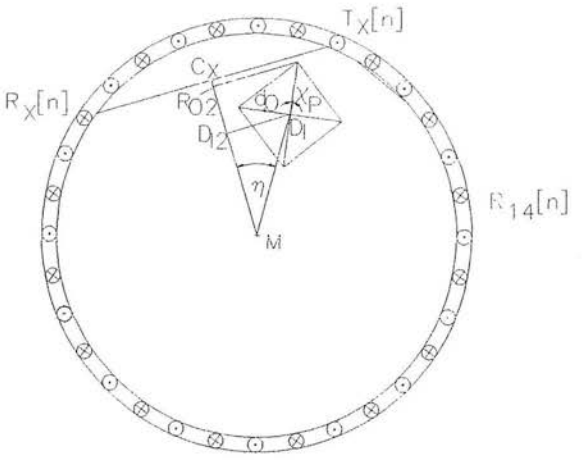

c) Polygon

Figure 5.3. Objects displaced from the centre of the ring

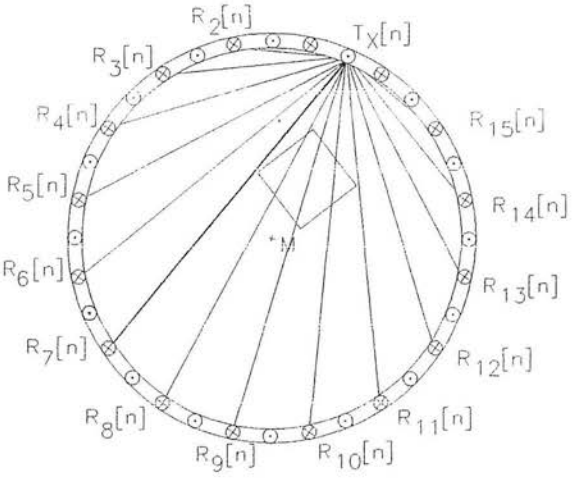

Figure 5.4. Polygon displaced in the ring

For every transmitter the touching chord with $m_B[n]$ must be determined (see T_X:$R_7[n]$ in figure 5.4). Therefore for each transmitter $T_X[n]$ of the ring all possible chords to each receiver $R_X[n]$ will be investigated (see $R_2[n]$ to $R_{15}[n]$ in the example in figure 5.4). All of this chords are determined by the number of receivers u between actual investigated transmitter $T_X[n]$ and receiver $R_X[n]$ with $1 < u < N_R$. The closest distance of every chord $T_X[n]$:$R_X[n]$ to the midpoint M of the ring circle is

$$|M{:}C_X| = r \cos(u\,\beta)$$

For finding the tangent of the object, parallel to the investigated chord the line $M{:}D_I$ and the actual $r_O[\chi_D]$ have to be displayed on the line $M{:}C_X$, giving the distances $|M{:}D_{I2}|$ and $|D_{I2}{:}R_{O2}|$ (see figure 5.3). The direction of $M{:}C_X$ is then

$$\chi_D = n\,\alpha - (u + \tfrac{1}{2})\,\beta \tag{5.4}$$

The distance $ro_D[u]$ between the midpoint M and the tangent in the direction of $M{:}C_X$ is with

$$r_O[u] = r_O[\chi_D] = |D_{I2}{:}R_{O2}|$$

equal

$$r_{OD}[u] = |M{:}D_{I2}| + r_O[u]$$

With the angle η between the lines of considered direction $M{:}C_X$ and the displaced object $M{:}D_I$ is

$$\eta = \psi - \chi_D$$
$$|M{:}D_{I2}| = |M{:}D_I|\ \cos(\eta)$$
$$|M{:}D_{I2}| = |M{:}D_I|\ \cos(\psi - n\,\alpha + (u + \tfrac{1}{2})\,\beta) \tag{5.5}$$

With $|D_{I2}{:}R_{O2}| = r_O[u] = r_O[\chi_D]$ depending on the kind of object as detailed in the previous chapter (equations 5.1 - 5.3), the distance r_{OD} is for all possible u

$$r_{OD}[u] = |M{:}D_{I2}\,[u]| + |D_{I2}{:}R_{O2}\,[u]|$$

The procedure is to find all $m_B[n]$ for the closest chord $T_X{:}R_X[n]$ (tangent) of all transmitters $0 < n < N_{OBJ}$ of the object with the mathematical equation

$$n = N_{OBJ},\ u = N_R$$
$$m_B[n] = \mathrm{MIN}\,(|M{:}C_X\,[u,n]|) > r_{OD}[u,n]$$
$$n = 0,\ u = 1$$

All determined numbers $m_B[n]$ will be included in the array Z0 (see chapters 6.2, 10.7) as primary data. In the case of the example in figure 5.4, $m_B[n]$ is describing chord $T_X{:}R_7[n]$. Eventually, the array Z0 will include as many 'back' chords as transmitters N_T for one cross-section (revolution).

5.1.3. Describing objects with different shapes of cross-sections

Using the algorithms described and methods developed, different objects can be constructed. Some examples of cross-sections are shown in figures 5.5-5.10. These figures also include images of 3-D objects, which will be explained in the following chapter. The largest cross-section of the object as a result of the simulation is shown on the right side in each figure 5.5-5.10. The simulated data are included in the primary data area Z0 (see chapters 6.2, 10.7) and have been analysed by using the algorithms described in chapters 3.2-3.5, 4.1-4.2. Inside the hull of the cross-section the spiral of the origin of the investigated distance $r_O[n]$ of the object is shown. It can be seen that the hull determined by the ring-sensor system does not touch the object, so will over-estimate the area. This over-estimation in area is caused by the fundamental operation of the ring and is determined by the resolution of the sensor. The circular shaped curves around polygons (see figure 5.8-5.10) show the distance of the closest chord found for each transmitter from the midpoint of the ring to the surface of the object $r_{OD}[m_B[n]]$ around the object. On round objects (see figure 5.5.-5.6) this cannot be seen because the object itself is round.

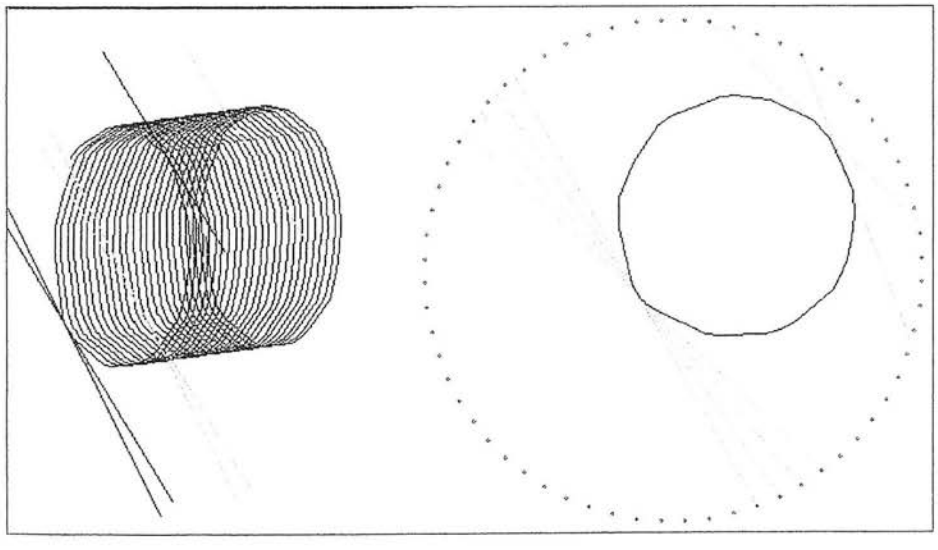

Figure 5.5. Simulated cylinder in the ring sensor system

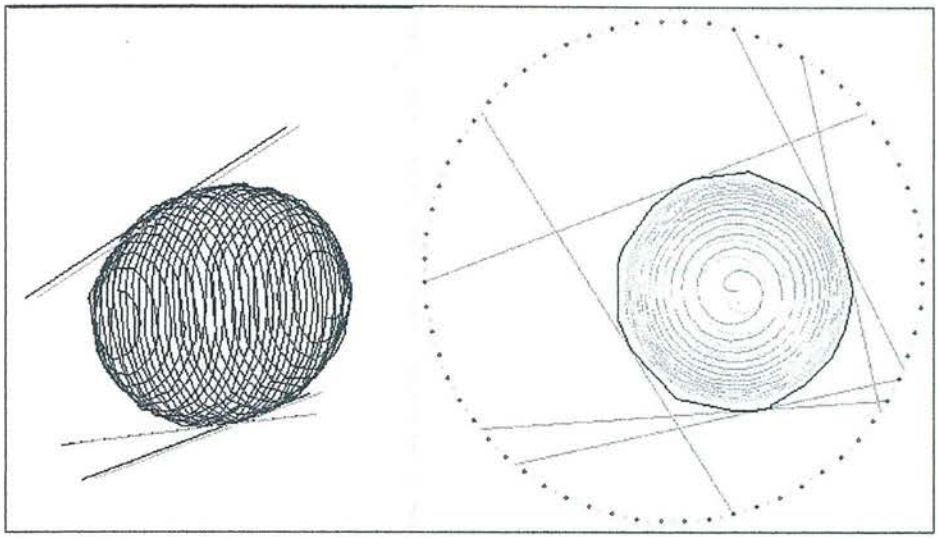

Figure 5.6. Simulated sphere in the ring

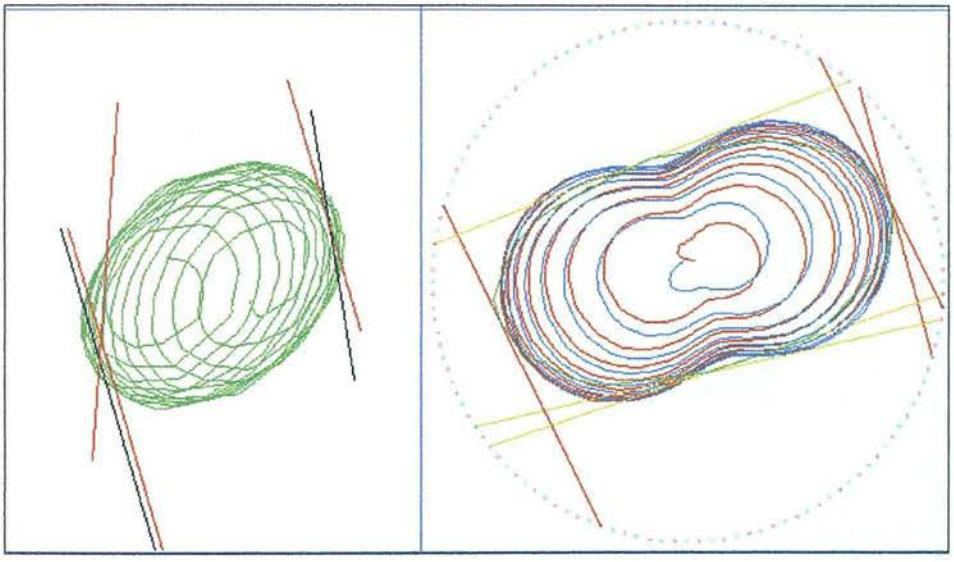

Figure 5.7. Simulated ellipsoid in the ring

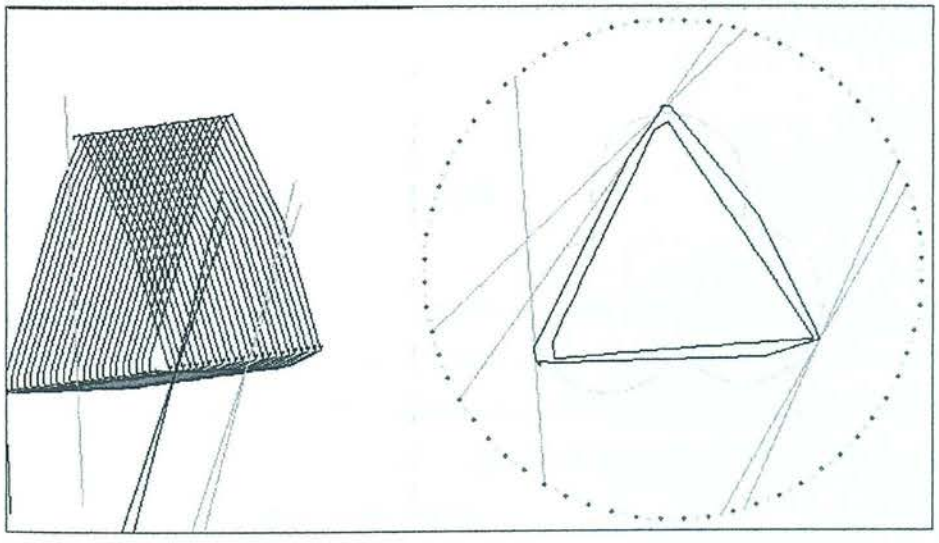

Figure 5.8. Simulated prismatic object with triangular cross-section

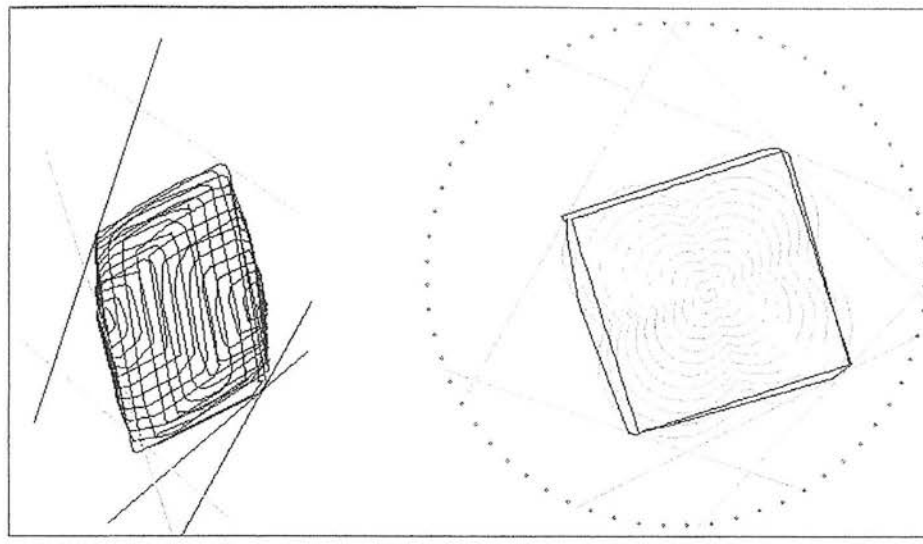

Figure 5.9. Simulated cube with 4 vertices in cross-section

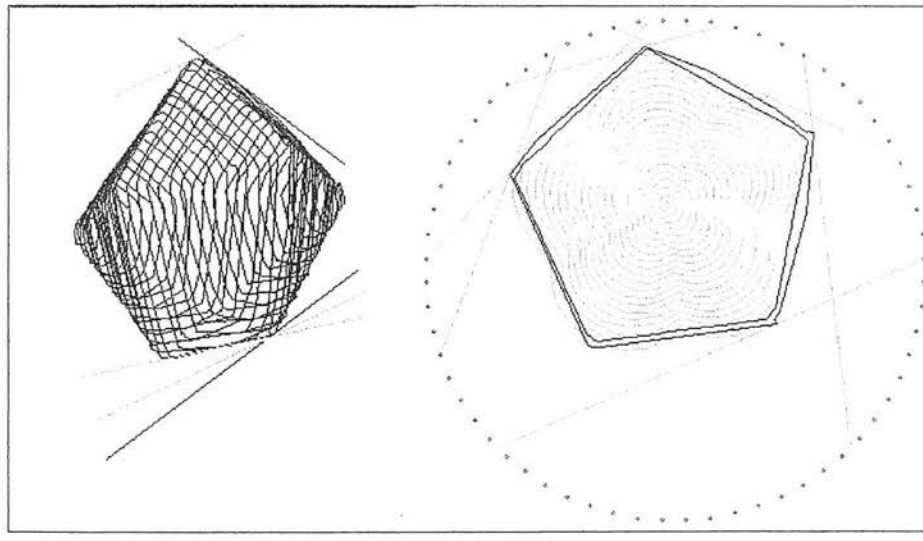

Figure 5.10. Simulated object with 5 vertices in cross-section

5.1.4. Three dimensional objects

The described model of the ring sensor system requires the translation of the objects in the longitudinal direction but does not depend on the position of the object within the ring (see chapter 3.4). The result of a simulation is an enveloping spiral (see figures 5.5-5.10). In the direction of movement, the length L of the object limits the spiral. For a sphere the length is equal to double the radius.

The location for each surface point and distance $r_{O3D}[n]$ of the spiral from the rotational axis (midpoint) of a symmetrical object is based on the 2-D result for the $r_O[n]$ (equations 5.1-5.4). It depends on each snapshot n in the range between 0 and the total number of snapshots of the object N_{OBJ}. The following are some examples for longitudinal shapes

Cylinder:	$r_{O3D}[n] = r_O[n]$
Sphere:	$r_{O3D}[n] = r_O[n]\ (1-(\ 1-2\ n\ /\ N_{OBJ}\ )^2)^{½}$
pyramid or cone	$r_{O3D}[n] = r_O[n]\ n\ /\ N_{OBJ}$
pyramid with 2 acute ends	$r_{O3D}[n] = r_O[n]\ (1-\|1-2\ n\ /\ N_{OBJ}\|)$

Other formulae are possible for different shapes, for example banana, helix or artificial shapes. The third dimension allows concave areas in the direction horizontal to the movement to be investigated. Figures 5.11-13 are examples of enveloping spirals.

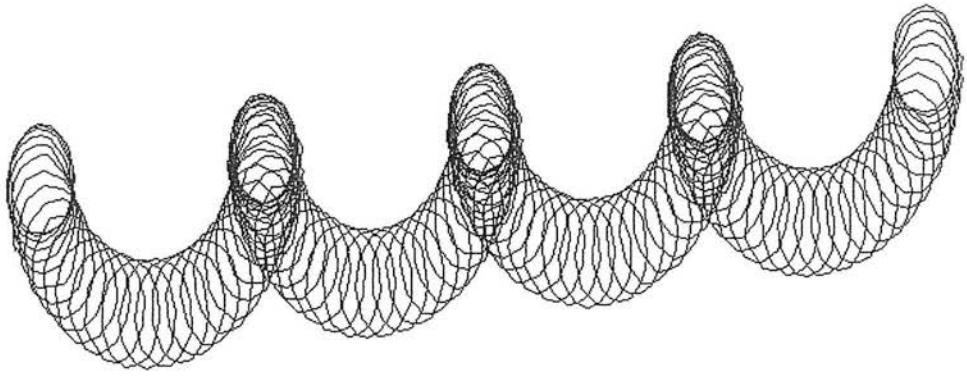

Figure 5.11. Simulated object in the form of a spiral with

variation of ψ (see equation 5.5)

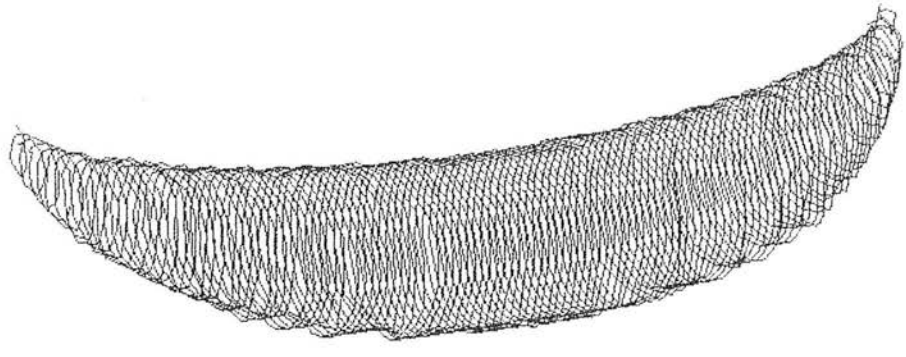

Figure 5.12. Simulated bean with variation of $|M{:}D_I|$ (see equation 5.5)

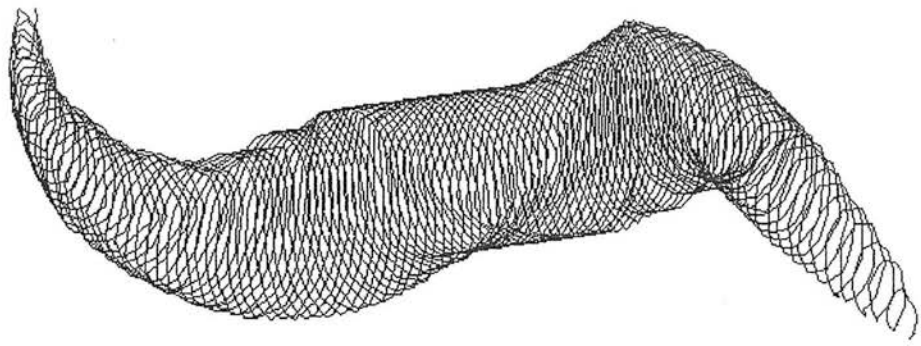

Figure 5.13. Ellipse with variation of $|M{:}D_I|$ and ψ (see equation 5.5)

Using the basic equation 5.5, in figure 5.11, $M{:}D_I$ is constant, $\psi[n]$ varies (k_R is a constant determining the slope of the spiral)

$$\psi\,[n] = k_R\ n$$

Because the formula is linear the result is a spiral with a constant pitch. In figure 5.12 ψ is constant and $M{:}D_I$ varies.

With k_Z a constant between

$$0 <= k_Z <= 19/20\ r - r_{03D}[n]$$

(on the shortest possible distance of the object to the ring)

$$|M{:}D_I[n]| = k_Z\ (1-(\ 1-2\ n\ /\ N_{OBJ}\ )^2)^{1/2}$$

The result is a bean shaped object. In figure 5.13 both $|M{:}D_I|$ and ψ are variable using the previous formulae. The object definitions are much more flexible in 3-D. Further improvements could be made by using non-linear functions. Any shape can be simulated provided that the objects are within the geometrical limits of the ring (cylinder) and the extension is in the horizontal direction. The main advantage of this system is its flexibility in scanning objects of any shape, which can then be described by a limited number of chords received from a practical ring sensor solution.

5.2. Simulation tests and errors

Simulations with different objects were carried out to determine the accuracy of the ring sensor system. The cross-sections which were used are shown in figure 5.14. The 3-D shapes investigated are cylinders, spheres and polyhedra of different shapes.

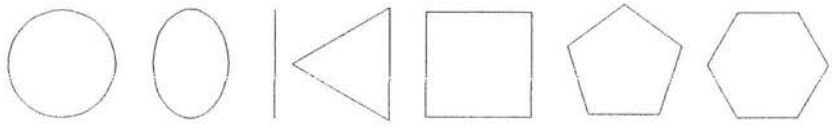

Figure 5.14. The cross-sections used for the simulations

5.2.1. Basic set up for the simulations

To investigate possible real conditions for a practical sensor solution, the following sensor parameters were chosen:

Number of transmitters:	64
Number of receivers:	64
Radius of ring sensor:	90 mm
Scanning speed of the ring:	400 rev/s
Speed of the objects:	1 m/s

The space within the sensor system is limited by the area of the ring. This limits the maximum possible distance between the midpoint of the ring sensor system and the 'midpoint' of an object $|M{:}D_I|$. In practice, the object must not touch the ring. For this reason, an excluded area around the ring is defined by the distance $D_{ED} = 5$ mm from the outside of the ring. For the simulations, rational random numbers N_{RAN} between 0..1 and the following formulae are used to define all possible distances $|M{:}D_I|$ of the centre of the object from the centre of the ring.

$$\text{Cylinder and sphere:} \quad |M{:}D_I| = N_{RAN}\ (r - D_{ED} - r_{OBJ})$$

Including the worse case of expansion

$$\text{Ellipsoid:} \quad |M{:}D_I| = N_{RAN}\ (r - D_{ED} - e_A)$$

$$\text{Polygon:} \quad |M{:}D_I| = N_{RAN}\ (r - D_{ED} - d_O)$$

The angles χ_P and ψ within the range of 0..2 π are also determined using different random numbers N_{RAN}.

$$\chi_P, \psi = N_{RAN} \; 2\,\pi$$

As a result of random values the objects are randomly positioned in different areas and positions in the sensor system. The diameter of objects in practice is limited to match typical agricultural products and is in the range of 20-140mm diameter, as for example potatoes. Most of the tests will be carried out in this range. For each test each object was simulated 1000 times. One major axis is the length L. Because in simulation this axis is built up by N_{OBJ} snapshots, a deviation will never occur.

Most of the tests will be based on this set-up. If different properties are used, they will be noted.

5.2.2. Basics about accuracy and errors

It must be remembered that cross-sections of the objects generally have to be convex, since concave areas can not be 'seen' because of the shadow principle of the ring. The errors are mainly caused by the discrete design of the ring since only a finite number of chords and intersections are possible.

In Gall (1992,1998) special cases on a cross-section have been investigated on the worst case that round objects (symmetrical polygons) are centrally positioned in the ring. Only a limited number of different regular convex polygons with their sides being tangential can be created with chords being tangents to a defined number of circles. Striped lines in figure 5.15 show an example of two neighboured circles with the radii r_A, r_S and the distance d_R between them. Centrally positioned cylinders (symmetrical polygons) between these circles can not be described there are no chords available. The resulting error for volume and axis determination is dependent on the number of transmitters and receivers.

For alternately arranged transmitters and receivers, the number of these polygons or rings is equal to half the number of transmitters or receivers. The number of sides of each polygon is the number of transmitters or receivers.

In the following chapters using 3-D, simulations and statistics are used to get an overview of the accuracy and errors created by different factors. Factors are volume, length of major/minor axis with and without error corrections for various test shapes.

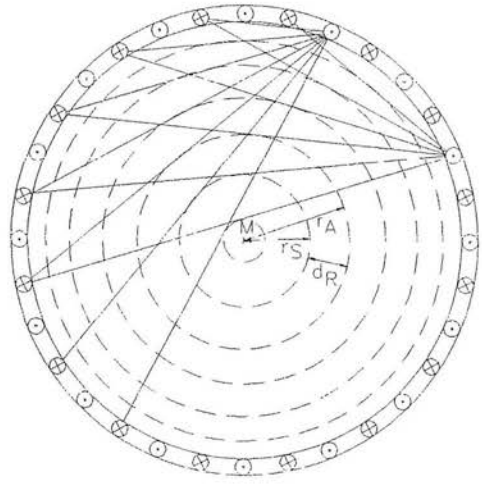

Figure 5.15. Possible chords from a transmitter to the receivers (2 snapshots)

5.2.3. Accuracy of volume of spheres using the 'back' chord

Simulated spheres of 14 different radii between 10mm and 70mm were chosen to investigate the possible accuracy of volume and axis determination of the 'back' chord spiral.

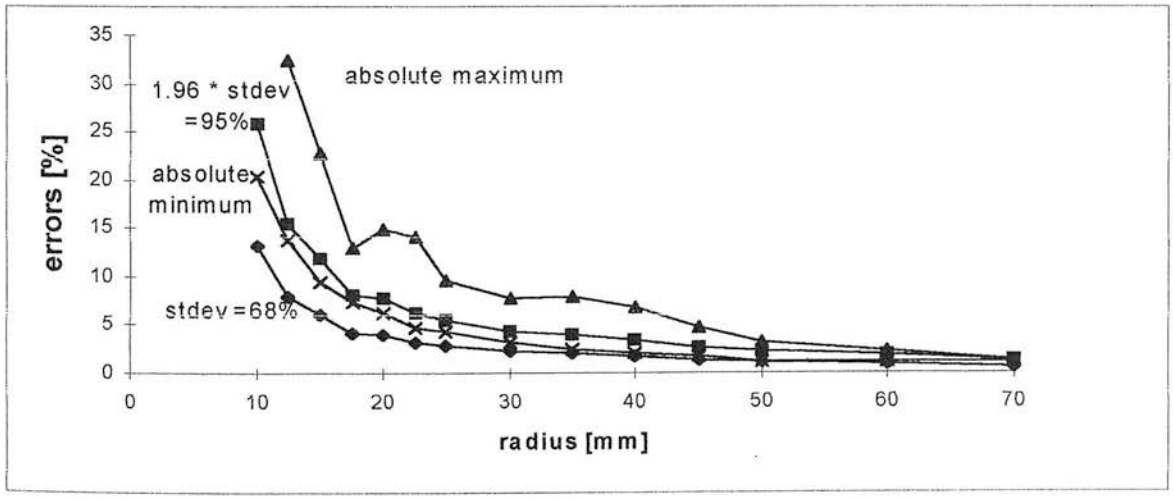

Figure 5.16. Errors in the volume determination of spheres

In figure 5.16 the absolute maximum and minimum values, the standard deviation, stdev, and the 95% line which is equal to 1.96 stdev are shown. The results show that for spheres in the practical range of interest between 17.5 and 30mm, 95% of all measurements have a random error less than 10%. For spheres with a radius between 35 and 70mm the error is better than 5%. However for a radius of less than 17.5 mm the error increases substantially.

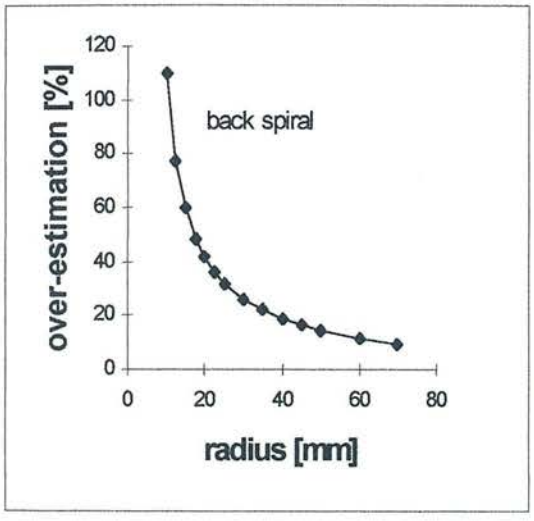

Figure 5.17. Over-estimation of the average measured volume from the real volume

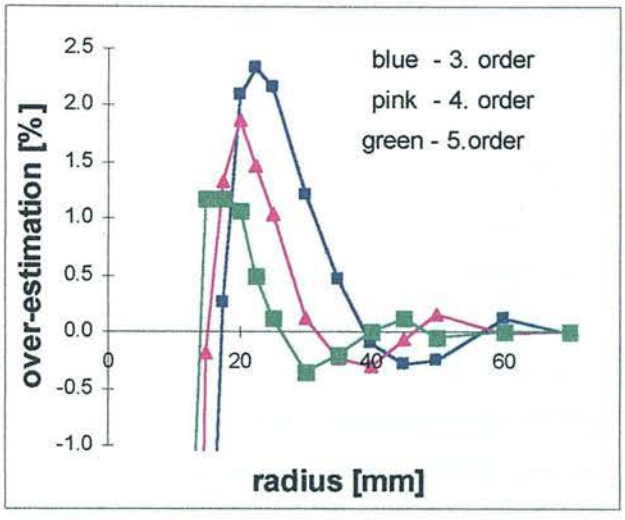

Figure 5.18. Corrected over-estimation of the average measured volume using regression

In figure 5.17, the over-estimation or systematic error of the technique is shown. The error for the corrected volume V_{C_MEAS} can be minimised by using the measured volume V_{MEAS}, the regression factors k_X (see table 5.1) and the regression formula

$$V_{C\_MEAS} = k5\ V_{MEAS}^{5} + k4\ V_{MEAS}^{4} + k3\ V_{MEAS}^{3} + k2\ V_{MEAS}^{2} + k1\ V_{MEAS} + k \qquad (5.5)$$

Order	k	k1	k2	k3	k4	k5
3.	-5.08	0.823	$1.108\ 10^{-4}$	$-3.345\ 10^{-8}$	0	0
4.	-3.92	0.791	$2.335\ 10^{-4}$	$-1.753\ 10^{-7}$	$4.85\ 10^{-11}$	0
5.	-3.1	0.759	$4.639\ 10^{-4}$	$-7.195\ 10^{-7}$	$5.41\ 10^{-10}$	$-1.47\ 10^{-13}$

Table 5.1. Factors for the regressions 3. - 5. order

After the correction using the regression function of the fifth order the results (see figure 5.18) show that for the parameters used for the simulation, the radius of the object should be a minimum of 15mm. The final error for objects smaller than 25mm is about 1%. In practice this scheme may be more efficiently implemented as a look-up table.

5.2.4. Comparison of use of 'back' and/or 'front' spiral for volume determination

In this test the results of the 'back', the 'front' and the combination of the two spirals are investigated using exactly the same random numbers for all cases. The combination of 'front' and 'back' spiral was carried out by taking each single result for an object and creating the average. As shown in chapter 3.6, the 'back' and 'front' spiral are in different locations round an object. The measurements are taken at the same time, but at a different point on the surface. If both volumes are independent measurements of the same accuracy $\sigma 1$ and $\sigma 2$, the theory of propagation of error (Gellert 1971) can be applied with the result that the middle error σ_M is

$$\sigma_M = \frac{1}{2}\sqrt{\sigma 1^2 + \sigma 2^2} = \frac{\sigma 1}{\sqrt{2}} = 0.7071\sigma 1$$

A reduction of the deviation error of 29.3 % of the single error of each passage of an object can be expected compared with the result using only one spiral.

The results of the simulations in figure 5.19 show that the expected reduction in error does not occur. This is because the precision for the 'back' and the 'front' spiral are similar but not the same. The reason for the small difference in the accuracy between 'back' and 'front' spiral could not be found. The independence of measurements of each spiral seems not to be given. This has to be investigated in the future.

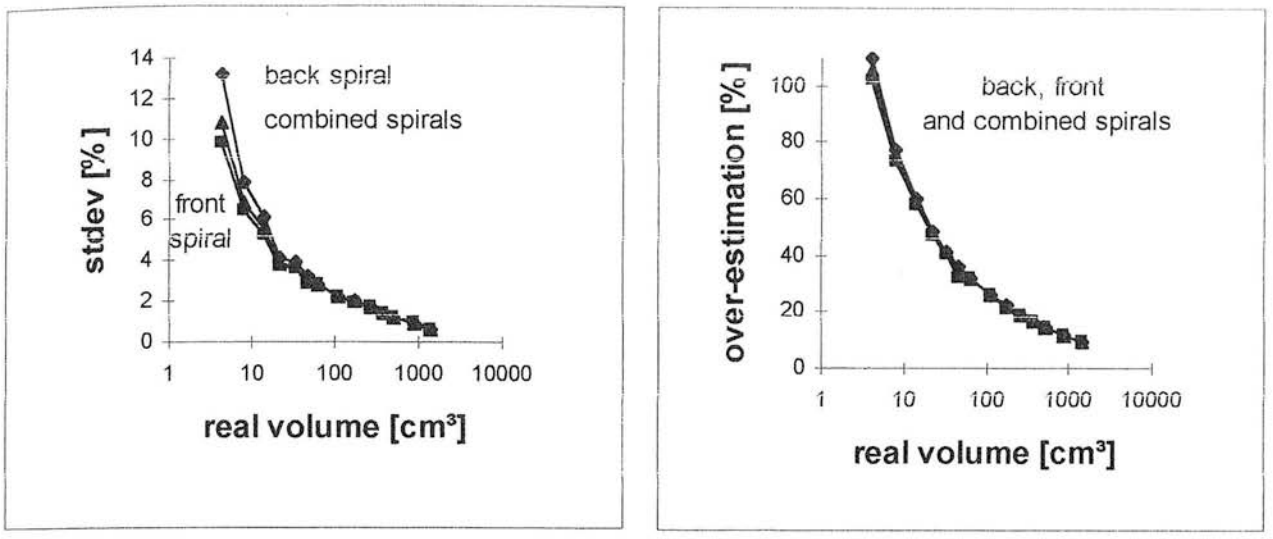

a) Standard deviation b) Over-estimation

Figure 5.19. Comparison of use of 'back' and 'front' spiral for volume determination

The over-estimation for all three variants is the same, so that the analysis from the chapter before can be used for all.

5.2.5. Major axes of cross-sections

The same test as described above for the 'back' spiral was used to investigate the largest slice and the middle slice. The largest slice is positioned at the largest diameter of the object in the vertical direction. The major axis is the largest axis of this slice. For spheres, the largest slice should be the middle slice.

One fundamental problem has first to be addressed regarding the use of algorithms for the determination of axes (see also chapter 4.2).

1. One possibility is to find and measure the distance from each chord to the opposite chord (if it is parallel) or vertex (see chapter 4.2). The determined distance can include a systematic error (see figure 5.20.a), but for 'nearly' round objects and a high resolution this method should be accurate enough.
2. The largest major axis can only be between two vertices. For this reason the second method and preferred solution is the investigation of the distance from one vertex of a chord to an opposite vertex.
3. Minor axes can be between parallels, a chord and a vertex or two vertices. That and a

limited resolution of the system can cause a problem for minor axes as shown in figure 5.20.b. Because of this, both algorithms will be independently tested. For minor axes the determination of parallels is always allowed.

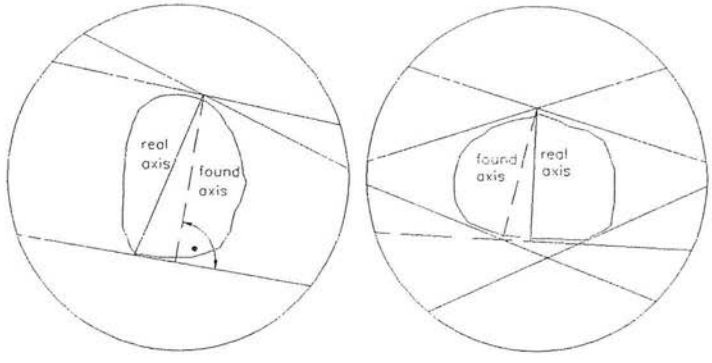

a) One vertex b) Two vertices

Figure 5.20. Problems with the determination of axes

In figure 5.21 the results for the standard deviation are shown, and are similar for both cases so that only the 'back' chords will be used for the investigations into the over-estimation of the middle and largest slice (see figure 5.22). Because the results are similar they can be corrected by using the polynomial regression (see equation 5.5 and table 5.2) of third order. The result shows that the final over-estimation is less ±1%.

	k	k1	k2	k3
Major axes of slices	5.48	0.914	$9.324\ 10^{-4}$	$-2.67\ 10^{-6}$

Table 5.2. Factor for the triple regression of major axes

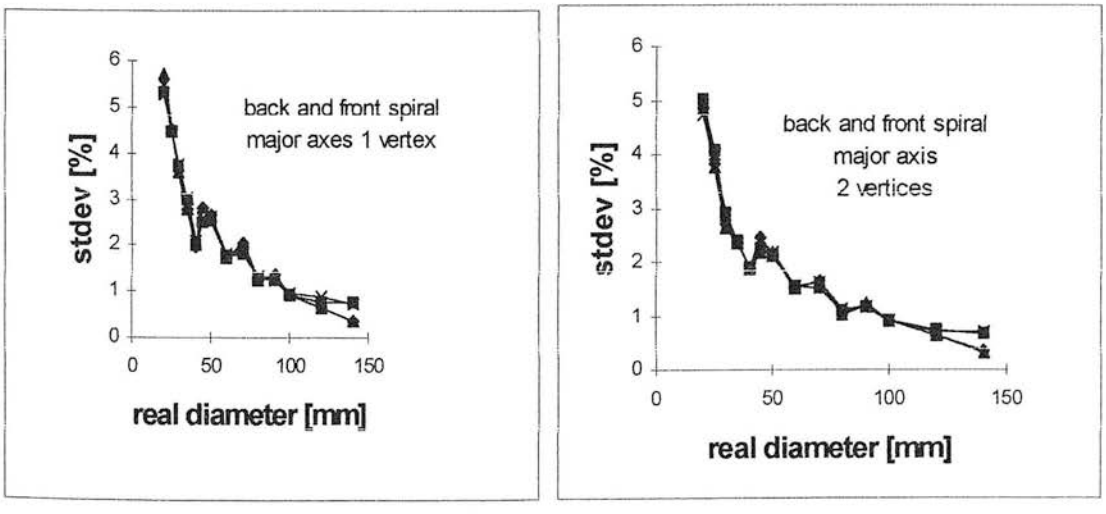

a) Use of one vertex opposite a line b) Use of two vertices at opposite side

Figure 5.21. Standard deviation of the major axes using 1 or 2 vertices

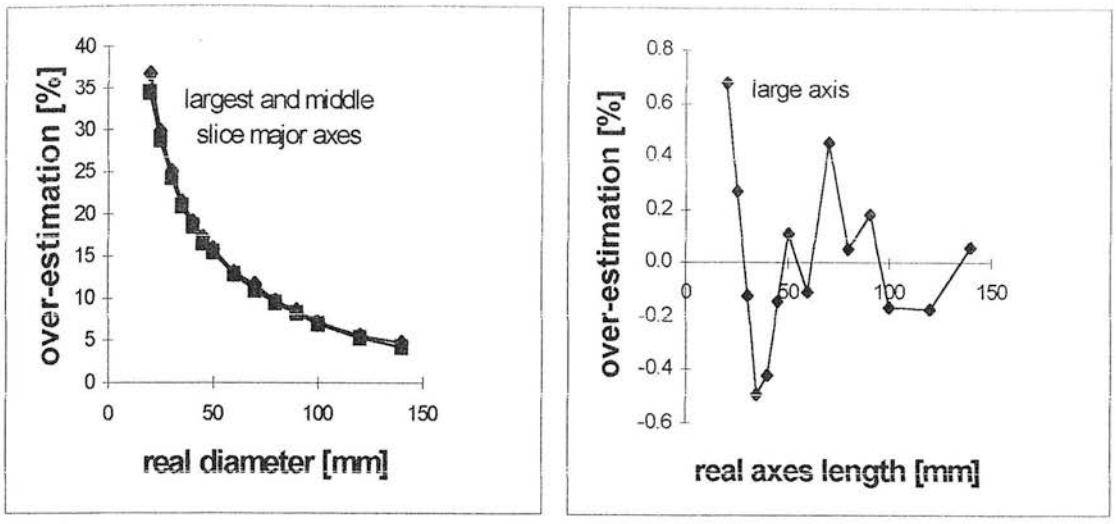

a) Over-estimation b) Corrected over-estimation

Figure 5.22. Over-estimation for the major axes before and after correction

5.2.6. Minor axes of cross-sections

The smallest diameter is found by checking the enveloping spiral a turn 'back' and forward. For the largest slice the larger of both axes is wanted .

As with the major axes, the one and two vertices solution will be investigated. In figure 5.23 it can be seen that the random error is significantly lower for the use of 2 vertices, due to the error (see figure 5.20.a) being avoided.

In figure 5.24, the over-estimation and the corrected over-estimation for the largest and the middle slice can be seen. To correct the over-estimation the polynomial regression (see equation 5.5) of third order was used. The results show that the final over-estimation is less than ±1.5%.

For objects like a sphere or an ellipsoid, a distinction between the middle and the largest slice is necessary since the largest slice is defined on the first discovery of the largest diameter, but is not necessarily combined with the largest minor axis. For the sphere this means that the actual largest slice is the middle slice. Some thought will be given to amending the algorithms to cope with this situation.

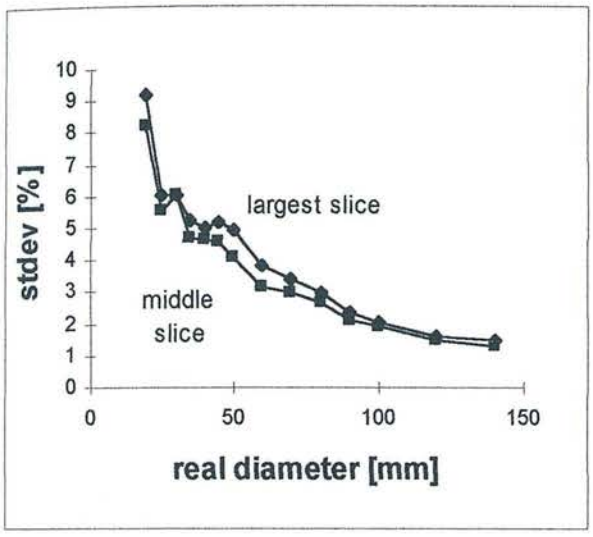

a) One vertex

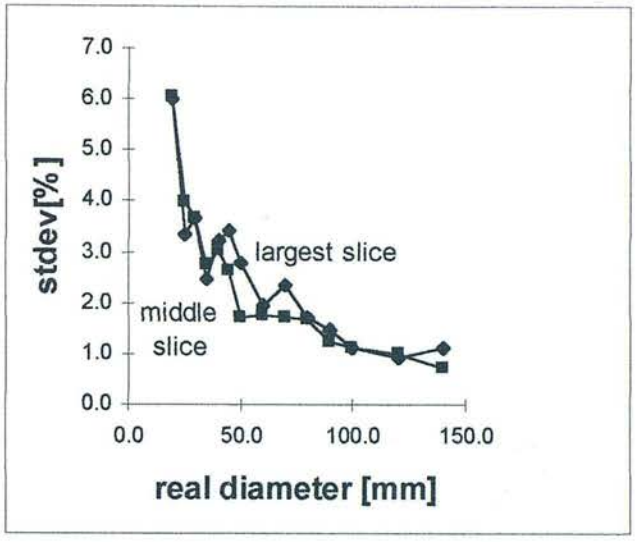

b) Two vertices

Figure 5.23. Standard deviation of the minor axes of the 'back' chord

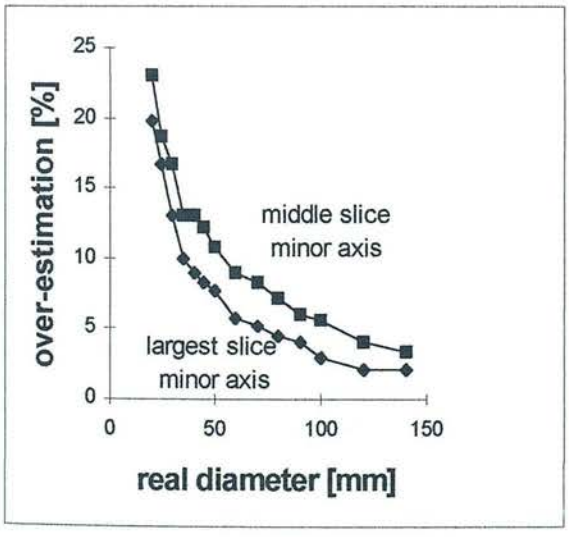

a) Over-estimation

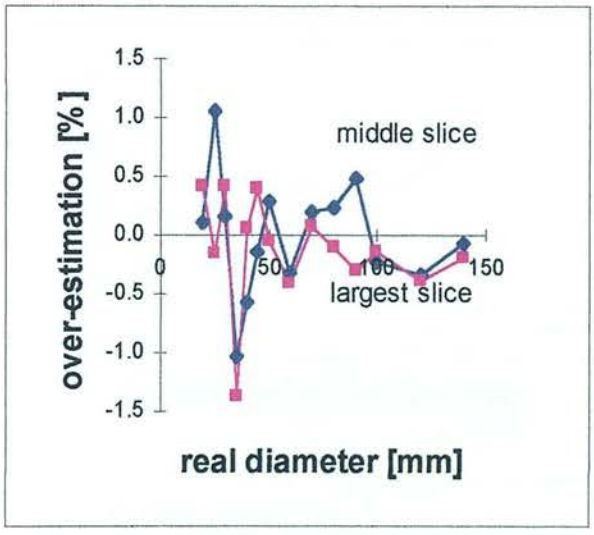

b) Corrected over-estimation

Figure 5.24. Over-estimation of minor axes before and after correction

Minor axes	k	k1	k2	k3
Largest slice	3.88	0.992	$2.7\ 10^{-4}$	$-1.199\ 10^{-6}$
Middle slice	-3.32	0.942	$3.572\ 10^{-4}$	$-2.493\ 10^{-7}$

Table 5.3. Factors for the triple regression of minor axes

For further tests, only the distance between 2 vertices will be used because the error is lower.

5.2.7. Position of the largest slice

One parameter of interest is the position of the largest cross-section of an object in the horizontal direction. It gives information about the shape (for example misshapen potatoes). Figure 5.25 shows that the standard deviation decreases rapidly with the increase of the radius. The over-estimation is permanent. One reason is explained in chapter 5.2.5 searching for the right axis. Another factor is the resolution of the system and the small changes in size of the cross-section around the midpoint of a sphere.

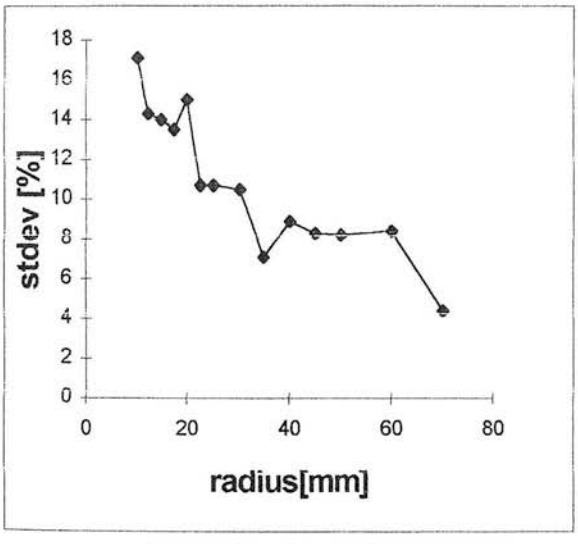

a) Standard deviation

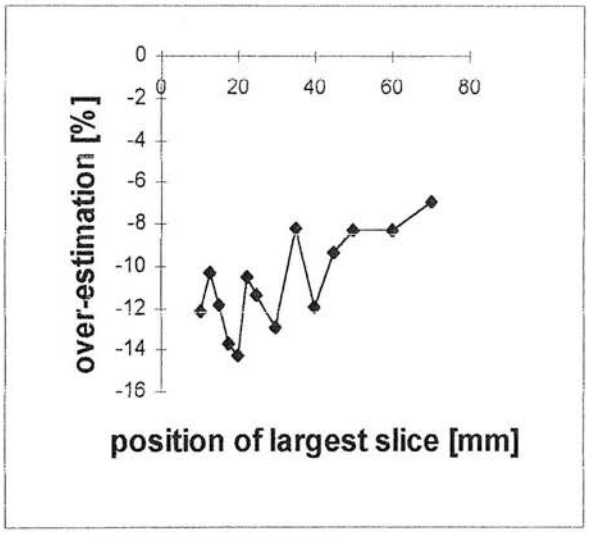

b) Over-estimation

Figure 5.25. Position of the largest slice

As shown in chapter 5.2.2, it concentrates on centred objects with a round cross-section, there are discrete steps for an accurate determination of the surface of objects in vertical direction depending on the resolution of the system.

5.2.8. The accuracy dependence on the position in the ring

In this test the determination of volume and the largest axis of spheres with a radius of 20, 30 and 40mm are investigated with reference to the distance from the midpoint of the sensor ring. Each object was simulated 1000 times in distance classes with steps of 5mm. Sensor systems with an equal number of alternately arranged transmitters and receivers (TE) have been investigated, with TE = N_T = N_R of 64 and 256.

The results for the volume (see figure 5.26) show that in the middle of the ring a higher over-estimation is obtained. This is caused by a lower number of intersections (see chapter 6.1) giving a lower resolution in the middle of the system. The standard deviation is relatively low, but increases quickly for small objects in the outer regions.

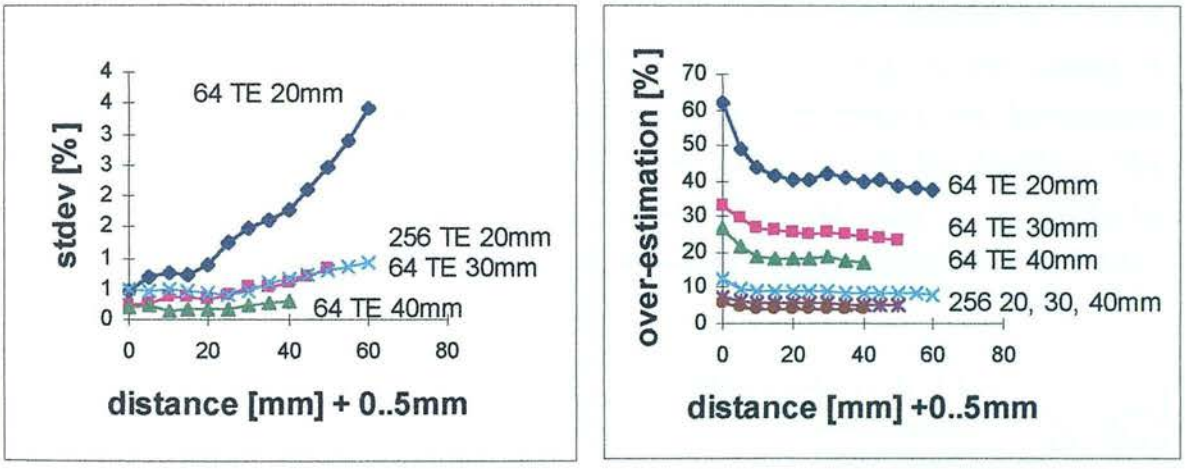

a) Standard deviation b) Over-estimation

Figure 5.26. Volume at different distances from the midpoint of the sensor system

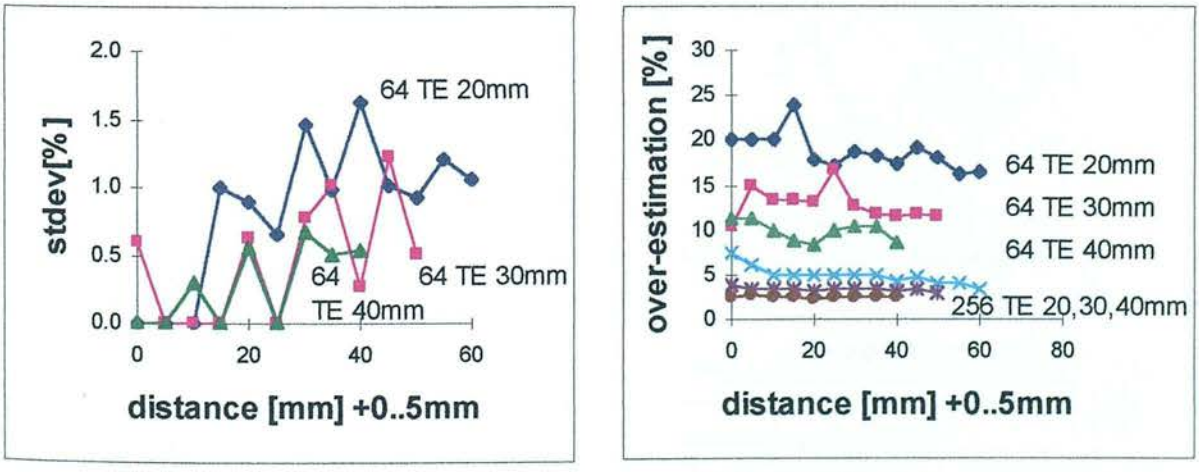

a) Standard deviation b) Over-estimation

Figure 5.27. Major axis at different distances from the midpoint of the sensor system

The investigation of the major axis of the largest slices (see figure 5.27) shows that the over-estimation is relatively constant in the different regions. The standard deviation is relatively low and increasing in the outside regions especially for small objects.

One further fact can be seen in figure 5.27.b. The deviations in the curves of the 64 transmitter solution are caused by the resolution. Different diameters of objects deliver different faults. This effect can also be seen in figures 5.21 and 5.25.a, but is improved with the higher resolution from 256 transmitters and receivers.

5.2.9. The effect of the resolution of the system on the accuracy

In this test the resolution of a different number of transmitters and receivers on volume measurements of spheres was investigated (see figure 5.28). Doubling the number of transmitters and receivers improves the standard deviation by about a half for medium sized spheres. The over-estimation is also cut by about 2 with the doubling. The investigation for the major axis of the largest slice gives the same improvement by cutting the errors by about 2 through doubling the number of transmitters and receivers.

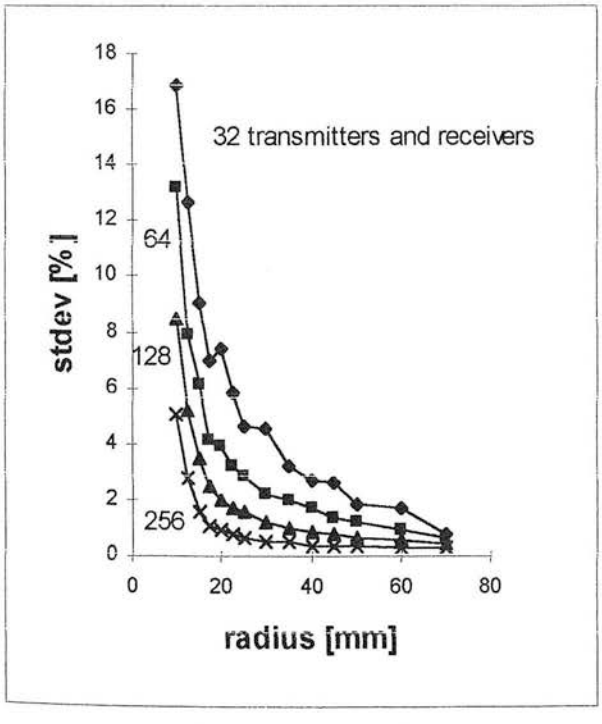

a) Standard deviation

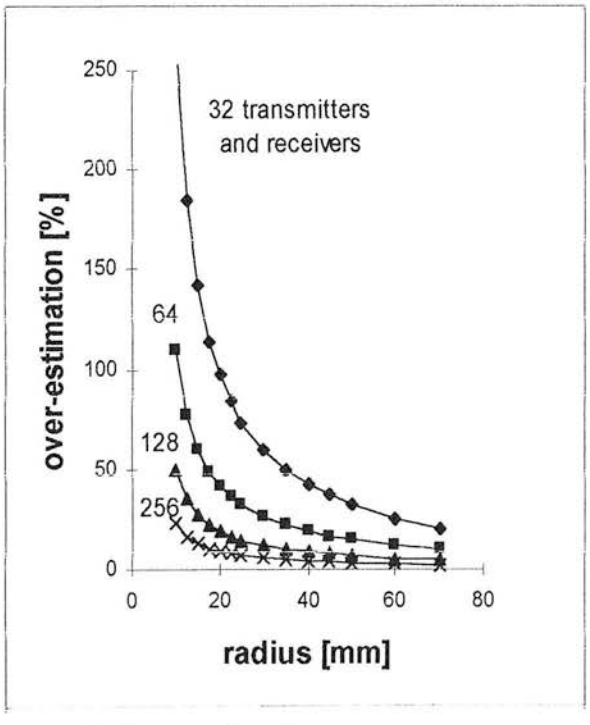

b) Over-estimation

Figure 5.28. Volume of spheres depending on the resolution (number of transmitters and receivers)

5.2.10. The effect of the speed of the ring or the object on the accuracy

In this test the speed was varied in the range of 200 up to 1000 revolutions per second. This has the same effect as changing the speed of the object. The following is the list of equivalents of revolutions and speed valid for this test.

Speed ring [rev/s]	200	400	600	800	1000
Speed object [m/s]	2	1	0.66	0.5	0.4

Table 5.4. List of equivalents of scanning rate and speed of object

The results for the volume of spheres (see figure 5.29) show that the standard deviation will not be efficiently reduced by the increase of the speed of the ring or by the decrease in speed of the objects. The over-estimation is nearly constant for all speeds, except the 200 rev/s test for small objects.

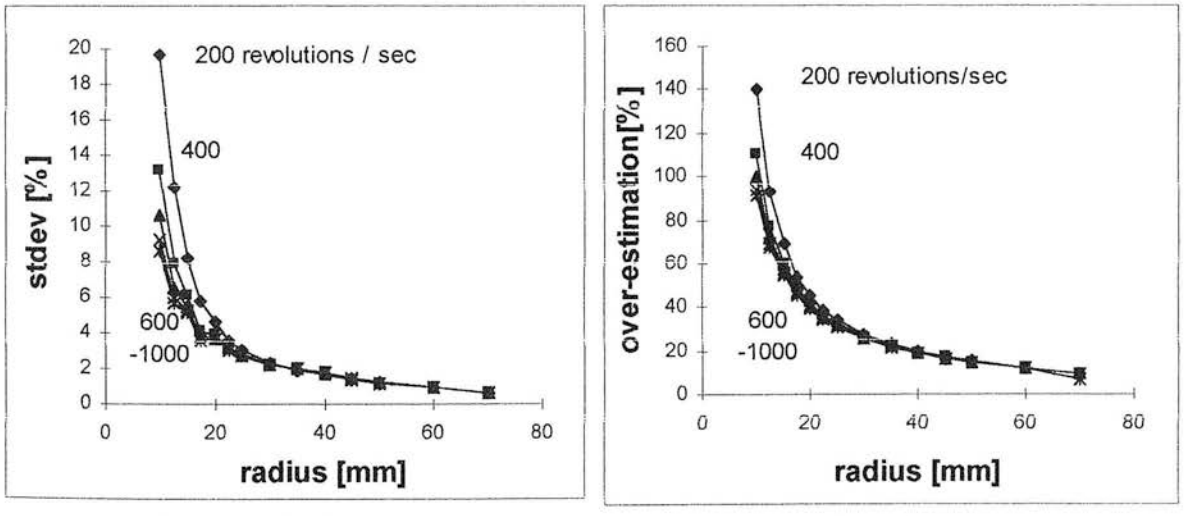

a) Standard deviation b) Over-estimation

Figure 5.29. Volume of spheres dependent on the speed of the ring

The results for the major axis (see figure 5.30) of the largest slice measurement show an independence from the speed, so it can be said that for the determination of axis measurements for spheres and ellipsoids the speed is not an issue. The results correspond with the results for the use of two spirals (see chapter 5.2.4). If the speed is doubled, the conditions are similar to comparing the use of two spirals.

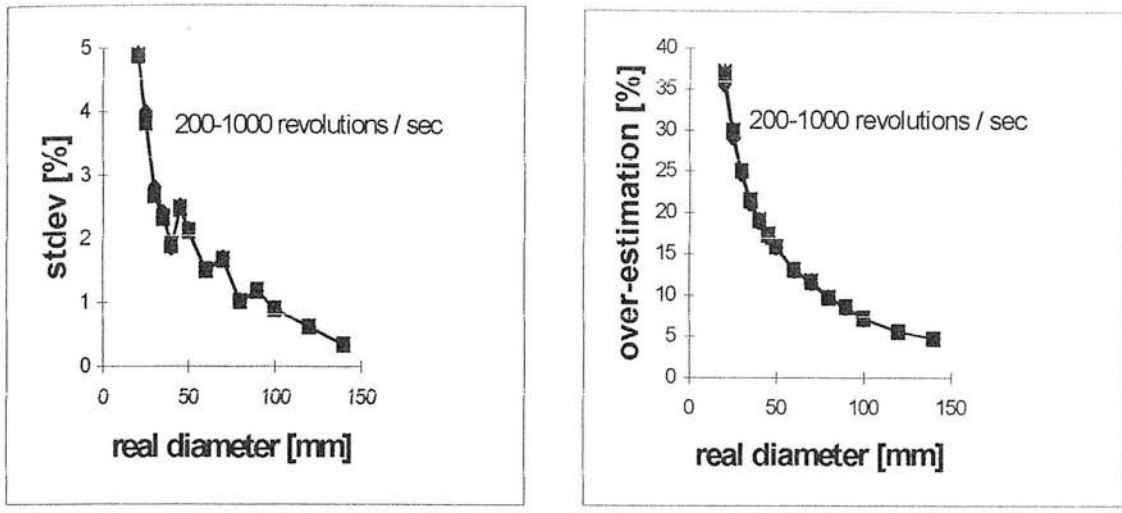

a) Standard deviation b) Over-estimation

Figure 5.30. Major axis dependent on the speed

5.2.11. The accuracy depending on the shape of cross-sections

In this test the influence of shape of cross-sections was investigated. The objects chosen have different cross-sectional shapes (see figure 5.14), but each had the same length of 100mm with a constant cross-section over the whole length. The radii were varied, so that a range of volumes and the major axis of the middle slice could be investigated.

The results for the volume (see figure 5.31) show that the over-estimation does depend on the shape. An object with a cross-sectional shape of a polygon with 3 vertices has about double the over-estimation error of an ellipse shape. The standard deviation is quite similar for all objects, but increases substantially with a small size. Not included in figure 5.31 is the result for 'thin polygons' with two vertices and a volume of zero, because the error is too high.

Because of the constant shape of the cross-sections about the whole length of the investigated objects, the results are also valid for the 2-D case.

For the major axis of the middle slice (see figure 5.32) objects with cross-sections of nearly round shapes have about 50% higher over-estimation than angular objects. This is due to the problem of low resolution on round objects as described in chapters 5.2.2 and 6.1. The standard deviation is relatively low and decreases with the increase in the volume.

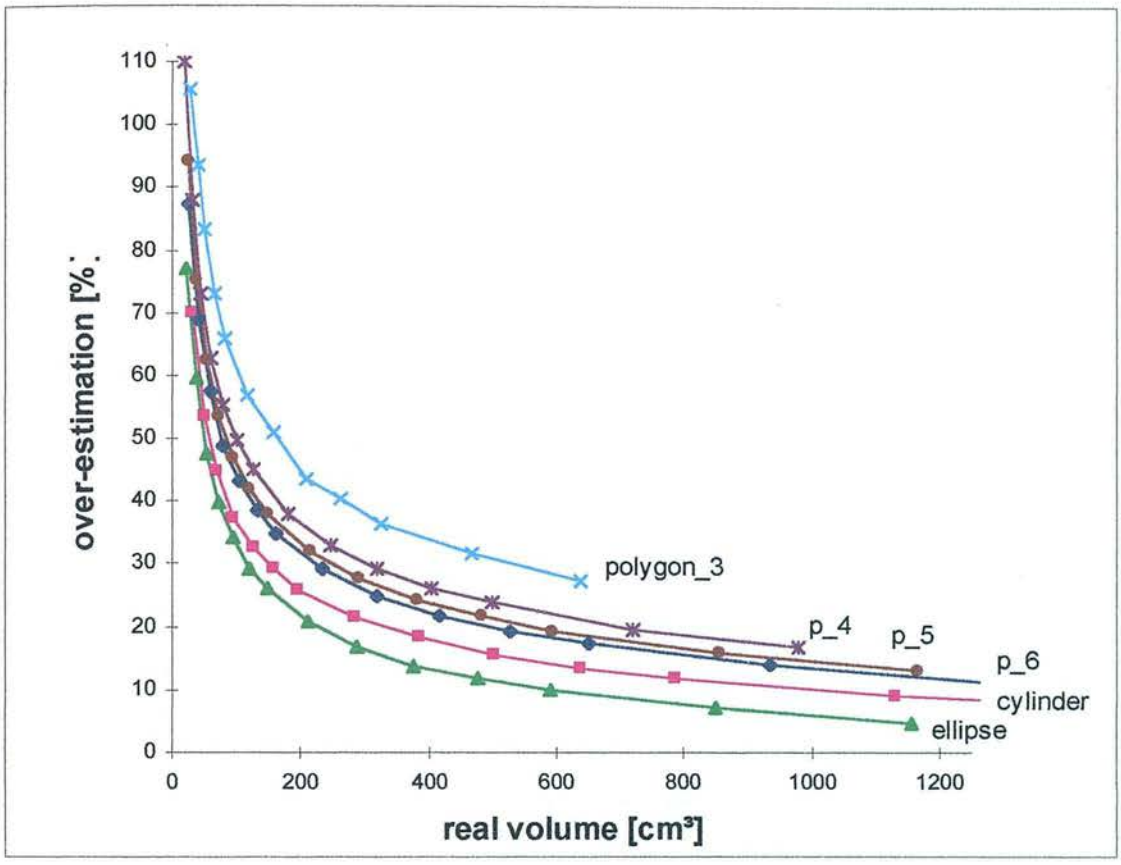

a) Over-estimation

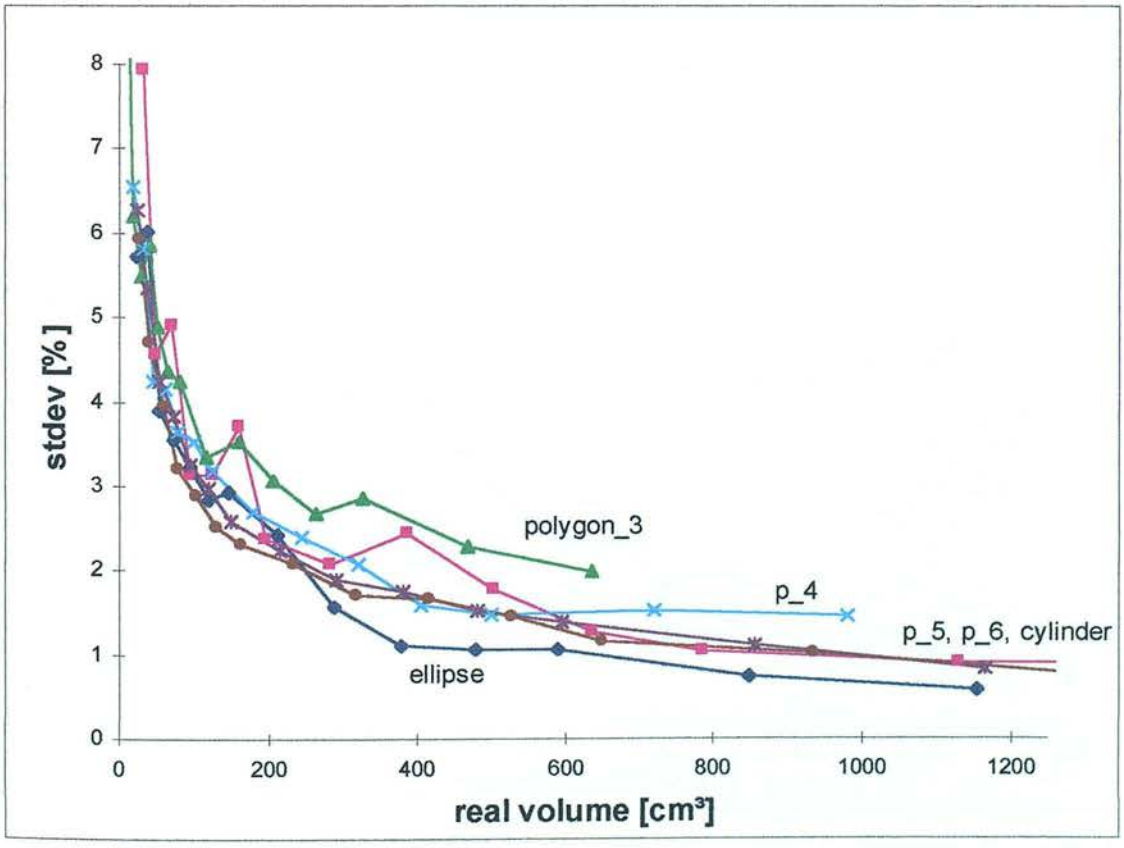

b) Standard deviation

Figure 5.31. Volume dependent on the shape of cross-sections

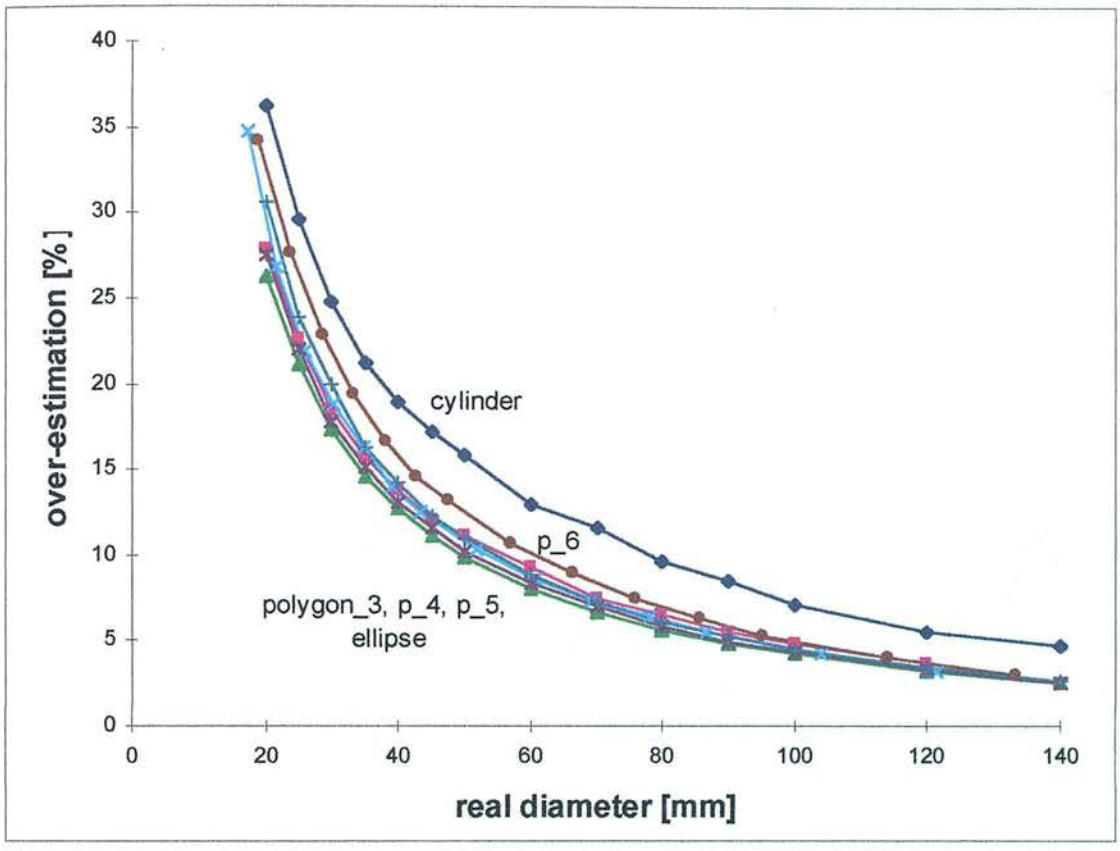

a) Over-estimation

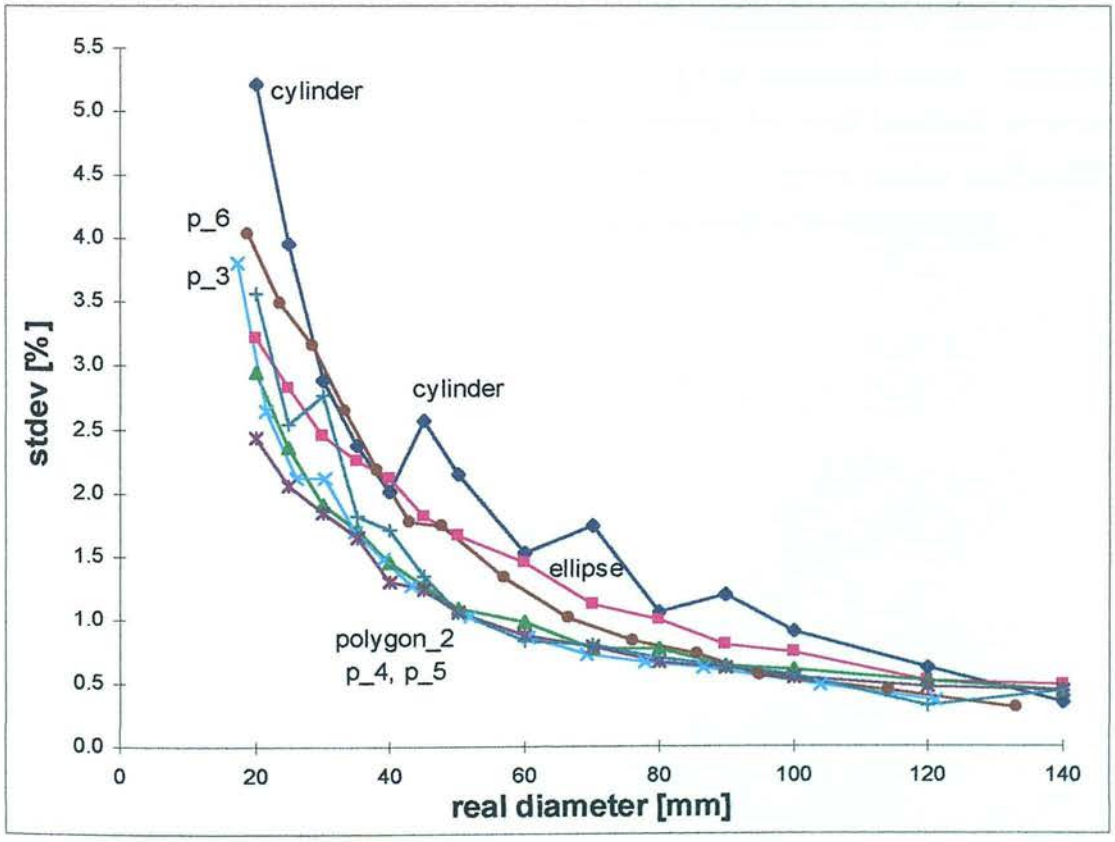

b) Standard deviation

Figure 5.32. Middle axis on different shaped cross-sections

Overall the shape has an influence. So far as the shape of objects is approximately known, the systematic error can be estimated and be kept under control. Another method is to increase the resolution as necessary for the particular use.

5.3. Summary

A model to create one object or cross-section at a time in the ring is described. The positions and shapes of objects are variable within the limits set by the ring. Tests were carried out to find the limits using comprehensive simulations of different objects, for instance in different areas of the sensor system, different arrangements, speed variation of the sensor system and using the 'back' and 'front' spiral to envelope objects. The system properties were formed flexibly in wide ranges, but require design and adaptation to the specific task.

Under the expected practical use with the expected parameters (see chapter 2.7) the set-up for a practical solution should have at minimum 64 transmitters and 64 receivers (see chapters 5.2.1, 7.1). For practical use the objects should be presented singly lengthways and not have major concave areas in the cross-sections. For crop handling, potatoes, cucumber and carrots are suitable in shape. Products such as onions, apples and bananas cause problems of presentation, concave areas and as a result a lower accuracy.

6. Other properties related to the sensor system

In this chapter some interesting accompanying properties of the system shall be investigated which are not directly related to the mathematics and type of algorithms necessary to determine the geometry of objects.

6.1. Number of intersections

An object can only be detected if at least one possible chord in a snapshot is not detected (excluding the chords between a transmitter and its two immediate neighbour receivers). In this case it can be said that all objects are enveloped by chords which intercept each other. There are four possible positions for an object around two chords (see figure 6.1.a). If a third chord intersects, twelve different positions are possible (see figure 6.1.b). This is also valid, even if the three chords intersect at one point.

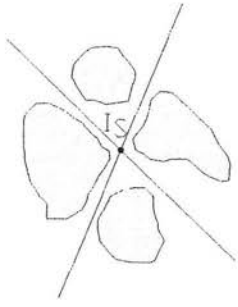

a) Possible positions of an object around an intersection

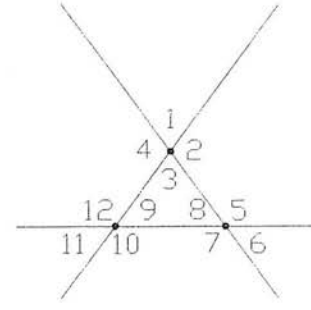

b) Possible positions around three intersections

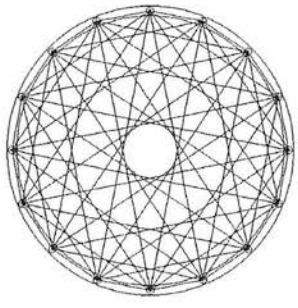

c) Intersections with 8 transmitters and receivers

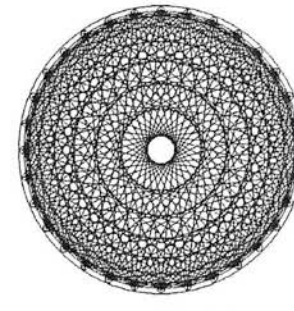

d) Intersections with 16 transmitters and receivers

Figure 6.1 Intersections in the ring

This means that the possible number N_I of intersections (see figure 6.1.c,d and 6.2) multiplied by 4 gives the value N_P, describing all possible positions of a part of an object in the ring. The functions for a ring with the same number of transmitters N_T and receivers N_R and $N_T > 2$ are

$$N_I = \frac{1}{2} N_T \sum_{i=3}^{i=N_T} (i-1)(i-2)$$

$$N_P = N_I * 4$$

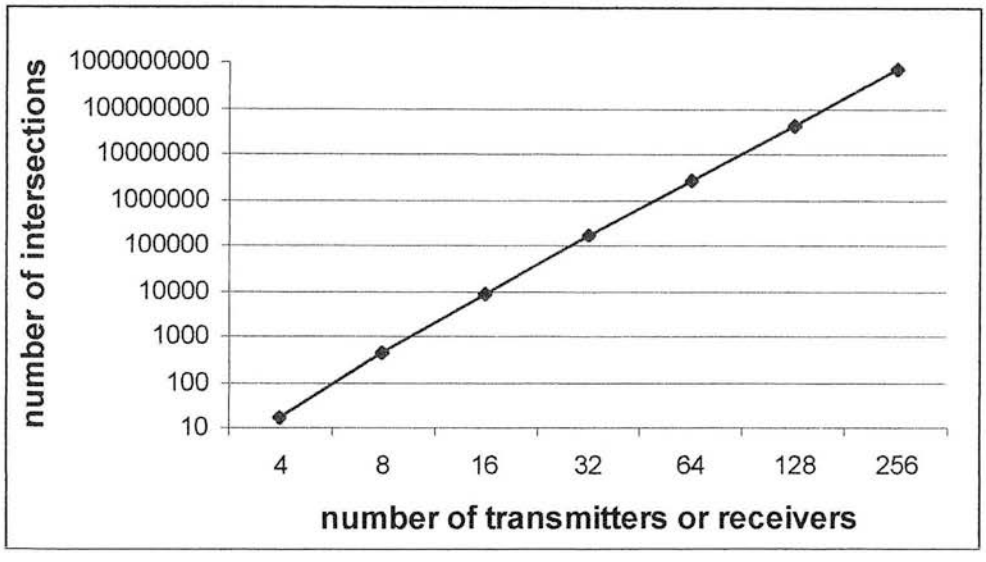

Figure 6.2. Numbers of intersections N_I in a ring

Because the chords lie closer together near the outside of the ring, more intersections are found there. This is why larger objects can be measured with a higher accuracy.

6.2. The amount of data and structure

Consider first the 'basic' picture which consists of the result of each snapshot (see figure 3.1). The transmitters are activated one by one. The snapshots can be numbered by a positive increasing integer number n. This number can be used to address a linear memory space in the computer.

A result of one snapshot using only the 'back' chord is one variable $m_B[n]$, the distance between the transmitter and the receiver, which will be stored in the memory. The necessary width in bits w_{BIT} for coding distance between transmitter and receiver is

$$w_{BIT} = \log_2 (N_R).$$

The width up to 256 receivers are preferably coded in a byte, although for a ring with 64 receivers with $w_{BIT} = 6$ there are only 6 bits required. The total number of bytes for one object with a system up to 256 receivers and each snapshot coded in a byte is calculated from the number of snapshots N_{OBJ} and the number of counted revolutions of the sensor N_{REV}

$$N_{OBJ} = N_{REV} * N_T$$

For a ring consisting of $N_T = 64$ transmitters and $N_R = 64$ receivers only 64 Bytes are necessary to describe a whole revolution and a cross-section. In the 3-D space that means for an object with a length of $N_{REV} = 23.5$ rounds, a total number of 1504 snapshots which are stored as primary data in the memory in the array Z0 (see chapter 3.1, 5.1.2, 6.3, 10.7).

$$Z0 = [m_B[0], m_B[1], m_B[2], m_B[3],... m_B[N_{OBJ}]]$$

In the case the 'front' chord is also used (see chapter 3.6, 5.2.4) the data are stored in

$$Z1 = [m_F[0], m_F[1], m_F[2], m_F[3],... m_F[N_{OBJ}]]$$

The 'basic' picture of the whole scene includes all necessary information to describe the object in the form of components of vectors, but also contains superfluous information about chords not part of the envelope (for pixel images 80-90% of data processed are redundant McEntee (1996)). The contour tracking algorithm (see chapters 3.2-3.5) excludes the redundant chords. As a result the structure of remaining data is different and linked to the future use as for example for the determination of volume and axis measurements and graphics (see also chapter 6.5). A compromise between minimised memory use and the choice of mathematical algorithms is recommended. Practical use results in i_{OBJ} remaining snapshots with data stored in arrays including the number of each remaining snapshot FCHN = n[i], the related distance of the receiver FCHM = m[n[i]] and the distance FCHR = $|T_A:C_P[n[i]]|$ (see table 6.1, chapter 10.7).

i	FCHN[i]	FCHM[i]	FCHR[i]
1	0	$m_B[0]$	$\|T_A:C_P[0]\|$
2	1	$m_B[1]$	$\|T_A:C_P[1]\|$
3	2	$m_B[2]$	$\|T_A:C_P[2]\|$
4	5	$m_B[5]$	$\|T_A:C_P[5]\|$
5	7	$m_B[7]$	$\|T_A:C_P[7]\|$
...			
i	n	$m_B[n]$	$\|T_A:C_P[n]\|$
i_{OBJ}	N_{OBJ}	$m_B[N_{OBJ}]$	$\|T_A:C_P[N_{OBJ}]\|$

Table 6.1. Data of remaining chords after processing

The amount of data in these arrays depends on the form of the object. The worst case is when the object is a cylinder positioned in the centre of the ring. Using 16 bit integer values for the variables n and for the distances $|T_A:C_P[n]|$ and a byte for $m_B[n]$ the total number would be N * 5 Bytes. Looking at the earlier example 7520 Bytes have to be stored. The amount of data has increased compared with the 'basic' picture, but it is still small for the description of an object in 3-D space.

6.3. Differential coding of primary data

For a cylinder passing centrally through the ring the description is simple. Only two numbers, n for the position in the horizontal direction of passage and $m_B[n]$ for the chord are needed.

There is always a way 'around' each object. Each object passing through the ring system can be put into a cylinder, which is again a part of the cylinder built up by the ring sensor system itself (see figure 3.10).

If the shape of the object becomes little different, the changes between two neighbouring snapshots caused by shape and position of the object in the ring during the enveloping

process are relatively small. Observing the primary data, the changes between the actual measured value of the transmitter $m_B[n]$, its predecessor $m_B[n-1]$ and successor $m_B[n+1]$ are mostly on the least significant bit, that is, +1, -1, or 0 if there is no change. Also on 'misshapen' objects the majority of changes from one snapshot to the next are minimal. As said, the ideal is a centrally positioned cylinder with no change over the whole object. The first differential is always 0.

This is the reason to recommend the use of differential coding for storage and transfer of data. Based on the assumption that with up to 256 receivers only one byte is needed per snapshot, the change between snapshot n+1 and snapshot n with $m_B[n+1] - m_B[n]$ is coded into a reduced number of bits (see table 6.2). The remaining data are sequentially lined up, then split into Byte format for storage.

Difference = $m_B[n+1] - m_B[n]$	0	-1	1	2	all other
number of bits used for coding	1	3	3	3	3+w_{BIT} (for 64 receivers 3+6)
code (binary)	0	100	101	110	111 + whole value

Table 6.2. Differential coding

Although for sudden big changes one additional bit is necessary, an overall compression of primary data down to 12-30% is possible depending on the size and shape (see figures 6.3).

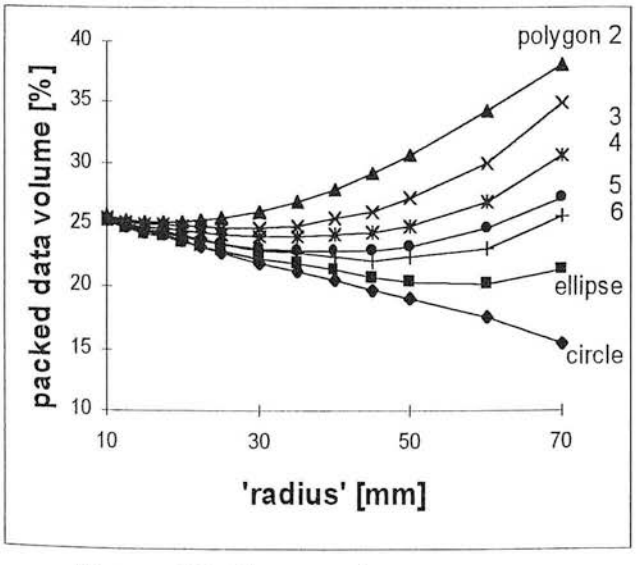

Figure 6.3. Compression

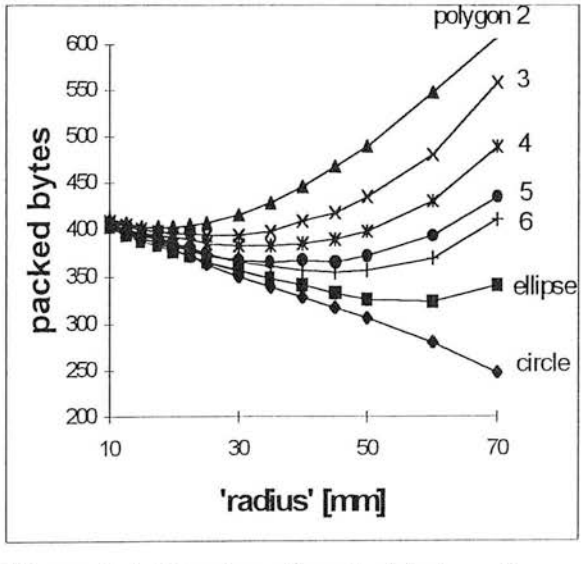

Figure 6.4. Number of packed bytes of 100mm long objects with different cross-sections enclosed by 25 helices

Some simulations have been carried out using the same objects of different shape in different positions of the ring as investigated in chapter 5.2.11. They are all described originally by 25 revolutions which gives 1600 bytes. Figure 6.3 and 6.4 show the percentage of compression and the number of bytes left after differential coding.

In figures 6.5 and 6.6 results are shown only for spheres as known from former tests (see chapter 5.2.3). The reason for the level and course of the standard deviation is

1. the immediate increase in the difference between two neighboured chords for small diameters on the enveloping spiral.
2. the relatively wide range of positions of small size objects in the ring up to a fixed position for the maximal diameter.

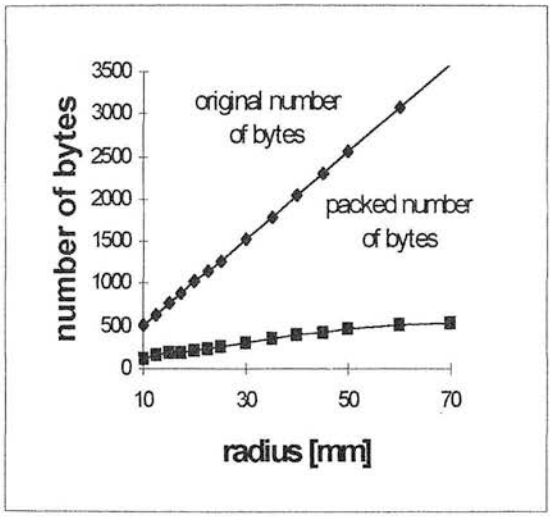

Figure 6.5. Number of bytes to describe a sphere with a radius between 10 and 70mm

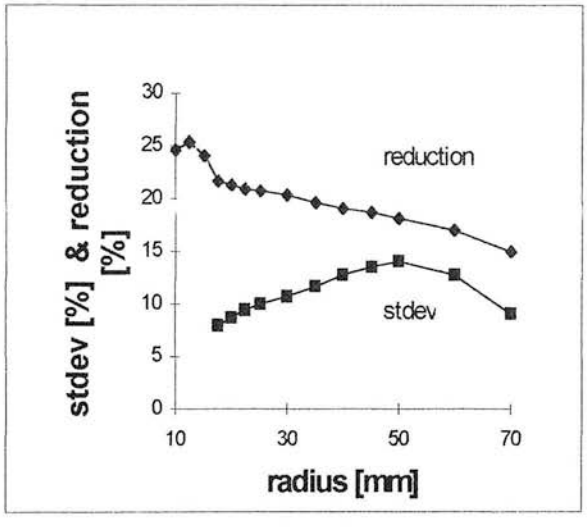

Figure 6.6. Standard deviation and data reduction of spheres

The advantage of differential coding of original data can be seen. This can be used for minimising data for transfer and storage. So far no other method is known which can include such flexible complex objects within so small an amount of primary data in 3-D space immediately after the scan.

6.4. Time consumption of main algorithms

There follows a short review of the time conditions for the computation. The time for the investigation of one chord includes the execution of all instructions carrying out case1-3 (see chapter 3.2.2) for the investigation of a present actual chord. The process

time for this part of the program is constant so long as the object is a cylinder in the centre of the ring, because case3 (see chapter 3.2.2) will not be repeated at the same actual chord. The worse case will be an object with a cross-section of a rectangle or triangle with a very thin side (e.g. piece of paper) with only three chords describing the convex hull during a revolution. The best, case3, will only take place N_T - 3 times in the cross-sectional 2-D area or in a 3-D spiral in one revolution. With the times t[case1], t[case2], t[case3] required for each case 1-3 the minimal total time t_{CMIN} is

$$t_{CMIN} = t\,[case1] + t[case2] + t[case3]$$

and the total time for a cross-section t_{TOT2D} is

circle	:	$t_{TOT2D} = N_T\, t_{CMIN}$
⇓		⇓
all other objects	:	t_{TOT2D}
⇓		⇓
thin rectangle or triangle	:	$t_{TOT2D} = N_T\,(t_{CMIN} + t[case3]) - 3\,t[case3]$

The total time t_{TOT3D} for the determination of a 3-D object with the total number of snapshots N_{OBJ} is

$$t_{TOT3D} = N_{OBJ}\ t_{CTOT2D} / N_T$$

and varies between the minimum of a cylinder with circular cross-section in central position and the maximum of an object with a cross-section of a rectangle or triangle with a thin side within the limits

cylinder	:	$N_{OBJ}\, t_{CMIN}$
⇓		⇓
all other objects	:	t_{TOT3D}
⇓		⇓
thin rectangle or triangle	:	$N_{OBJ}\,(t_{CMIN} + t[case3]) - 3\,(N_{OBJ} / N_T)\,t[case3]$

The time can be further reduced by investigating that the situation regarding the predecessor and successor is the same as before. If no change occurred, the same results for the actual chord can be taken. This reduces especially t_{CMIN}.

In chapter 7 a practical ring solution is introduced using a Motorola 68332 processor running on clock rate of 16MHz and without cache and with 512 KByte of RAM. The system can determine volume and axes measurements of 10 medium sized potatoes (100g) within a second. The program is optimised using look-up tables and on time consuming parts assembler programs.

6.5. Amount of data left after determination of touching chords

In this chapter, the performance of algorithms (case1-3) on the necessary amount of data which are used to find the finally touching chords as described in chapters 3.2-3.5 is investigated. This is only important if the data are used for axis determination and for graphic purposes, otherwise the data could be destroyed. Simulations (see chapter 5.2.11) have been carried out with different shaped cross-sections of cylindrical objects. The results for the first algorithms case 1-2 shown in figure 6.7 delivers a reduction of chords down to 45% - 90% depending on the shape and size of the object. Angular objects have an advantage with fewer remaining chords. By integrating case 3 the algorithm determines finally the touching chords with a reduction down to between 30 - 85 % depending on the shape (see figure 6.8). Angular objects end up with less data than round.

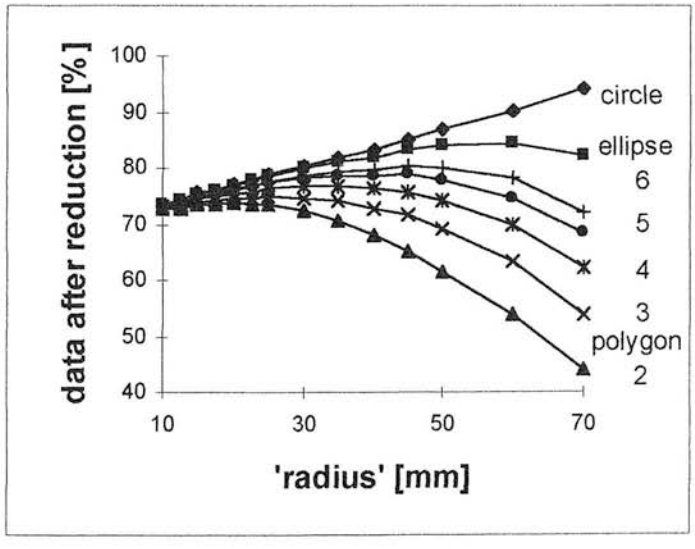

Figure 6.7. Elimination of non-cutting chords case 1-2, data left after reduction

Differential coding could also be used for the storage of the final data. Because this has to include the position of each point in the horizontal direction n (2 Bytes), the distance $m_B[n]$ (1 Byte) and the distance from the transmitter to the predecessor $|T_A:C_P|[n]$ (2 Bytes), 5 Bytes are necessary (see chapter 6.2) per intersection. The result is that the total amount of memory necessary is higher than for primary data.

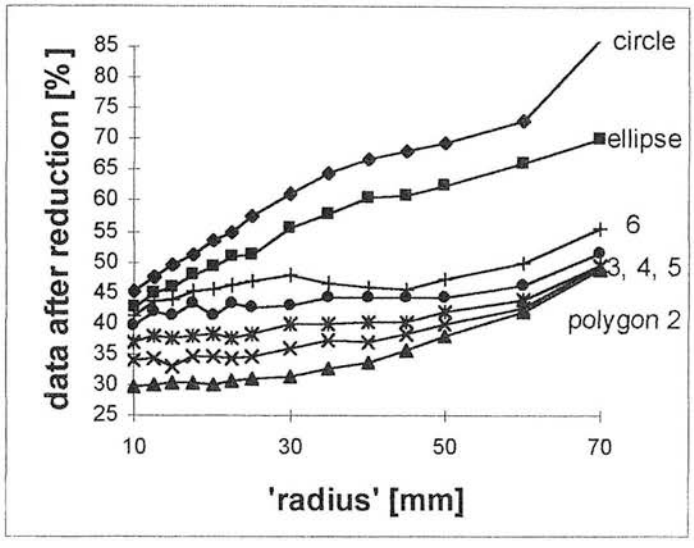

Figure 6.8. Final determination of touching chords case 3, data left after reduction

6.6. Summary

In this chapter related properties are investigated which do not have a direct impact on the determination of the geometry of the objects. The number of all intersections between chords within the ring is related to the possible resolution and accuracy. The necessary amount of primary data and data after handling reflects how effectively compact objects can be described. The object surrounding architecture and enveloping function of the ring sensor system supports further significant data reduction using differential coding. The time consumption of the algorithm can be defined for best and worst case conditions and is linear growing with the length of the object.

7. Practical tests

As the main interest in the ring sensor system has come primarily from agriculture and more particularly from the potato industry, a practical solution was developed with tests being carried out to locate the actual properties of the system predominantly on potatoes.

7.1. Measurements on potatoes of different size

As proposed in chapters 2.7 and 5.2.1 a ring consisting of 64 transmitters and 64 receivers was developed and built by Gall and Argus Electronic GmbH (1997, see figure 7.1). The proposed algorithms, proposed by Gall (1997, 1998) were used to develop a complex software system. This work was carried out from Gall and Argus Electronic GmbH.

The ring diameter is 175 mm with a scan rate of 25,6 kHz equal to 400 revolutions per second. Using the basic two-dimensional algorithms, volume, length, major (MSL) and minor (MSS) axes of the middle slice (see figure 7.2), and position of the largest slice (SPO) of an object, major (LSL) and minor (LSS) axes of the largest slice, mass (if density is known) or density (if mass is known) can be determined.

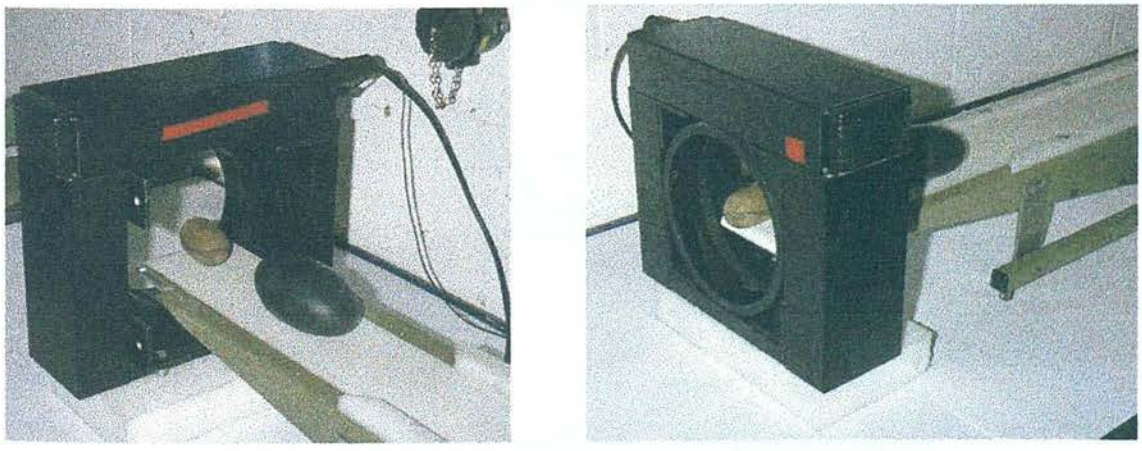

a) Two views of the actual ring sensor system positioned on a flat feeding belt

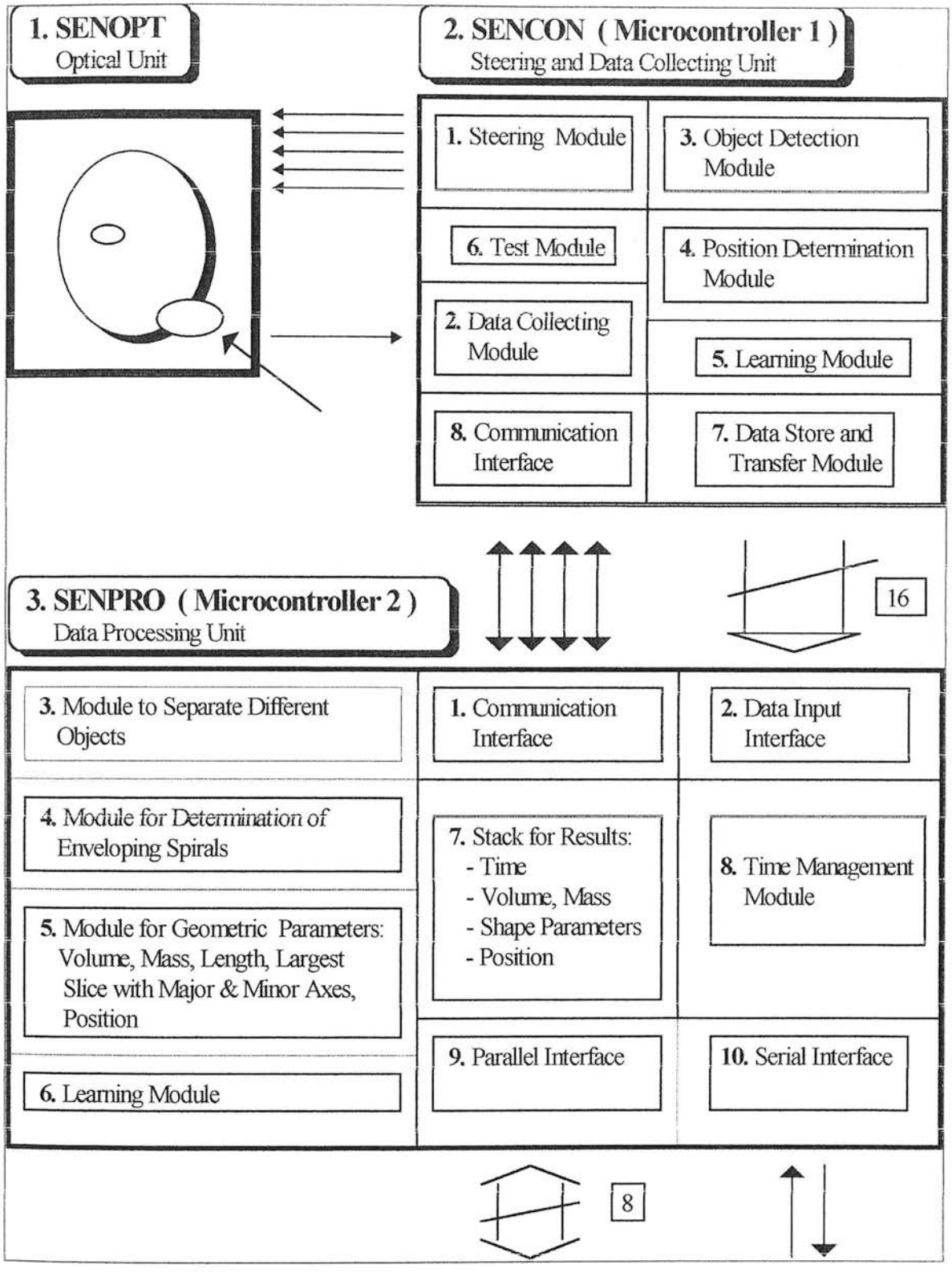

b) Structure of hardware for a ring sensor system

Figure 7.1. Structure, realisation of the ring sensor system

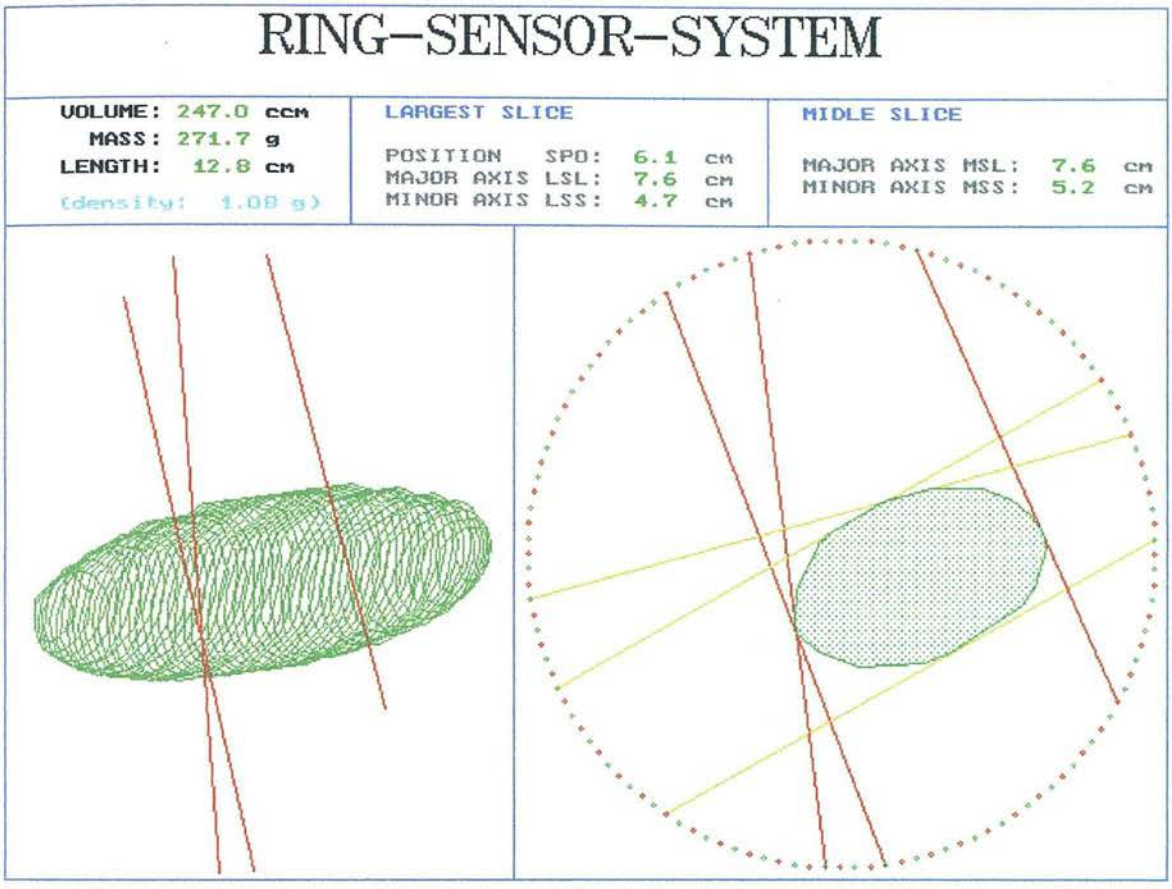

Figure 7.2. A scan of a potato on the computer including the drawing of the whole object and of the largest cross-section. The important axis measurements are marked and the results are shown

A test was performed which showed the results of volume and axis determination of 24 different potatoes in a varying size range, passing through the ring at a constant speed of $1.0ms^{-1}$. Each object was measured fifty times using different positions in the ring.

The method of feeding material into the system is very important. The speed of the feeding system must be stable, and the alignment and stability of the potatoes are crucial for accurate results. For this test, objects were positioned by hand longitudinally on a simple flat conveyor belt before being launched through the ring. The real volume of the potatoes was determined by measuring the weight of the potatoes in air and in water with a balance with 0.1g resolution.

7.1.1. Volume

The results for the deviation of 95% of the measured volumes, the maxima and the minima are shown in figure 7.3. It can be seen that the error varies over the whole range of potato sizes and decreases with the size. The 95% curve means that this quantity of all potatoes are definitely within this random error range and it is defined as 1.96 standard deviation. This is a common method to classify the accuracy of grading systems in agriculture (Barganz 1991).

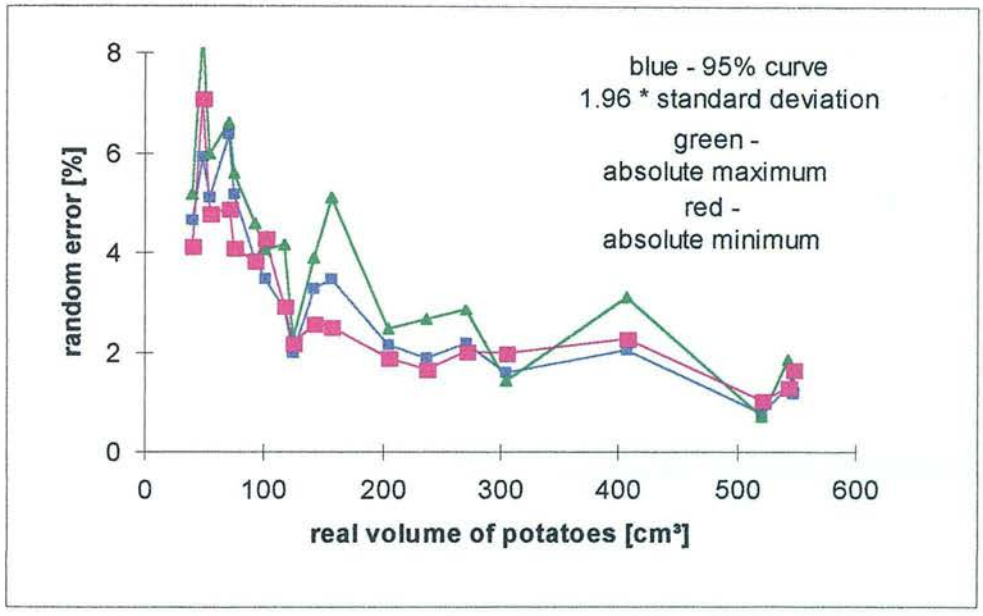

Figure 7.3. The deviation of volume

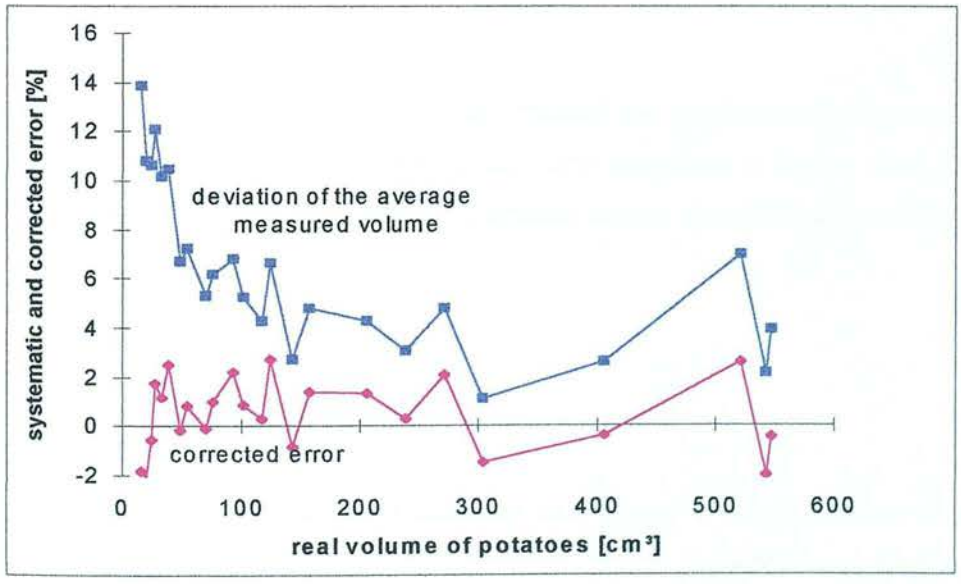

Figure 7.4. Absolute error and correction

The absolute error is shown in figure 7.4. The small potatoes have on average a larger positive deviation, because the size is over-estimated. In this case it is a systematic error, a polynomial regression reduces the error (see also chapter 5.2.3).

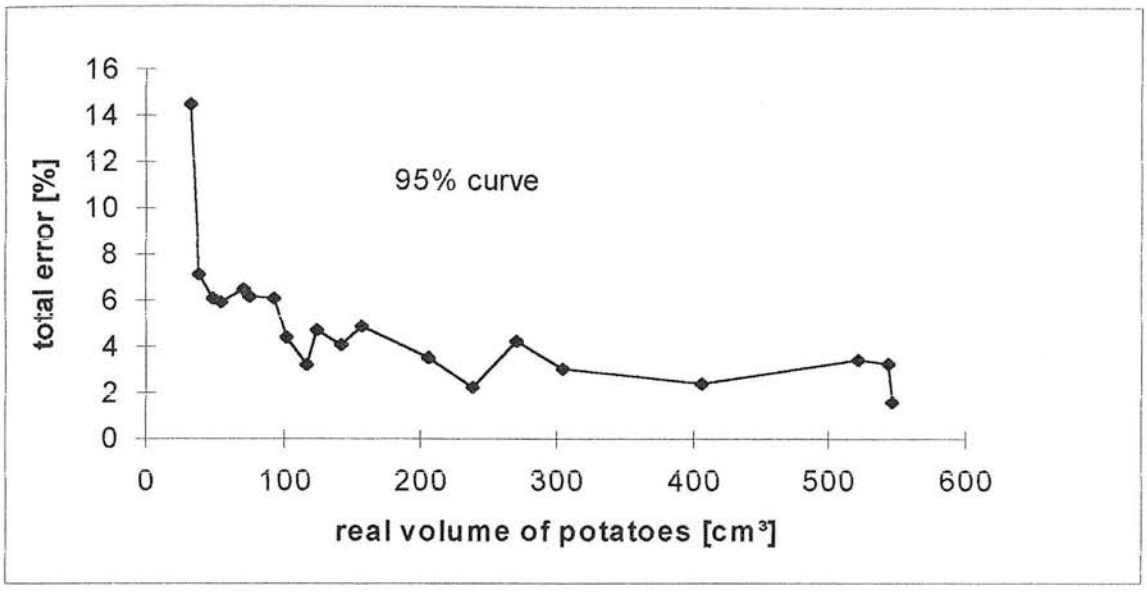

Figure 7.5. Total error - 95% curve

Finally the total error, the sum of the 95% curve plus the absolute deviation from the corrected systematic error is shown in figure 7.5.

There are several factors, which can account for this result. There is the influence of the presentation, which has not been investigated but was minimised. The effect of size and shape was discussed in chapter 5.2.

It can be seen that for potatoes of more than 100cm³ the total error is about or less than 5%. For potatoes smaller than 50cm³ the standard deviation is higher than 7% which suggests that the cut-off point for using the present device should be around 75 cm³.

7.1.2. Axis measurements

The investigation of the length measurement also shows a deviation (see figure 7.6). This is caused by the not quite 100% accurate stable presentation and the varying horizontal direction of the object, underlining the importance of the presentation.

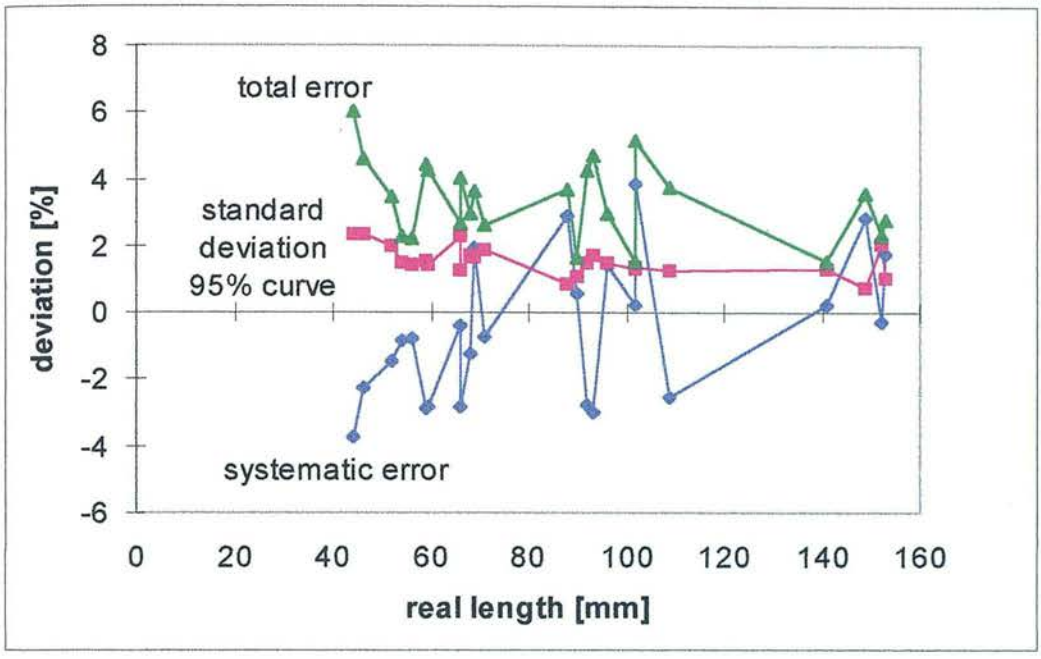

Figure 7.6. Error of the length

For the major axis LSL of the largest slice, it can be seen in figure 7.7 that the total error would be less if systematic error could be corrected. The reason for this is again the over-estimation of small objects. The final error is mainly caused by the presentation of the potatoes and the discrete architecture of the ring.

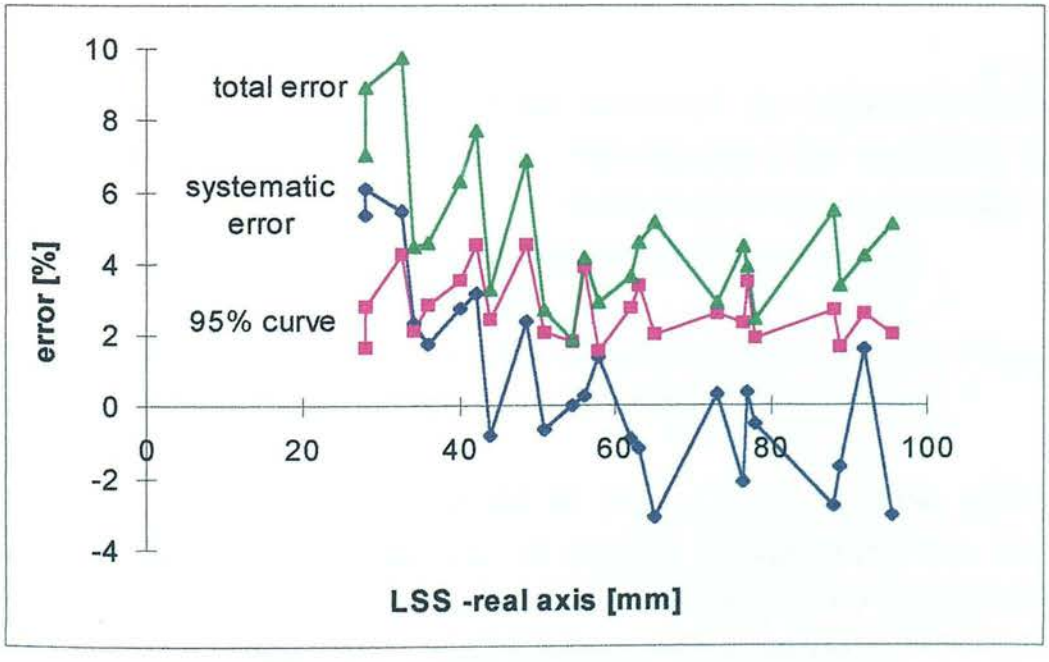

Figure 7.7. Error of the major axis of the largest slice

The random error for the minor axis LSL (see figure 7.8) of the largest slice is generally higher than that of the major axis. The reason is that this axis is determined from the position found for the major axis. This position varies as will be shown later. Another fact is that method 2 of axis determination (see chapters 4.2.2, 5.2.5) is used, the combined error is cumulative especially on small objects. One additional result of this is that it cannot be seen as an over-estimation.

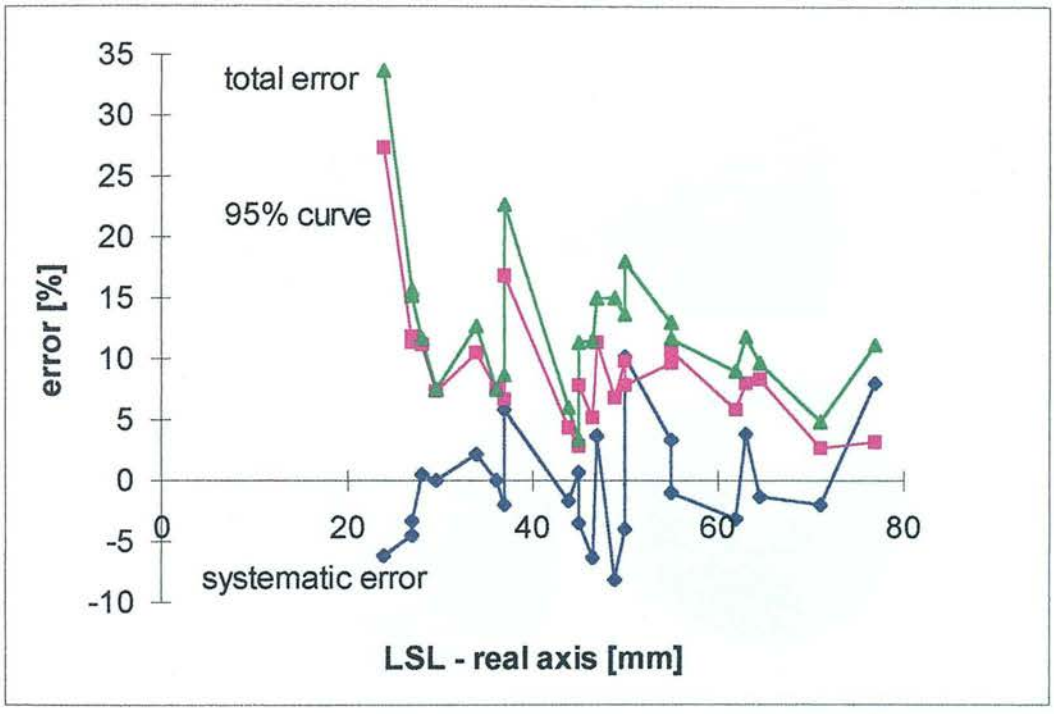

Figure 7.8. Error of the minor axis of the largest slice

The position of the largest slice SPO was determined (see appendix 7 figure 10.1). Because of the general shape of potatoes (ellipsoid) with a low variation in diameter around the largest slice and also due to the resolution of the system, the random error is so high, that a practical use of the largest slice can not be recommended.

For the major MSL and minor axis MSS of the middle slice (see appendix 7 figure 10.2-10.3) the same judgement can be given as for the axes of the largest slice.

Finally it can be said that volume and the axes L, LSL, LSS, MSL, MSS can be determined within the required range of accuracy for agricultural use. For higher requirements an optimum has to be found, increasing the number of transmitters and receivers for the particular use to which the ring is being employed.

7.2. Four artificial objects

In a second test, the random and absolute error of volume determination of objects of different shapes was investigated (see figure 7.9). Table 7.1 includes examples of four objects, a small and a larger rectangular block, a diagonally cut block with triangular shape and a symmetrical object in the shape of a ring doughnut. The presentation conditions were the same as for the potatoes. It can be seen that for objects with more sharp edges, the error increases.

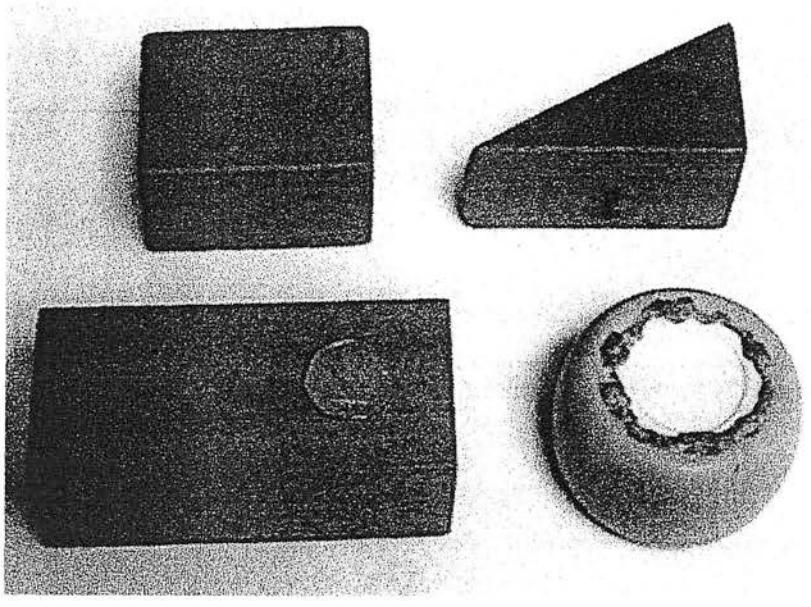

Figure 7.9. Four objects of different shape

	Real volume [cm³]	Measured volume [cm³]	Absolute error [%]	Random error 95% value [%]
Block 1	159	162	1.9	4.5
Block 2	318	324	1.9	2.5
Triangle	116	125	7.8	6.9
Doughnut	194	195	0.5	1.4

Table 7.1. Average measured and random error for four different objects

The axis measurements of the object in form of a round doughnut were also investigated, with a real maximum diameter of 76 mm and minimum diameter of 49mm. The object could be presented in a very stable position because of the shape. The results of the measured dimensions of this object are shown in table 7.2.

	L	LSL	LSS	SPO	MSL	MSS
Real measurements [mm]	76	76	49	38	76	49
Average measured distance [mm]	72.8	76.1	54.5	31.0	75.8	55.9
95% value = 1.96 standard deviation [%]	0.6	1.2	5.1	14.7	1.0	2.5

Table 7.2. Additional measurements of the doughnut shaped object

The calibrating factor for the length L based on the speed of presentation was not set right and has to be increased by the factor 1.044. The major axes LSL and MSL are correct, but the minor axes LSS and MSS are over-estimated be caused of the method of axis determination as discussed earlier.

7.3. Comparison of the actual ring sensor system and the Accu Pack system

A test was set up to compare the accuracy of weight determination of the Accu Pack machine (see figure 7.10) with the actual ring solution on baker potatoes (200g-400g).

The Accu Pack system (Exeter 1994) is used in the British and American potato industry in packing houses for weight sizing on a large scale. It is based on a rectangular frame including two cross-wise arranged sensing lines using the principle shown in figure 2.2.c. The x-y lines scanning cross-wise with a rate of about 5KHz. The sensing area is a rectangle of about 170 x 170 mm. The analogue signal, received by one receiver on each scanning line, is converted by an 8bit Analogue Digital Converter. A computer puts together the rectangular cross-sections and calculates the total volume of all sections of an object. Using an average density the weight is calculated.

For the test 15 clean potatoes and four artificial objects were chosen within a spectrum of size (see figure 7.11). The weight and underwater weight of each potato was determined using a balance with an accuracy of 0.1g. The potatoes were firstly presented the Accu Pack Test/Training Unit consisting out sensor head and the feeding three wire

transport system. They were then presented to the ring sensor, placing them up on a conveyer belt to jump freely through the ring sensor system.

The following conditions are valid for both:

- kind of sensor	optical
- measured value	cross-sections, volume
- determined value	volume, weight
- speed of objects:	90 m/min
- infeed:	in predominantly horizontal direction
- test range:	30 times each

Figure 7.10. Accu Pack system with square shaped sensor system

Figure 7.11. 15 potatoes and 4 artificial objects

Looking at the results, it can be seen, that the ring sensor gives about half the random, absolute and total error of the Accu Pack system(see figure 7.12-7.15). The weight (see figure 7.15) gives the same result, because a general density factor based on the dry matter content of objects is used for the weight determination. Changes in the dry matter content and adhering soil cause additional errors.

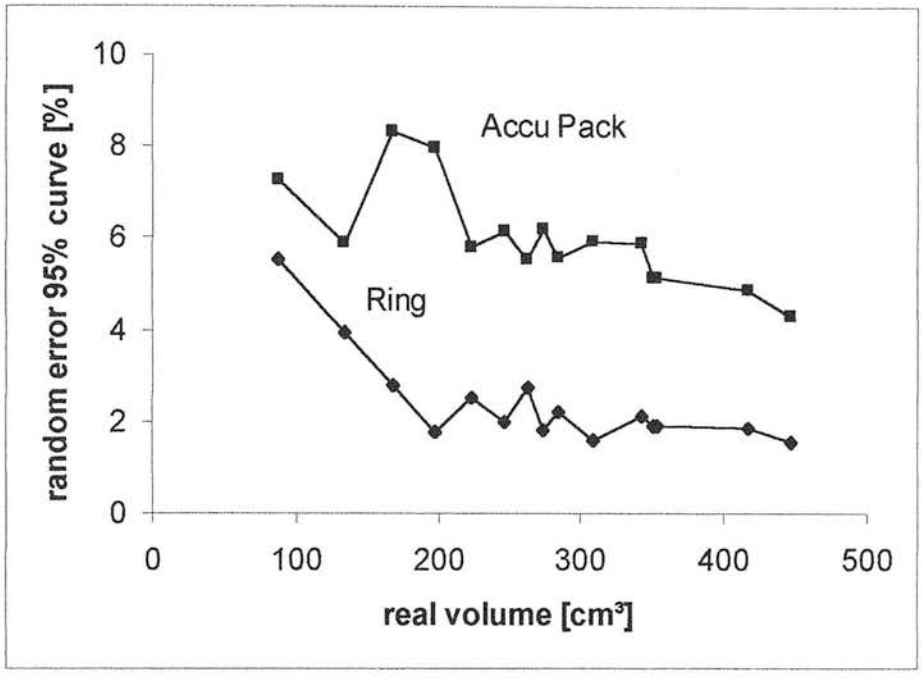

Figure 7.12. Random error for the volume measurement

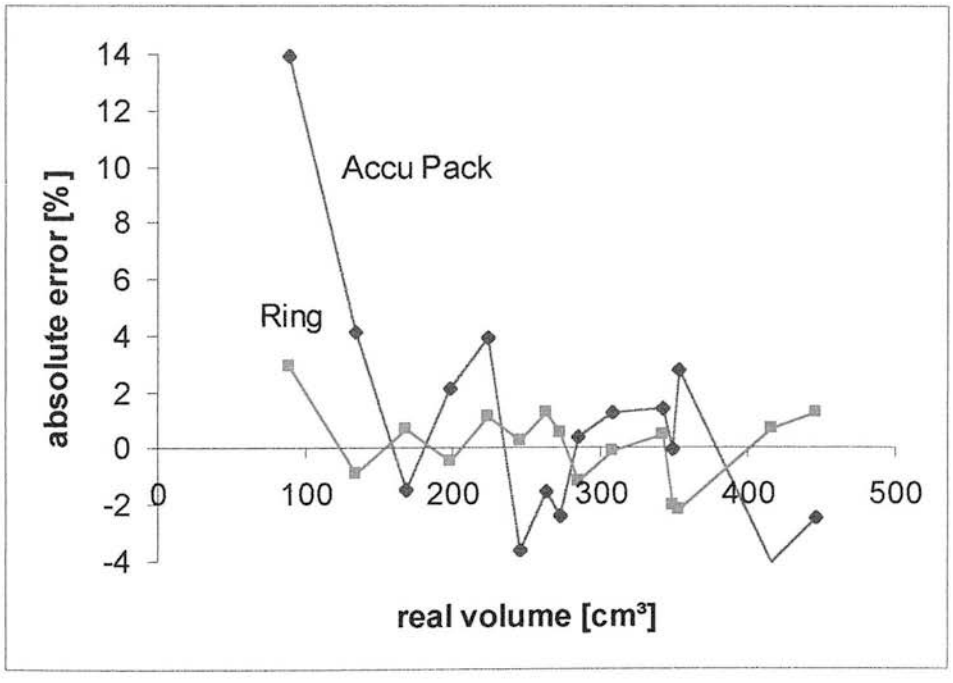

Figure 7.13. Absolute error of the average of the volume measurements

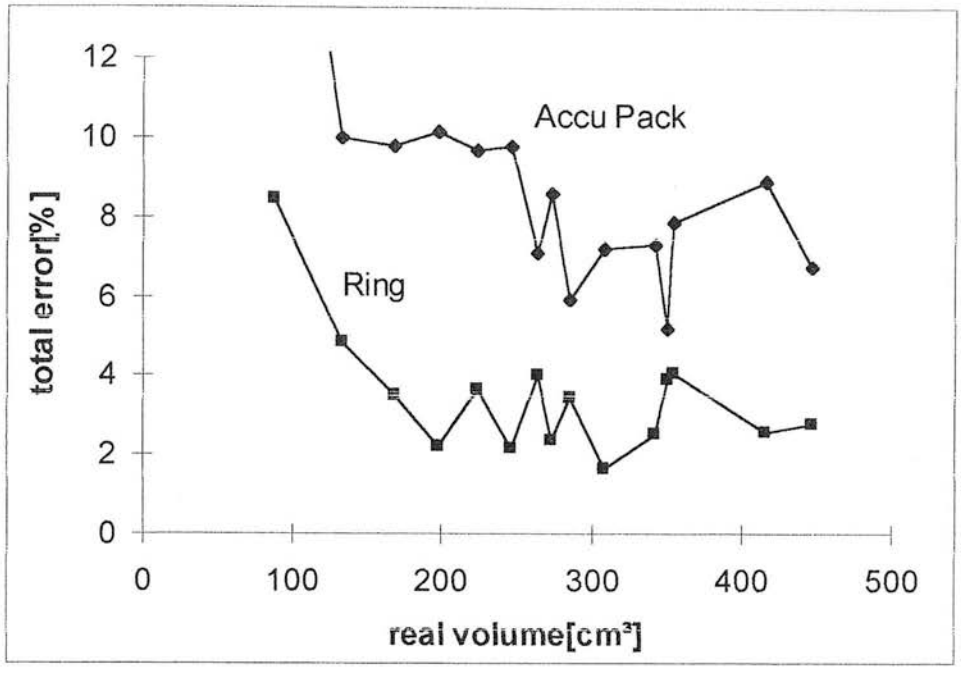

Figure 7.14. Total error 95% curve for volume

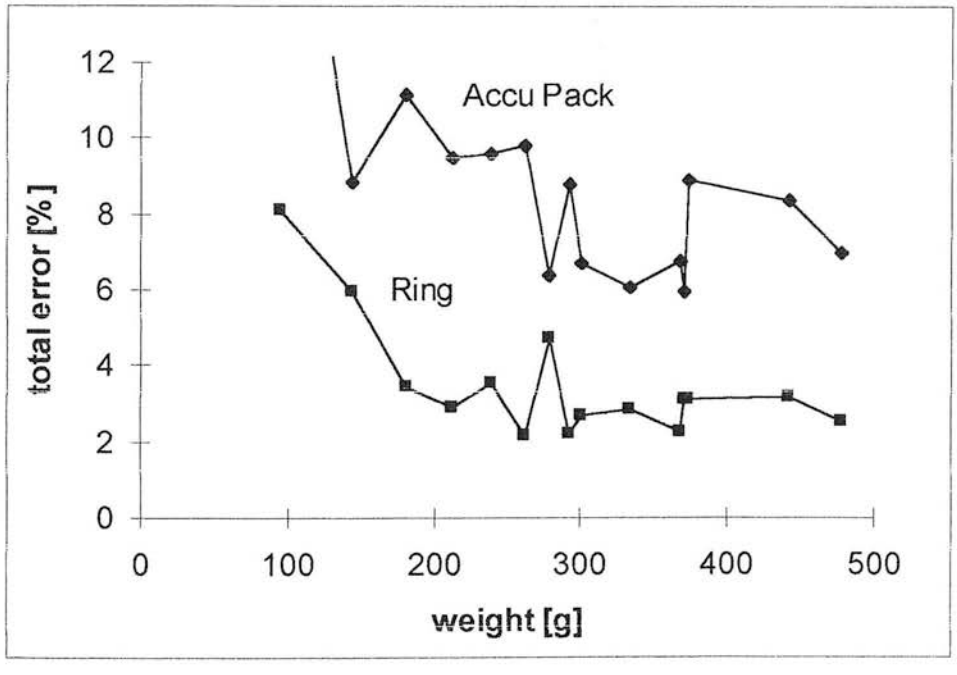

Figure 7.15. Total error 95% curve for the weight measurements

For the four artificial objects shown in figure 7.11 only the random error for volume detection was investigated (see table 7.3). It shows that the ring system is significantly better. The same error on the pin is a result of variable position in horizontal direction on the belt for the ring sensor system during the tests.

Test object	Small ellipsoid	Small brick	Large brick	Pin
Accu Pack (stdev [%])	4.9	3.3	2.7	1.7
Argus ring (stdev[%])	2.8	2.3	1.6	1.7

Table 7.3. Random error for four test objects as shown in figure 7.11

7.4. Summary

Practical tests were carried out using a practical ring sensor solution which confirmed the working principle of the ring sensor system. Artificial objects and potatoes have been used to determine the limits for a practical solution. The ring sensor system was compared with a system used in practice in the potato industry and achieves about twice the accuracy.

8. Multiple objects in the ring sensor system

So far all investigations have only considered one object in the ring at a time. In practice some times two or more objects could pass through the sensor system at the same time, for example two overlapping objects or a complex shaped object like the doll (see figure 3.14). In this chapter an introduction will be given into a model for the simulation and a method for the separation of multiple objects with flexible positions in the ring.

8.1. Basics

The practical number of objects in the ring is limited by the influence of self-shadowing of the objects, causing additional false captured area or ghosting around each object and a reduction in resolution and accuracy (see especially the triangle in figure 8.1.a). Normally there must not be more than three objects in the ring with an unknown shape and position. This also includes objects like the doll (see figure 3.14), which will have a maximum of three cross-sections as it passes through.

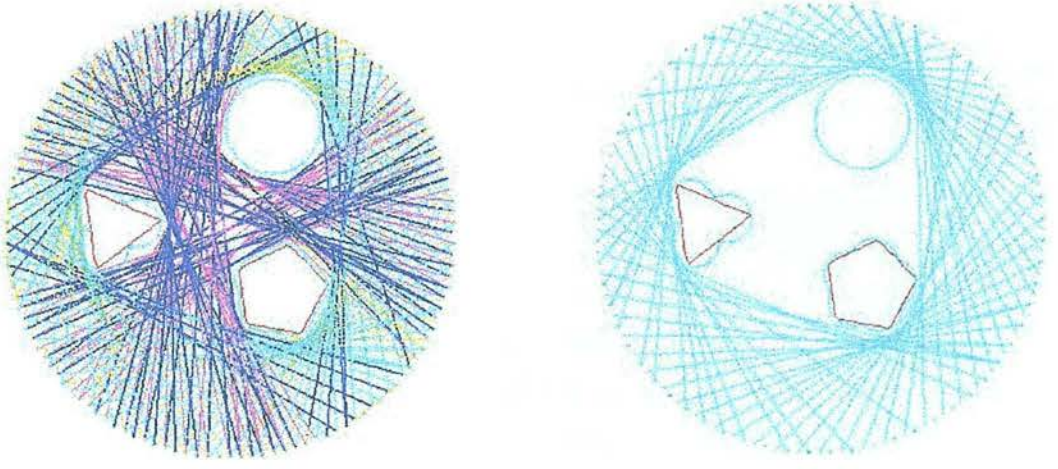

a) All chords b) The 'back' chords only

Figure 8.1. Multiple objects in the ring

Investigating multiple objects is much more complex as will be shown. Using only the algorithm developed for one object (see chapter 3) with only the 'back' chord then only the global envelope of all objects will be found. Multiple objects can not be separated using the 'back' chord alone, so additional information on the basis of other chords has to be used.

If one object is in the ring, one 'back' chord TR0 and one 'front' chord TR1 are available to describe the situation from each snapshot (see figure 8.2.a). The chords are described by the number of receivers anti-clockwise between the actual determined receivers m_{TR0} and m_{TR1}.

If a second object comes into the ring, the situation changes. Four different situations can occur (see figure 8.2.b-e).

In the first case the object chords TR0, TR1 related to object 1, TR2, TR3 related to object 2 can be found in a snapshot (see figure 8.2.b). They have the values m_{TRO}, m_{TR1}, m_{TR2} and m_{TR3}. Each snapshot is described by four chords with the values m_B1, m_F1, m_B2, m_F2 without any relation to the real position of objects. These data are stored for processing in the primary data arrays Z0-Z3 (see chapter 6.2, 10.7). The main point is to link the snapshot chords to the objects for the splitting process and vice versa for the simulation. Following different links are shown by only exchanging the object number in figure 8.2.b and c.

In figure 8.2.b	$m_B1 = m_{TR0}$
	$m_F1 = m_{TR1}$
	$m_B2 = m_{TR2}$
	$m_F2 = m_{TR3}$,
in figure 8.2.c	$m_B1 = m_{TR2}$
	$m_F1 = m_{TR3}$
	$m_B2 = m_{TR0}$
	$m_F2 = m_{TR1}$.

In the second case on a different snapshot the gap between the objects is becoming narrow and so they are only split by one chord TR1=TR2 with the describing values m_{TR0}, $m_{TR1}= m_{TR2}$ and m_{TR3} (see figure 8.2.d).

In the third case one object shadows the other totally (see figure 8.2.e) or partially (see figure 8.2.f).

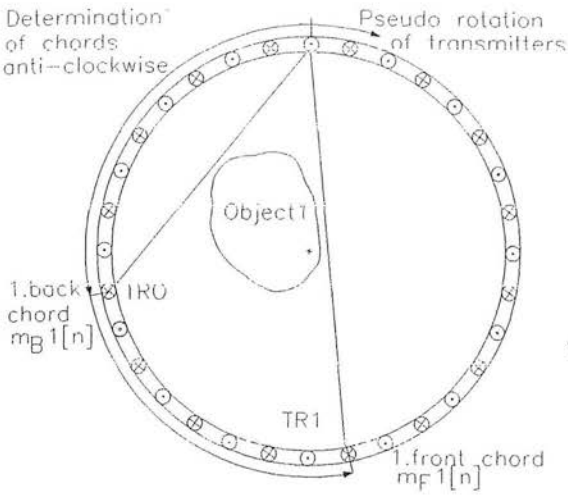

a) One object described by two chords

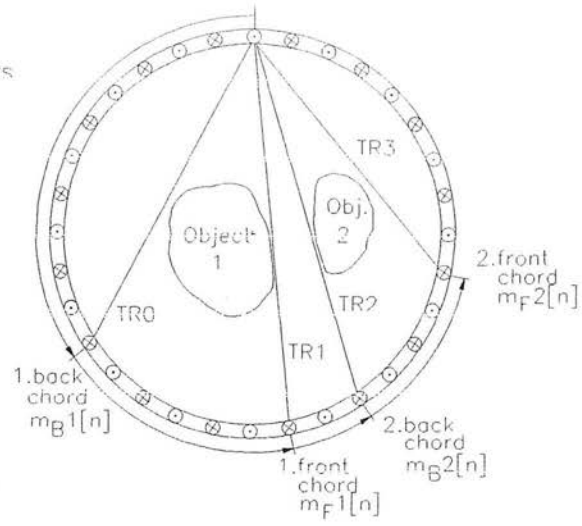

b) Two objects described by 4 chords

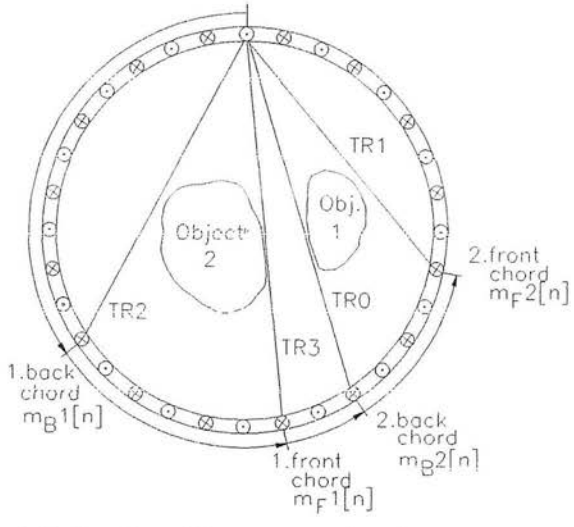

c) 4 chords with a reversed order of object chords

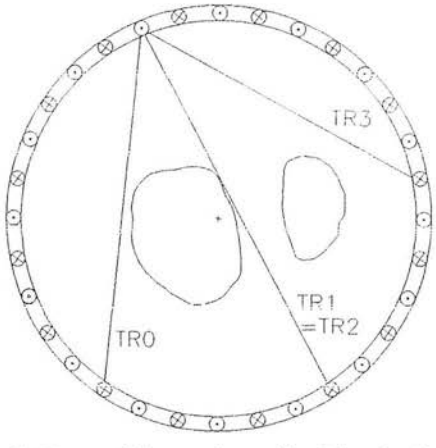

d) Two objects described by 3 chords

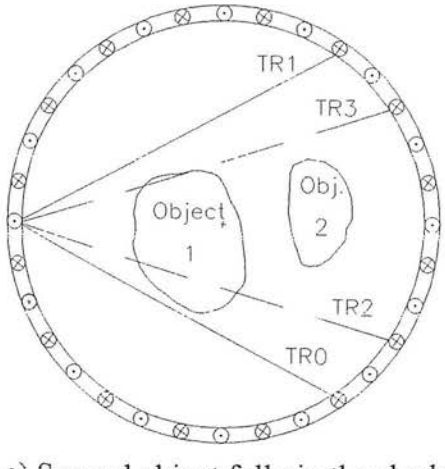

e) Second object fully in the shadow

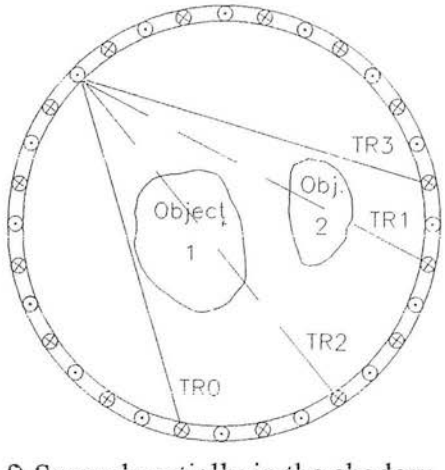

f) Second partially in the shadow

Figure 8.2. Possible snapshots with one or two objects in the ring

It is obvious that information is lost if one object is in the shadow of the other and the objects cannot be separated from this angle of view. This is a major disadvantage of all shadow systems. A minimum of one snapshot in one revolution of the ring system with a chord through the gap between two objects is necessary to split them.

As mentioned previously, as a result of the described algorithm (see chapter 3) the hardware of the actual sensor system (see chapter 7) rotates clockwise, but the determination of the chords is anti-clockwise orientated. This means, a 'back' chord will always be determined first (see figure 8.2.a-b). Further, for all snapshots:

$$m_B1[n] < m_F1[n] <= m_B2[n] < m_F2[n] .$$

For multiple objects, more information is required in the form of more chords. Every chord for a system of up to 256 receivers requires one byte. Using four chords for two objects, four times as many primary data values are required for a complete description of the scene.

For three objects in the ring the situation becomes much more complex. For a full description of the scene a further two chords are needed (see figure 8.3.a).

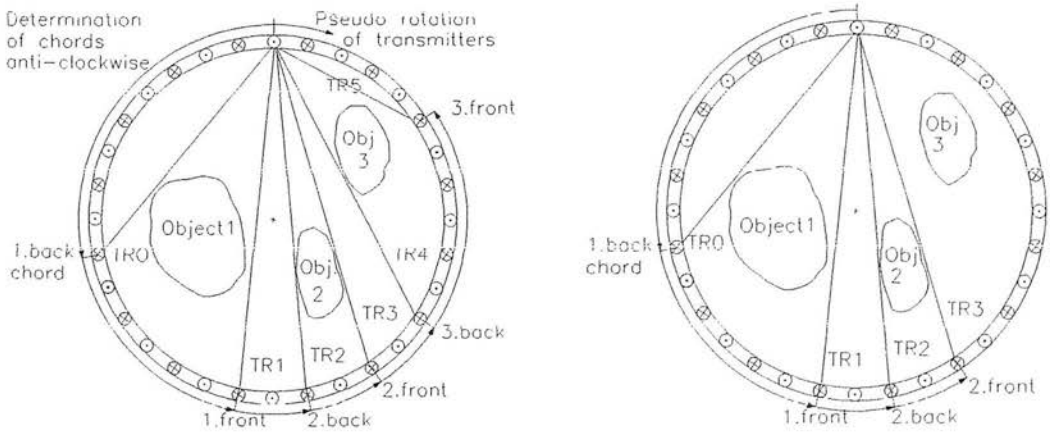

a) Snapshot with 6 chords

b) Same snapshot with only 4 chords

Figure 8.3. Snapshot of a scene using a different number of chords.

For 3 objects, 6 bytes of data for each snapshot are necessary to describe the situation completely,

m_B1	=	m_{TR0}	1. 'back' chord
m_F1	=	m_{TR1}	1. 'front' chord
m_B2	=	m_{TR2}	2. 'back' chord
m_F2	=	m_{TR3}	2. 'front' chord
m_B3	=	m_{TR4}	3. 'back' chord
m_F3	=	m_{TR5}	3. 'front' chord

The hardware of the practical ring sensor allows a maximum of four chords per snapshot to be recorded (see figure 8.3.b). This limitation is not a problem, since the objects shadow each other in a whole cross-section in different snapshots (see figure 8.2.d-e) resulting in a reduction of obtainable chords per scene. So the influence of a reduced used number of chords is minimal.

As shown, the first chord per snapshot analysed anti-clockwise is always a 'back' chord. During analysis of the following snapshots clockwise around the ring, if the second object gets closer, the first 'back' chord will touch object 2 instead of object 1 (see figure 8.4.a). Comparing the order of objects NPO for two objects in figure 8.2.b and 8.4.b, NPO is now 21 instead of 12. The relation of chords to the objects in different snapshots changes and for figure 8.4.b is

m_B1	=	m_{TR2}	1. 'back' chord
m_F1	=	m_{TR3}	1. 'front' chord
m_B2	=	m_{TR0}	2. 'back' chord
m_F2	=	m_{TR1}	2. 'front' chord

For three objects six different positions NPO related to each other are possible (see figure 8.4.a with the order 132, or figure 8.6 with 321):

NPO: 123, 132, 321, 312, 213, 231.

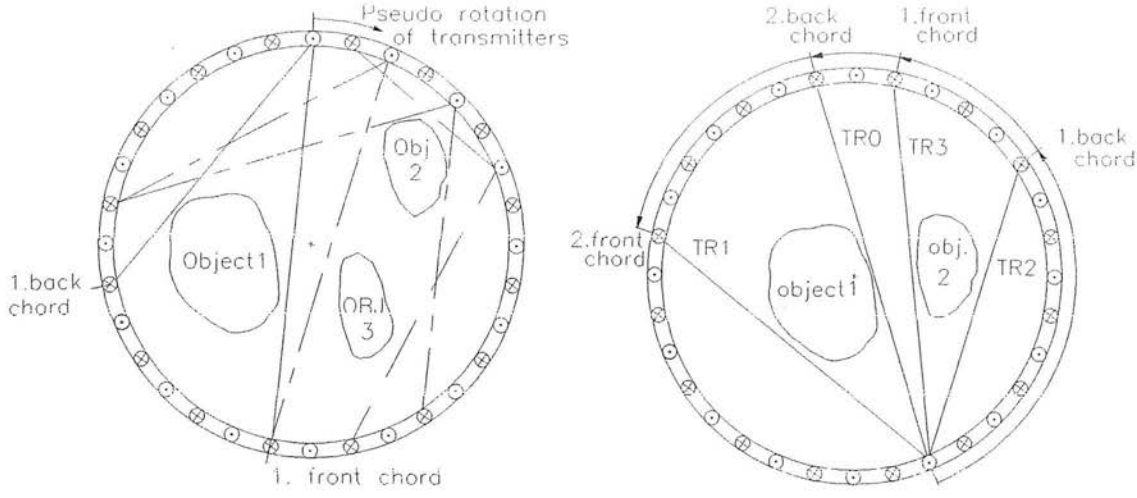

a) Movement of the 1.'back'/'front' chord from object 1 to 2

b) Order of objects and chords from side

Figure 8.4. Change of the order of objects

On the basis of this fundamental explanation, a further example for a cross-section is shown in figure 8.5. The first 'back' chord always builds up the global envelope containing all objects (see figure 8.5.a). As said, it can not on its own be used for separation. At a minimum one other chord is necessary to describe and split objects. The most convenient is the first 'front' chord with the value $m_F1[n]$ with N_T chords per revolution (see figure 8.5.b). The number of second 'back' and 'front' chords (see figure 8.5.c-d) is limited because of the shadowing, but they are necessary for a more accurate description of the scene as can be seen in figure 8.5.e-f showing all four chords used.
The shadowing causes an error in the form of an additional ghost area attached to each object. This increases with the number of objects in the system and limits the practical use. For the following explanations only four chords will be used and the number of objects is set to three.

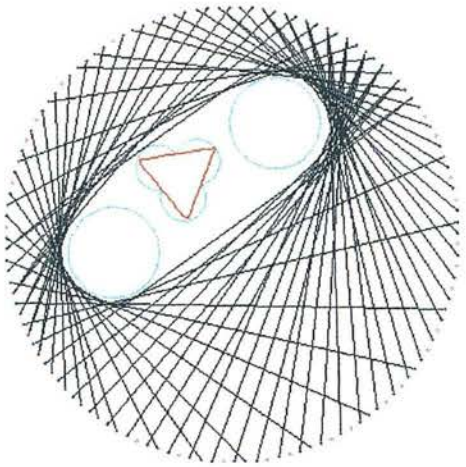

a) 1.'back' chords

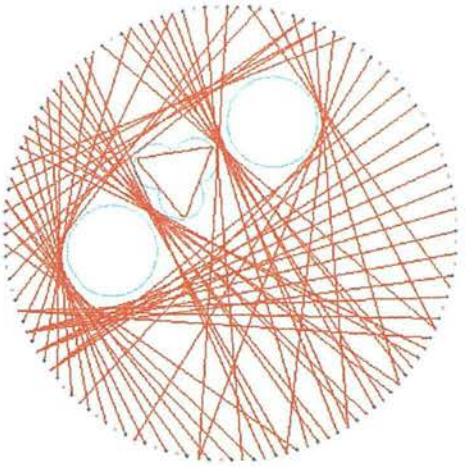

b) 1.'front' chords

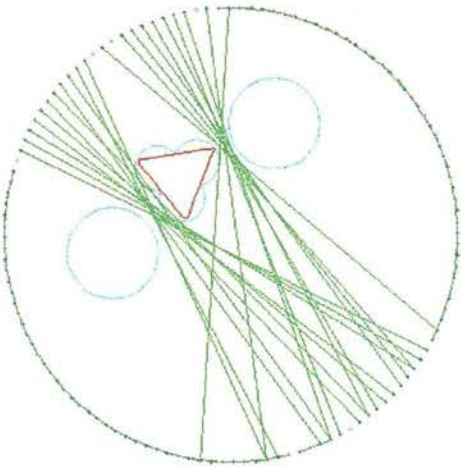

c) 2.'back' chords

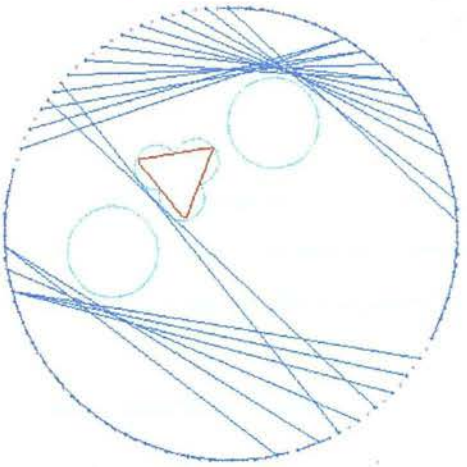

d) 2.'front' chords

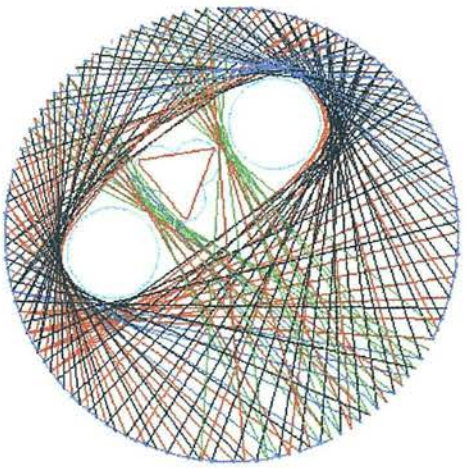

e) All 4 chords on 3 objects in line

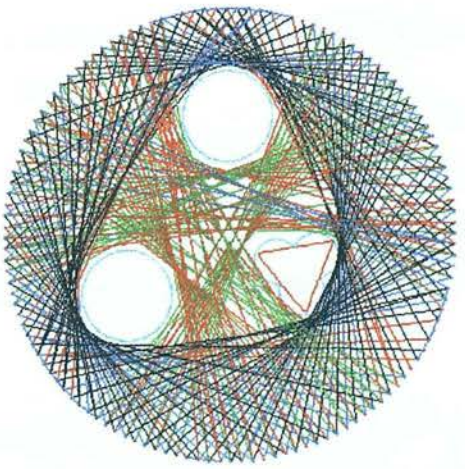

f) All chords on 3 objects not in line

Figure 8.5. Different chords building up a scene of objects within the ring

8.2. Model for simulation of multiple objects

8.2.1. Cross-sections of multiple objects in the ring

The simulation is quite simple and follows the procedure:

- The objects have to be placed separated in the ring.
- For the creation of multiple objects the algorithm for the simulation of one object as described in chapter 5.1 is used.
- The 'back' and 'front' chords are simulated for each object independently (data are stored in the arrays OBJ0-5, see appendix 10.8)
- The results are six chords per snapshot for single independent objects in the ring.
- This data has to be linked to create each snapshot describing the scene containing all objects with maximal 4 touching chords in the scene stored in the snapshot arrays.

For the determination of snapshot the following steps have to be made:

- For positioning the objects the number NPO has to be set. It is arbitrary, but once set it is not changed.
- Depending on NPO and the different possibilities of overlapping of the objects in the scene, the chords for each snapshot can be determined.

For example in figure 8.6 the order of chords in anti-clockwise direction is TR4,5,2,0,3,1. Object 3 (TR4,5) is the first touched object and object 2 (TR2,3) is shadowed by object 1 (TR0,1). As a result the first four visible chords TR4,5,2,1 have to be taken for this particular snapshot.

m_B1	=	m_{TR4}	1. 'back' chord = 'back' chord of object 3 (TR4)
m_F1	=	m_{TR5}	1. 'front' chord = 'front' chord of object 3 (TR5)
m_B2	=	m_{TR2}	2. 'back' chord = 'back' chord of object 2 (TR2)
m_F2	=	m_{TR1}	2. 'front' chord = 'front' chord of object 1 (TR1)

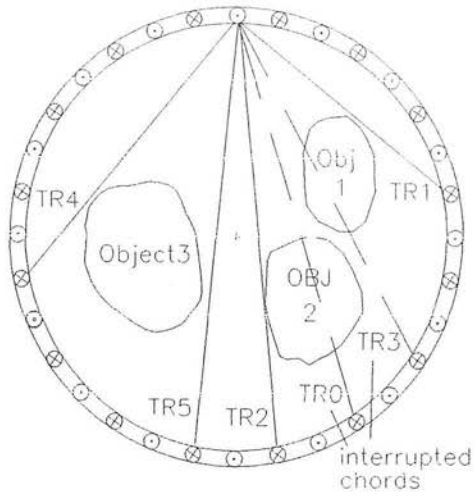

a) Scene in the ring

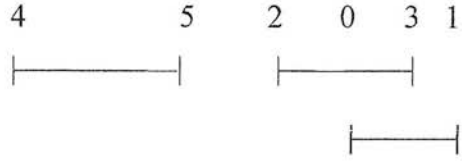

b) Related code constellation

Figure 8.6. Possible collection of the 3 objects within the ring

There are the six possible constellations of three objects given by NPO, for each 15 different situations including different overlapping of chords are possible. This means in total 90 solutions, which will be used to set up a look-up table called the TRC-code (transfer code). For NPO = 123 for example the coding is shown in table 8.1 (TR0 and TR1 are bold in the table to show the way of development).

Order of chords TR0 - TR5	**Chords used for the snapshot**	
0,1,2,3,4,5	0,1,2,3	all objects are separated
0,1,2,4,3,5	0,1,2,5	object 2 and 3 are overlapped
0,1,2,4,5,3	0,1,2,3	object 3 behind object 2
0,2,**1**,3,4,5	0,3,4,5	object 1 and 2 overlapped
0,2,**1**,4,3,5	0,5	all objects overlapping
0,2,**1**,4,5,3	0,3	object 1 and 2 overlapping, object 3 fully covered by object 2
0,2,3,**1**,4,5	0,1,4,5	object 2 hidden behind object 1
0,2,4,**1**,3,5	0,5	all objects overlapping or covering each other
0,2,4,**1**,5,3	0,3	-"-

0,2,3,4,**1**,5	0,5	-"-
0,2,4,3,**1**,5	0,5	-"-
0,2,4,5,**1**,3	0,3	-"-
0,2,3,4,5,**1**	0,1	-"-
0,2,4,3,5,**1**	0,1	-"-
0,2,4,5,3,**1**	0,1	-"-

Table 8.1. TRC-transfer-code for the coding of three objects with the position
(The full table is given in appendix 10.9)

Using the look-up table the primary data including the right order of chords for each snapshot can be created to include all three objects.

8.2.2. Entire multiple objects

For entire objects the extension of the algorithm into 3-D space is done in the same way as described in chapter 3.5. In figure 8.7 an example is given of a scene with three cylinders with an original circular cross-section within the ring. They start at the same point in the horizontal direction and have the same length.

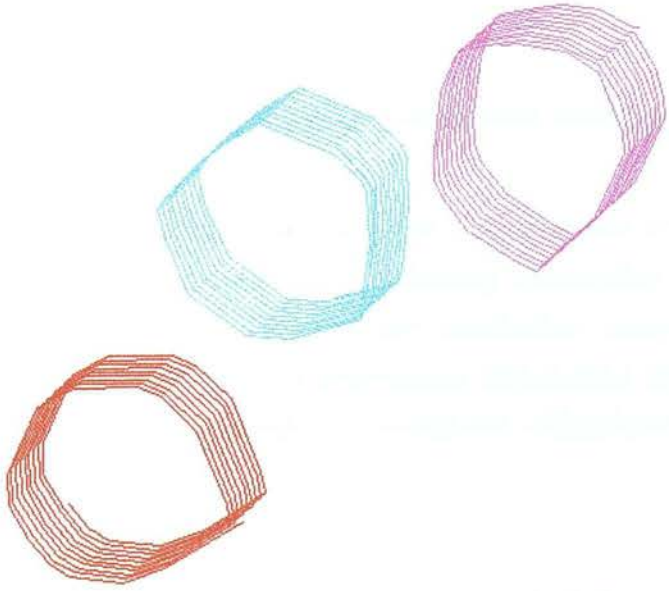

Figure 8.7. Three simulated cylinders in the ring sensor

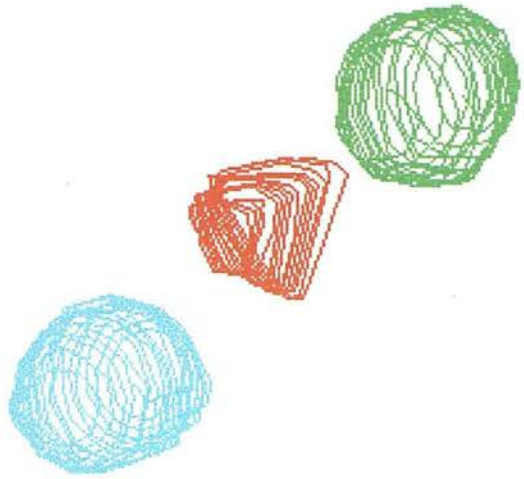

Figure 8.8. Two balls and a cone simulated in the ring

As can be seen, the shadowing causes the shape to be changed and additional volume is added. In figure 8.8 two balls and a cone are shown. The self-shadowing also has an influence on the shape of the simulated objects as can be seen especially on the extension on parts of the balls. To show the objects in images in figure 8.7 and 8.8 the separation algorithm was used and this is described in the following chapter.

8.3. Separation of objects

8.3.1. Introduction, conditions, restrictions and basic rules

There are different procedures to find and envelope objects within a scene as discussed in chapter 3.2.1. The main interest in the following description is a method and algorithm for the separation suitable for real time application using only logical links without any real arithmetic. This is only a preliminary introduction into this method and will not discuss all problems under special circumstances, which have to be investigated in the future.

During the investigations the following conditions and restrictions were used;

- Three objects are in the ring.
- Only objects with convex cross-sections are investigated.
- All objects start at the same horizontal position and have the same length.

- Four chords of each snapshot are used.
- All objects are separated by at least two chords from opposite sides (see figure 8.9).
- Only the logical analysis of vectors (chords) characterised by the values $m_B1[n]$, $m_F1[n]$, $m_B2[n]$, $m_F2[n]$ will be used to split, sort and assign the chords to each object in the scene. No real arithmetic will be applied for this process.
- Finally the known algorithms for single objects described in chapter 3 and 4 will be used for each object.

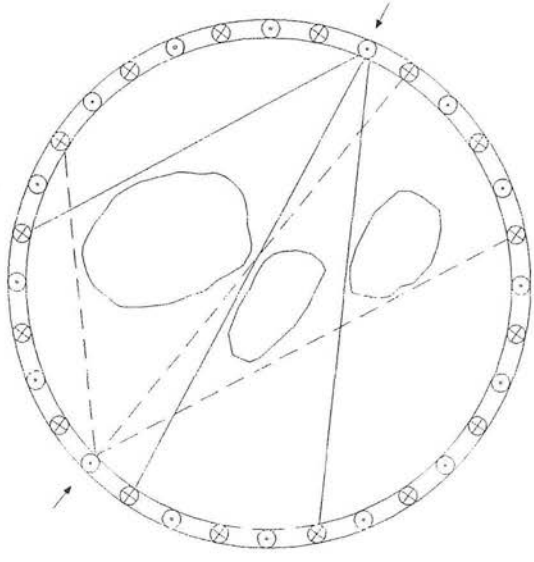

Figure 8.9. Objects separated by at least two opposite chords

There are some remarks about the problem of separation of three objects:

- The first 'back' chord with $m_B1[n]$ can only be used to build up a global enveloping spiral of all objects (see figure 8.5.a).
- If more than one object is in the ring, the use of at least the first 'front' chords with $m_F1[n]$ is necessary, because it is most likely to be the one which envelopes and separates all objects (see figure 8.5.b).
- The first and second 'front' and the second 'back' chord can be closer to the object than the 'back' chord (see figure 8.5.b-d).
- If objects are separated by a narrow gap, first 'front' and second 'back' chord can be congruent. They will be investigated independently.
- The second 'back' chord can split the second and third object from a view of a snapshot.
- The position and geometry of objects in the ring is not known.
- Because the position and geometry are not known, the use of reverse algorithms of the simulation of multiple objects (chapter 8.2) is impossible.

- It is necessary to determine the position of each object from the view of each snapshot.
- It is required to use all available four chords from a snapshot to get a relatively accurate envelope of each object. This requires the transformation of the 'front' chords into the same direction of rotation as the 'back' chords, themselves becoming 'back' chords. The transmitter will become a receiver and vice versa. Related problems regarding this transformation are discussed in chapter 3.6.

8.3.2. Overview of the different steps required for the separation

The process of separation requires a number of different procedures to get the necessary information about the scene and the objects. Based on this a transformation and allocation of chords to each object can be carried out and the objects are separated. Finally the geometrical properties of each object can be determined.

The whole process of separation and determination of the objects can be organised in 6 steps as shown in figure 8.10. These steps will be explained in the succeeding chapters.

1. IIC-code (see chapter 8.3.3)

Description: Finding snapshots, where gaps between objects appear and disappear
Method: All chords in each snapshot n and predecessor n-1 are investigated
Result: The number n of snapshot i of change and the related IIC-code[i]

⇓

2. POT-code (see chapter 8.3.4)

Description: For each remaining snapshot anti-clockwise the shadowing is investigated
Method: IIC-code [i] and successor [i+1] of remaining snapshots are investigated
Result: The POT-code[i] is added to the list of the IIC-results above. Because of algorithms used later to determine the geometry (chapter 3 and 4) the POT-code also contains information about necessary inversion of chords into 'back' chords

⇓

3. Special case 9 (see chapter 8.3.5)

Description: If there is no change in a detected gap between two totally shadowing situations (or at the beginning of the scan) the POT[i] can not be determined
Method: IIC[i] and successor [i+2] snapshots or the opposite side are investigated
Result: The right POT[i] is determined

⇓

4. OOC-code (see chapter 8.3.6)

Description: The objects are now identified by a number 1-3. The OOC-code gives the order of these three existing objects in the scene from remaining snapshot i
Method: POT[i], OOC[i], the predecessors and opposite of scene are investigated
Result: The OOC[i] is noted to the other results

⇓

5. Separation of objects (see chapter 8.3.7)

Description: All chords are now allocated as 'back' chords to each object they belong too
Method: On the basis of the remaining snapshots, the related OOC-code gives the real order and the POT-code the additional information about one or two gaps between the objects and required inversions. Between the remaining snapshots i all other snapshots n of primary data are transferred as the last actual OOC[i] and POT[i]- code setting
Result: One data-set for each object 1-3 containing the primary data of 'back' chords

⇓

6. Determination of the geometry of all three objects

The algorithms for each object are applied as described in chapters 3 and 4

Figure 8.10. Procedure to obtain the separation of objects

8.3.3. Step 1: Generation of the Image Improvement Code (IIC-code)

The scene including all snapshots has first to be analysed and judged. Each snapshot and its predecessor have to be investigated for changes in the number of usable chords (2-4) or one or more chords change by touching a different object. It is like walking around the ring, watching the scene (chords) and writing down the position of each transmitter, where and how gaps between the objects appear or disappear. Carrying out this operation does not give information about which object is which! The IIC-code is defined by nine different relationships between the chords of actual and predecessor snapshots, describing the progress in the scene, each defined by m_B1, m_F1, m_B2, m_F2 from [n] or [n-1]:

IIC-code

1: 2 chords; all objects are fully or partly shadowing each other (see figure 8.11.a)

For all following cases 4 chords detected:

2: the first time (after case 1) that 4 chords are detected within the image; the order of chords and their relation to the objects is unknown (can be case 3-8)

3: value of $m_F2[n] < m_F2[n-1]$ the first time (see figure 8.11.b)

4: value of $m_F2[n] > m_F2[n-1]$ the first time (see figure 8.11.c)

5: $m_F1[n] < m_F1[n-1]$ and $m_B2[n] < m_B2[n-1]$ the first time (see figure 8.11.d)

6: $m_F1[n] > m_F1[n-1]$ and $m_B2[n] > m_B2[n-1]$ the first time (see figure 8.11.e)

7: case 3 and 5 together (see figure 8.11.f)

8: case 4 and 6 together (see figure 8.11.g)

9: is case 1 after case 2. Because it is not case 3-8 the order of chords related to the objects is not known at this stage

If only one chord is in the first gap between two objects seen anti-clockwise in a snapshot (see figure 8.2.d), the 1. 'front' and 2. 'back' chord cover each other and $m_F1[n] = m_B2[n]$. They will always be seen and investigated as two independent chords.

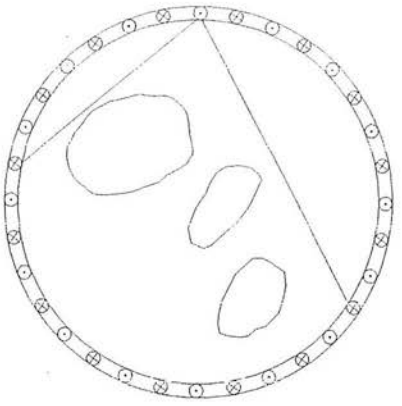

a) All objects are fully or partly shadowed (case1)

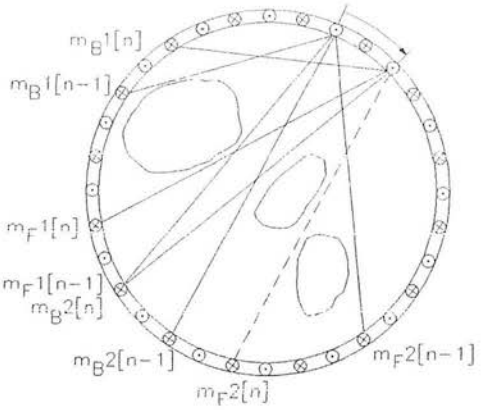

b) $m_F2[n] < m_F2[n-1]$ (case 3)

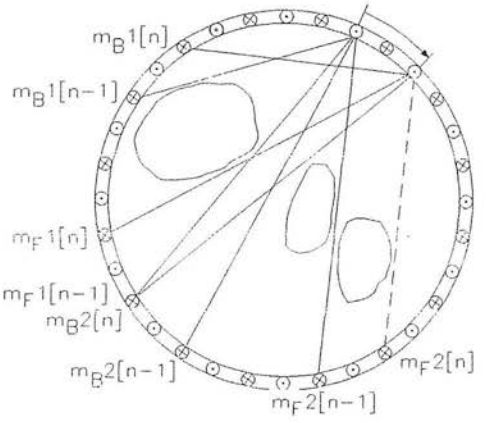

c) $m_F2[n] > m_F2[n-1]$ (case 4)

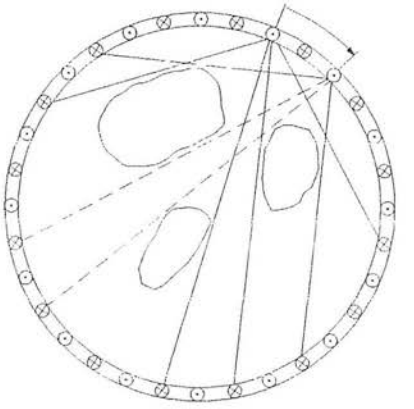

d) $m_F1[n]$, $m_B2[n]$ < predecessor (case 5)

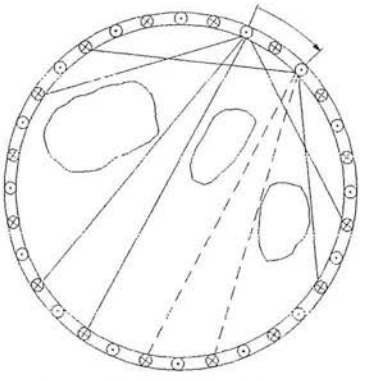

e) $m_F1[n]$, $m_B2[n]$ > predecessor (case 6)

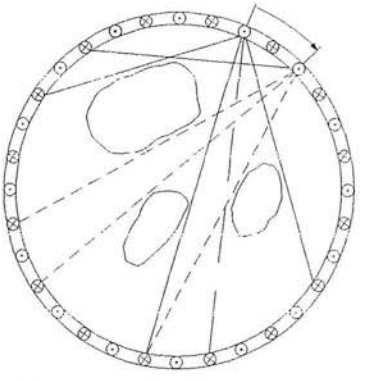

f) Case 3 and 5 together (case 7)

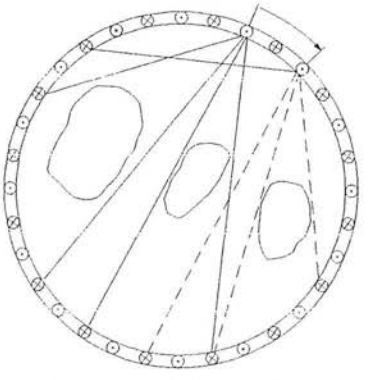

g) Case 4 and 6 together (case 8)

Figure 8.11. Possible development of two neighboured snapshots

For all snapshots where changes occur in the image, the changes are coded in the Image Improvement Code and together with the number of change i, the appearances in the scene (snapshot) n and stored. Four examples of cross-sections are shown in figure 8.12.a-d and for figure 8.12.a-b the related results are in tables 8.2.a-b.

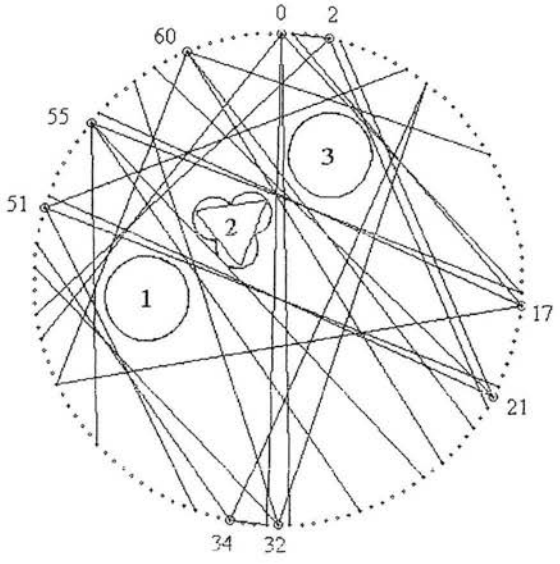

a) Three objects in a line

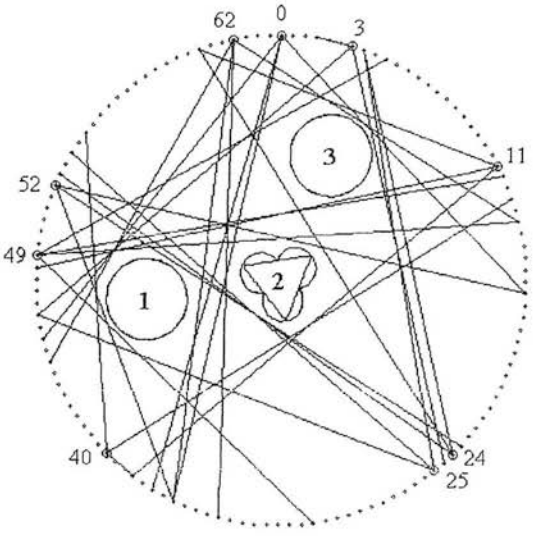

b) Three objects not in line

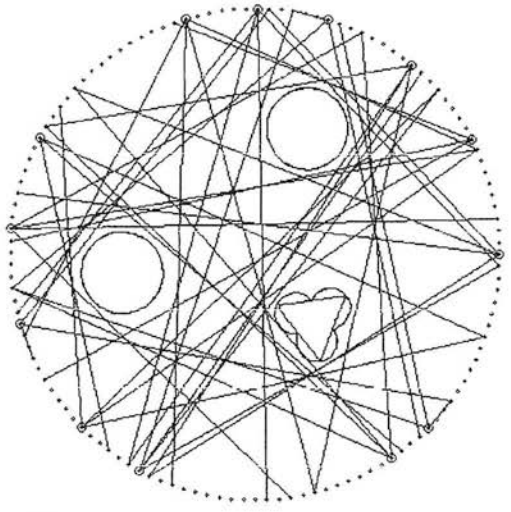

c) Nearly symmetrical distribution and space between the objects

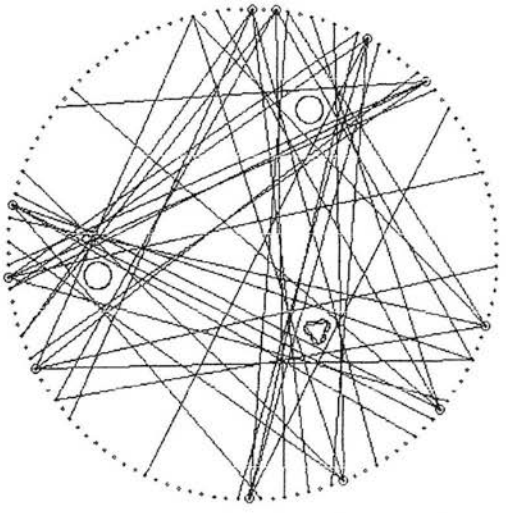

d) Never more than one object hidden

Figure 8.12. Examples of IIC images

i	0	**1**	2	3	4	5	6	7	8	**9**	10
n of remaining snapshots of a change	0	**2**	17	21	32	34	51	55	60	**66**	81
IIC-code	9	**1**	2	3	8	1	2	3	8	**1**	2
POT-code Correction case 9	9 3	**0**	2	1	3	0	2	1	3	**0**	2
OOC-code	2	**2**	11	11	12	12	1	1	2	**2**	11

a) For example shown in figure 8.12.a

i	0	**1**	2	3	4	5	6	7	8	**9**	10
n of remaining snapshots of a change	0	**3**	11	24	25	40	49	52	62	**67**	75
IIC-code	9	**1**	2	4	8	1	2	7	4	**1**	2
POT-code Correction case 9	9 2	**0**	2	1	3	0	3	1	2	**0**	2
OOC-code	1	**1**	9	11	12	12	2	1	1	**1**	9

b) For example shown in figure 8.12.b

Table 8.2. Number of change i, snapshot of change n, IIC- Code , POT-Code (explained in chapter 8.3.4), correction case 9 (explained in chapter 8.3.5), OOC-Code (explained in chapter 8.3.6)

The IIC-code is based on the change in the scene from one viewpoint to the next around the ring. There are two problems. Firstly, if there is no complete self-shadowing in the beginning of the analysis of the scene, the situation can not be clearly identified using only four chords. The first 'front' and second 'back' chord could be between the first and second or second and third object. Secondly the same problem can occur during the analysis, if between two totally self-shadowing situations only a small gap is determined without the change of the chord situation. This results in the IIC-code 9 (see table 8.2). The solution of the problem will be discussed in chapter 8.3.5.

8.3.4. Step 2: Generation of the Primary Object Transformation Code (POT-Code)

Using the IIC-code the number of objects, which can be seen from any related snapshot, must be investigated. This is coded in the POT-code together with the numbering of the objects in the sequence of their appearance in the scene for the investigated snapshots (see figures 8.2.b, 8.3.b). Also at this stage the real objects are not fixed and numbered, because there is yet not enough information!

The information about the order of 'back' and 'front' chords of each snapshot related to the objects in the ring is needed. There are four possibilities (see table 8.3). The object order is how they appear anti-clockwise in the image from the viewpoint (snapshot).

Because the algorithm described in chapter 3 requires only 'back' chords, the 'front' chords have to be partially inverted into 'back' chords to split and envelope each object and make it possible to use the known algorithm to determine the geometry of the objects. The information about a necessary negation (complementation) of the 'front' chord is always linked to the POT-Code. It is marked in table 8.3 with '-' for a required negation, otherwise with a '+' . For POT-code =1 the situation is as shown in figure 8.13, so for the 1.object the 1. 'front' chord has to be inverted, as for the 2.object the 2.'front' chord to become 'back' chords, but for the 3. object the second 'front' chord is a 'back' chord.

POT-code	Object 1	Object 2	Object 3	Object order	Description
0	$+m_B1[n]$ $-m_F1[n]$	$+m_B1[n]$ $-m_F1[n]$	$+m_B1[n]$ $-m_F[n]$	123	All 3 objects are shadowing each other
1	$+m_B1[n]$ $-m_F1[n]$	$+m_B2[n]$ $-m_F2[n]$	$+m_F2[n]$	1_2_3	Object '1' is separated from object '2' and object '2' from '3'
2	$+m_B1[n]$ $-m_F1[n]$	$+m_B2[n]$ $-m_F2[n]$	$+m_B2[n]$ $-m_F2[n]$	1_23	Object '1' is separated from objects '2' and '3', which are shadowing each other
3	$+m_B1[n]$ $-m_F1[n]$	$+m_B1[n]$ $-m_F1[n]$	$+m_B2[n]$ $-m_F2[n]$	12_3	Object '3' is separated from objects '1' and '2', which are shadowing each other

Table 8.3. POT-code for each snapshot for three objects (+ = normal, - = inverted chord)

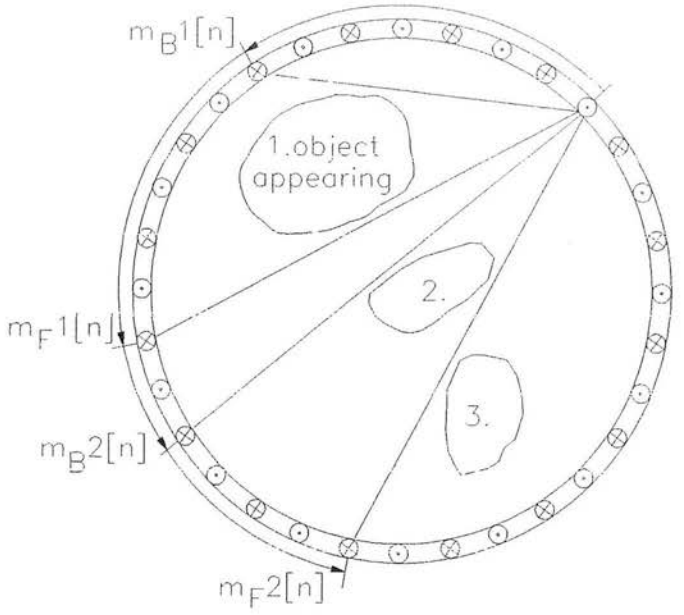

Figure 8.13. POT-code =1. situation

IIC[i]	IIC[i+1]	POT[i]	relation to figure 8.11.a-g
1	-	0	a
2	4,8	1	b,g
2	3,6	2	d,e
2	5,7	3	d,f
3,7	-	1	b,f
4,5	-	2	c,d
6,8	-	3	e,g
9	-	9	b-g (case3-8) possible (see chapter 8.3.5)

Table 8.4. POT-code transfer table for the POT-Code using the IIC-Code

Depending on the IIC-code 1-8 the POT transfer code is shown in table 8.4. Case 2 is a special case, because the order has to be determined using the successor of the IIC-Code array to give the precise information. The POT-Code for two examples shown in figures 8.12.a,b is given in table 8.2.

8.3.5. Step 3: Solution of the case 9 problem

Case 9 is a situation where the chords can not yet be assigned to the situation in the ring. This situation can occur:

1. At the beginning of multiple objects with a detected split of objects and the first IIC-code entry 2 the next entry is 1 (see figure 8.12.a-b),
2. A split between two objects can be seen from one snapshot n[i], the predecessor and successor do not detect a split, so that the IIC-code does not change within the gap. This can only happen when two objects are separated by a small gap (see figure 8.14.a).

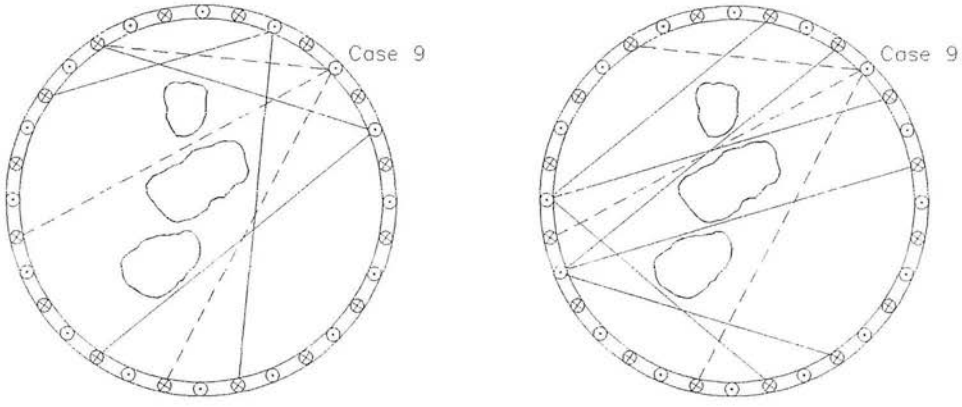

a) The case 9 problem in a current scan

b) One solution by looking from the opposite site

Figure 8.14. The case 9 problem

The problem can be solved

1. If there is an IIC-code 2 in the table (see table 8.2.a-b) at the place i+2 and the chords have the same receiver or neighbours, the same position of objects is valid, or
2. the chords $m_F1[i]$, $m_B2[i]$, $m_F2[i]$ have to be investigated looking on the opposite side until a similar matching chord is found in the opposite direction (see figure 8.14.b). Using the POT-code of these chords the problem can be solved. In the case where is also a case 9 situation the IIC-code has to be used. If a similar chord cannot be found, for example if a new gap between objects would be in the scene, it has to be investigated further, a full revolution ahead.

Based on this the POT-code can be corrected (see tables 8.2.a-b). The problem cannot be solved this way if the number of objects in the ring changes. This has to be investigated in the future.

8.3.6. Step 4: The generation of the Object Order Code (OOC-code)

On the basis of the POT-code it now becomes possible to identify and number the objects themselves and give the real order of the chords related to the real objects in the ring. Every possibility is coded in the Object Order Code (see examples in the tables 8.2.a-b).

The assignment of a number for each object is done by the defined separated appearance of each object within the scene. Once defined each object retains its number. The basic OOC-code is given below (see table 8.5), for example OOC-code 1 means
the real object order

1_23: the object with the number 1 is separated from shadowed objects 2 and 3 (POT-code 2),

but it also covers the situation

1_2_3 : as above, but objects 2 and 3 are also split

The OOC-code does not distinguish between these two cases, but this information is already part of the POT-code.

OOC-Code	Object order	OOC-Code	Object order	OOC-Code	Object order
1	1_23 or 1_2_3	5	2_31 2_3_1	9	3_12 3_1_2
2	12_3	6	23_1	10	31_2
3	1_32 1_3_2	7	2_13 2_1_3	11	3_21 3_2_1
4	13_2	8	21_3	12	32_1

Table 8.5. Basic OOC-code of different object orders

The determination of the OOC-code is split into two steps

1. The OOC-code within the first round must first be found.
2. If the OOC-code for the chords across the actual investigated transmitter becomes available from carrying out analysis backwards on the spiral, it is simpler to use this.

In the first round the algorithm is based on the use of look-up tables used until the first 'front' chord passes the transmitter 0 the first time (see figure 8.15).

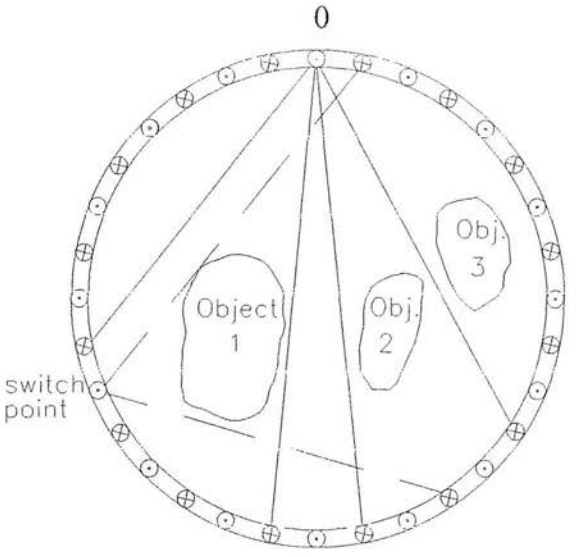

Figure 8.15. Switch point between first round and general detection of the OOC-Code

At the beginning of the procedure the object order is set to 123 with the OOC–Code 1 or 2 depending on the first snapshot. The OOC-code related to each i can be determined using the actual POT[i]–code, the predecessor POT[i-1] and OOC[i-1]. For different cases different OOCT-transformation tables containing the OOC-code are necessary depending on the POT-code.

POT[i-1]	**POT[i]**	**related OOCT-transformation table**
3	1,2	OOCT 3_12 transfer table (see table 8.6.a)
0	1,3	OOCT 20_31 transfer table (see table 8.6.b)
2	1	OOCT 20_31 transfer table (see table 8.6.b)
0	2	OOCT 0_2 transfer table (see table 8.6.c)
1	3	OOCT 1_3 transfer table (see table 8.6.d)

All situations with

POT[i-1]	->	**POT[i]**
any		0
0		2
1		3

have no impact on the object order and the OOC-code.

With the chosen look-up table and the OOC[i-1] code the actual OOC[i]-code can be determined (see tables 8.6.a-d).

Predecessor OOC[i-1]	New OOC[i]	Object order
2	5	2_31
4	11	3_21
6	9	3_12
8	3	1_32
10	1	1_23
12	7	2_13

a) The OOCT 3_12 table

Predecessor OOC[i-1]	New OOC[i]	Object order
1	3	1_32
3	1	1_23
5	7	2_13
7	5	2_31
9	11	3_21
11	9	3_12

b) The OOCT 20_31 table

Predecessor OOC[i-1]	New OOC[i]	Object order
1	9	3_12
3	7	2_13
5	1	1_23
7	11	3_21
9	5	2_31
11	3	1_32

c) The OOCT 0_2 table

Predecessor OOC[i-1]	New OOC[i]	Object order
1	2	12_3
3	4	13_2
5	6	23_1
7	8	21_3
9	10	31_2
11	12	32_1

d) The OOCT 1_3 table

Table 8.6. The Object order code transformation OOCT-tables for the first cycle

The real positions in form of the OOC-code are now known for the first part of the object.

For all following investigated snapshots i the OOC-code across the ring for the investigated chords is known. Therefore a different procedure can now be applied.

The following algorithm to determine the OOC-code for the objects is based on the analysis of the OOC-code of the transmitter n[i] backwards across the sensor. Five look-up tables are needed to determine the situation. The POT[i]-code from the predecessor opposite (see table 8.7) determines the use of the OOCT table (see tables 8.8).

POT[i]	Temporary tables	Final OOCT- tables
0	-	always OOC-code 0
1	FOTX_11 (see table 8.8.a) FOTX_13 (see table 8.8.b)	FOTX_1 (see table 8.8.c)
2	-	FOTX_2 (see table 8.8.d)
3	-	FOTX_3 (see table 8.8.e)

Table 8.7. Determination of the required OOCT-table

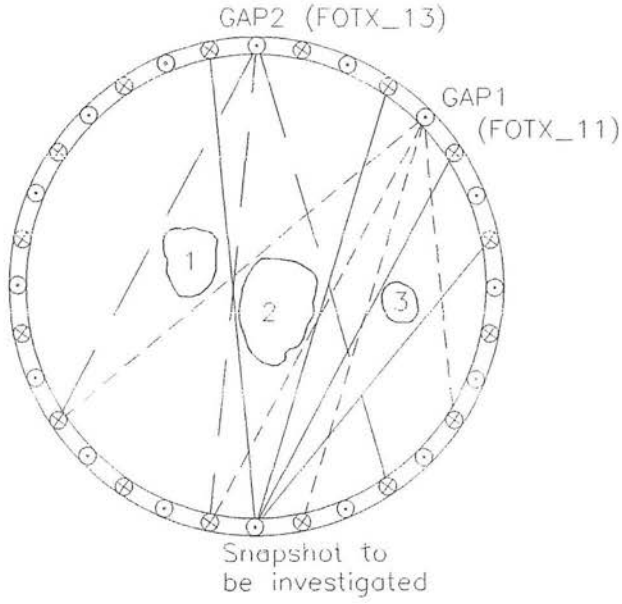

Figure 8.16. Situation on the opposite side and need for tables FOTX_11, FOTX_13

The temporary tables FOTX_11, FOTX_12 are necessary, because the objects are not shadowing each other (object order e.g. 3_2_1, see figure 8.16) and instead of one gap between the objects two have to be investigated. The OOC-code from the opposite sides of the two 'front' chords of the two gaps defines the final OOC-code given in the FOTX_1 table. The linked object number will give the 6 possible orders of the objects within the scene.

OOC-code across	Temporary code
1	3
2	3
3	2
4	2
5	1
7	1
7	3
8	3
9	2
10	2
11	1
12	1

a) FOTX_11

OOC-code across	Temporary code
1	1
2	1
3	1
4	1
5	2
7	2
7	2
8	2
9	3
10	3
11	3
12	3

b) FOTX_13

Link between results of FOTX_11 and FOTX_12	OOC-code of actual chord
1 2	3
2 1	5
2 3	7
3 2	9
1 3	1
3 1	11

c) FOTX_1

OOC-code across	OOC-code of actual chord
1	-
2	9
3	9
4	5
5	-
7	1
7	1
8	9
9	-
10	5
11	5
12	1

d) FOTX_2

OOC-code across	OOC-code of actual chord
1	6
2	-
3	6
4	6
5	10
7	-
7	10
8	10
9	2
10	-
11	2
12	2

e) FOTX_3

Table 8.8. Transfer tables for the OOC-code from the situation across backwards

8.3.7. Step 5 and 6: Transfer of data and determination of objects

Based on the OOC-code and the POT-code the primary chords can be assigned to object 1, object 2 and for object3. Because all chords have to have the 'back' chord direction a number of 'front' chords have to be 'inverted'. This requires an artificial doubling in the number of transmitters and receiver. Each transmitter is now also a receiver and vice versa.

For the generated primary data for each object the known algorithm (see chapter 3, 4) can be applied to determine the geometrical properties. A result of simulation is shown in figure 8.17, using a cylinder, a pyramid and half of an ellipsoid (more examples see figure 8.7, 8.8). The deformation rises with the increase of the diameter of the objects and the decrease of their distance from each other.

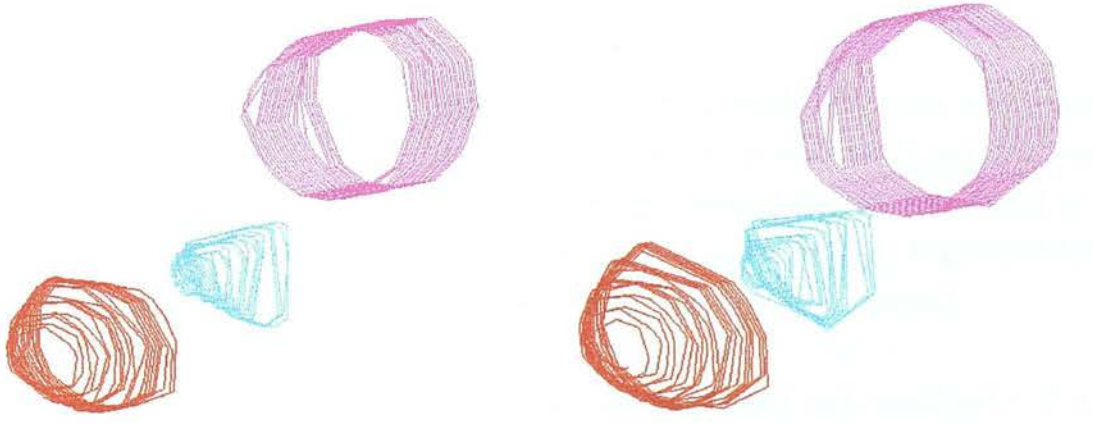

a) Smaller diameter b) Larger diameter

Figure 8.17. Three objects simulated, separated and determined

8.3.8. Problem of the method of separation used

The principle of separating the objects works within limitations. The main problem is the right decision for the right IIC, POT, OOC-code at any time, especially if the objects within the ring are under narrow angles from the viewpoint (snapshot). One mistake causes the wrong result for the following investigations concerning all objects. In the future more investigations have to be carried out, to make this method more flexible and safer or to develop a different method. One different possibility could be the determination of one certain point within the cross-section of each object. Using these points all chords can be investigated and transferred related to each object. Overall it can be said, when there is more than one unknown object passing through the ring, the situation is much more complex than with a single object.

8.4. Separation of one unknown object from objects with a known position

In practice one special case of multiple objects is known, which will allow a different simplified approach. The mechanical transport machine of the Accu Pack machine (see chapter 7.3) consists of 2 or 3 plastic cables moving with constant speed. The objects are transported and presented to the sensor system, including the cables, cross-sectional images are shown in figure 8.18. The position of the cables is always constant.

The situation concerning the clear ring (only the cables are in the ring, see figure 8.18.a) is analysed and recorded. The situation for every snapshot is known. The procedure is to scan the situation in the ring, and as soon as a change in one snapshot occurs the object is detected and can be targeted.

The data handling can be characterised by the following steps:

- All 'front' chord data have to be transferred into 'back' chords. This means the two spirals are joined together again and the Nyquist criteria has to be considered.
- Starting with the chord firstly recognised as touching a new object, all chords have to be investigated and separated as part of the object or as the cables (see figure 8.18.b).

- If in the image the object is touching the cable (see figure 8.18.c), under special circumstance concerning the angle of chord from a snapshot the envelope can be corrected by the use of an 'artificial' chord taking out the width of the cable.

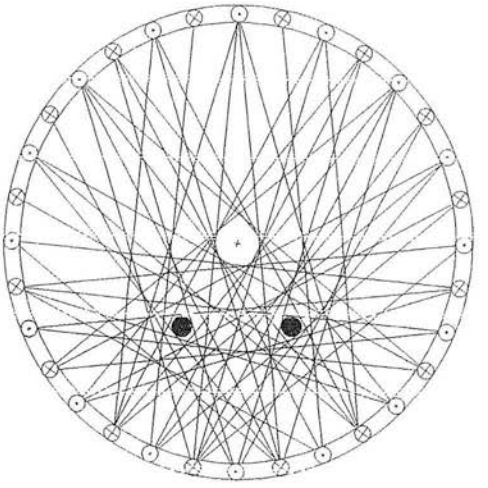

a) No unknown object is in the ring

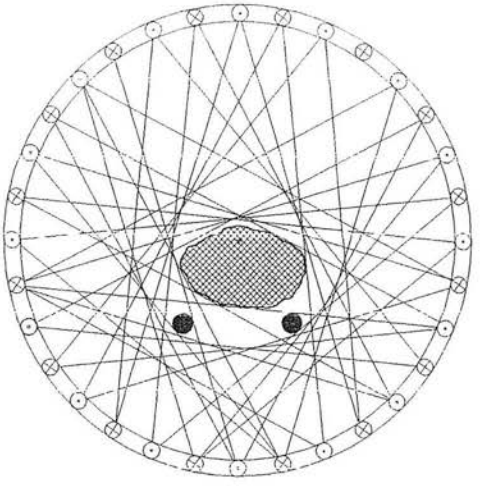

b) Object is in the ring

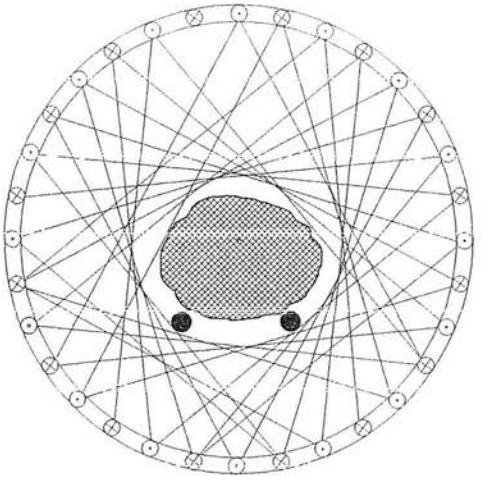

c) Object is in the ring with maximum cross-section

Figure 8.18. One unknown and two permanent objects of known position in the ring

This special case has to be investigated in the future. It could deliver the possibility of an alternative to the Accu Pack system (see chapter 7.3). The problems associated with the handling of multiple unknown objects (see chapter 8.3) do not occur, because the situation is much more controlled with only one unknown object passing through the ring.

8.5. Summary

In this chapter multiple objects were investigated. A model to simulate objects in the ring was described. The self-shadowing of objects creates shape errors of the objects. The separation of multiple objects is a complex operation. For this reason the number of objects was set to three. It is possible to use only logical analysis of the chords to split three objects and use the algorithms described earlier to determine the properties of objects. There are problems in the method concerning certain orders of objects from some viewpoints. In the future the method of separation should be improved. A simpler case with an immediate practical use is the situation with objects of fixed position and one variable object of interest.

9. Conclusions

Visual systems are becoming more important in the automated world. New kinds of light sources and sensors allow new arrangements of sensor systems, not comparable with solutions seen in nature. These sensor systems have properties giving them each advantages in practical use under different requirements. Systems can be classified by the kind of lighting, light interaction with the objects, characteristic of receivers, presentation of the objects, movement either of the sensor system or the objects, models used by the system to describe object parameters. The separation and presentation of objects require much attention in the first place, in order to arrive at the correct choice of sensor system, optimising the performance and cost of the system.

The ring-sensor system for the determination of 2-D and 3-D properties of objects described in this thesis has a different mechanical structure to most other visual systems. The closest comparison can be found in sensors for tomography, but instead of transmitted light, shadow is used. Alternately arranged transmitters and receivers with Lambertian characteristic are fixed on a circular ring, building up an environmentally stable multiple light-beam configuration. Each transmitter is activated in sequence around the ring and light beams are built up to every receiver giving a snapshot of the scene. All light beams in one snapshot (viewpoint) are investigated to find the shadow of the object. Every object is touched by two non-interrupted light beams, the so called 'back' and the 'front' chords. For every snapshot the result of measurement is one number containing the number of receivers between the activated transmitter and the closest non-interrupted light beam. The system carries out a pseudo-rotation, building up a cylinder-tunnel, where singulated objects pass through. Because of a shift in space and phase, 'back' and 'front' chords are preferred to be investigated independently for single objects in the ring.

With a modified polar co-ordinate system and special algorithms it is possible to describe the surface of 3-D objects with two enveloping spirals, one on the basis of the 'back' chords, the other on the 'front' chords. The objects passing through one by one are caught in a limited symmetrically built space, however their position is variable. Data received from the sensor system are components of describing vectors. The number of possible vectors is limited from each viewpoint. This allows the predominant use of pointer instructions for the calculations.

The data necessary to describe objects is minimal compared with other systems, in particular as compared to pixel based systems. There is a significant disadvantage, concave areas in cross-section can not be seen, because the system uses the shadow principle. However for 3-D objects, concave sections along the direction of travel can be seen.

For the determination of geometrical properties the image has to be segmented. In the case of the ring sensor system, the area between the ring and the object is studied. The main parts are triangles, each with an accompanying circle segment. The determination of these segments allows the calculation of the cross-sectional areas of an object. If objects are predominantly convex, the objects can pass through in any orientation for determination of volume of the object and the position in the ring. The algorithms introduced for the determination of axis-measurement require passage through the ring in longitudinal direction.

Besides weight and volume, axis measurements are vital to describe the shape of objects. Many agricultural objects are ellipsoid in shape. For these, the axes of the middle slice and the length are adequate for a description.

The parameters that can be determined by the ring sensor system are

- volume
- length
- position of the largest slice of an object in longitudinal direction
- position of the object in space
- major and minor axes of the largest and the middle slice
- circumferences in crosswise direction
- mass (if the density is known)
- density (if the mass is known)

An advantage of the system is that the determination of all geometric parameters is based on values known from the determination of the contour. The expansion in the third dimension and the determination of volumes of objects is straightforward using the same algorithms as for the 2-D case. This supports real time use and keeps the necessary computer power low.

.

A model is described to simulate one object or cross-section in the ring at a time. The positions and shapes of objects can be variable in a wide range within the limits set by the ring.

Using real measurements and simulations of objects it becomes possible to build up artificial 3-D worlds on a minimum data basis.

Tests were carried out to find the limits using comprehensive simulations of different objects, for instance in different areas of the sensor system, different arrangements, speed variation of the sensor system and using the 'back' and 'front' spiral to envelope objects. The results show the increase of accuracy with the cross-sectional size of the objects and with more transmitters and receivers. The measured size of objects (over a minimum size) is independent of the position in the ring. The speed of spheres and ellipsoids passing the system is unimportant for the accuracy of the determination of geometrical properties above a minimum diameter. The cross-sectional shape of objects has an influence on the determined value, but if the approximate shape is known this error can be minimised.

Some other interesting properties were investigated. The number of all available intersections between chords in the ring increases sharply with any increase in the number of transmitters and receivers. The amount of primary data for one object created whether by simulations or measurements is low. It can be further reduced by differential coding for data transfer and storage. During processing, the amount of data increases. The time consumption of the algorithms can be defined for best and worst case conditions depending on shape, and is linear growing with the length of the object.

The system properties are very flexible in wide ranges as for example the size of the system, number of transmitters and receivers, and sampling rate. This requires design and adaptation to the desired task. Under the expected use for agricultural products, a practical solution of a ring sensor system was designed with 64 transmitters, 64 receivers, a diameter of 175mm and running at 400 rev/s, including the comprehensive software to control the system, to handle and analyse the data. It can scan 3-D objects in real time with up to 10 average potatoes per second which equates up to about 3.6 tonnes per hour. Practical tests were carried out with artificial objects and potatoes and confirmed the expected performance of the ring sensor system for volume and axis determination. The accuracy was better than 7% for a volume larger than $50cm^3$ and 5% when larger than 100g. The ring sensor system is compared with a system used in practice in the potato industry (Accu Pack system) and achieves about half the error.

For practical use the objects should be presented one by one in horizontal direction and not have major concave areas in the cross-sections. For objects such as agricultural products the ring sensor system offers the potential for a relatively fast and accurate determination of geometric parameters.

The ring can be used for example in plant breeding, in the vegetable handling industry, in baking, meat, fish and timber industries for sorting products and/or quality control. In crop handling it is useful for shapes such as potatoes, cucumber and carrots. Products such as onions, apples and bananas cause problems of presentation, since concave areas result in lower accuracy.

Finally an introduction into the situation of multiple objects in the ring sensor is given. A model to simulate objects in the ring is described, extending the method known from the simulation of single objects. Additional errors occur caused by the self-shadowing of objects and a shape error of the objects in the view of the sensor system is also created.

The separation of objects introduced here is a complex operation. It is possible to use only logical analysis of the chords to split three objects and use the algorithms described earlier to determine the properties of objects. It is necessary therefore to combine the two spirals of the 'back' and 'front' chord under the consideration of the Nyquist criteria. The surrounding conditions cause problems in the determination of the positions of the objects from some viewpoints. In future the method of separation should be improved. A simpler case is the situation with objects of fixed position and one variable object of interest in the ring, as occurs in practice with potatoes presented on three stable wires (Accu Pack system).

The following should be considered for further investigation in the future:

- minimising the geometrical size of the system to investigate smaller products
- different geometry of the ring e.g. partial ring solutions, rectangular solutions
- effect of increase of either the transmitters or receivers on the resolution
- method of finding characteristic axes of objects independently from the orientation of passage
- development of further methods of splitting multiple objects
- the situation of changing numbers of objects in the ring
- as a special practical case, one unknown object presented on 2 or 3 wires with a known position and size

It is desirable that more work should be put into the further development of this unique sensor solution in the future.

10. Appendix

10.1. Appendix 1: Distance between transmitter and intersection with predecessor

x,y	label for the actual chord A, the predecessor P or the successor S
$k_{Tx,TRy}$	numbers of receivers between different transmitters or receivers determined using the variables n for the marked transmitter or $m_B1[n]$ for the marked receivers. Multiplied by angle β, angles $\omega_{M,Tx,TRy}$ will be determined.
$\omega_{M,Tx,TRy}$	angle at the circumference centred on a transmitter $T_X[n]$ created with the radius of the ring (with the midpoint M) and a further transmitter or receiver.

$$\omega_{M,TA,Tp} = \pi / 2 - k_{TA,Tp}\ \beta$$

$$\omega_{M,TA,RA} = \pi / 2 - (k_{TA,RA} + ½)\ \beta$$

$$\tau1 = \omega_{M,TA,Tp} - \omega_{M,TA,RA} = (½ + k_{TA,RA} - k_{TA,Tp})\ \beta$$

$$\omega_{M,Tp,Rp} = \pi / 2 - (k_{TA,Rp} - k_{TA,Tp} + ½)\ \beta$$

$$\tau2 = \omega_{M,TA,Tp} + \omega_{M,Tp,Rp} = \pi - (k_{TA,Rp} + ½)\ \beta$$

$$\tau3 = \pi - \tau1 - \tau2$$

$$|T_A{:}C_P[n]| = |T_A{:}T_P[n]|\ \sin \tau2 / \sin \tau3$$

10.2. Appendix 2: Distance between transmitter and intersection with successor

$$\omega_{M,Ts,TA} = \pi / 2 - k_{TA,Ts}\ \beta$$

$$\omega_{M,Ts,Rs} = \pi /2 - (k_{Ts,Rs} + ½)\ \beta$$

$$\tau1 = \omega_{M,Ts,TA} - \omega_{M,Ts,Rs} = (½ + k_{Ts,Rs} - k_{TA,Ts})\ \beta$$

$$\omega_{M,TA,RA} = \pi / 2 - (k_{Ts,RA} - k_{TA,Ts} + ½)\ \beta$$

$$\tau2 = \omega_{M,Ts,TA} + \omega_{M,TA,RA} = \pi - (k_{Ts,RA} + ½)\ \beta$$

$\tau 3 = \pi - \tau 1 - \tau 2$

$|T_A:C_S[n]| = |T_A:T_S[n]| \sin \tau 1 / \sin \tau 3$

10.3. Appendix 3: Distance between two parallel chords

$\alpha 1 = 2 (k_{TA,RA} + 1) \beta$

$\alpha 2 = 2 (k_{TX,RX} + 1) \beta$

$|C_A:M| = r \cos \alpha 1 / 2$

$|C_X:M| = r \cos \alpha 2 / 2$

$|C_A:C_X| = |C_A:M + C_X:M|$

$|C_A:C_X| = r \, | \cos (k_{TA,RA} + 1) \beta + \cos (k_{TX,RX} + 1) \beta |$

10.4. Appendix 4: Distance between chord and intersection

$\varphi = \varphi 2 - \varphi 1$

$\varphi = \pi / 2 - (k_{TX,RX} + 1) \beta - (\pi / 2 - (k_{TX,RX^*} + 1) \beta)$

$\varphi = (k_{TX,RX^*} - k_{TX,RX}) \beta$

$|C_X:C_X^*| = |T_X:C_X| \sin \varphi$

$|C_A:C_X| = |C_A:C_X^*| + |T_X:C_X| \sin ((k_{TX,RX^*} - k_{TX,RX}) \beta)$

10.5. Appendix 5: Distance between two intersections

$|T_X:C_X^*| = |T_X:C_X| \cos \varphi$

$|T_X:C_Z| = \frac{1}{2} (|T_X:R_X^*| - |T_A:R_A|)$

$|R_A:C_A| = |T_A:R_A| - |T_X:C_X^*| + |T_X:C_Z|$

$|R_A:C_A| = \frac{1}{2} (|T_A:R_A| + |T_X:R_X^*|) - |T_X:C_X^*|$

10.6. Apendix 6: Additional information about the practical sensor solution

The Ring Sensor - how it works

The main part of the system is an **optical ring**, which the objects/potatoes pass through one by one. This ring consists of a large number of IR-emitters and receivers which are alternately arranged. The emitters emit infrared light in succession. Each receiver is able to 'see' each activated transmitter. As an objects pass through the ring lots of **shadow zones** are created (figure 1). Around the object/potato the shadows zones are noted and assembled to create a **cross section**. The scanner generates 400 cross sections of an object in one second. Fig. 2 shows a cross section of a typical potato. As the object moves through the scanner/ring, an enveloping spiral of scans creates a 3D representation of the outline of the object. (figure 3).

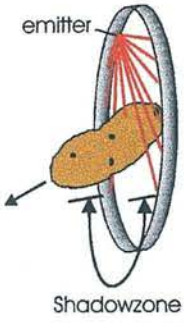

Fig.1: Shadow zones

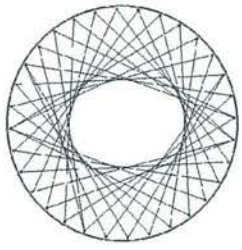

Fig.2: Cross section of a potato

Fig.3: A scanned cuboid

The following geometrical properties can be calculated with the help of these cross sections in real time:

- Volume
- Length
- Position of the largest slice of an object
- Major and minor axis of the largest and the middle slice
- Mass (if the density is known)

Hardware requirements and Software features

The 3D scanner is connected to a standard **PC** via an industrial bus system (CAN). A PC-program initialises and supervises the sensor. On demand it saves scanned data (volume and axes) of each object to a simple name.**txt file** which can be used by any calculating programme or spreadsheet.

RESULTS

	A	B	C	D	E	F	G
1	Volume	Length	max. Slice			middle Slice	
2			Position	max. Ø	min. Ø	max. Ø	min. Ø
3	1580	203	114	110	91	96	83
4	1310	180	95	84	79	80	76
5	1259	169	93	83	78	81	69

Technical data

Max. diameter of objects:	120 mm
Max. length of objects:	depending on speed, typically > 300 mm
Accuracy of volume:	3% (for a typical potato), at a speed of 1.4 m/s
Accuracy of length:	1% (for a typical potato), at a speed of 1.4 m/s
Max. throughput:	4-5 objects/second with a length of less than 200 mm each at a speed of 1.4 m/s
Power supply:	110-240V AC/ 50 Hz, 1A
Size over all:	360mm * 280 mm * 140 mm

argus electronic gmbh
Joachim-Jungius-Straße 9
18059 Rostock
Germany

Tel.: +49 / 381 / 4059 815
Fax: +49 / 381 / 4059 200
http: //argus.in-mv.com

SIEMENS

SFH420

GaAs Infrared Emitter
SMT-TOP-LED™

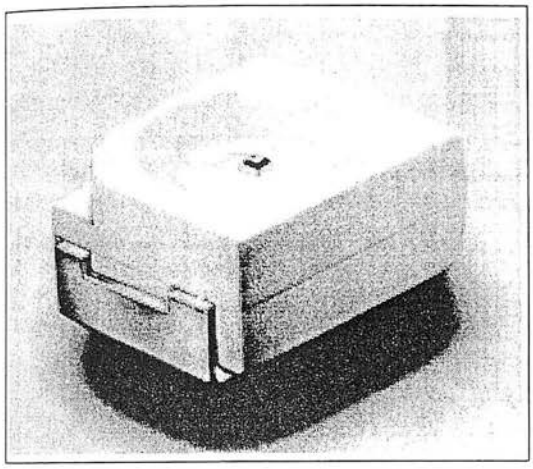

Package Dimensions in Inches (mm)

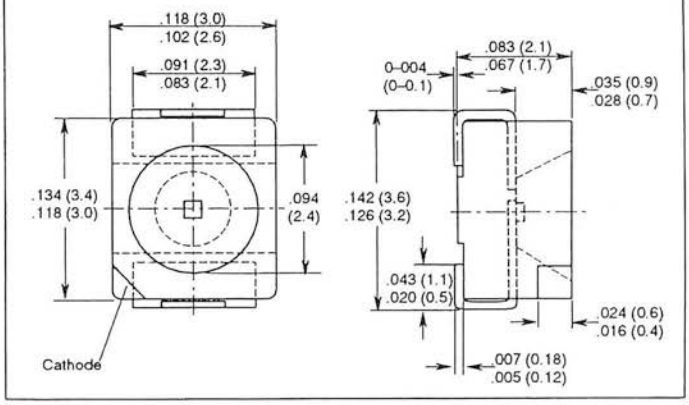

FEATURES

- **Surface Mountable PL-CC-2 Package**
- **Suitable for Vapor-Phase Reflow, Infrared Reflow, Wave Solder Processes**
- **Compatible with Automatic Placement Equipment**
- **GaAs IR LED with Wide Viewing Angle**
- **Good Linearity [Ie = f (I_F)] at High Currents**
- **High Reliability/Long Lifetime**
- **Fast Response Time**
- **Matches with SFH320/SFH320F Phototransistor**
- **Applications**
  - **Measurement and Control**
  - **Touch Screens**
  - **Light Curtains**

DESCRIPTION

The SFH420 is a wide angle GaAs LED in a compact surface mountable package. The device is compatible with automatic placement equipment and can withstand IR reflow, vapor phase reflow and solder processes. Their small size makes them suitable for dense packaging in array applications such as touch screens and precise position measurement.

Maximum Ratings

Operating and Storage Temperature (T_A, T_{STG}) ..... –55 to +100°C
Junction Temperature (T_J) ..... 100°C
Reverse Voltage (V_R) ..... 5 V
Forward Current (I_F) ..... 100 mA
Pulse Current (I_{FSM}) τ=10 µs, D=0 ..... 1A
Power Dissipation (P_{tot}) T_A=25°C ..... 160 mW
Thermal Resistance, Junction to Ambient
Mounting on PC Board (R_{thJA}) ..... 450 K/W
Chip to Solder Area (R_{thJA}) ..... ≈250 K/W

Characteristics (T_A=25 °C)

Parameter	Symbol	Value	Unit
Peak Wavelength (I_F=100 mA, t_p=20 ms)	λpeak	950±20	nm
Spectral Bandwidth (50% of I_{max}, I_F=100 mA)	Δλ	55	nm
Half Angle	φ	±60	Deg.
Radiant Sensitive Area	A	0.09	mm^2
Radiant Sensitive Area Dimensions	L x W	0.3 x 0.3	mm
Response Time (I_F=100 mA, R_L=50 Ω, from 10% to 90% or 90% to 10% of I_E)	t_R, t_F	0.5	µs
Capacitance (V_R=0 V, f=1 MHz)	C_O	25	pF
Forward Voltage			
(I_F=100 mA, t_p=20 ms)	V_F	1.3 (≤1.5)	V
(I_F=1 A, t_p=100 µs)	V_F	2.3 (≤2.8)	V
Reverse Current (V_R=5 V)	I_R	0.01 (≤1)	µA
Total Radiant Flux (I_F=100 mA, t_p=20 ms)	Φ_e	22	mW
Temperature Coefficient, (I_e or Φ_e)(I_F=100 mA)	TC_I	–0.5	%/K
Temperature Coefficient, V_F (I_F=100 mA)	TC_V	–2	mV/K
Temperature Coefficient, λpeak (I_F=100 mA)	TC_λ	+0.3	nm/K
Radiant Intensity: SFH420-N			
(I_F=100 mA, t_p=20 ms)	I_{Emin}	2.5	mW/sr
(I_F=100 mA, t_p=20 ms)	I_{Emax}	5	mW/sr
(I_F=1 A, t_p=100 µs)	I_{Etyp}	38	mW/sr

Relative spectral emission
$I_{REL}=f(\lambda)$

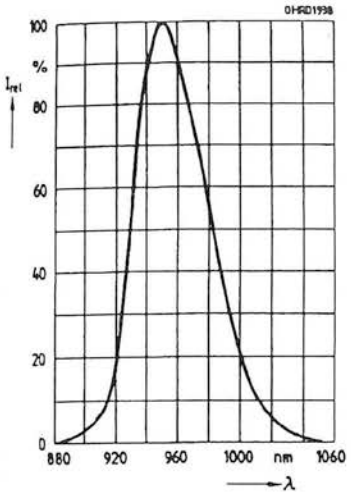

Relative radiant intensity
I_E/I_E 100 mA = f(I_F), one pulse, τ = 20 µs

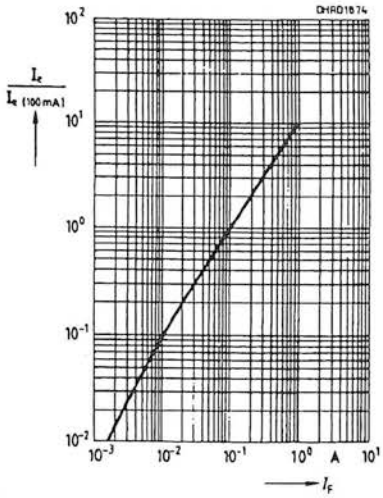

Radiation characteristics $I_{REL}=f(\varphi)$

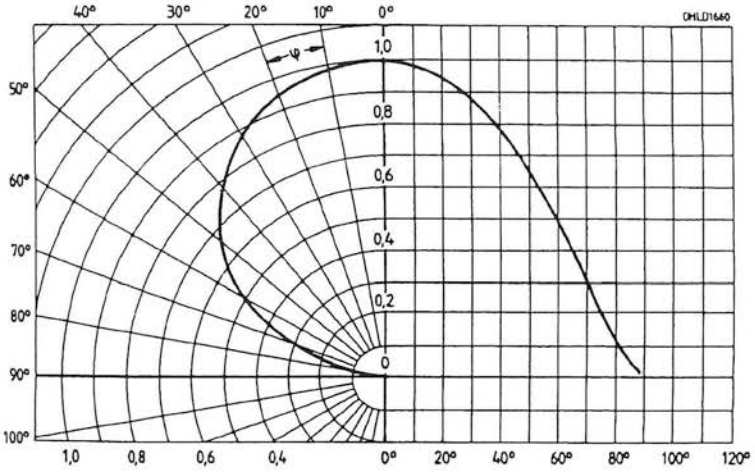

Permissible pulse handling capability $I_F=f(\tau)$, $T_A \leq 25°C$
duty cycle D=Parameter

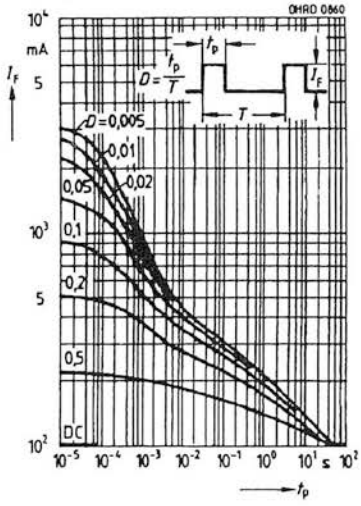

Maximum permissible forward current $I_F=f(T_A)$

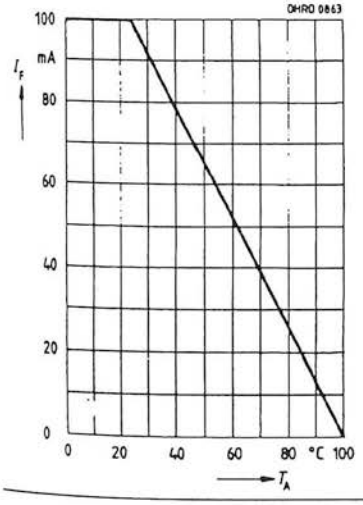

Forward current
$I_F=f(V_F)$, one pulse, τ = 20 µs

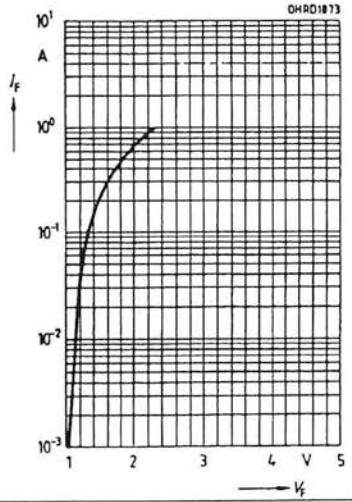

SIEMENS

SFH320
DAYLIGHT FILTER SFH320F
NPN Silicon Phototransistor
SMT-TOPLED™

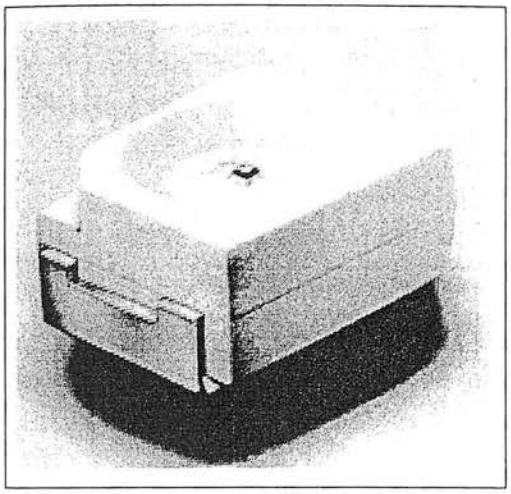

Package Dimensions in Inches (mm)

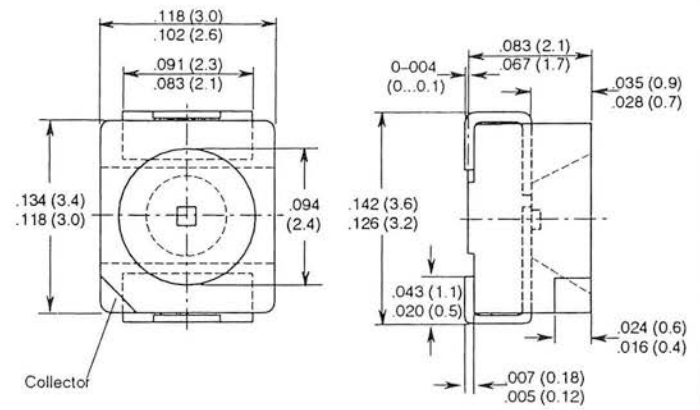

FEATURES

- **NPN Silicon Phototransistor**
- **Daylight Filter Option–SFH320F**
- **Suitable for Vapor-Phase Reflow, Infrared Reflow, Wave Solder Processes**
- **Compatible with Automatic Placement Equipment**
- **High Photosensitivity**
- **High Reliability**
- **No Measurable Degradation**
- **Three Photocurrent Bin Options**
- **Matches with SFH420–SMT IRED**
- **Surface Mountable PL-CC-2 Package**
- **Applications**
  - **– Measurement and Control**
  - **– Touch Screens**
  - **– Miniature Light Curtains**

DESCRIPTION

The SFH320/320F are high-sensitivity NPN silicon phototransistors in a compact surface-mountable package. Available with or without a daylight filter, they are compatible with automatic placement equipment and can withstand IR reflow, vapor phase reflow, and wave solder processes. Their small size makes them suitable for dense packaging in array applications such as touch screens and precise position measurement.

Maximum Ratings

Operating & Storage Temperature (T_{OP}, T_{STG}) ..... –55 to +100°C
Collector-Emitter Voltage (V_{CE}) ..... 35 V
Collector Current (I_C) ..... 15 mA
Peak Collector Current (I_{CS}) τ<10 µs ..... 75 mA
Power Dissipation (P_{tot}) T_A=25°C ..... 165 mW
Thermal Resistance, Junction to Ambient
Mounting on PC Board (R_{thJA}) ..... 450 K/W

Characteristics (T_A=25 °C, λ=950 nm)

Parameter	Symbol	SFH320	SFH320F	Unit
Maximum Sensitivity Wavelength	λ_{Smax}	860	900	nm
Spectral Range, Photosensitivity (S = 10% of S_{max})	λ	380 to 1150	730 to 1120	nm
Radiant Sensitive Area	A	0.045	0.045	mm^2
Radiant Sensitive Area Dimensions	L x W	0.45 x 0.45	0.45 x 0.45	mm
Distance, Chip Surface to Case Surface	H	0.5 to 0.7	0.5 to 0.7	mm
Half Angle	φ	±60	±60	Deg.
Capacitance (V_{CE}=0 V, f=1 MHz, E=0)	C_{CE}	5.0	5.0	pF
Dark Current (V_{CEO}=25 V, E=0)	I_{CEO}	1(≤200)	1(≤200)	nA

Photosensitivity ranges by dash numbers.

Parameter	Symbol	-1	-2	-3	-4	Unit
Photocurrent (E_e=0.1 mW/cm², V_{CE}=5 v)	I_{PCE}	10–20	16–32	25–50	≥40	µA
SFH320: (E_V=1000 lx, std. light A, V_{CE}=5 V)	I_{PCE}	260	420	650	1000	µA
Rise Time/FallTime (I_C=1 mA, V_{CC}=5 V, R_L=1 kΩ)	t_r, t_f	5	6	7	8	µs
Collector-emitter Saturation Voltage (I_{PCE}=I_{PCEmin}(1) • 0.3, E_e=0.1 mW/cm²)	V_{CEsat}	150	150	150	150	mV

Note: 1. I_{PCEmin} is the minimum photocurrent for each group.

Relative spectral sensitivity–SFH320
$S_{REL}=f(\lambda)$

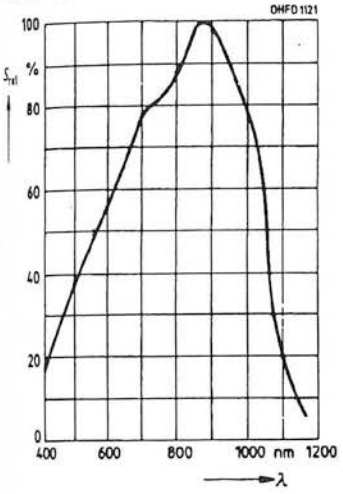

Relative spectral sensitivity–SFH320F
$S_{REL}=f(\lambda)$

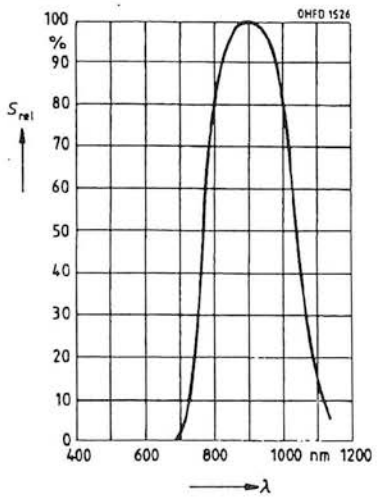

Photocurrent $I_{PCE}=f(E_e)$, V_{CE} =5 V

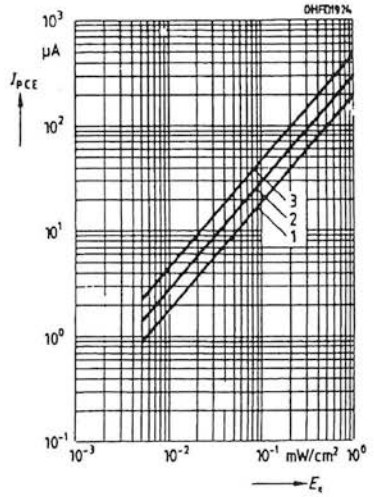

Directional characteristic
$S_{REL}=f(\varphi)$

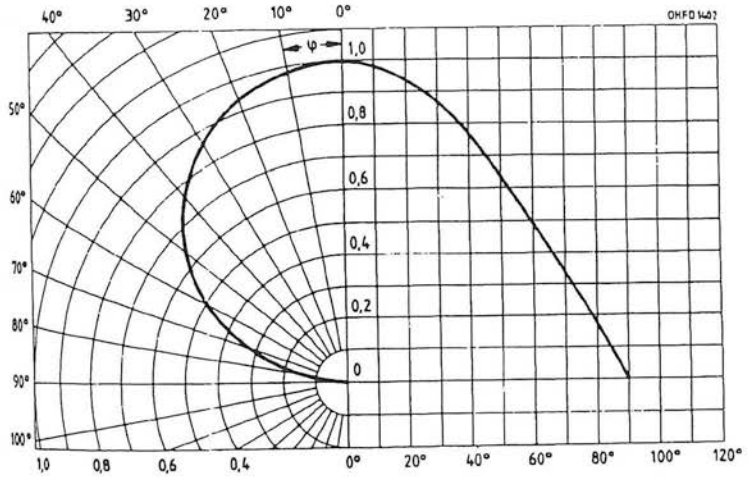

Total power dissipation
$P_{TOT}=f(T_A)$

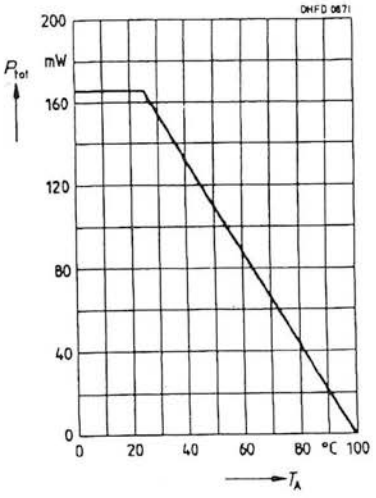

Photocurrent
$I_{PCE}=f(V_{CE})$, E_e=Parameter

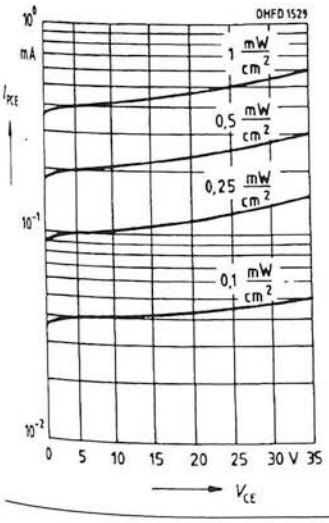

Dark current $I_{CEO}=f(V_{CE})$, E=0

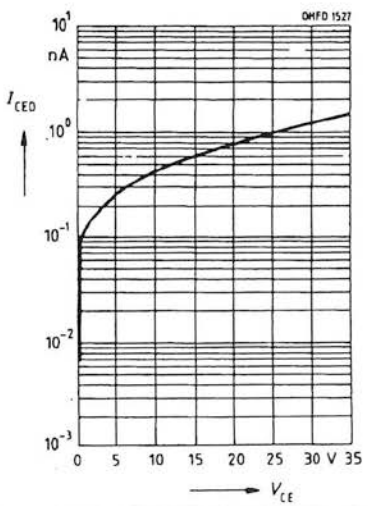

Dark current $I_{CEO}=f(T_A)$,
V_{CE}=25 V, E=0

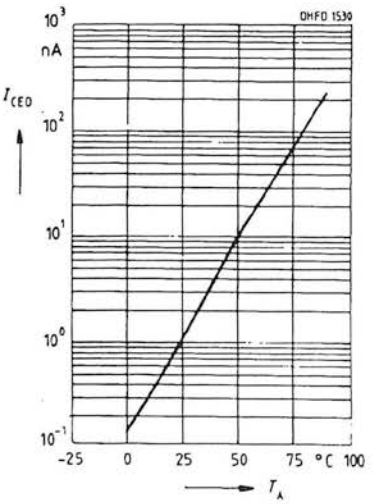

10.7. Appendix 7: Diagrams concerning results of practical measurements

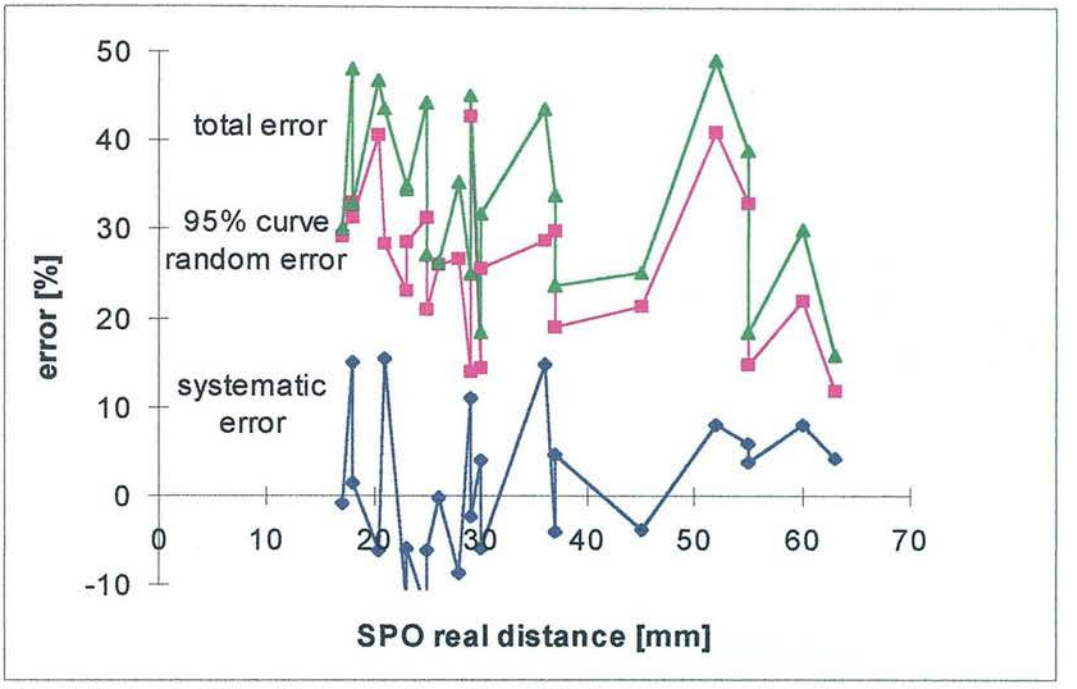

Figure 10.1. Position of largest slice

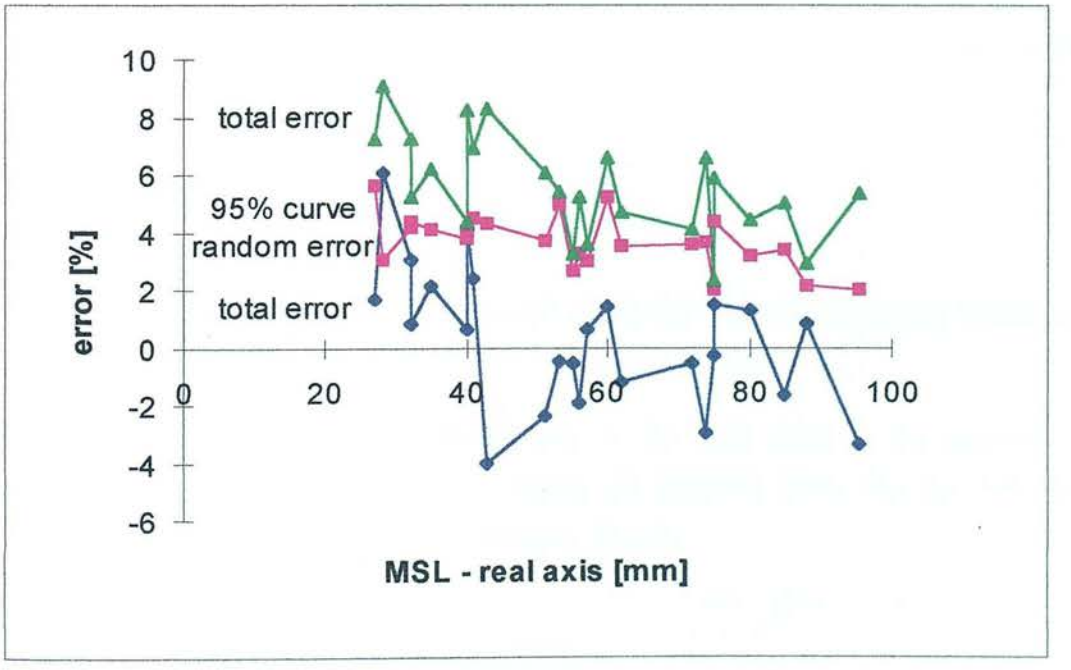

Figure 10.2. Major axis of the middle slice

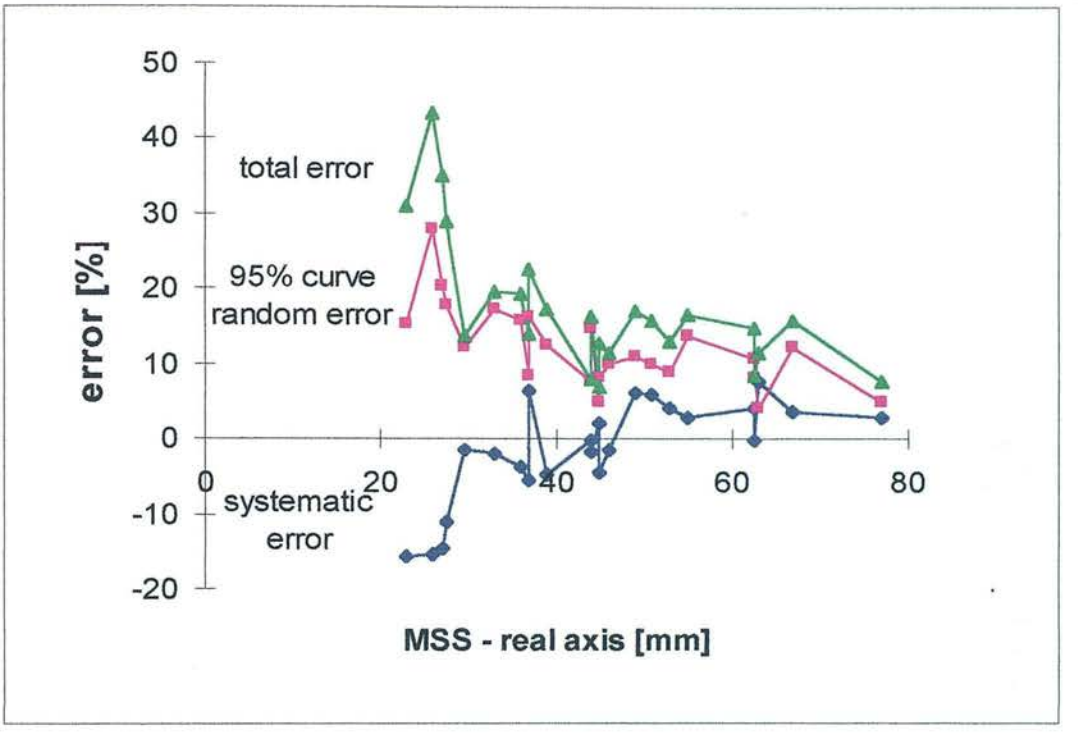

Figure 10.3. Minor axis of the middle slice

10.8. Appendix 8: Arrays of data in the computer memory

It is essential to keep linear arrays of data in the right order in the memory of the computer. The amount of data is depending on different tasks (for the 1-D case see chapters 6.2, 6.3) and increasing for multiple objects.

Name of the arrays	Definition	Info
1. Arrays for original snapshots (primary data)		
Z0	1. 'back' chords	*
Z1	1. 'front' chords	**
Z2	2. 'back' chords	***
Z3	2. 'front' chords	***
2. Final arrays for object determination (spiral)		
FCHN	numbers of the remaining chords	*
FCHM	related distance of receiver to transmitter $m_B1[n]$	*
FCHR	distance from transmitter to the related intersection $\|T_A{:}C_P[n]\|$	*
3. Arrays for primary data for multiple objects		
OBJ0	Object 1 'back' chords	***
OBJ1	'front' chords	***
OBJ2	Object 2 'back' chords	***
OBJ3	'front' chords	***
OBJ4	Object 3 'back' chords	***
OBJ5	'front' chords	***
4. Arrays for separation of objects		
n	Number of snapshot with change of chords	***
IIC_A	Image improvement code array	***
POT_A	Primary object transformation code array	***
OOC_A	Final object order code array	***
5. Look-up tables		
TRC	Code for chord position during simulation of multiple objects	***
IIC	Code of change of chords within the image	***
POT	Transfer code from IIC to POT-code	***
OOCT 20_31	\	***
OOCT 0_2	\	***
OOCT 20_31	> Transfer code for 1.round for OOC-determination	***
OOCT 3_12	/	***
OOCT 1_3	/	***
FOTX_11	\	***
FOTX_13	\	***
FOTX_1	> Transfer code for the general OOC-determination	***
FOTX_2	/	***
FOTX_3	/	***
SIN	discrete sinus values for arithmetic operations of the unit circle	*
SIN2	discrete 1/sinus values of the unit circle	*
COS	discrete cosines values of the unit circle	*

* Used for all investigations (see chapters 3-5), ** Used if also 'front' chord is investigated (see chapter 3.6, 5, 8) *** Used for the simulation and separation of multiple objects (see chapter 8)

Table 10.1. Arrays of data in the computer memory

10.9. Appendix 9: TRC-code for 3 objects

Table containing the TRC-code (90 possibilities) for 3 objects in the ring (see chapter 8.2.1) depending on the order NPO of the objects:

INPUT	OUTPUT	INPUT	OUTPUT	INPUT	OUTPUT
1 - 2 - 3		**1 - 3 - 2**		**3 - 2 - 1**	
0,1,2,3,4,5	0,1,2,3	0,1,4,5,2,3	0,1,4,5	4,5,2,3,0,1	4,5,2,3
0,1,2,4,3,5	0,1,2,5	0,1,4,2,5,3	0,1,4,3	4,5,2,0,3,1	4,5,2,1
0,1,2,4,5,3	0,1,2,3	0,1,4,2,3,5	0,1,4,5	4,5,2,0,1,3	4,5,2,3
0,2,1,3,4,5	0,3,4,5	0,4,1,5,2,3	0,5,2,3	4,2,5,3,0,1	4,3,0,1
0,2,1,4,3,5	0,5	0,4,1,2,5,3	0,3	4,2,5,0,3,1	4,1
0,2,1,4,5,3	0,3	0,4,1,2,3,5	0,5	4,2,5,0,1,3	4,3
0,2,3,1,4,5	0,1,4,5	0,4,5,1,2,3	0,1,2,3	4,2,3,5,0,1	4,5,0,1
0,2,4,1,3,5	0,5	0,4,2,1,5,3	0,3	4,2,0,5,3,1	4,1
0,2,4,1,5,3	0,3	0,4,2,1,3,5	0,5	4,2,0,5,1,3	4,3
0,2,3,4,1,5	0,5	0,4,5,2,1,3	0,3	4,2,3,0,5,1	4,1
0,2,4,3,1,5	0,5	0,4,2,5,1,3	0,3	4,2,0,3,5,1	4,1
0,2,4,5,1,3	0,3	0,4,2,3,1,5	0,5	4,2,0,1,5,3	4,3
0,2,3,4,5,1	0,1	0,4,5,2,3,1	0,1	4,2,3,0,1,5	4,5
0,2,4,3,5,1	0,1	0,4,2,5,3,1	0,1	4,2,0,3,1,5	4,5
0,2,4,5,3,1	0,1	0,4,2,3,5,1	0,1	4,2,0,1,3,5	4,5

INPUT	OUTPUT	INPUT	OUTPUT	INPUT	OUTPUT
3 -1 - 2		**2 - 1 - 3**		**2 - 3 - 1**	
4,5,0,1,2,3	4,5,0,1	2,3,0,1,4,5	2,3,0,1	2,3,4,5,0,1	2,3,4,5
4,5,0,2,1,3	4,5,0,3	2,3,0,4,1,5	2,3,0,5	2,3,4,0,5,1	2,3,4,1
4,5,0,2,3,1	4,5,0,1	2,3,0,4,5,1	2,3,0,1	2,3,4,0,1,5	2,3,4,5
4,0,5,1,2,3	4,1,2,3	2,0,3,1,4,5	2,1,4,5	2,4,3,5,0,1	2,5,0,1
4,0,5,2,1,3	4,3	2,0,3,4,1,5	2,5	2,4,3,0,5,1	2,1
4,0,5,2,3,1	4,1	2,0,3,4,5,1	2,1	2,4,3,0,1,5	2,5
4,0,1,5,2,3	4,5,2,3	2,0,1,3,4,5	2,3,4,5	2,4,5,3,0,1	2,3,0,1
4,0,2,5,1,3	4,3	2,0,4,3,1,5	2,5	2,4,0,3,5,1	2,1
4,0,2,5,3,1	4,1	2,0,4,3,5,1	2,1	2,4,0,3,1,5	2,5
4,0,1,2,5,3	4,3	2,0,1,4,3,5	2,5	2,4,5,0,3,1	2,1
4,0,2,1,5,3	4,3	2,0,4,1,3,5	2,5	2,4,0,5,3,1	2,1
4,0,2,3,5,1	4,1	2,0,4,5,3,1	2,1	2,4,0,1,3,5	2,5
4,0,1,2,3,5	4,5	2,0,1,4,5,3	2,3	2,4,5,0,1,3	2,3
4,0,2,1,3,5	4,5	2,0,4,1,5,3	2,3	2,4,0,5,1,3	2,3
4,0,2,3,1,5	4,5	2,0,4,5,1,3	2,3	2,4,0,1,5,3	2,3

10.10. Copies of publications

Meas. Sci. Technol. 8 (1997) 1228–1235. Printed in the UK PII: S0957-0233(97)85246-0

A ring sensor system using a modified polar coordinate system to describe the shape of irregular objects

Hartmut Gall

Crop Systems, Scottish Agricultural College, Penicuik EH26 0PH, UK

Received 23 June 1997, in final form 21 August 1997, accepted for publication 2 September 1997

Abstract. For agricultural produce such as potatoes, size and shape determination is very important in grading lines. If electronic sensor systems are installed, weighing cells and optical sensors such as cameras or simple shadow solutions are predominantly used. These systems are limited with regard to the numbers of 'views' of the object, which determines the accuracy for the determination of geometrical parameters. A ring sensor system is described consisting of a large number of optical transmitters and receivers which are arranged alternately. The emitters strobe infrared light in sequence round the ring, creating a large number of 'viewpoints'. Optical connections to each receiver are made. As an object passes through the ring, a shadow zone of each transmitter beam is created. As a result, the tangential chords can be found. A modified polar coordinate system, an algorithm and trigonometrical functions are described which allows the contour of the convex hull of three-dimensional objects to be formed. One advantage of this system is that the data from the ring is in the form of components of vectors and can be used to describe the whole object. As a result an enveloping spiral of the object is created.

1. Introduction

For the determination of the quality of agricultural produce, size and shape are necessary as are primary parameters. The major problem is that agricultural products have large variability in shape and size. As growers of agricultural produce experience increasing demand for their crops in both quality and quantity, so sorting processes have to be enhanced to a higher degree of automation. A great deal of attention today is paid to quality control, for example disease detection using camera systems (Porteous *et al* 1981), but there is also a lot of interest in size and shape determination and sorting (Brice 1996, McRae 1995).

In the UK, the potato industry is probably second to none with regard to quality criteria in terms of shape and disease. Most other crops, for example apple and orange, have a built-in symmetry which simplifies the sorting problem, whereas the potato tuber by its very nature is ill-formed, oddly shaped and knobbly.

For efficient sorting it is necessary to get a picture of the entire surface of the tuber. This may be accomplished in one of two ways. The objects may be rotated in normal or near infrared light, x-ray, laser light or structured light and viewed by one or two camera systems (Loctronic 1989, Samro 1995, Marchant *et al* 1990, Crowe 1996, Yonekawa et al 1994). Alternatively, several cameras, or a mirror viewing system may be positioned around a channel, where the potatoes pass through one by one (Weimar Werk 1996, Mörtl 1992). Depending on the number of mirrors or cameras giving different viewpoints, it is possible to get a picture of the whole object. These systems all use pictures built up by pixels to get the information about the size and shape.

It is also possible to use sensor systems which are not related to the human eye such as a camera. A number of packaging companies are using machines such as the electronic Accupack System (Exeter Engineering 1994). The sensor in this system consists of a rectangular frame with optical transmitters and receivers, effectively using the shadow principle. The weight can be calculated from the size and the shape. The potatoes pass through one by one and are scanned by the sensor system from only two viewpoints. The number of viewpoints around an object is very important to accurately describe the potatoes in three dimensions. Most of the existing systems are limited in this respect or do not work in real time.

This paper will describe the basic algorithm and mathematics for contour detection using a ring sensor

0957-0233/97/111228+08$19.50

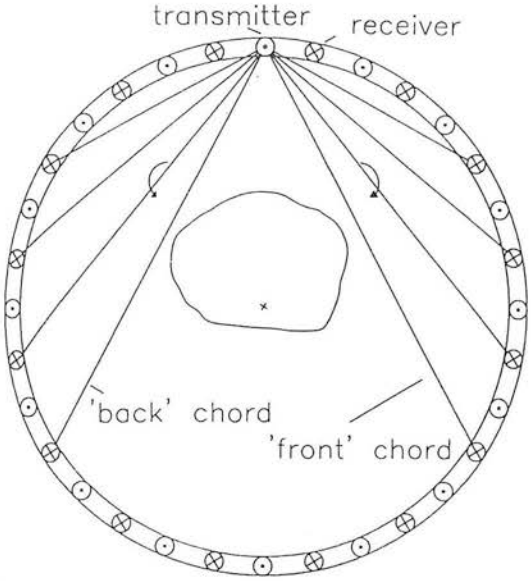

Figure 1. 'Snapshot' from one viewpoint indicating tangential light paths at the 'front' and the 'back' of an object.

system and a modified coordinate system based on the fundamental developments of Gall and Farchmin (1990) and Gall (1992, 1994).

2. The ring sensor system

The ring sensor system (see figure 1) consists of a number of single emitters and receivers arranged alternately and equispaced on the circumference of a circle (ring). Other arrangements are possible, for example double the number of receivers can be used. The emitters and receivers have a Lambertian angular response. The emitters are switched in sequence round the ring. From one activated transmitter, the signal at each optical receiver can be likened to a 'snapshot'. If no object is present within the ring, for each switched on transmitter, each detector will detect light. If an object is introduced, then one or more receivers will be obscured from the emitter. The two closest non-interrupted light paths (chords in the circle) can be used to describe the curvature of objects. They are called the 'front' and 'back' chord of each 'snapshot' (transmitter).

Only the 'back' chord of each 'snapshot' shall be used, because the 'front' chord touches the object at another point. It is permissible to make this restriction because results will be similar to those obtained using only the 'front' chords.

After a scanning revolution of the ring when there is a static object within the scanned area, a 'basic' picture showing all 'back' chords including the cross section of the object (see figure 2) is obtained. There is no restriction on the position of the object in the ring.

The information is coded in an array Z whose size in the two-dimensional case is equal to the number of transmitters N_T. For each transmitter n with $0 \leq n < N_T$ the relative position of the receiver $m[n]$ will be given (the determination of $m[n]$ will be discussed later).

$$Z = [m_0, m_1, m_2, m_3 \ldots m_{N_{T-1}}].$$

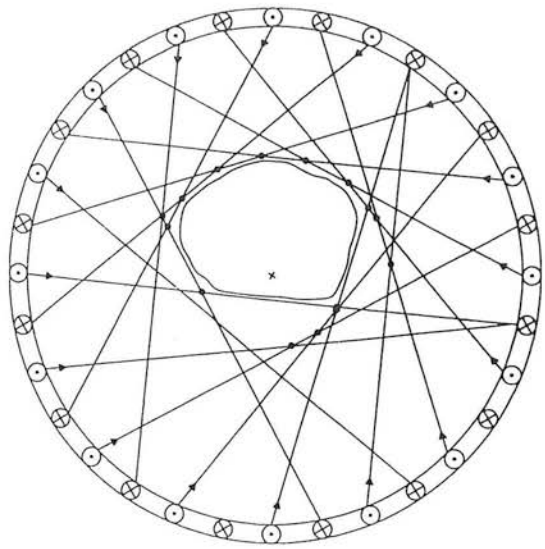

Figure 2. The 'back' chords of one revolution including the cross-section of an object (the intersections between the adjacent chords are marked).

3. Contour-tracking conditions

Consider first the two-dimensional case. The following conditions are set.

(1) There must never be more than one object in the ring.

(2) Transmitters and receivers will be arranged alternately. Pairs of transmitters are diametrically opposite each other, as are pairs of receivers.

(3) To simplify the following description, the ring shall scan clockwise and from each 'snapshot' (see figure 1) only the 'back' chords will be investigated.

As shown in figure 2 the description of the curvature of a section of the object is contained within this set of chords. Using any shadow method it is impossible to scan concave areas in the curvature in the two-dimensional case, so under these conditions, the result of determination will always be a convex hull.

Determination of a convex hull has often been discussed in mathematics and computer geometry literature. For a given set (cloud) of points (pixels) the task is to find the smallest polygon by excluding extraneous points (Jarvis 1973, AKL 1979, Petkov 1990, Preparata 1985).

Starting with components of vectors instead of a pixel picture offers a different situation. The following points define the geometric conditions.

(1) The chords and intersections (marked points in figure 2) of the adjacent chords are all on or outside the convex hull.

(2) The number of intersections with adjacent chords is limited, is equal to the number of chords and also equal to the number of transmitters.

(3) The chords are formed sequentially around the object.

This problem is similar to the intersections of half-planes (Preparata, 1985, Teillaud, 1993). They describe the set-up of a polygon limited in size by a large number of half-planes and methods to exclude redundant constraints in the polygon description. In our case (see figure 2), if the

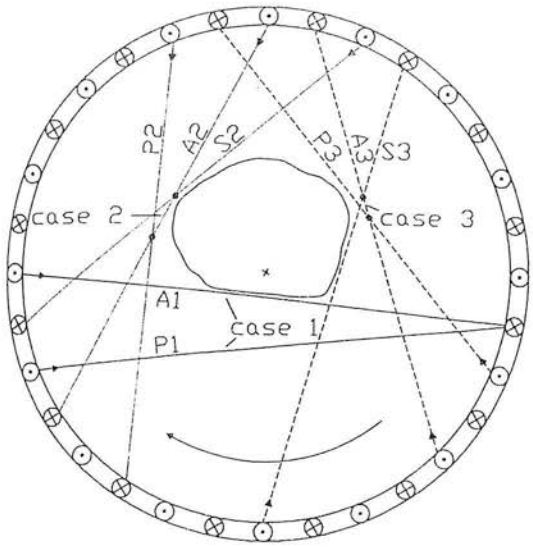

Figure 3. The three different cases of adjacent chords.

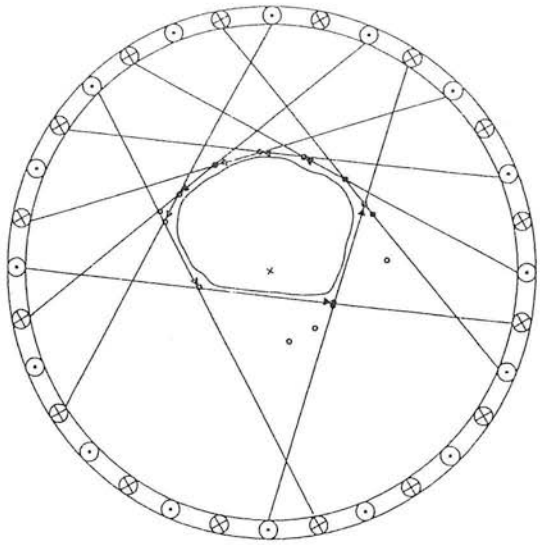

Figure 4. Remaining chords building up the convex hull (included and excluded intersections are marked).

chords were stretched to form segments of the circle, or into straight lines building up half-planes around the convex hull, the same conditions hold and this same method could be used. In practice the ring sensor has limited numbers of transmitters and receivers and the object has to be in the area of the ring, which means that the conditions are much more controlled. So a simplified algorithm can be used.

4. Contour-tracking method

The 'basic' picture is generated in one scan consisting of N_T sequential 'snapshots' which gives a set of N_T 'back' chords. All chords will be sequentially investigated as they are generated. All redundant chords have to be excluded from further consideration, since they are not coincident with the contour of the object.

To do this, each chord (actual chord), its successfully tested predecessor and successor have to be investigated (see figure 3).

The following cases are possible.

(1) The actual chord A1 reaches the same receiver as the predecessor P1, which is therefore redundant and is excluded from further investigations.

(2) The intersection of the actual investigated chord A2 with the predecessor P2 lies further from the transmitter than does the intersection with the successor S2. The actual chord A2 will therefore be part of the convex hull. It may, however, be excluded by investigation on subsequent steps.

(3) The intersection of the actual investigated chord A3 with the predecessor P3 lies closer to the transmitter than does the intersection with the successor S3. The actual chord is redundant and has to be excluded from further investigations. At this point, the predecessor P3 will become the actual chord, and the chord tested before the predecessor is now the predecessor chord. The successor remains the same. The turning back and excluding of previously successfully tested, but in this instance recognized as redundant chords, will run until case (2) occurs.

The chords are then renumbered and rechecked sequentially using the above rules until no more chords can be excluded (see figure 4).

The contour is described using the remaining chords and the distance to the intersections of the chords.

5. The modified polar coordinate system

Using the 'basic' picture and a modified polar coordinate system it can be shown how the positions of intersections of the actual chord and the predecessor $C_P[n]$ of the convex hull can be described. From each transmitter n we get one distance $m[n]$ stored in an array Z (see section 2). These values will be components of the vectors and intersections, which will describe the convex hull of the object. The origin of the coordinate system is the transmitter $T_A[0]$ (see figure 5).

The parameters of the ring are: α, the angle between the adjacent transmitters (in this case also between the receivers); β, is the angle (displacement) between the transmitter and the receiver; N_T, is the number of installed transmitters; N_R, is the number of installed receivers; r, is the radius. The variables are: n, the number of the actual activated transmitter with $0 \leq n < N_T$; $m[n]$ the number of receivers from the actual activated transmitter n anticlockwise to the receiver of the 'back' chord with $0 \leq m < N_R$.

The maximum possible number chords N_{CH} with respect to the numbers of transmitters N_T and receivers N_R is:

$$N_{CH} = N_T N_R.$$

We will show first, how the position of the vector $T_A[0]C_P[0]$ from the chord with the first transmitter $T_A[0]$ to the intersection with the predecessor starting in $T_P[0]$ can be described. For equally spaced transmitters and receivers, we have:

$$\alpha = 2\pi/N_T \qquad \beta = \alpha/2.$$

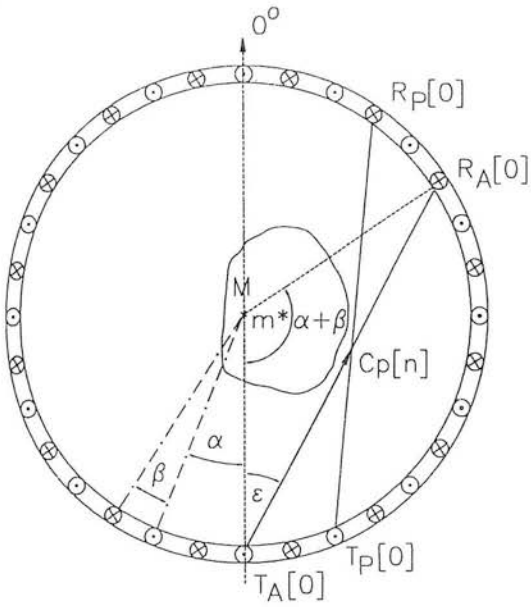

Figure 5. The vector $T_A C_P[0]$ in the coordinate system.

The position of the actual receiver $R_A[0]$ from the touching chord depends on the shape of the object. With

$$\varepsilon = \pi/2 - \tfrac{1}{2}(m\alpha + \beta)$$

so giving

$$R_A[0] = [\varepsilon, 2r\cos\varepsilon].$$

Because $T_A[0]$ has the coordinates $[0, 0]$ two points are known. Having the position of two points the chord can be described accurately.

The distance between the transmitter of the actual chord $T_A[0]$ and the interception with the predecessor $C_P[0]$ (determination, see figure 6) can be used to determine the position of the intersection.

$$C_p[0] = [\varepsilon, |T_A C_P[0]|].$$

The first step for the investigation of all chords is the use of $m[n]$ from the actual chord with the transmitter $T_A[0]$ as the origin for the determination of the temporary vector $T_A[0]C'_P[n]$ (see figure 6). The advantage is that the same mathematic algorithms can be used as for the transmitter $T_A[0]$. This can be done because the ring is symmetrical.

It is now necessary to move the vector $T_A[0]C'_P[n]$ into the right position. The position of the starting point with the angle φ to the zero axis and the distance from $T_A[0]$ to $T_A[n]$ will be determined.

With

$$\varphi = \pi/2 - n\beta$$

then

$$|T_A[0]T_A[n]| = 2r\cos\varphi.$$

The position of $T_A[n]$ is

$$T_A[n] = [\varphi, 2r\cos\varphi].$$

The angle δ of the real vector $T_A C_P[n]$ in the area will be determined by the angle $T_A[0]$, M, $T_A[n]$ and ε

$$\delta = n\alpha + \varepsilon.$$

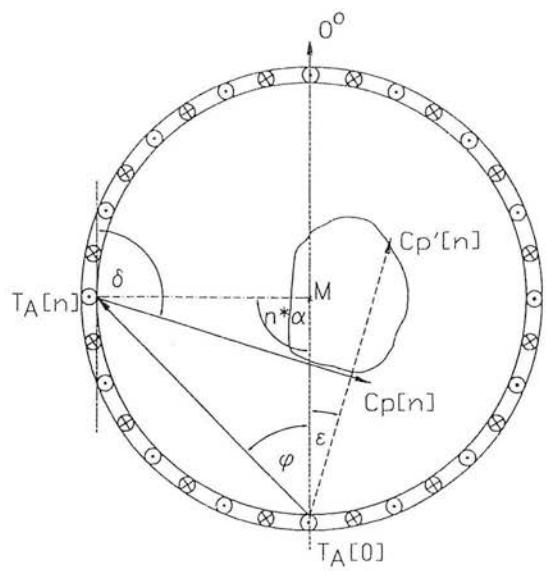

Figure 6. Creation of the vector $T_A C_P[n]$ in the right position.

The position of $C_P[n]$ is

$$C_P[n] = [T_A[n], \delta, |T_A C_P[n]|]. \quad (1)$$

The use of this coordinate system makes mathematical equations more simple than the use of the polar coordinate system with the origin in the midpoint. The position of the intersections with the successor chords $C_S[n]$ can be described in the same way. $C_S[n]$ is the same intersection as $C_P[n+1]$.

6. Determination of intersections

To find the redundant chords where the successor does not have an intersection as shown in case 1 (see figure 3), $m[n]$ and $m[n-1]$ have to be observed. If $m[n] = m[n-1] - 1$ then there will not be an intersection.

The main task is the determination of the distances from the transmitter of the actual chord $T_A[n]$ to the intersections with the adjacent chords. It would also be possible to use the distances of the intersections to the receiver of the actual chord. As said previously the determination of the distance between the actual transmitter $T_A[n]$ to the intersection $C_P[n]$ is independent from $T_A[n]$, because it is the same distance between $T_A[0]$ and $C'_P[n]$ (see figure 6).

The distance between each transmitter $T_A[n]$ and the intersection with the predecessor $T_A C_P[n]$ will be determined (see figure 7).

Using trigonometry,

$$|T_A C_P[n]| = |T_A T_P[n]| \sin\tau 2 / \sin\tau 3$$

(see appendix 1).

The distance between the transmitter and the intersection with the successor $|T_A C_P[n]|$ can be determined (see figure 8).

$$|T_A C_S[n]| = |T_A T_S[n]| \sin\tau 1 / \sin\tau 3$$

(see appendix 2).

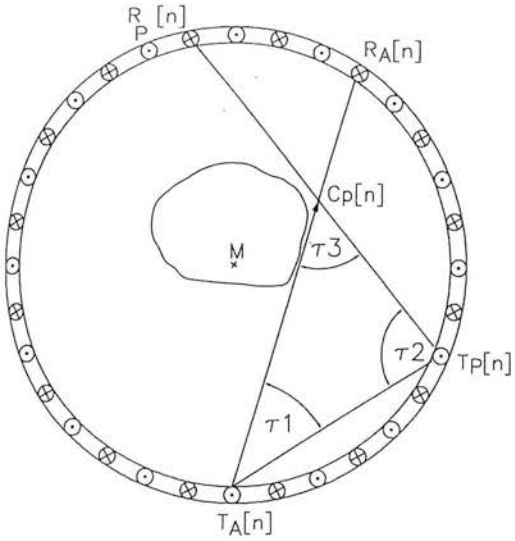

Figure 7. Intersection between actual chord and predecessor.

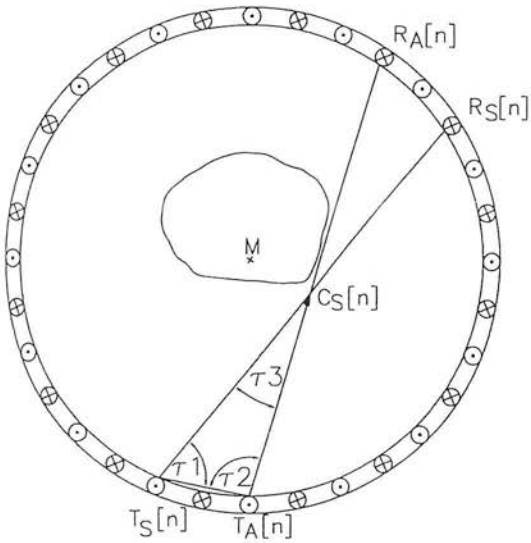

Figure 8. Intersection between actual chord and successor.

If

$$|T_A C_P[n]| < |T_A C_S[n]|$$

the actual investigated chord has to be eliminated (case (3), see section 4). In the other case the chord can be a tangential chord of the convex hull. Clockwise each chord has to be checked in this way. The equations are valid for all $T_A[n]$.

7. The three-dimensional system

There are a range of theories regarding the shape and surface detection of three-dimensional objects. One theory is to wrap the objects with a flexible elastic band with geodesics in many directions (Stewart, 1993). Closed geodesics will be found but on most surfaces, geodesics wander around forever without closing up. A mathematical method for the construction of piecewise surfaces which can be parametrized as single-valued surfaces in spherical coordinates is described by Sánchez-Reyes 1994. The

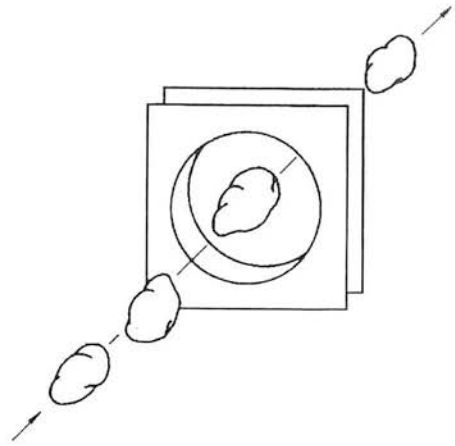

Figure 9. Potato on the way through the sensor system.

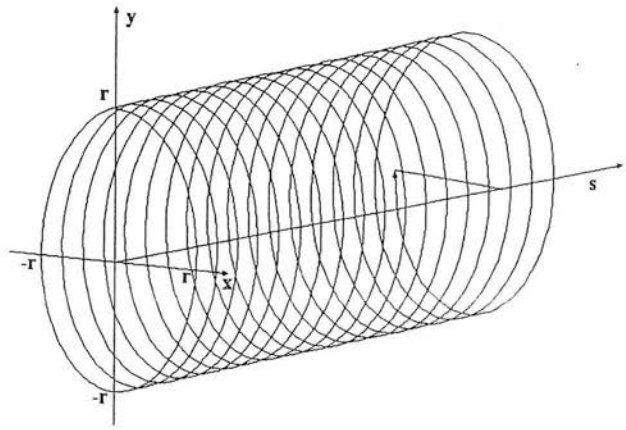

Figure 10. The sensor ring building up a three-dimensional cylinder space.

problems discussed are similar, but in the two-dimensional case the limitation imposed by the sensor ring makes special solutions possible.

The extension of the coordinate system (see section 5) into the three-dimensional space can easily be done with the ring sensor determining the object section at intervals and the object moving through the sensor (see figure 9). If the movement is at constant speed, this will guarantee a constant distance 's' between each 'snapshot'. In relation to the object the ring is now an enveloping helix describing a cylinder of the sensor system (see figure 10). The helix will have a pitch of $2\pi s$ where s is the sampling distance in the third dimension determined by the speed of the object. The object has to pass through the ring and will be positioned in the cylinder.

The apparent number n of transmitters is now unlimited. N_T transmitters will be activated in one revolution. The distance m between each activated transmitter and the receiver building up the touching chords on the object is the same as in the two-dimensional case $0 \leq m < N_R$.

The algorithms used are the same as described in section 4. An object starts if $m < N_R$. The end is reached when $m = N_R$ again.

Analogous to the two-dimensional case (see equa-

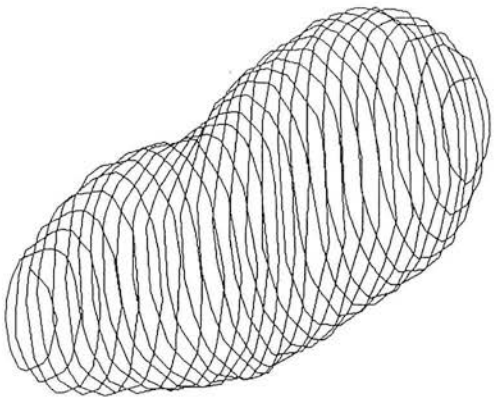

Figure 11. An enveloping spiral of a potato.

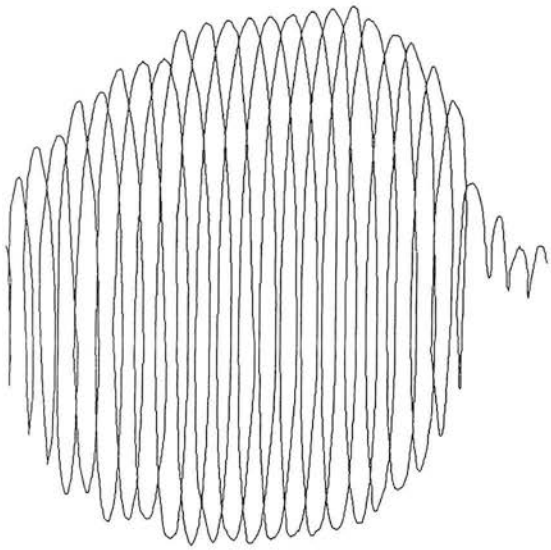

Figure 12. An enveloping spiral of an apple.

tion (1)) the intersection C_p can be determined by

$$C_P[n] = [T_A[n], \delta, |T_A C_P[n]|, ns].$$

It should be noted that in this description only two variables are necessary, the number of the activated transmitter n and the distance to the receiver m.

The picture of the object is composed of part of the chords including the determined intersections. The result is an enveloping spiral (see figures 11, 12 and 13). These show pictures created by a ring with $N_T = 64$ and $N_R = 64$ using the 'back' spiral. It should be noted that one difference with the two-dimensional case is that concavities can be seen in the direction of movement of the system (see figure 13); however, concave areas in the cross section cannot be seen.

The probability of concave areas on the longest axis of an object (potato) is larger than in other directions, and is the reason for a preferred direction of an object passing the sensor system. As an additional result of this condition the determination of the length L of the object is simply $L = ns$.

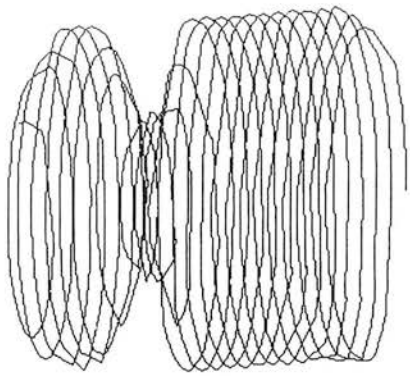

Figure 13. Example for an object with concave area.

8. Some effects for use in the computer

The 'basic' picture consists of the result of each 'snapshot' (see figure 2). The transmitters are activated one after the other. The number after each 'snapshot' is $n = n + 1$. This number can be used to address a linear memory space in the computer. As a result only one variable, $m[n]$, the distance between the transmitter and the receiver, is left which is stored in the array Z (see section 2). This 'basic' picture of the whole scene includes the necessary information to describe the object in the form of components of vectors. The power necessary for the determination of shape/size by pixel pictures (standard two-dimensional image processing) including contrast and edge triggering algorithms is eliminated and the use of vectors reduces the amount of memory needed. A further advantage is that for most functions, pointer instructions can be used as the system is built up symmetrically and discretely and the number of possible values are limited. This supports the possibility of practical real time use.

9. The practical use of the ring and its accuracy

On the basis of the results of the algorithms above, the following characteristics of objects can easily be determined (the description shall follow in a further article): volume; length; position of the largest slice of an object; the major and the minor axis of the largest and the middle slice; the circumferences in the crosswise direction; mass (if the density is known); density (if the mass is known).

The ring can be used for example in plant breeding, in the vegetable-handling industry, in baking, meat, fish and timber industries for sorting products and/or quality control. The accuracy of the ring depends on the number of transmitters and receivers and the size of the object. For example, a ring consisting of 64 transmitters and 64 receivers and with a ring diameter of 175 mm was built. If an average potato of 100 g passes through the ring and is described by a spiral of 20 revolutions, the error for volume determination is around ±3%. If the object is larger, the error decreases, if smaller it increases. A compromise in the construction and resolution of the ring for a particular application is necessary.

10. Conclusions

The ring sensor system described in this paper has a different mechanical structure than any other visual system. With a modified polar coordinate system and special algorithms it is possible to describe the surface of three-dimensional objects. The advantages are self evident. The three-dimensional surface of variable-shaped objects can be described relatively accurately. The object is caught in a limited symmetrically built space; however, its position is variable. Received data from the sensor system are components of the describing vectors. The number of possible vectors is limited. The algorithms are the same for two- and three-dimensional objects. The limited number of vectors allows the predominant use of pointer instructions. The necessary memory space to store the data is minimal. The necessary computer power is low. Concave areas in the direction of movement can be seen.

There are two disadvantages. The preferred direction of passage is the longitudinal axis of the object, and concave areas in cross-section cannot be seen, because the system uses the shadow principle.

For the description of very oddly shaped objects, such as those found in agriculture, the use of this system offers a good alternative.

Acknowledgments

The work was funded by the European Commission. The project 'Quality control using image analysing systems for sizing and sorting potatoes' was carried out at the Scottish Agricultural College/Crop Systems Department at Bush Estate Penicuik.

Appendix 1

x, y	label for the actual chord A, the predecessor P or the successor S
$k_{T_x.TR_y}$	numbers of receivers between different transmitters or receivers determined using the variables n for the marked transmitter or $m[n]$ for the marked receivers. Multiplied by angle β, angles $\omega_{M.T_x.TR_y}$ will be determined.
$\omega_{M.T_x.TR_y}$	angle at the circumference centred on a transmitter $T_X[n]$ created with the radius of the ring (with the midpoint M) and a further transmitter or receiver.
$\omega_{M.T_A.T_P}$	$\pi/2 - k_{T_A.T_P}\beta$
$\omega_{M.T_A.R_A}$	$\pi/2 - (k_{T_A.R_A} + \frac{1}{2})\beta$
$\tau 1$,	$\omega_{M.T_A.T_P} - \omega_{M.T_A.R_A} = (\frac{1}{2} + k_{T_A.R_A} - k_{T_A.T_P})\beta$
$\omega_{M.T_P.R_P}$	$\pi/2 - (k_{T_A.R_P} - k_{T_A.T_P} + \frac{1}{2})\beta$
$\tau 2$	$\omega_{M.T_A.T_P} + \omega_{M.T_P.R_P} = \pi - (k_{T_A.R_P} + \frac{1}{2})\beta$
$\tau 3$	$\pi - \tau 1 - \tau 2$
$\lvert T_A C_P[n]\rvert$	$\lvert T_A T_P[n]\rvert \sin \tau 2 / \sin \tau 3$

Appendix 2

$\omega_{M.T_S.T_A}$	$\pi/2 - k_{T_A.T_S}\beta$
$\omega_{M.T_S.R_S}$	$\pi/2 - (k_{T_S.R_S} + \frac{1}{2})\beta$
$\tau 1$	$\omega_{M.T_S.T_A} - \omega_{M.T_S.R_S} = (\frac{1}{2} + k_{T_S.R_S} - k_{T_A.T_S})\beta$
$\omega_{M.T_A.R_A}$	$\pi/2 - (k_{T_S.R_A} - k_{T_A.T_S} + \frac{1}{2})\beta$
$\tau 2$	$\omega_{M.T_S.T_A} + \omega_{M.T_A.R_A} = \pi - (k_{T_S.R_A} + \frac{1}{2})\beta$
$\tau 3$	$\pi - \tau 1 - \tau 2$
$\lvert T_A C_S[n]\rvert$	$\lvert T_A T_S[n]\rvert \sin \tau 1 / \sin \tau 3$

List of symbols

A1–3	actual chords
$C_P[n]$	intersection of the actual chord with the predecessor
$C'_P[n]$	temporary position of the intersection $C_P[n]$
$C_S[n]$	intersection of the actual chord with the successor
$k_{T_x.TR_y}$	numbers of receivers between different transmitters or receivers determined using the variables n for the marked transmitter or $m[n]$ for the marked receivers. Multi-plied by angle β, angles $\varphi_{M.T_x.TR_y}$ will be determined.
L	length
$m[n]$	number of receivers from the actual activated transmitter n anticlockwise to the receiver of the 'back' chord
n	number of the actual activated transmitter
N_{CH}	maximum possible number of chords
N_T	number of installed transmitters
N_R	number of installed receivers
P1–3	predecessor chords
r	radius
$R_x[n]$, $R_y[n]$	receiver
s	displacement of the object between each 'snapshot'
S2–3	successor chords
$T_x[n]$, $T_y[n]$	transmitter
x, y	label for the actual chord A, the predecessor P or the successor S
$Z = [m_0, m_1, m_2, m_3 \ldots m_{NT-1}]$	array with coded information of the 'snapshots'
α	angle between adjacent transmitters
β	angle (displacement) between transmitter and receiver $= \frac{1}{2}\alpha$
$\varepsilon, \varphi, \delta$	angles
$\tau 1$–3	angle in the triangles
$\omega_{M.T_x.TR_y}$	angle at the circumference centred on a transmitter $T_X[n]$ created with the radius of the ring (with the mid-point M) and a further transmitter or receiver.

References

AKL S G 1979 Two remarks on a convex hull algorithm *Inform. Proc. Lett.* **8** 108–9

Brice A 1996 An eye on the fry *Potato Business World* **4** 24–32

Crowe T G and Delwiche M J 1996 Real-time defect detection in fruit—part I: Design concepts and developments of prototype hardware *Trans. ASAE* **39** 2299–308

Exeter Engineering 1994 Automatic grading and sizing systems. *Information Journal* Exeter, California p 6

Gall H 1992 Sichtsystem mit ringförmigem Sensor zur On-Line Vermessung der Geometrie unregelmäßig geformter konvexer Objekte. Universität Rostock, Germany p 117

Gall H 1994 Viewing system with ring-shaped sensor for on-line determination of the geometry of irregularly formed convex objects *International Agrophysics* **8** 565–6

Gall H and Farchmin U 1990 Sensor zur Bestimmung geometrischer Abmessungen *Sensor Magazin 4* Magazin Verlag 16–17

Jarvis R A 1973 On the identification of the convex hull of a finite set of points in the plane *Inform. Proc. Lett.* **2** 18–21

Loctronic 1989 Autoselector Ro-Ro 'C'&'D', Information sheet. Loctronic Graders Ltd, Danburry, Chelmsford, Essex, England p 2

Marchant J A, Onyango C M and Street M J 1990 Computer vision for potato inspection without singulation *Comput. Electron. Agric.* **4** 235–44

McRae D C 1995 Größen- und Qualitätssortierung bei Kartoffeln *Kartoffelbau* **9** 380–3

Mörtl W 1992 Indirekte Massebestimmung von Kartoffeln und Äpfeln aus optisch ermittelten Abmessungen der Frucht. Rostock, Universität Rostock, Germany p 98

Petkov N 1990 Ein Näherungsverfahren zur Bestimmung der konvexen Hülle und verwandte Probleme der algorithmischen Geometrie *Bild und Ton* **3** 76–9

Porteous R L, Muir A Y and Wastie R L 1981 The identification of diseases and defects in potato tubers from measurements of optical spectral reflectance *J. Agric. Eng. Res.* **26** 151–60

Preparata P F and Shamos I M 1985 *Computational Geometry an Introduction* (New York: Springer) pp 398

Samro 1995 Samro Video—Elektronischer Größensortierer, Information Sheet. Samro Bystronic Maschinen AG, Burgdorf, Switzerland p 2

Sánchez-Reyes J 1994 Single-valued surfaces in spherical coordinates *Comput. Aided Geom. Des.* **11** 491–517

Stewart I 1993 A million ways to wrap a rubber band round a potato *New Scientist* **137** 16

Teillaud M 1993 Towards dynamic randomised algorithms in computational geometry (Berlin: Springer) pp 149

Yonekawa S, Sakai N and Kitani O 1994 Three-dimensional measurement of loam using machine vision *Trans. ASAE* 1003–9

Weimar-Werk 1996 Agroselector 5000 und Varianten. Information Sheet. Select GmbH, Hartmannsdorf, Germany p 2

Meas. Sci. Technol. 9 (1998) 1809–1820. Printed in the UK PII: S0957-0233(98)92122-1

A ring sensor system for the determination of volume and axis measurements of irregular objects

Hartmut Gall†, Andrew Muir†, John Fleming†, Rolf Pohlmann‡, Lothar Göcke‡ and Will Hossack§

† Crop Systems, Scottish Agricultural College, Bush Estate, Penicuik EH26 0PH, UK
‡ Argus Electronic GmbH, Joachim-Jungius-Straße 9, 18059 Rostock, Germany
§ Department of Physics, The University of Edinburgh, Edinburgh EH9 3JZ, UK

Received 2 March 1998, in final form 14 July 1998, accepted for publication 21 August 1998

Abstract. In agriculture, a large variability of objects in a range of sizes and shapes is found, leading to problems in size grading. For example, for a low-cost product such as potatoes, the predominantly used mechanical size-determining systems have errors of up to 30% and can cause damage, but they are cheap and have a throughput up to 20 tonnes per hour. Alternatives which can guarantee an improvement in accuracy and a financial gain for the companies are required. In this paper methods for the determination of volume and axis measurements using a simple ring sensor system are described. A modified co-ordinate system and the segmentation of the area between the ring and the object are used. The volume determination is independent of the direction of presentation of the objects. For the determination of axes, the objects must be presented in the longitudinal direction to allow the use of simple 2D algorithms. The accuracy of the system depends both on the number of transmitters and receivers placed on the ring and on its diameter. A small ring sensor system was developed, which can scan 3D objects in real time (36 000 potatoes, 3.6 tonnes per hour) with an accuracy of better than 5% for a volume larger than 100 cm^3.

Keywords: ring sensor, three-dimensional objects, volume, size, axis measurement, shape

Nomenclature

A_C	area of a segment of the ring (circle)
A_O	cross sectional area of an object
A_R	area of the ring
A_S	segment in the ring consisting of one triangle and a segment of the ring (circle)
A_S^*	A_S in a circle with radius 1
A_T	area of the triangle
C_A	intersection on the actual chord with the perpendicular from the intersection opposite
C_X, C_X^*	intersection between the perpendicular of the actual chord and the apparent parallel chord or the opposite intersection
C_P, C_S	intersection of the actual chord with the predecessor or successor
C_Z	intersection of the perpendicular from the actual receiver $R_A[n]$ to the apparent chord
d_R	difference between two neighbouring radii
d_S	distance which the object moves during one scanning revolution
E_A, E_D	error of area or distance
i	actual segment number
i_{OBJ}	total number of determined remaining area segments A_S or volume segments
IN	intersection
$k_{TA,TP}$, k_{TX,RX^*}, $k_{TX,RX}$	numbers of receivers between different transmitters and/or receivers
L	length
L-LARGE	largest slice, major axis
L-SLICE	position of the largest slice
L-SMALL	largest slice, minor axis
$m[n]$	number of receivers from the actual activated transmitter n anti-clockwise to the receiver of the 'back' chord
M	midpoint
M-LARGE	middle slice, major axis
M-SMALL	middle slice, minor axis
n	number of the actual activated transmitter

0957-0233/98/111809+12$19.50

n_{OBJ}	total number of 'snapshots' of one object
N_I	number of intersections
N_P	number of possible positions of parts of objects
N_T	number of transmitters installed
N_R	number of receivers installed
r	radius of the ring
r_A, r_S	radii to neighbouring round cross sectional areas
P	parallels
R_A, R_S, R_P	actual receiver, successor and predecessor
$R_X[n], R_Y[n], R_X^*$	receiver on the opposite side
s	displacement of the object between each 'snapshot'
S	axis of movement of the object
T_A, T_S, T_P	actual transmitter, successor and predecessor
$T_X[n], T_Y[n], T_X^*$	transmitter on the opposite side
v	number of viewpoints
V_C	volume of cylinder
V_O	volume of the object
V_R	volume of spline
V_S	volume of segment
x, y	two axes in the three-dimensional space
α	angle between adjacent transmitters
$\alpha_1, \alpha_2, \varphi, \varphi_1, \varphi_2$	angles
β	angle (displacement) between transmitter and receiver ($=1/2\alpha$)
π	pi
τ_1	angle in the triangle of area A_T

1. Introduction

The main criteria used to describe the geometry of agricultural objects are volume (weight) and axis measurements. Today accuracy of 10–30% is common in mechanical size-grading systems for potatoes. Electronic systems reach about 10%. The market standards are increasing and tolerance values are reducing. A system with tighter sizing parameters is definitely required, although it is envisaged that there will never be a need for micrometre resolution in size and general shape detection. Resolution in the range of about 1–2 mm is adequate. Agricultural products have a low unit value and many of them have to be handled in a short time period (10 tonnes or about 100 000 or more potatoes in 1 h). Fast simple sensors are therefore needed, which will also allow a pay-back period of 3 years. A simple, compact mechanical construction is also necessary in order to keep the equipment's footprint small.

A lot of time and effort has been invested in the development of automated systems to obtain geometrical measurements, including electronic sensors, mathematical methods and improvements in computer technology. Different sensor systems require different mathematical methods and models to determine geometrical measurements used in agriculture. All try to 'box in' the whole 3D object as perfectly as possible. The accuracy depends on the number of viewpoints around the object.

The following are some examples of 'boxing-in' methods which are used for calculation of size and shape. The principles shown in figures 1(a)–(e) are for the scanning of 2D cross sections in the vertical plane of a horizontally moving object. The principle in figure 1(f) requires the rotation of the object in front of the sensor system in order to get a number of viewpoints from which to scan horizontal cross sections.

(i) Mechanical riddles with different square mesh sides in a shaker for sorting potatoes (until today the most commonly used in agriculture) use the square measurement of the largest slice (see figure 1(a)). The size of the potatoes is calculated solely from this one measurement.

(ii) Rectangular frames with optoelectronic elements (Larsson 1994, Exeter Engineering 1994) use the view from two sides, the result is a rectangle of a cross section (see figure 1(b)). A number of adjacent rectangular slices will describe the object and the size can be calculated.

(iii) If three or more line-camera systems and diffuse lighting are used (Baganz *et al* 1991, Hiroshi 1989) the edge detection presents vertical cross sections (see figure 1(c)). Size and axes can then be calculated from a discrete number of slices (Mörtl 1992). In theory this problem is also similar to the inverse of decomposition of an object into slices (Phillips and Rosenfeld 1988).

(iv) Using the principle of triangulation, the 3D shape of a surface can be determined (see figure 1(d)). An extension is the use of structured light from one or more sides (Zwahlen 1992, Yang 1995), indicating the 3D shape or outline of the surface.

(v) The ring sensor system (see figure 1(e)) uses a large number of optical transmitters and receivers alternately arranged round a ring. Light paths can 'box in' predominantly convex cross sections (Gall and Farchmin 1990, Gall 1992, 1997).

(vi) Matrix camera systems with diffuse lighting are primarily developed and used for disease and defect detection in the food industry. The objects are rotated in front of the camera (Wright *et al* 1984, McClure and Morrow 1987, Marchant *et al* 1988) or pictures of the whole object are taken in a tunnel of mirrors (Ross 1995). Using edge detection, a limited number (3–12) of silhouettes (horizontal cross sections) of the object (see figure 1(f)) in front of a white or black background can be captured. The size and shape can be derived using these intersecting cross sections (Mörtl 1992). Camera systems with defined flash lighting from two sides of the object (Crezee 1996) use in principle the same 'boxing-in' method.

Another method is use of an artificial retina (Karnali *et al* 1997), like a bell or hull over the fixed positioned object. It can be used to determine the volume but not axis measurements.

This paper describes the basic mathematics and algorithms for the determination of volume and axis measurements of objects using a ring sensor system and the modified co-ordinate system described by Gall (1997). An introduction to the detection of theoretical errors will also be given. Tests confirm the practicability of the system and methods.

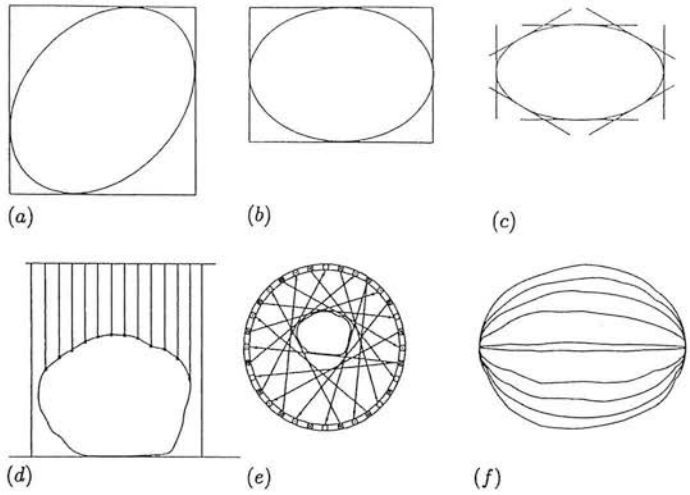

Figure 1. Methods of "boxing in' objects with typical numbers of viewpoints 'v': (a) a vertical central slice, square mesh, $v = 2$; (b) a vertical slice, variable rectangle, $v = 2$; (c) a vertical slice, variable convex polygon, $v = 3$–18; (d) a vertical slice from one side of a variable polygon, $v \geq 10$; (e) a vertical slice, variable convex polygon, $v \geq 32$; and (f) a star of horizontal slices, variable shape $v = 3$–12.

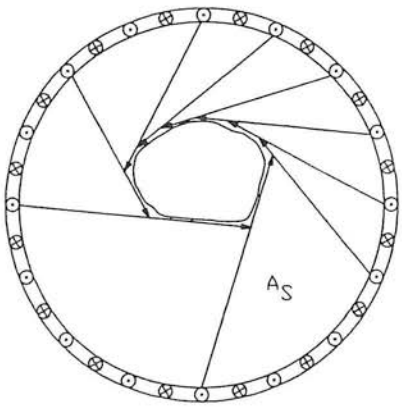

Figure 2. Segmentation anticlockwise.

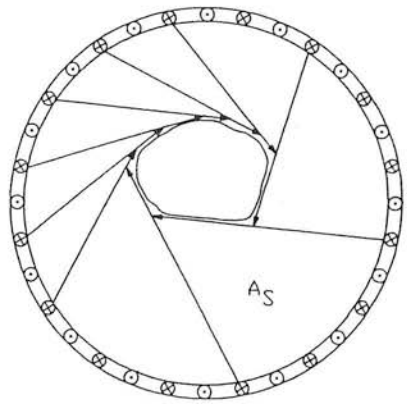

Figure 3. Segmentation clockwise.

2. Segmentation of the picture

One main step in computer vision is the segmentation of a picture into known simple geometrical units. So far as is known, all of these systems try to segment the objects and the origin of the co-ordinate system is placed within the object.

The ring sensor is built with the same number of transmitters N_T and receivers N_R symmetrically arranged on the circumference of a circle (Gall 1992, 1997). The environment around the object is defined by the ring and the data obtained describe the outline curvature of the object. Since there is no information about the inside of the silhouette, it is more logical to segment the space between the ring and the object.

The surface of the object is described by vectors from each transmitter of the remaining chords to the intersection with its predecessor (Gall 1997). In figure 2 a cross section built up by these vectors is shown. The segmentation of the picture becomes obvious.

There are two possibilities for segmenting the picture, anticlockwise (see figure 2) or clockwise (see figure 3). Both ways are feasible and will deliver the same results for the area and volume determination. Each element of area A_S is defined by part of one chord and part of the predecessor chord, which intersect, and an arc of the ring.

In the following investigations, the anticlockwise orientation was used. Each element A_S is made up of a triangle of area A_T and a segment of a circle A_C (see figure 4). These units are basic geometrical figures and can be calculated and used for area and volume determination.

3. Areas and volume determination

3.1. Areas of the segments

The segmentation of the picture offers a simple method of determination of cross sectional areas and volumes of objects with the sensor ring system. The investigation uses results from Gall (1997). The solution of the geometrical shapes is shown in figure 5. $T_A[n]$ and $T_P[n]$ are transmitters and $R_P[n]$ and $R_A[n]$ are receivers of two neighbouring touching chords of the object. n is the number of the actual activated transmitter which creates the specified chord in the image. α is the angle between two neighbouring transmitters or receivers and β is the angle

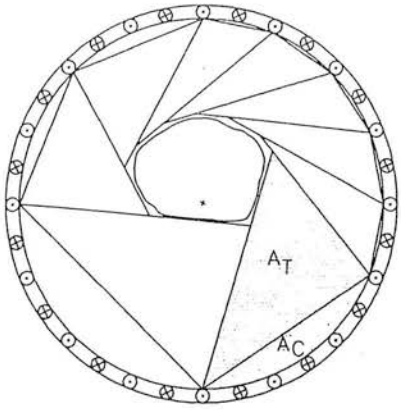

Figure 4. Segmentation into definite elements– the triangle A_T and segment of circle A_C.

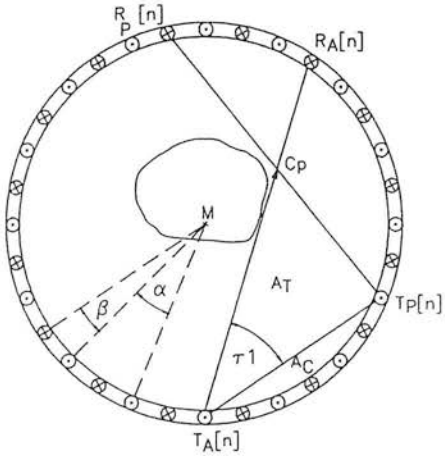

Figure 5. The intersection between an actual chord and its predecessor creating a triangle of area A_T, a segment of area A_C and the vector T_AC_P.

between a neighbouring transmitter and a receiver. All values are known, except for the areas A_T and A_C.

The area of the triangle A_T for all possible circles with radius r is

$$A_T = \tfrac{1}{2}r^2|\boldsymbol{T_AC_P}||\boldsymbol{T_AT_P}|\sin\tau_1$$

The area for the segment of the circle using the number $k_{TA,TX}$ of receivers between the transmitters $T_A[n]$ and $T_X[n]$ and the angle α is

$$A_C = \tfrac{1}{2}r^2[k_{TA,TP}\alpha - \sin(k_{TA,TP}\alpha)].$$

The sum of A_T and A_C gives the area for the element A_S:

$$A_S = \tfrac{1}{2}r^2[|\boldsymbol{T_AC_P}||\boldsymbol{T_AT_P}|\sin\tau_1 + k_{TA,TP}\alpha - \sin(k_{TA,TP}\alpha)].$$

In the case of the unit circle,

$$A_S^* = A_S/r^2.$$

An advantage of this method is that main values such as the length of the vector $\boldsymbol{T_AC_P}[n]$ and angle τ_1 can be taken from previous investigations and the determination of all the other values is not difficult. This allows real-time use.

3.2. The area of a cross section

The area for the whole circle (inside the ring), A_R, is simply

$$A_R = \pi r^2.$$

The sum of the determined remaining i_{OBJ} segments A_S gives the area surrounding the object. Subtracted from A_R this gives the resulting cross sectional area A_O of the object

$$A_O = A_R - \sum_{i=1}^{i=i_{OBJ}} A_S(i).$$

3.3. The volume of an object

Using the ring sensor system, the extension of algorithms into 3D space is simple, as already described by Gall (1997). First take the ring with no object and the maximal cylinder described by it (see figure 6(a)). The ring describes a cylindrical spiral about the length L of the object. The length is the product of n_{OBJ} 'snapshots' of the object and the distance s the object moves between each 'snapshot'. The volume of this cylinder V_C is the sum of the splines V_R (see figure 6(b)). The volume of a spline is given by the area (circle sector) demarcated by the centre of the ring, the part of the circle between adjacent transmitters and the distance d_S which the object moves during one scanning revolution. For its determination, the displacement s of the object between each 'snapshot' and the number of transmitters N_T is used:

$$d_S = N_T s$$

$$V_R = \pi r^2 d_S/N_T = \pi r^2 s$$

$$V_C = \sum_{n=1}^{n=n_{OBJ}} V_R(i) = \sum_{n=1}^{n=n_{OBJ}} i\pi r^2 s$$

$$V_C = n_{OBJ}\pi r^2 s.$$

The area elements A_S surrounding the object become volumes V_S when multiplied by the distance d_S:

$$V_S = A_S d_S = A_S s N_T.$$

The volumes V_S have to be subtracted from the cylinder's volume V_C to get the object's volume V_O:

$$V_O = V_C - \sum_{i=1}^{i=i_{OBJ}} V_S(i)$$

$$V_O = n_{OBJ}\pi r^2 s - \sum_{i=1}^{i=i_{OBJ}} A_S(i) s N_T.$$

In the last formula the radius of the ring r is constant and the distance s between consecutive 'snapshots', is dependent on the speed of the object. They can be excluded during the data processing until the final calculation using A_S^*.

$$V_O = r^2 s\left(n_{OBJ}\pi - \sum_{i=1}^{i=i_{OBJ}} A_S^*(i) N_T\right).$$

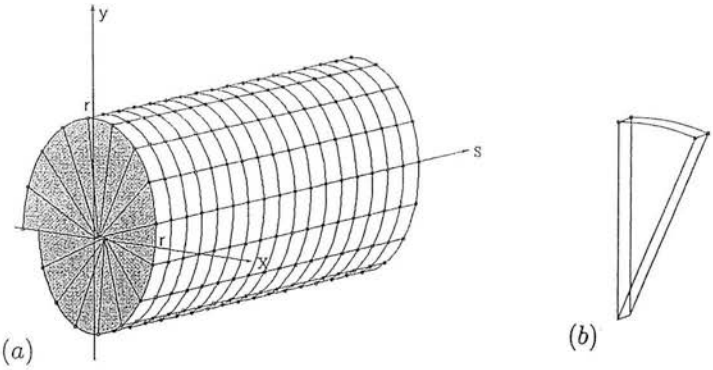

Figure 6. The volume of a 3D ring (cylinder): (a) the basic volume cylinder for an object and (b) the basic spline.

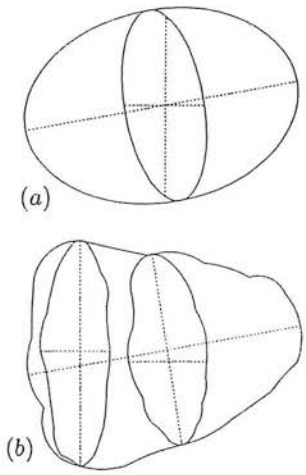

Figure 7. An ellipsoid (a) and an irregular object (b).

4. Axis measurements

4.1. Characteristic axes of an object

Axis measurements have been used in agriculture to estimate the shape and volume of objects (Mörtl 1992, McRae *et al* 1986). In this paper a simple description of the determination of major axes is presented, which requires the largest axis of the object to be parallel to the axis of passage through the ring sensor. The advantages of this are that only a two-dimensional investigation is necessary in order to determine the axis measurements and the co-ordinate system (Gall 1997) need not be changed. If the presentation of objects were random, a different co-ordinate system would be necessary with subsequently more complex 3D algorithms.

The determination of the length L of the object has been discussed previously (Gall 1997). One revolution of the enveloping spiral of the object creates a cross section normal to the longitudinal direction. The minor and major axes of the middle slice will give the parameters of an ellipsoid (see figure 7(a)).

In nature, many variable forms of fruit and vegetables can be found. If the object is not an ellipsoid, these three parameters need not suffice for describing the shape.

One possible solution (see figure 7(b)) is based on finding the position of the largest slice and measuring the major and minor axes. The relationships among the length, the axes of the largest slice and of the middle slice and the position of the largest slice can give a description of the object's (see section 6).

4.2. Positions of the chords for axes at a cross section

Three different positions of axes are possible in an object. They can be defined as lying between:

(i) two parallel chords P (see figure 8(a));
(ii) a chord and an intersection IN_2 (see figure 8(b));
(iii) two intersections IN_{3A} and IN_{3B} (see figure 8(a)).

For the minor axis, variants 1, 2 and 3 are possible, a major axis in each case requires variant 3. The following sections describe the mathematical background of the axis determination.

4.3. The distance between parallel chords (variant 1)

Looking for minor and major axes of cross sections, each chord touching an object will be investigated for a parallel chord opposite (see figure 9). This case is valid when the distances $|T_A R_X|$ and $|R_A T_X|$ are the same. The distance $|C_A C_X|$ is

$$|C_A C_X| = r|\cos(k_{TA,RA} + 1)\beta + \cos(k_{TX,RX} + 1)\beta|$$

(see appendix A).

If parallel chords are found, the investigation is finished. The distance $|C_A C_X|$ includes no information about the position of the axis.

4.4. The distance between a chord and an intersection of chords (variant 2)

In most cases parallel chords will not be found (see figure 10). In this case, the most distant intersection C_X on the opposite side has to be found and the shortest distance $C_A C_X$ to the actual chord $T_A R_A$ has to be determined.

The first step is to find the first chord $T_X R_X$ in the clockwise direction of rotation of the ring, which precedes a possible parallel chord. Next an apparent parallel chord $T_x R_x^*$ has to be fixed for the determination of the distance $|C_A C_X^*|$ using the method from the previous section. The

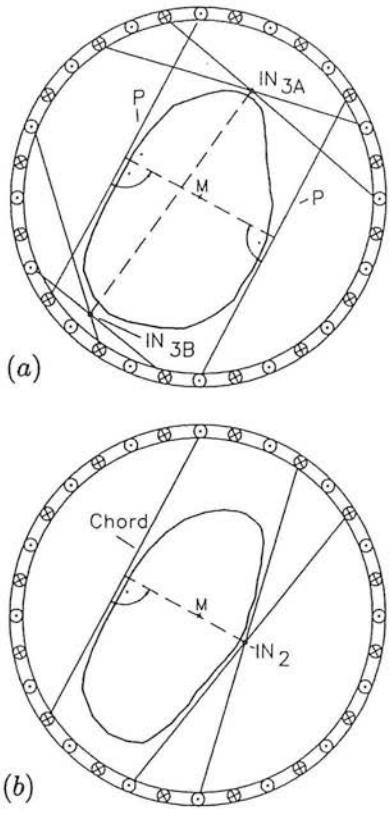

Figure 8. Possible axes in an object with parallels and opposite intersections.

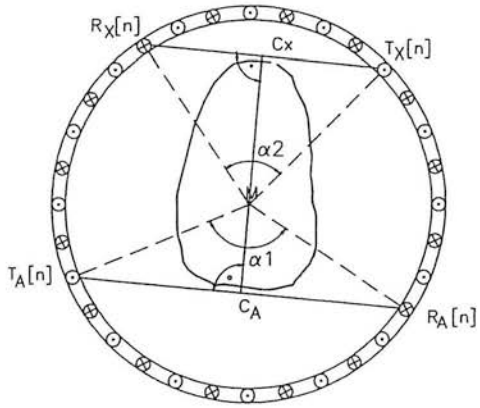

Figure 9. The distance between two parallel chords.

intersection C_X is always further from the chord $T_A R_A[n]$ than this parallel.

Finally the distance $|C_A C_X|$ can be determined:

$$|C_A C_X| = |C_A C_X^*| + |C_X C_X^*|$$

$$|C_A C_X| = |C_A C_X^*| + |T_X C_X| \sin[(k_{TX,RX^*} - k_{TX,RX})\beta]$$

(see appendix B). The distance $|T_X C_X|$ is known from the determination of intersections (Gall 1997).

4.5. The distance between two intersections of chords (variant 3)

Because the major axis of a cross section can only lie between two intersections and the minor axis could also do

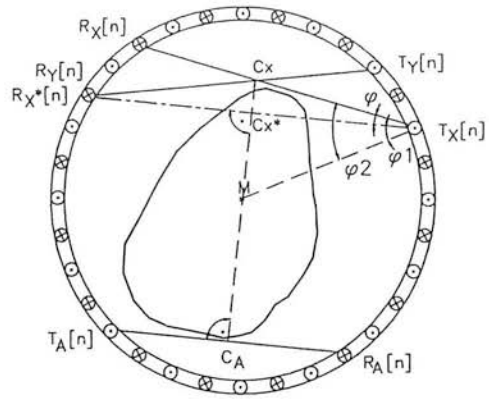

Figure 10. The distance between a chord and an intersection.

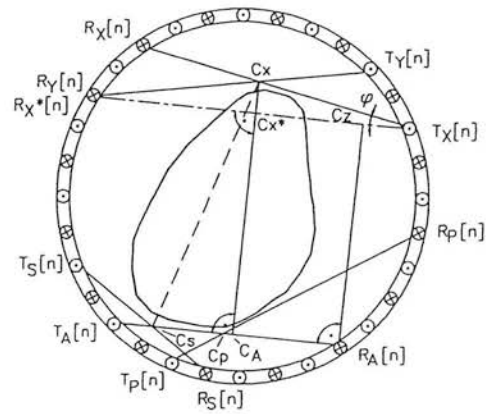

Figure 11. The distance between two oppositely positioned intersections.

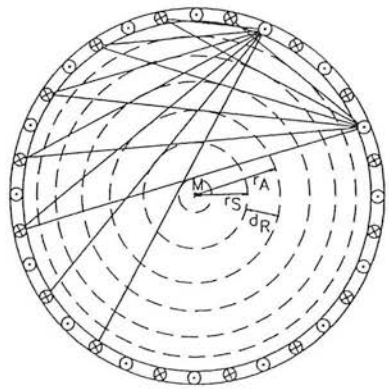

Figure 12. Possible chords from a transmitter to the receivers (two 'snapshots').

this, it follows from section 4.4. that a second intersection has to be found by investigating the distance from the receiver of the actual chord to the intersection with the predecessor $|R_A C_P|$ and also $|R_A C_S|$, the distance to the intersection with the successor chord (see figure 11). Both can simply be produced as a 'by-product' during the determination of the intersections (Gall 1997). The distance $|R_A C_A|$ is also required:

$$|R_A C_A| = \tfrac{1}{2}(|T_A R_A| + |T_X R_X^*|) - |T_X C_X^*|$$

(see appendix C).

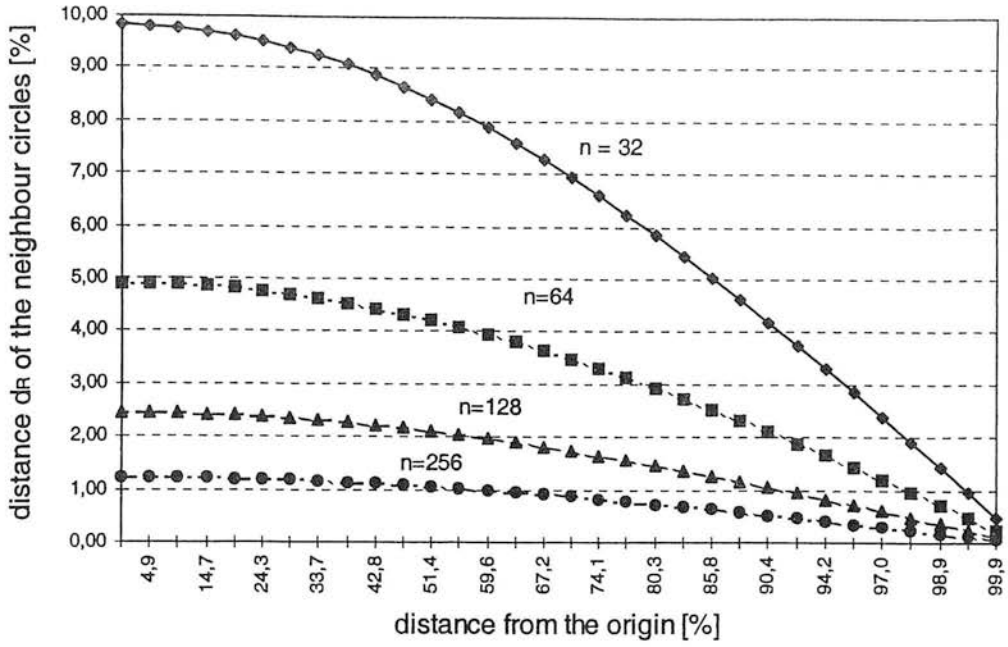

Figure 13. The distance d_R (%) of neighbouring circles to the radius of the ring.

Table 1. Volumes and descriptions of the shapes of the 12 potatoes used.

Number of potato	Real volume (cm^3)	Evaluation of shape
1	24	Long oval
2	39.6	Long oval
3	48.5	Long flat
4	54.5	Long oval
5	70.8	Long flat
6	117.8	Oval flat
7	144	Long flat
8	242.2	Oval flat
9	276.8	Nearly ellipsoid
10	308.5	Oddly shaped, oval and flat
11	550.9	Long flat
12	779	Long oval

Investigating the distances $|C_A C_P|$ and $|C_A C_S|$, the larger has to be evaluated:

$$|C_A C_P| = |R_A C_P| - |R_A C_A|$$

$$|C_A C_S| = |R_A C_S| - |R_A C_A|.$$

The larger distance determines the required intersection (C_S in figure 11). Using Pythagoras' theorem the result is either

$$|C_X C_S| = (|C_A C_X|^2 + |C_A C_S|^2)^{1/2}$$

or

$$|C_X C_P| = (|C_A C_X|^2 + |C_A C_P|^2)^{1/2}.$$

All requirements for the evaluation of the length of the axes are now known. The largest value found around the cross section is the major axis. The positions of the axes in the cross sections and in the ring are unknown and not necessary for the planned use.

5. Sources of errors

It must be remembered that cross sections of the objects generally have to be convex, since concave areas cannot be 'seen' because of the shadow principle of the ring. The errors are mainly caused by the discrete design of the ring since only finite numbers of chords and intersections are possible. The determination of the errors is very complex (Gall 1992) and is a major part of current investigations.

5.1. Round objects centrally positioned in the ring

For the investigation a simplified case is used. There are certain preconditions.

(i) The ring shall consist of a large number of transmitters and the same number of receivers equispaced on the circumference.

(ii) Clockwise scanning and the back chords are used.

(iii) The objects used shall have a circular cross section. They are placed centrally in the ring.

With no object each possible 'snapshot' shows the same result (see figure 12).

A few different regular convex polygons are created with back chords which can be used to describe the same number of touching circles in the ring. For alternately arranged transmitters and receivers, the number of these polygons is equal to half the number of transmitters or receivers because the system is symmetrical about the origin. The number of sides of each polygon is the number of transmitters or receivers.

The formulae for the radii between the actual possible circular cross sections r_A and the successor r_S using the number of receivers $m[n]$ between the actual activated transmitter n and the receiver of the touching chord are

$$r_A = r\cos(m[n] - 0.5)\pi/N_R$$

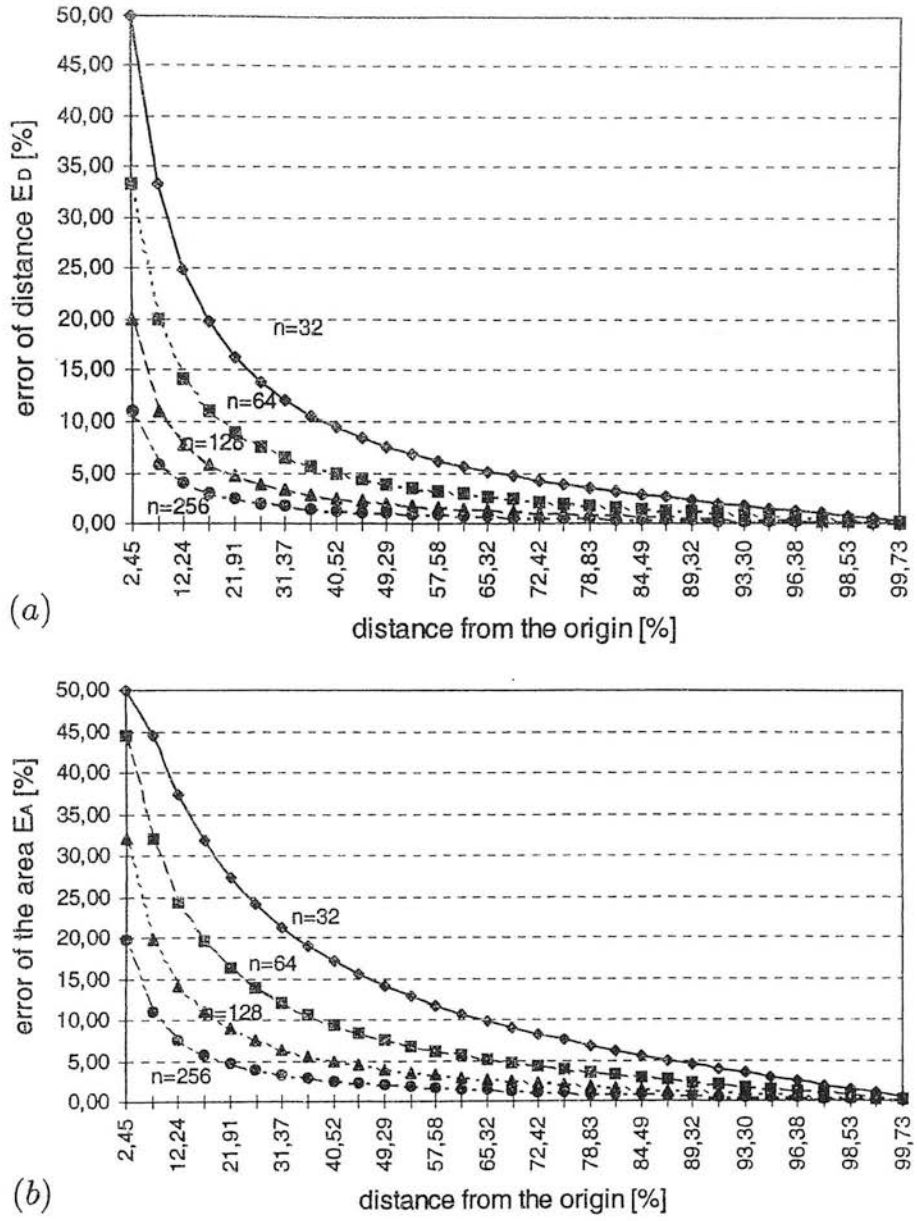

Figure 14. Errors between the possible measurable circular cross sections: (a) of the distance E_D (%) and (b) of the area E_A (%).

and

$$r_S = r\cos(m[n] + 0.5)\pi/N_R.$$

The difference gives the distance $d_R = r_A - r_S$ between the possible cross sections, shown in figure 13 in relation to the radius of the ring.

The average error for the distance E_D (see figure 14(a)) and the area between the circles E_A (see figure 14(b)) are

$$E_D(\%) = 100 \times \tfrac{1}{2}(1 - r_A/r_S)$$

$$E_A(\%) = 100 \times \tfrac{1}{2}[1 - (r_A)^2/(r_S)^2].$$

The error in determination of the diameter and area (see figures 14(a) and (b)) decreases as the diameter of the cross section of the object increases. This is because the chords between transmitters and receivers are closer together with growing distance from the origin of the ring. If the number of transmitters and receivers is doubled, the number of polygons also doubles, as does the resolution for round objects.

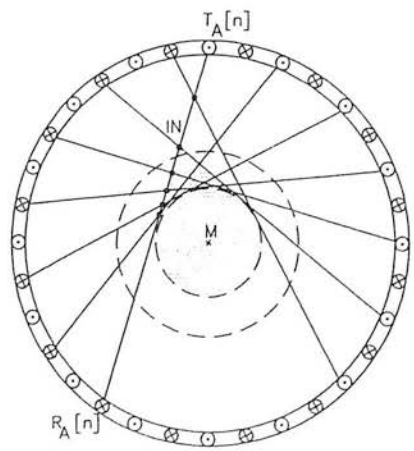

Figure 15. Chords from different transmitters touching the same polygon.

Until now, with each connection from one transmitter to each receiver, a different polygon was touched. One of

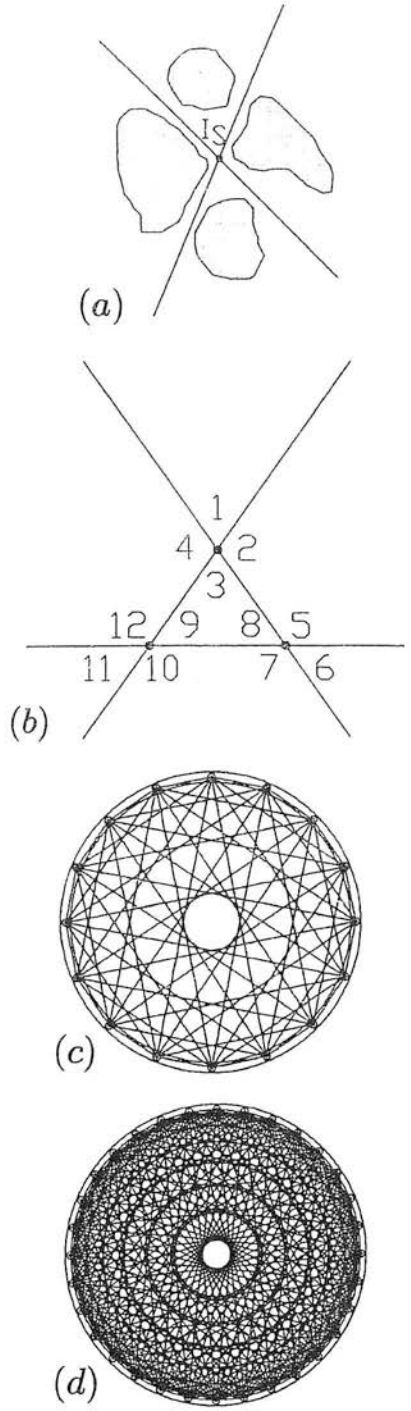

Figure 16. Intersections in the ring. (a) Determined possible positions of an object around an intersection. (b) Possible positions around three intersections. (c) Intersections with eight transmitters and receivers. (d) Intersections with 16 transmitters and receivers.

these described polygons shall now be taken and the chords from the other transmitters to this polygon (see figure 15) used to create a deviation from a circle.

The chord $T_A R_A$ shows that a determinable and limited number of successor chords cut it at different places between the polygons (circles) discussed above. Additional shapes and deviations can be described for non-centrally located and non-circular objects, which improves the resolution and the accuracy.

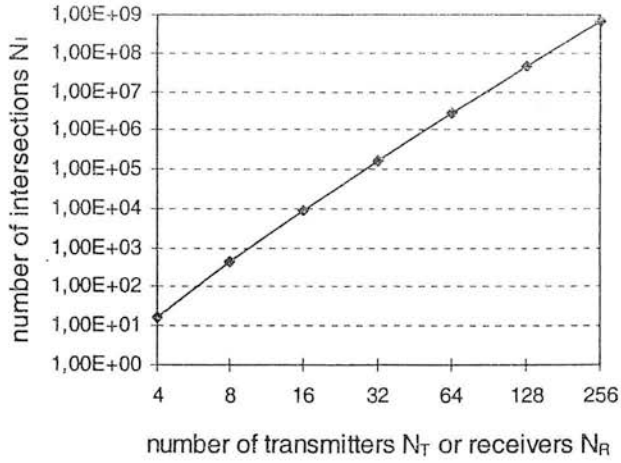

Figure 17. Numbers of intersections N_I in a ring.

5.2. The number of intersections

An object can be detected only if at least one possible chord in a 'snapshot' is not detected, excluding the chords between a transmitter and its two immediately neighbouring receivers. In this case it can be said that all objects are enveloped by chords with intersections between them. There are four possible positions for an object around two chords (see figure 16(a)).

If a third chord intersects at the same point, 12 different positions are possible. The number of possible positions is the same as if they did not intersect at the same point (see figure 16(b)).

This means that the possible number N_I of intersections (see figures 16(c) and (d) and 17) multiplied by 4 gives the value N_P, describing all possible positions of a part of an object in the ring. The functions for a ring with the same number of transmitters N_T and receivers N_R are

$$N_I = N_T^2(N_T - 1)(N_T - 1)/6$$

$$N_P = 4N_I.$$

Because the chords lie closer together near the outside of the ring, more intersections are found there. This is why larger objects can be measured with a higher accuracy.

5.3. Three-dimensional objects

The former investigations can be directly transferred to the three-dimensional case if the objects are considered as centrally positioned cylinders passing with constant speed through the ring. Normally, agricultural products have a form closer to an ellipsoid. This means that it is better to use a number of central positioned circular 'cross sections' with different radii building up a special ellipsoid. In this case the errors are averaging for the determination of volume.

The sampling rate of the ring sensor system determines the number of coils in the spiral which describes the object. Increasing this rate will increase the accuracy for non-cylindrical objects such as ellipsoids, but not for centrally placed cylinders. If the front and the back chords are both

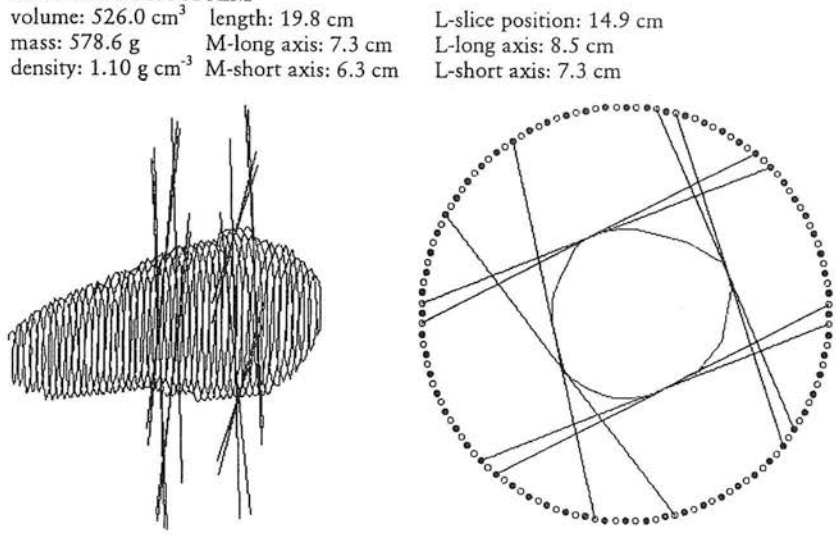

Figure 18. A scan of a potato on the computer including the drawing of the whole object and of the largest cross section. The important axis measurements are marked and the results are shown.

Table 2. The volumes and errors for four different objects.

	Real volume (cm^3)	Measured volume (cm^3)	Standard deviation (%)	Absolute minimum (%)	Absolute maximum (%)
Block 1	159	162	2.3	−3.4	5.8
Block 2	318	324	1.3	−3.2	3.4
Triangle	116	125	3.5	−9.0	7.8
Doughnut	194	195	0.7	−1.5	1.8

used, two shifted spirals envelop the object. This is also a way of increasing the accuracy.

The speed of the object passing through the ring should be constant. If it is not, the speed has to be determined and included during the processing of the data. It is also responsible for the number of coils in the spiral describing the object. Reducing the speed increases the number of coils and the accuracy.

6. Practical tests

A ring consisting of 64 transmitters and 64 receivers was built (Argus Electronic 1997). The ring's diameter is 175 mm with a scanning rate of 400 revolutions per second. Using the basic two-dimensional algorithms, the volume, length, major (M-LARGE) and minor (M-SMALL) axes of the middle slice (see figure 18) and the position of the largest slice (L-SLICE) of an object, major (L-LARGE) and minor (L-SMALL) axes of the largest slice, mass (if the density is known) and density (if the mass is known) can be determined.

A test was performed which showed the results of volume determinations of 12 different potatoes (table 1) passing through the ring at a constant speed of 1.0 m s^{-1}. Each object was measured 50 times using different positions in the ring.

The method feeding material into the system is very important. The belt speed must be stable and the alignment an stability of the potatoes are crucial for accurate results. In practice V belts or a a three-wire-system, for example, are used. For this test, objects were positioned by hand longitudinally on a simple flat conveyor belt before being launched through the ring. The real volume of the potatoes was determined by measuring the weight of the potatoes in air and in water with a balance with 0.1 g resolution (table 1). The shape was estimated and described using terminology normally applied to tubers.

The results for the maximal and average deviations of the measured volume from the real volume are shown in figure 19. It can be seen that the error varies over the whole range of potato sizes used. There are several factors which can account for this result. There is the influence of the presentation, which has not been investigated but was minimized. The effect of size can be seen from the results on error estimation (see section 5.1). The small potatoes have on average a larger positive deviation, because the size is overestimated. In this case, a function could reduce the error. The shape also has an influence. The extrema in shape relative to the average (potatoes 9 and 10 in table 1) give a large deviation in a relatively close range.

The results for the random error and the standard deviation in estimating the measured volume are shown in figure 20; the absolute minimum and maximum are also shown. It can be seen that, for potatoes of more than 100 cm^3, the standard deviation is less than 2.5%. For potatoes smaller than 50 cm^3 the standard deviation is higher than 5%, which suggests that the cut-off point for using the present device should be around 70 cm^3.

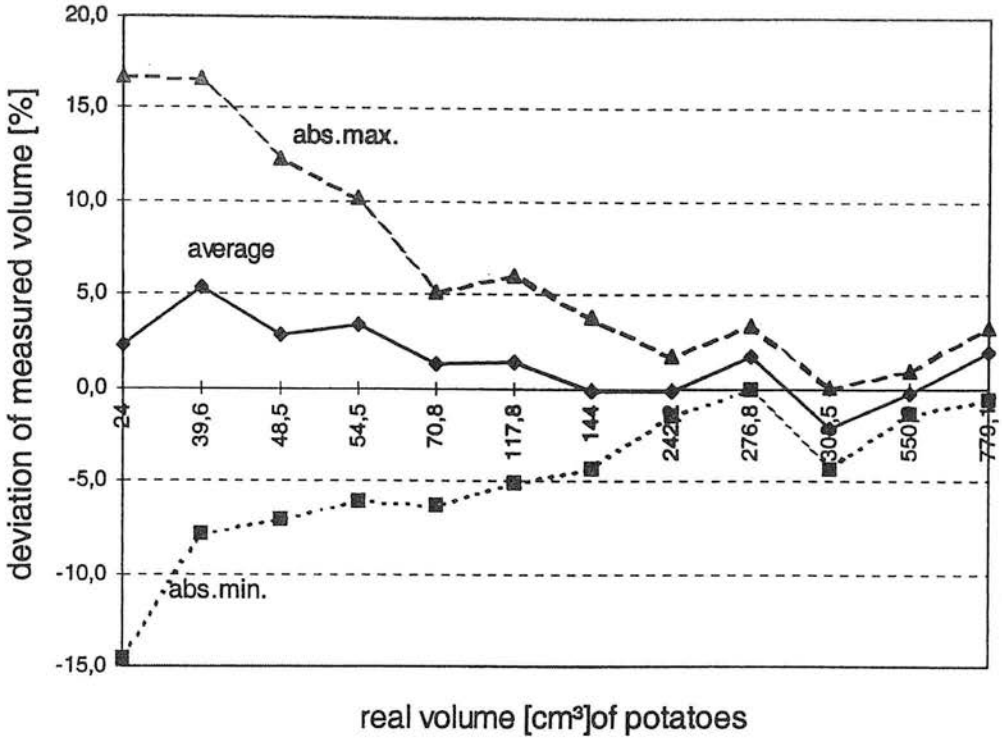

Figure 19. The deviation of the average measured volume from the real volume.

Table 3. Additional measurements of the doughnut-shaped object.

	L	L-LARGE	L-SMALL	L-SLICE	M-LARGE	M-SMALL
Real measurements (mm)	76	76	49	38	76	49
Measured distance (mm)	72.8	76.1	54.5	31.0	75.8	55.9
Standard deviation (%)	0.3	0.6	2.6	7.5	0.5	1.3
Absolute minimum (%)	0.3	1.4	4.5	13.0	1.1	6.9
Absolute maximum (%)	0.4	1.2	2.8	24.1	0.3	0.3

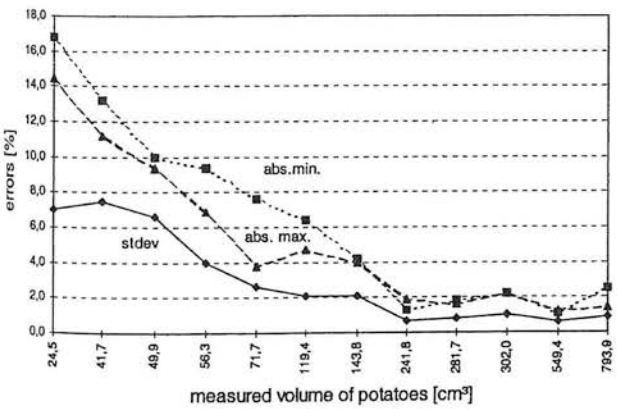

Figure 20. The deviation of the average measured volume from the real volume of potatoes.

In a second test, objects of different shapes were investigated. Table 2 includes examples of other objects, a small and a larger rectangular block, a diagonally cut block with triangular shape and a symmetrical object in the shape of a ring doughnut. The presentation conditions were the same as those for the potatoes.

The object in the form of a round doughnut had a maximum diameter of 76 mm and and a minimum diameter of 49 mm. The results of the measured dimensions of this object are shown in table 3.

The error for the position of the largest slice, L-SLICE, is relatively high because there is little variation in diameter around the mid-section of this object. The deviations of the average measured small axes, L-SMALL and M-SMALL, are consistent with a systematic error dependent on the shape of the object and caused by the principle of determination of the small axis. The errors shown can be reduced by increasing the number of transmitters and receivers and this indicates that an optimum has to be found for the particular use to which the ring is being put.

7. Conclusions

For the determination of area and volume measurements, a segmentation of the picture included in the ring is necessary. The main parts are triangles each with an accompanying circle segment. The determination of these areas allows the calculation of the cross sectional areas of an object. If objects are predominantly convex,

passage through the ring in the longitudinal direction is not necessary for volume but is necessary for cross sectional areas and axis measurements.

Axis measurements are vital to describe the shape of objects. Many agricultural objects are ellipsoidal in shape. For these, the length and the axes of the middle slice are adequate for a description. Other objects deviate from an ellipsoid. To cope with this, the position of the largest slice and the axis measurements can be calculated and used.

An advantage of the system is that the determination of all geometrical parameters is built up by known values from the determination of the contour. The expansion in the third dimension and the determination of volumes of objects is straightforward using the same algorithms as those for the 2D case. This facilitates real-time use.

The theoretical analysis of errors is a complex problem depending on the position, size and shape of objects and number of transmitters and receivers. The accuracy is greater with larger objects. The total number of intersections in the ring gives the possible number of positions of edges of various objects.

For the determination of ellipsoids an average error can be determined because the area of cross sections varies along the whole object. Tests were used to find random and systematic errors with a prototype ring and showed that the ring could be designed to keep errors within acceptable limits for the type of objects being measured.

For objects such as agricultural products the ring sensor system offers the possibility of a relatively fast and accurate determination of geometrical parameters. One small ring sensor system was developed, which can scan 3D objects in real time (36 000 potatoes, 3.6 tonnes per hour) with total accuracies of better than 6% for a volume larger than 70 cm^3 and 5% when objects are heavier than 100 g.

Appendix A

$$\alpha_1 = 2(k_{TA,RA} + 1)\beta$$

$$\alpha_2 = 2(k_{TX,RX} + 1)\beta$$

$$|C_A M| = r\cos(\alpha_1/2)$$

$$|C_X M| = r\cos(\alpha_2/2)$$

$$|C_A C_X| = |C_A M + C_X M|$$

$$|C_A C_X| = r|\cos(k_{TA,RA} + 1)\beta + \cos(k_{TX,RX} + 1)\beta|.$$

Appendix B

$$\varphi = \varphi_2 - \varphi_1$$

$$\varphi = \pi/2 - (k_{TX,RX} + 1)\beta - [\pi/2 - (k_{TX,RX'} + 1)\beta]$$

$$\varphi = (k_{TX,RX'} - k_{TX,RX})\beta$$

$$|C_X C_X^*| = |T_X C_X|\sin\varphi$$

$$|C_A C_X| = |C_A C_X^*| + |T_X C_X|\sin[(k_{TX,RX'} - k_{TX,RX})\beta]$$

Appendix C

$$|T_X C_X^*| = |T_X C_X|\cos\varphi$$

$$|T_X C_Z| = \tfrac{1}{2}(|T_X R_X^*| - |T_A R_A|)$$

$$|R_A C_A| = |T_A R_A| - |T_X C_X^*| + |T_X C_Z|$$

$$|R_A C_A| = \tfrac{1}{2}(|T_A R_A| + |T_X R_X^*|) - |T_X C_X^*|.$$

References

Argus Electronic GmbH 1997 *The Ring Sensor System* Information leaflet, Joachim-Jungius-Straße 9, 18059 Rostock, Germany

Baganz K, Herold B and Mörtl W 1991 Optoelektronische Sortierung andwirtschaftlicher Früchte *Landtechnik* 46 (1/2) 23–5

Crezee L P 1996 Method and apparatus for measuring form parameters of items, European patent applications EP 0 707 192 A1

Exeter Engineering 1994 Automatic grading and sizing systems *Information J.* 109 West Pine Street, PO Box 457, Exeter, California, USA

Gall H and Farchmin U 1990 Sensor zur Bestimmung geometrischer Abmessungen *Sensor Magazin* **4** 16–7

Gall H 1992 Sichtsystem mit ringförmigem Sensor zur On-Line Vermessung der Geometrie unregelmäßig geformter konvexer Objekte *Dissertation* Universität Rostock

Gall H 1997 A ring sensor system using a modified polar coordinate system to describe the shape of irregular objects *Meas. Sci. Technol.* **8** 1228–35

Hiroshi M 1989 Method and apparatus for visual inspection of material Japanese patent JP1035205

Karnali C, Murase H and Honami 1997 Image recognition by artificial retina using the charge simulation numerical technique *Proc. 5th Int. Symp. on Fruit, Nut, and Vegetable Production Engineering, (University of California, Davis, USA, September 6–9)* section 15

Larsson K 1994 *Bildbehandlingsteknik för sortering av potatis* Teknik för Lantbruket Jordbrukstekniska institutet

Marchant J A, Onyango C M and Street M J 1988 High speed sorting of potatoes using computer vision American Society of Agricultural Engineers paper 88-3540

McRae D C, Glasbey C A, Melrose H and Fleming J 1986 Size grading and their relationship to the dimensions, mass and volume characteristics of potato cultivars *Potato Res.* **29** 477–86

McClure J E and Morrow C T 1987 Computer vision sorting of potatoes, American Society of Agricultural Engineers paper 87-6501

Mörtl W 1992 Indirekte Massebestimmung von Kartoffeln und Äpfeln aus optisch ermittelten Abmessungen der Frucht *Dissertation* Universität Rostock

Phillips T H and Rosenfeld A 1988 Decomposition of 3D objects into compact subobjects by analysis of cross-sections *Image Vision Computing* **6** 33–51

Ross D 1995 Viewing apparatus UK patent application UK9502197.8

Wright M E, Sistler F E and Watson R M 1984 Measuring sweet potato size and shape with a computer *Louisiana Agriculture* **28** 12–3

Yang Q 1996 Apple stem and calyx identification with machine vision *J. Agric. Eng. Res.* **63** 229–36

Zwahlen H 1992 Verfahren und Vorrichtung zur Messung einer Dimension eines Körpers und Anwendung dieses Verfahrens, Europäische Patentanmeldung EP 0 500 490

11. References

Affeldt H A Jr., Brown G K, Brusewitz G H , Delwiche M J, Hetzroni A, Kranzler G A, Peleg K, Searcy S, Sistler F E 1993 Dimension, shape and surface texture measurment on agricultural commodities *Nondestructive Technologies for Quality Evaluation of Fruits and Vegetables. Proceedings of the Internatiuonal Workshop funded by BARD, Spokane, Washington, June 1993,* 50-62

AKL S G 1979 Two remarks on a convex hull algorithm. *Information Processing Letters* **8**(2) 108-119

Alt P 1992 Optisch-elektronische Sortiersysteme in der kartoffelverarbeitenden Industrie Bericht über die 13.Kartoffel-Tagung 1991 *Granum-Verlag, Detmold*

Arnarson H and Pau L F 1993 Apparatus and method for determining the volume, form and weight of objects *US-Patent 5,184,733*

Arnarson H and Pau L F 1994 PDL-HM: morphological and syntactic shape Classification algorithm *Machins Vision and Applications* 7 59-68

Antonsson E K 1989 Apparatus for measuring three-dimensional surface geometries *US-Patent* 4,957,369

Aquametric 1995 Product info *AquaMetric AS Trondheim Norway* 4pp

Argus Electronic GmbH 1997 The ring sensor system. *Information Leaflet, Joachim-Jungius-Strasse 9, 18059 Rostock, Germany* 2pp

Baganz K, Herold B and Mörtl W 1991 Optoelektronische Sortierung landwirtschaftlicher Früchte. *Landtechnik* **46** (5) 23-25

Barco 1999 www.barco.com

Belhumeur P N, Kriegman D J 1996 What is the Set of Images of an Object Under All Possible Lighting Conditions? *Proceedings IEEE Computer Society CONF on Computer Vision & Patt recog* 270-277

Besl P J 1988 Geometric Modeling and Computer Vision *Proceedings of the IEEE* **76** 8 930-958

Bhatia G, Vannier M W, Smith K E, Commean P K, Riolo J, Young V L 1994 Quantification of Facial Surface Change Using a Structured Light Scanner *Plastic & Reconst Surg* **6** 768 - 774

Birkle G 1993 Optical Components for opticaally Scanning sthe Surface of an Object whose surface is capable of reflecting, scattering or refracting light *Patent* WO 93/03350

Biswas A K, Nieschwitz P J, Schubert H A 1990 Verfahren und Vorrichtung zum Bestimmen der Geometrie eines Körpers *European Patent* 364 907 A2

Boyer E, Berger M O 1997 3D Surface Reconstruction Using Occluding Contours *Int. J. of Computer Vision* **22(3)** 219 - 233

Brice A 1996 An eye on the fry *Potato Business World* **4** 1 24-32

Brooks M J and Chojnacki W 1994 Direct Computation of Shape from Shading *Proceedings International Conference on Pattern Recognition* **1** 114-119

Chen G H, Chern Maw-Sheng , Lee R C T 1987 New systolic architecture for convex hull and half-plane intersection problems *BIT* **27** 141-147

Chen S, Fon D S, Hong S T 1992 Electro-optical citrus sorter *ASAE Paper* 92-3520

Chiyokura H and Kimura F 1983 Design of solids with free-form surfaces *Computer Graphics* **17** 3 289-299

Chung R, Nevatia R 1996 Recovering LSHGCs and SHGCs from stereo *Int. J. of Computer Vision* **20** (5) 43-58

Cinque L and Lombardi L 1995 Shape description and recognition by a multiresolution approach *Image and Vision Computing* **13** 8 599 - 607

Cipolla R, Fletscher G, Giblin P 1997 Following Cusps *Int. J. of Computer Vision* **23** 2 115-129

Crezee L P 1996 Method and apparatus for measuring form parameters of items *European Patent EP 0 707 192 A1*

Crowe T G and Delwiche M J 1996 Real-time defect detection in fruit - part I: Design concepts and developments of prototype hardware. *Transactions of the ASAE* **39**(6) 2299-2308

Davies E R 1990 Machine Vision *Academic Press, HarcourtBrace Jovanovich, Publishers* 538pp

Delibasis K, Undrill P E 1994 Anatomical object recognition using deformable geometric models *Image and Vision Computing* **12** 7 423-433

De Silva C W, Gosine R G, Wu Q M, Wickramarachchi N, Beatty A 1993 Flexible Automation of Fish Processing *Engng Applic. Antif.Intell.* **6** 2 165-178

Eigler H, Möller W 1988 Dreidimmensionale Lagebestimmung und Formerkennung durch aktive Triangulation *Bild und Ton* **41** 12 366-368

Elad D, Einav S 1990 Three-dimensional measurement of biological surfaces *ISPRS Journal of Photogrammetry and Remote Sensing* **45** 247-66

Exeter Engineering 1994 Automatic grading and sizing systems *Information Journal, Exeter*, 6pp (109 West Pine Street P.O. Box 457 Exeter, California)

Farchmin U, Gall H 1990 Vorrichtung zum optoelektrischen Erfassen und zur rechentechnischen Auswertung von Querschnittsabmessungen, Querschnittsflächeninhalten,Querschnittsumfängen, Querschnittsformen, Querschnittspositionen und dem Reflektionsverhalten von Produkten *German patent Offenlegungsschrift DE 40 12 038 A1*

Fatehi D, Schneider B 1991 Visuelles Sensorsystem zur Überwachung von Förderbändern *Vision & Voice Magazine* **5** (2) Kennziffer 115

Faux D and Pratt M J 1985 Geometry for Design and Manufacture *Ellis Horwood Ltd.*

Foley D, van Dam A, Feiner St K, Hughes J F, Philipps R L 1997 Introduction to Computer Graphics *Addison-Wesley Publishing Company* 513pp

Fon D S, Chen S, Yang C Y 1990 Size sorting of fruits using array phototransistors *ASAE Paper 90-7058*

Forsyth D, Zisserman A 1990 Shape from shading in the light of mutual illumination *Image and vision computing* **8** 1 42-49

Gall H and Farchmin U 1990 Sensor zur Bestimmung geometrischer Abmessungen. *Sensor Magazin* **4**, *Magazin Verlag*, 16-17

Gall H 1992 Sichtsystem mit ringförmigem Sensor zur On-Line Vermessung der Geometrie unregelmäßig geformter konvexer Objekte. *Dissertation Universität Rostock, Germany* 117pp

Gall H 1994 Viewing system with ring-shaped sensor for on-line determination of the geometry of irregularly formed convex objects. *International Agrophysics Volume* 8, *Lublin, Poland* 565-566

Gall H, Pohlmann R 1996a Optisches Sensorsystem zur Größen- und Formvermessung von Lebensmitteln *LVT Fachzeitschrift für Lebensmittel- und Verpackungs - technik* **4** 9, Verlag E F Beckmann KG 207-209

Gall H 1996b Determining the size and shape of potatoes *Potato Newsletter SAC Scottish Agricultural College* December 8-9

Gall H 1997 A ring sensor system using a modified polar co-ordinate system to describe the shape of irregular objects. *Measurement Science and Technology, Institute of Physics Publishing November* **8** 1228-1235

Gall H, Muir A, Fleming J, Pohlmann R, Göcke L and Hossack W 1998 A ring sensor system for the determination of volume and axis measurements of irregular objects *Measurement Science and Technology, Institute of Physics Publishing* **9** 1809-1820

Gall H, Muir A, Fleming J 1999 Alternative method for determination geometrical parameters of agricultural produce *Proc. SPIE Vol.3543, Precision Agriculture and Biological Quality, George E. Meyer, James A. DeShazer* 385-388

Gardner R J 1995 Geometric tomography *Encyclopedia of mathematics and its applications Cambridge University Press* 416pp

Gellert W, Küstner H, Hellwich M, Kästner H. 1971 Kleine Enzyklopädie Mathematik *VEB Bibliographisches Institut Leipzig* 837pp

GREEFA 1995 The NEW revolutionary GREEFA electronic measuring system *Product Information* (Nieuwsteg 62, 4196 Am Tricht Holland)

Gronewäller L, Dickmann K 1990 Laser-Triangulation zur Bestimmung geometrischer Werkstückgrößen *Sensor Magazin* **2** 30-34

Hata S, Okada T, Ariga M, Okabe T 1988 Three-dimensional vision system *US-Patent 4,731,853*

Heinemann P H, Hughes R., Morrow C T, Sommer H J, Beelman R B, Wuest P J 1994 Grading of mushrooms using a machine vision system *Transaction of the ASAE* **37** 5 1671-1677

Herbert R J 1998 The Upgrader 1200 Information Leaflet 2pp (R J Herbert Engineering Ltd, Middle Drove, Marshland St James, Wisbech, Cambridgeshire, PE14 8JT U.K.)

Herbert R J 1989 Agri-Sort Information *Leaflet 1pp* (R J Herbert Engineering Ltd, Middle Drove, Marshland St James, Wisbech, Cambridgeshire, PE14 8JT U.K.)

Hermann G T 1980 Image reconstruction from projections *Academic Press New York-London-Toronto*

Hiroshi M 1989 Method and apparatus for visual inspection of material *Japanese Patent JP1035205*

Hirotoshi T 1991 Method for judging shapes of fruits and vegetables *Japanese Patent JP3221175*

Horn B K P, Brooks M J 1989 Shape from shading *The MIT Press Cambridge, Massachusetts, London, England* 577pp

Inoue Y, Nishumara T, Ipposhi T, Iwamatsu T 1995 Three-dimensional shape Measuring device and three-dimensional shape measuring sensor *US-Patent 5,381,235*

Jarvis R A 1973 On the identification of the convex hull of a finite set of points in the plane *Information Processing Letters* **2** (1) 18-21

Kajiki Y 1997 Three-dimensional moving image recording/reproducing system Which is compact in size and easy in recording and reproducing a three-dimensional moving image *US-Patent 5,694,235*

Karnali C, Murase H and Honami 1997 Image Recognition by Artificial Retina Using the Charge Simulation Numerical Technique. *Proceedings 5th International Symposium on Fruit, Nut, and Vegetable Production Engng., Davis, USA, Sep.6-9,* Section 15 6pp

Kim J H, Cho H S 1995 Neural network-based inspection of solder joints using a circular illumination Image and Vicion Computing **13** (6) 479-490

Klein A 1986 Modelling 3D shaped solids of arbitrary shape using an edge-orientated algorithm *Comput. & Graphics* **10** (4) 327-331

Klingenberg K, Reinfelder H E 1990 Medical imaging techniques *ISPRS Journal of Photogrammetry and Remote Sensing* **45** 203-226

Knight E D, Purssell P 1973 Formerkennungsystem *German patent Offenlegungsschrift DE-2256103*

Koendrink J J 1990 Solid shape *The MIT Press Cambridge*

Konecny G, Schiewe J 1996 Mapping from digital sattelite image data with special reference to MOMS-02 *ISPRS Journal of Photogrammetry & Remote Sensing* **51** 173-181

Lanzl F 1985 The monecular electro-optical stereo scanner (MEOSS) *DFVLR D-8031 Oberpfaffenhoffen Germany* 4pp

Larsson K Bildbehandlingsteknik för sortering av potatis *Technik för Lantbruket* (Jordbrukstekniska institut Box 7033, 750 07 Uppsala Sweden)

Lee S 1990 Distributed proximity sensor system having embedded light emitters and detectors *US-Patent 4,893,025*

Leu M C, Ji Z 1992 Non-linear displacement sensor based on optical triangulation principle *US-Patent 5,113,080*

Lefebre M, Gil S, Brunet D, Natonek E, Baur C, Gugerli P, Pun T 1993 Computer vision and agricultural robotics for disease control: The potato operation *Computer and Electronics in Agriculture* **9** 85-102

Limbach D C 1997 Optical method and apparatus for measuring surface topography of an object *US-Patent 5,636,030*

Liu T Y, Hsu W H, Chen Y S 1992 Shape description via shading images *Image and Vision Computing* **10** (1) 46-54

Loctronic 1989 Autoselector Ro-Ro 'C'&D', *Information sheet. Loctronic Graders Ltd* 2pp (Danburry, Chelmsford, CM3 4NH, Essex, England)

Mafroda 1998 Carrot grading for the 21st century *MAF France* (546, Rue G. Jay, B.P. 112, 82001 Montauban France)

Marchant J A, Onyango C M, Street M J 1988 High speed sorting of potatoes using computer vision. *ASAE Paper no. 88-3540* 6pp

Marchant J A, Onyango C M and Street M J 1990 Computer vision for potato inspection without singulation *Computers and electronics in agriculture* **4** 235-244

Marel 1999 www.marel.is

McEntee J 1996 'Shape camera' will highlight edges for product inspection *OLE October* 33-34

McCrea P G 1981 Microcomputer-controlled potato sizing and selecting machinery *IECI proceedings San Franzisco 9-12 Nov 1981* 433-438

McRae D C, Glasbey C A, Melrose H and Fleming J 1986 Size grading methods and their relationship to the dimensions, mass and volume characteristics of potato cultivars. *Potato Research* **29** 477-486

McRae D C 1988 Singulator for potatoes and other produce *Information Leaflet 2pp* (Scottish Centre of Agricultural Engineering, Bush Estate, Penicuik, Midlothian, EH26 0PH, Scotland U.K.)

Miller W M 1992 Classification analysis of Florida grapefruit based on shape parameters *Proceedings Food Automation II* 339-347

Minowa M 1994 Three-dimensional shape measurement of a pig *Technical bulletin of the faculty of agriculture* 4pp

Mitchell H L 1995 Applications of digital photogrammetry to medical investigations *ISPRS Journal of Photogrammetry and Remote sensing* **50** (3) 27-36

Molitor M 1988 Berührungslose optoelektronische Meßautomaten für die Geometrieerfassung an Werkstücken *VDI-Verlag GmbH Düsseldorf* 183pp

Monnin M 1994 Machine Vision Gauging in a bakery *Proceedings of FPAC III conference food processing automation III* 62-71

Mörtl W 1992 Indirekte Massebestimmung von Kartoffeln und Äpfeln aus optisch ermittelten Abmessungen der Frucht. *Rostock, Universität Rostock, Germany* 98pp

Mullani N A 1986 Position emmision tomography camera *US-Patent 4,563,582*

Namco 1990 Wo (Laser-) Licht ist, ist auch Schatten *Sonderdruck aus Sensor report Heft 5 Oktober*

Nayar S K, Ikeuchi K 1989 Photometric Sampling: A method for determining shape and reflectance of surfaces *Machine vision for inspection and measurement Academic Press Inc.* 137-184

Noborio H, Fukuda S, Arimoto S 1988 Construction of octree approximating three-dimensional objects by using multiple views *IEEE transactions on pattern analisys and machine intelligence* **10** (6) November 769-781

O'Rourke J, Badler N 1979 Decomposition of three-dimensional objects into spheres *IEEE transactions on pattern analysis and machine intelligence* Vol.PAMI 1, No. 3, July

OLE 1996 Potato sorting and more: smart optics eyes new market *Product info OLE December* 6

Oren M, Nayar S K 1996 A theory of specular surface geometry *International Journal of Computer vision* **24** (2) 105-124

Pepperl+Fuchs GmbH 1995 Optical Size and volume measurement – for production line inspection *Information leaflet* 6 pp (68301 Mannheim Germany)

Petkov N 1990 Ein Näherungsverfahren zur Bestimmung der konvexen Hülle und verwandte Probleme der algorithmischen Geometrie. *Bild und Ton* 43 **3** 76-79

Pillow N, Utcke S, Zissermann A 1995 Viewpoint-invariant representation of generalized cylinders using the symmetry set *Image and Vision Computing* **13** (5) 355-365

Preparata P F and Shamos I M 1985 Computational geometry an introduction. *Springer-Verlag New York* 398pp

Rashid H U, Burger P 1992 Differential algorithm for the determination of shape from shading using a point light source *Image and Vision Computing* **10** (2) 119-127

Raggam J, Almer A, Strobl D 1994 A combination of SAR and optical line scanner Imagery for stereoscopic extraction of 3-D data *ISPRS Journal of Photogrammetry and Remote Seensing* **49** (4) 11-21

Resource 1995 High speed, high-resolution citrus sorter is cost-effective *Resource (presenting the 1995 A50 aword winners) AE50/23* 1pp

Riese U 1992 Elektronisch gesteuerte Verlesesysteme – für ungeschälte und geschälte Kartoffeln *Kartoffelbau* **43** (6) 275-277

Robert L, Faugeras O D 1995 Relative 3D positioning and 3D convex hull Computation from a weakly calibrated stereo pair *Image and Vision Computing* **13** (3) 189-196

Rosenfeld A 1987 Zukünftige Entwicklungslinien des maschinellen Sehens *Bild und Ton* **40** (11) 332-335

Rosenfeld A, Kak A C 1982 Digital picture processing second edition *Volume 1-2 Academic Press Inc.*

Ross D 1995 Viewing Apparatus. *United Kingdom Patent Application number UK9502197.8*

Samro 1994 Samro Video - Elektronischer Größensortierer, *Information Sheet. Samro Bystronic Maschinen AG, CH-3400 Burgdorf, Switzerland* 2pp

Samro 1995 Schweizer Qualität – Unsere Modellreihe *Information Sheet Samro Bystronic Maschinen AG, CH-3400 Burgdorf, Switzerland* 4pp

Sánchez-Reyes J 1994 Single-valued surfaces in spherical co-ordinates. *Computer Aided Geometric Design* **11** 491-517

Schaffrath H, Looks H 1989 Adaptive Verarbeitung von medizinischem Bildgut *Bild und Ton* **42** (12) 363-367

Schulz K P, Röhl A 1986 Sichtsystem mit CCD-Zeilenkameras zur On-Line-Vermessung und -Sortierung bewegter Objekte *Inaugural-Dissertation University Rostock* 261pp

Select 1998 Agroselector spectrum colour TWIN 10T-3 *Information leaflet - Select Ingenieurgesellschaft für Optoelektronik und Qualitätsprüefung mbH, D-09232 Hartmannsdorf Germany 2pp*

Shafer S A 1985 Silhouettes in computer vision *Kluver Academic Publishers*

Shen X, Hogg D 1994 Shape models from image sequences *Lecture Notes in Computer Science, Vol.800 Computer Vision - ECCV '94 Springer-Verlag Berlin Heidelberg* 225-230

Shen X, Hogg D 1995 3D shape recovery using a deformable model *Image and Vision Computing* **13** (5) 377-383

Siemens 1993 Optoelectronics Data Book *Siemens Components, Inc., Optoelectronics Division 1900 Homestead Road, Cupertino, California 95014*

Sistler F E 1991 Machine vision techniques for grading and sorting agricultural products *Postharvest News and Information* **2** 2 81-84

Slusallek P, Seidel H P 1995 Vision – an architecture for global illumination calculations *IEEE transactions on visualization and computer graphics* **1** (1) 77-96

Stewart I 1993 A million ways to wrap a rubber band round a potato. *New Scientist* 1854 **137** 16

Strachan N C J 1993 Recognition of fish species by colour and shape *Image and Vision Computing* **11** (1) 2-10

Strachan N C J 1993 Length measurement of fish by computer vision *Computers and Electronics in Agriculture* **8** 93-103

Streenstrup C, Christiansen K, Rasmussen A 1993 System and method for testing and/or identification of objects including especially living fish-objects *PCT-Patent WO 93/16351*

Takada M 1983 Object solid figure recognizing method and apparatus *US-Patent 4,404,684*

Tao Y, Morrow C T, Heinemann P H, Sommer H J 1995 Fourier-based separation Technique for shape grading of potatoes using machine vision *Transactions of the ASAE* **38** (3) 947-957

Teillaud M 1993 Towards dynamic randomised algorithms in computational geometry, *Springer-Verlag Berlin Heidelberg* 149pp

Tellkamp H, Rosenkranz G 1989 Osteoporosediagnostik unter Anwendung moderner bildgebender Verfahren *Bild und Ton* 42 (12) 357-359

Texas Instruments 1975 Das Opto – Kochbuch: Theorie Praxis der Optoelektronik *Texas Instruments Deutschland Learning Center, Freising*

Terzopoulos D, Witkin A, Kass M 1987 Symmetry – seeking models and 3D object reconstruction *International Journal of Computer Vision* **1** 211-221

Thomson W H, Pomeranz Y 1991 Classification of wheat kernels using three-dimensional image analysis *Cereal chemistry* **68** (4) 357-361

Tillet R D 1991 Image analysis for agricultural processes: a review of potential opportunities *Journal of agricultural engineering research* **50** 247-258

Times 1997 Revealed: secret of how flies see *The Sunday Times Business 19 October 1997* 3.12

Turing 1999 www.turing.gla.ac.uk

Vosseler H G 1997 Messvorrichtung zur kontaktlosen Messanalyse von Körpern oder Oberflächen *European Patent EP 0767357*

Wallack A S, Canny J F 1995 Object recognition and localization from scanning beam sensors *Proceedings International Conference on Robotics and Automation* **1** 247-254

Wallack A S, Canny J F 1997a Object recognition and localization from scanning beam sensors *Proceedings The International Journal of robotics research* **16** (5) 631-659

Wallack A S, Canny J F 1997b Generalized polyhydral object recognition and localization using crossbeam sensing *The International Jornal of robotics research* **16** (4) 473-496

Wallack A S, Canny J F 1993 A geometric matching algorithm for beam scanning *SPIE Vol. 2060 Vision Geometry II* 143-160

Wartenberg 1989 Project grading potatoes *Ingenieurhochschule Wartenberg, East-Berlin, GDR* (was seen by the Author, no more information)

Weinshall D 1994 Local shape approximation from shading *Journal of Mathematical Imaging and Vision* **4** 119-138

Wögenbauer J P, Hindiger S, Wachter B R 1991 Einrichtung zum Erfassen der Masse eines gegebenenfalls bewegten Gegenstandes *European Patent EP 0442252*

Wright M E, Sistler F E and Watson R M 1984 Measuring sweet potato size and shape with a computer. *Louisiana Agriculture* **28** 1 12-13

Wu X, Murai S 1997 Image matching using a three line scanner *ISPRS Journal of Photogrammetry & Remote Sensing* **52** 20-32

Yamazaki K, Aoyama H 1995 Non-contact type measuring device for measuring three-dimensional shape using optical probe *US-Patent 5,410,410*

Yang Q 1996 Apple stem and calyx identification with machine vision. *J. Agric. Engng Res.* **63** 229-236

Yang M C, Tsai W H 1989 Recognition of single 3D curved objects using 2D cross-sectional slice shapes *Image and vision computing* **7** (3) 211-216

Zerroug M, Nevatia R 1996 Volumetric descriptions from a single intensity image *International Journal of Computer Vision* **20** (1/2) 11-42

Zwahlen H 1992 Verfahren und Vorrichtung zur Messung einer Dimension eines Körpers und Anwendung dieses Verfahrens. *European Patent EP 0500490*